Heavy-to-light Decays on the Lattice

Eike Hermann Müller

A thesis submitted in fulfilment of the requirements for the degree of

Doctor of Philosophy

to the

University of Edinburgh

2009

Abstract

Precise predictions of hadronic matrix elements in heavy meson decays are important to constrain the fundamental parameters in the Standard Model of particle physics. The CKM matrix element V_{ub} can be extracted from experimental data on the decay $B \to \pi\ell\nu$ if the hadronic form factor is known. In addition, loop suppressed rare decays of B-mesons, such as $B \to K^*\gamma$ and $B \to K^{(*)}\ell\ell$, provide valuable insight into new physics models.

Hadronic form factors for exclusive meson decays can be calculated in the framework of lattice QCD. As the wavelength of heavy quarks is not resolved on currently available lattices I use an effective nonrelativistic theory to discretise the heavy degrees of freedom. In addition, the discretisation errors in the final state meson are reduced by working in a moving frame.

I review the phenomenology of rare B decays and describe how lattice QCD can contribute to calculating the relevant form factors. As the short distance physics in the effective theory is different from that of QCD, the Lagrangian and decay currents need to be renormalised. I show how this can be achieved in the framework of lattice perturbation theory.

I calculate the perturbative renormalisation constants of the leading order operators in the heavy quark Lagrangian. Motivated by nonperturbative studies I extend this approach to higher order kinetic terms which break rotational invariance. In combination with simulations in the weak coupling regime of the theory, results from diagrammatic lattice perturbation theory are used to calculate the heavy quark self-energy corrections and predict the fundamental parameters of QCD. I calculate the one loop correction on a finite lattice with twisted boundary conditions which is used for the extraction of higher order perturbative corrections. I renormalise the heavy-light current to one loop order in lattice mNRQCD and present results from nonperturbative studies. Finally, I discuss how the results are used in the calculation of hadronic form factors.

Declaration

I do hereby declare that this thesis was composed by myself and that the work described within is my own, except where explicitly stated otherwise.

Sections 4.1 and 5.1.1 follow work published as [1]. As one of the lead authors of this paper I carried out the perturbative calculations presented there and contributed significantly to writing the text.

Eike Hermann Müller
August 2009

Contents

List of Figures

List of Tables

Overview

This work is organised as follows:

After a brief review of the particles and forces in the Standard Model I discuss how the measurement of B meson decays helps to constrain the CKM matrix in chapter 1. In this chapter I also discuss the impact of lattice QCD calculations on the CKM parameters and comment on indirect new physics searches. Chapter 2 focuses on the prediction of rare B meson decays. These processes are described by integrating out physics at the electroweak scale to construct a Lagrangian which is written as an expansion in local operators of the low energetic fields. I outline how theoretical predictions both for inclusive and exclusive decays can be obtained. In the second part of this chapter I discuss how heavy quarks are treated in an effective theory which can be discretised on a lattice. Basic concepts of lattice QCD and the discretisation of fermionic fields using improved actions are reviewed in chapter 3. Chapter 4 is more technical and specific to this work. I construct the heavy quark lattice action and explain how it can be radiatively improved by calculating corrections in lattice perturbation theory. My calculation of the heavy quark self-energy and renormalisation parameters of operators in the mNRQCD action is presented in chapter 5. I compare to nonperturbative simulations and describe how my results are used to constrain the polynomial fit of high-β data. In chapter 6 I extend the analysis to higher order kinetic terms in the NRQCD Lagrangian. I pay particular attention to regulating IR divergences in the integrand. Finally, in chapter 7, I calculate the one loop correction to the heavy-light vector- and tensor current. I review results of the nonperturbative calculation and comment on the extrapolation of the relevant form factors. My results are summarised in chapter 8 which also contains a detailled discussion of systematic errors. Several more technical aspects are relegated to the appendices.

Chapter 1

Introduction and motivation

1.1 The Standard Model of particle physics

The so called "Standard Model of Particle Physics" is the widely accepted theory describing the interactions of subatomic particles (for an overview see for example [2, 3]). It is a relativistic quantum field theory with local $SU(3) \times SU(2) \times U(1)$ gauge symmetry and it describes the forces between the matter fields as being mediated by the exchange of integer spin gauge bosons. The only particle that has not been detected yet is the Higgs boson [4] which is responsible for spontaneous electroweak symmetry breaking and gives mass to fields in a gauge invariant way. Over the last 30 years all other particles have been observed and their properties have been measured extensively[1]. So far the Standard Model has withstood all experimental tests to very high accuracy.

1.1.1 Particles and interactions

The following table lists the four forces in nature together with their relative strength at a lengthscale of $L \sim 1$ fm [6]:

Force	Relative strength
The strong force (binding together protons and nuclei)	1
Electromagnetism	10^{-2}
The weak force (responsible for radioactive beta decay)	10^{-7}
Gravitation	10^{-39}

I will not discuss gravitation as it is so weak that it does not play a role in present high energy experiments and as yet it has not been possible to successfully quantise the gravitational field.

[1] See, for example, [5] for a comprehensive listing of particle properties.

Lepton	T	T^3	Q	Y
$(\nu_e)_L$	$1/2$	$1/2$	0	-1
e^-_L	$1/2$	$-1/2$	-1	-1
e^-_R	0	0	-1	-2

Quark	T	T^3	Q	Y
u_L	$1/2$	$1/2$	$2/3$	$1/3$
d_L	$1/2$	$-1/2$	$-1/3$	$1/3$
u_R	0	0	$2/3$	$4/3$
d_R	0	0	$-1/3$	$-2/3$

Table 1.1: Electroweak quantum numbers of quarks and leptons as in [2]. T is the total weak Isospin, T^3 its three component, $Q = T^3 + Y/2$ the electric charge and Y the hypercharge. The subscripts L and R denote left- and right-handed particles.

The fundamental matter fields carry spin 1/2 and can be split into two groups: leptons, experiencing the electromagnetic and weak force and quarks which in addition interact via the strong force.

The electroweak interactions are described by the Glashow-Salam-Weinberg Model [7, 8, 9].

Before spontaneous symmetry breaking the gauge group is $SU(2)_L \times U(1)_Y$, where the index L indicates that only left-handed particles can interact via charged weak currents and $U(1)_Y$ is the hypercharge group. $SU(2)_L$ is often called the Weak Isospin group. The whole group is broken down to the electromagnetic gauge group $U(1)_{\mathrm{em}}$ by the vacuum expectation value of the Higgs field.

The matter fields can be organised into multiplets according to their quantum numbers under the different gauge groups (see Tab. 1.1). The left handed leptons are organised into an Isospin doublet containing a massless, neutral neutrino and an electron with charge $-e$. In addition there is an Isospin singlet containing the right handed electron. There are no right handed neutrinos in the Standard Model.

A similar structure exists for the quarks, the left-handed particles are organised into an Isospin doublet with an up quark of charge $+2/3e$ whereas the down quark has charge $-1/3e$. The right-handed quarks come in $SU(2)_L$ singlets and each quark belongs to the fundamental $SU(3)_c$ colour-triplet.

It turns out that in addition to the electron, its neutrino and the two quarks, there are two further families of particles with the same quantum numbers but different masses as shown in Tab. 1.2 where I also list the masses of the other fundamental particles. It is common to refer to the u (up), d (down) and s (strange) quarks as *light* as their masses are much smaller than the hadronic scale $\Lambda_{\mathrm{QCD}} \approx 500$ MeV. This hierarchy of scales can be used to construct an effective low energy theory that exploits the chiral symmetry of the Lagrangian in the massless limit [10, 11]. The mass of the heavy quarks c (charm) and b (bottom or beauty) is larger than Λ_{QCD}. Here a different

Leptons	e^-	511 keV	μ^-	105.66 MeV	τ^-	1.78 GeV
	ν_e	0	ν_μ	0	ν_τ	0
Quarks	u	$1.5 - 3.3$ MeV	c	$1.27^{+0.07}_{-0.11}$ GeV	t	171.2 ± 2.1 GeV
	d	$3.5 - 6.0$ MeV	s	104^{+26}_{-34} MeV	b	$4.20^{+0.17}_{-0.07}$ GeV
Photon			γ	0		
Gluons			G	0		
Weak gauge-			$W^\pm$	80.4 GeV		
bosons			Z^0	91.2 GeV		

Table 1.2: Masses of fundamental particles as in [5], see the notes there for an explanation of the quark mass definitions.

effective theory can be constructed where in the lowest order approximation the quarks are treated as infinitely heavy [12, 13, 14]. In chapter 4 it is shown how this effective theory can be discretised on a space time lattice and used to predict decays of heavy B mesons to light final states. The t (top) quark is so heavy that it decays before it can form bound states and it only has an indirect impact on low energy phenomena. In the effective theory I discuss in section 2.2 it will only affect the numerical value of the Wilson coefficients which multiply low energy operators.

The forces between the matter fields are mediated by the gauge bosons of the corresponding group. For the electromagnetic force this is the photon and for the strong force there are 8 gluons which themselves carry colour charges and interact with each other. In contrast to these the mediators of the weak force are not massless but have masses of the order of the vacuum expectation value of the Higgs field which spontaneously breaks the electroweak symmetry group down to the electromagnetic subgroup. The two charged gauge bosons $W^\pm$ have a mass of around 80 GeV and the mass of the neutral Z^0 is about 90 GeV. Like the top quark the weak gauge bosons can be integrated out and do not appear as independent degrees of freedom at hadronic scales.

In its minimal form the Higgs field is a charged scalar Isospin doublet which acquires a vacuum expectation value by spontaneous symmetry breaking. Three of its four degrees of freedom turn into the longitudinal polarisations of the massive weak gauge bosons. Direct detection of the remaining uncharged scalar is one of the main goals of the LHC and this discovery will complete the Standard Model.

1.2 Flavour changing currents and the CKM matrix

As the quarks have non-zero masses, their mass eigenstates can be different from their weak interaction eigenstates. This introduces interactions between the families via the exchange of charged $W^{\pm}$-bosons. The interaction term in the Lagrangian contains the Cabibbo-Kobayashi-Maskawa matrix [15, 16] V_{CKM} and can be written as

$$W_{\mu}^{+}(\overline{u}_L, \overline{c}_L, \overline{t}_L)\gamma^{\mu}V_{CKM}(d_L, s_L, b_L)^T + (h.c.) \tag{1.1}$$

where W_{μ}^{+} is the field of a weak gauge boson. The matrix

$$V_{CKM} = \begin{pmatrix} V_{ud} & V_{us} & V_{ub} \\ V_{cd} & V_{cs} & V_{cb} \\ V_{td} & V_{ts} & V_{tb} \end{pmatrix} \tag{1.2}$$

is unitary in the Standard Model and experiments indicate that the off diagonal elements are small (for an overview see [5]). V_{CKM} can be parametrised by four parameters, three real angles and one CP-violating phase. If this phase is non-zero, as measurements of the CKM-triangle show, weak interactions are not invariant under a simultaneous charge (C) reversal and parity (P) transformation.

The standard parametrisation is the approximation proposed in [17] which uses $\lambda = |V_{us}| \approx 0.22$ as a small expansion parameter

$$V_{CKM} = \begin{pmatrix} 1 - \frac{\lambda^2}{2} & \lambda & A\lambda^3(\rho - i\eta) \\ -\lambda & 1 - \frac{\lambda^2}{2} & A\lambda^2 \\ A\lambda^3(1 - \rho - i\eta) & -A\lambda^2 & 1 \end{pmatrix} + \mathcal{O}(\lambda^4). \tag{1.3}$$

Unitarity leads to a set of relations among the CKM parameters which can be interpreted geometrically as triangles in the complex plane. Only one of these triangles is not near-degenerate, after normalisation the corresponding relation is

$$\frac{V_{ud}V_{ub}^*}{V_{cd}V_{cb}^*} + \frac{V_{td}V_{tb}^*}{V_{cd}V_{cb}^*} + 1 = 0. \tag{1.4}$$

This can be used to relate the sides and angles to elements of the CKM matrix, see Fig. 1.3. The apex of the triangle lies at $\rho + i\eta$ so that a finite value of η is a sign of CP violation.

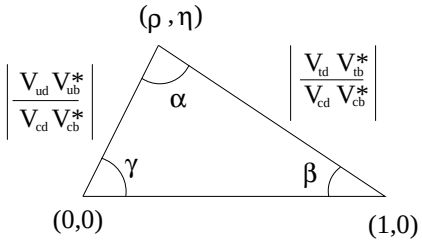

Table 1.3: CKM triangle in the complex plane

1.2.1 Measuring the sides of the CKM triangle

In nature free quarks can not be observed and V_{CKM} can only be extracted from decays of strongly bound particles. In Tab. 1.4 I list the absolute values of the CKM matrix elements which are obtained by combining results from different sources, including both inclusive and exclusive decays[2] and B meson mixing [5]. In the last column I also give examples for exclusive observables which can be used in this extraction; experimentally these have the advantage of a well defined final state. The prediction of inclusive and exclusive decays requires different techniques and it is useful to consider both as inconsistencies between them can provide information on contributions from new physics.

Note that the dominant uncertainty in $|V_{ud}V_{ub}^*/(V_{cd}V_{cb}^*)|$, which is one of the sides of the CKM triangle in Fig. 1.3, comes from $|V_{ub}|$ (see dark green circle in Fig. 1.1). The value quoted in Tab. 1.4 is dominated by the inclusive measurement. To extract V_{ub} from exclusive measurements matrix elements of heavy-light operators need to be calculated. Hadronic form factors have been predicted by the HPQCD collaboration [18]. With experimental input from the BaBar, Belle and Cleo collaborations they report $|V_{ub}| = (3.55 \pm 0.25(\text{exp.}) \pm 0.50(\text{theor.})) \cdot 10^{-3}$ where the dominant error is theoretical. Results obtained using other parametrisations with theoretical uncertainties of comparable or larger size are collected in [19]. In a recent calculation [20] the form factors are parametrised in a model independent way; using input from a lattice calculation and combining with data from the BaBar experiment the authors of this study find $|V_{ub}| = (3.38 \pm 0.36) \cdot 10^{-3}$.

In Fig. 1.1 I show all constraints on the CKM triangle in the complex (η, ρ)-plane [5]. The plot clearly demonstrates that so far the measurements from a wide range

[2]The hadronic final state in an inclusive decay contains an arbitrary number of particles and is only specified by its quantum numbers. For example, in the decay $B \to X_s\gamma$ the symbol X_s describes any number of hadrons with total strangeness $s = 1$. Exclusive decays have a defined final state, as in $B \to \pi\ell\nu$.

$(V_{CKM})_{ij}$	value	rel. error	observable
$\lvert V_{ud}\rvert$	0.97418 ± 0.00027	0.028%	Nuclear beta decay, $\pi \to \ell\nu$
$\lvert V_{us}\rvert$	0.2255 ± 0.0019	0.84%	$K \to \pi\ell\nu$
$\lvert V_{ub}\rvert$	$(3.93 \pm 0.36) \cdot 10^{-3}$	9.2%	$B \to \pi\ell\nu$
$\lvert V_{cd}\rvert$	0.230 ± 0.011	4.8%	$D \to \pi\ell\nu$
$\lvert V_{cs}\rvert$	1.04 ± 0.06	5.8%	$D \to K\ell\nu$, $D_s \to \ell\nu$
$\lvert V_{cb}\rvert$	$(41.2 \pm 1.1) \cdot 10^{-3}$	2.7%	$B \to D\ell\nu$
$\lvert V_{td}\rvert$	$(8.1 \pm 0.6) \cdot 10^{-3}$	7.4%	$B\overline{B}$-mixing
$\lvert V_{ts}\rvert$	$(38.7 \pm 2.3) \cdot 10^{-3}$	5.9%	$B_s\overline{B}_s$-mixing
$\lvert V_{tb}\rvert$	> 0.74		top decay, $Br(t \to Wb)/Br(t \to Wq)$

Table 1.4: Absolute values of CKM matrix elements from [5] and selection of (exclusive) processes which can be used for extraction of these matrix elements. Each value in the second column is obtained from a combination of inclusive and processes, not necessarily the ones listed in the last column.

of observables are consistent with each other and it is desirable to reduce theoretical uncertainties even further to keep up with the increasing precision of experimental measurements.

CKM triangle and lattice QCD

The differential decay rate of the semileptonic decay $B \to \pi\ell\nu$ is proportional to the product of $|V_{ub}|^2$ and the square of the strong form factor $f_+(q^2)$. In this process $q = p - p'$ is the momentum transfer between the initial- and final state mesons and the Fermi constant is denoted by G_F:

$$\frac{d\Gamma(B \to \pi\ell\nu)}{dq^2} = \frac{G_F^2 |V_{ub}|^2}{192\pi^3 m_B^3} \left[(m_B^2 + m_\pi^2 - q^2)^2 - 4m_B^2 m_\pi^2\right] |f_+(q^2)|^2 \qquad (1.5)$$

The form factors f_+ and f_0 parametrise heavy-light matrix elements of the vector current,

$$\langle \pi(p')|\overline{s}\gamma^\mu b|B(p)\rangle = f_+(q^2)\left(p^\mu + p'^\mu - \frac{M_B^2 - M_\pi^2}{q^2} q^\mu\right) + f_0(q^2)\frac{M_B^2 - M_\pi^2}{q^2} q^\mu. \qquad (1.6)$$

In [18] these form factors are calculated in lattice QCD. This is done using two approximations which are also crucial for this work:

1. The heavy quark is treated in an effective nonrelativistic theory.

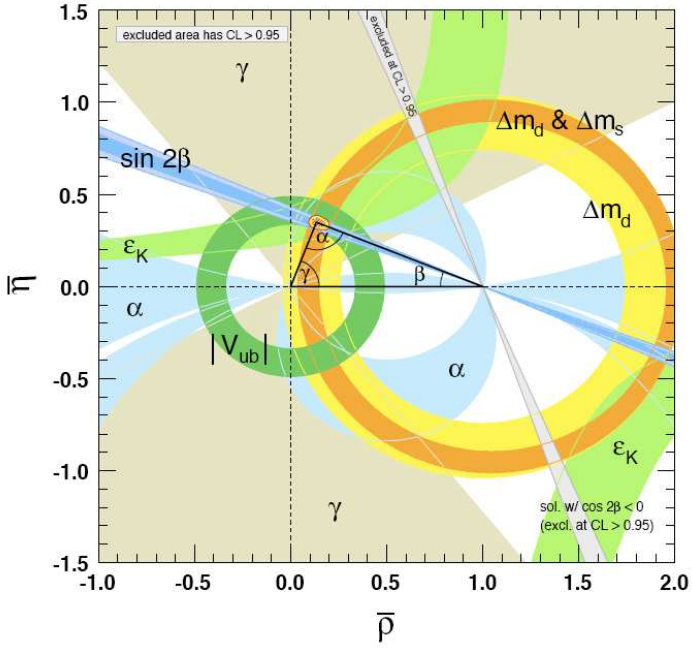

Figure 1.1: Constraints on the CKM triangle from [5]. The shaded regions have 95% confidence level.

2. Vacuum polarisation effects of light quarks can be included for masses close to the physical value by using an improved discretisation of the light fermion action.

As the hadronic particles in the final state are light, the squared momentum transfer q^2 can become very small. In the rest frame of the decaying B the pion in the final state has large momentum and the lattice calculation is spoilt by the associated substantial discretisation errors. On the other hand, most experimental measurements are obtained at small q^2 [21, 22, 23] so extending the prediction of form factors to this region is important to improve the constraints on $|V_{ub}|$. The same problem arises in other decays with light hadronic particles in the final state such as $B \to K^{(*)}\ell^+\ell^-$ or $B \to K^*\gamma$ where $q^2 = 0$. As will be discussed in detail in section 4.1.2 this problem can be solved by another improvement over previous work, namely

3. The heavy quark is discretised in a moving frame.

The resulting formalism has been developed in [1, 24, 25, 26, 27, 28] and is known as moving NRQCD. Calculation of radiatively improved non-perturbative lattice matrix elements is currently carried out by the HPQCD collaboration [29, 30].

In addition, lattice QCD can contribute to improving the constraints on CKM parameters by calculating the B and K bag parameters. The neutral B_q meson mass

splitting is proportional to $|V_{tq}|^2$ and the bag parameter B_{B_q}, defined by [31]

$$\langle \overline{B}^0 | (\overline{b}q)_{V-A} (\overline{b}q)_{V-A} | B^0 \rangle = \frac{8}{3} m_{B_q} B_{B_q} f_{B_q}^2 \tag{1.7}$$

where the subscript $V-A$ denotes the vector-axialvector structure of the weak interaction. This quantity can be calculated in lattice QCD from matrix elements of four quark operators; theoretical uncertainties are reduced in the ratio $f_{B_s}\sqrt{B_{B_s}}/(f_{B_d}\sqrt{B_{B_d}})$, so it is advantageous to use the experimental measurement of $\Delta m_{B_s}/\Delta m_{B_d}$ instead of Δm_{B_b} alone. As $V_{ts} \approx -V_{cb}$ this helps to constrain the other side of the CKM triangle (yellow and orange circles in Fig. 1.1). Recently the HPQCD collaboration has calculated B_{B_d} and B_{B_s} using a nonrelativistic action for the heavy quark and including vacuum polarisation effects from light sea quarks [32].

Similarly, the CP-violating parameter ϵ_K in neutral kaon mixing is proportional to the kaon bag parameter B_K

$$\begin{aligned} \langle \overline{K}^0 | (\overline{s}d)_{V-A} (\overline{s}d)_{V-A} | K^0 \rangle &= \frac{8}{3} m_K B_K f_K^2, \\ |\epsilon_K| &= B_K \eta \left[(1-\rho) c_1 + c_2 \right], \end{aligned} \tag{1.8}$$

where c_1 and c_2 are known constants [31]. This leads to another constraint on the CKM triangle (light green band in Fig. 1.1).

1.2.2 Measuring CP violation

The angles of the unitarity triangle can be inferred from CP-violating processes. The angle β is constrained by measuring the time-dependent asymmetry in $B \to J/\psi K_S$. For the decay to the CP eigenstate $f = J/\psi K_S$ [33] the asymmetry is

$$A_{CP}(t) = \frac{\Gamma(B^0(t) \to f) - \Gamma(\overline{B}^0(t) \to f)}{\Gamma(B^0(t) \to f) + \Gamma(\overline{B}^0(t) \to f)} = -\sin(2\beta)\cos(\Delta m_B t). \tag{1.9}$$

The time dependent asymmetry in this process is a very clean observable which does not suffer from large hadronic uncertainties. As can be seen from Fig. 1.1 this leads to very tight constraints on β.

The other angles of the CKM triangle can be constrained by other processes which, however, suffer from larger uncertainties .

1.2.3 Flavour changing neutral currents

In addition to these charged currents there are also flavour changing neutral currents (FCNCs). In the Standard Model these are forbidden at tree level but generated at one

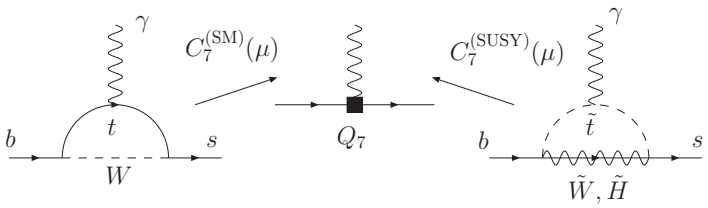

Figure 1.2: Loop suppressed flavour changing neutral current (FCNC) in the Standard Model (left) and SUSY (right). The local operator in the effective theory, which is obtained by integrating out physics at the electroweak scale, is shown in the centre.

loop level (see the left diagram Fig. 1.2 for an example). At energies well below the electroweak scale these currents can be written as the product of a Wilson coefficient, which encodes the physics at very small length scales, and a local effective operator which is usually suppressed by some powers of $1/m_W$. This factorisation simplifies the problem significantly: different extensions of the Standard Model will only modify the value of the Wilson coefficients $C(\mu)$, while QCD matrix elements of the effective operator are independent of the physics at the electroweak scale. I will discuss rare B decays and effective theories for flavour changing currents in more detail in chapter 2.

1.3 Searching for new physics

Although until now the Standard Model has passed all experimental tests there are reasons why it is believed that it has to be interpreted as an effective approximation of a more fundamental model. The parameters of the theory like masses and coupling constants are not predicted and a successful extension of the Standard Model has to explain the hierarchy in particle masses spanning several orders of magnitude. It is also highly desirable to unify all forces in nature, including gravitation. Numerous models have been put forward for solving all these problems but to date there is no consensus on a unique "Theory of Everything".

There are two strategies for extending our knowledge beyond what we know about the Standard Model. The first approach is the direct production of new particles. As these have not been observed in the energy range that is currently accessible this requires an increase of the collision energy in new particle accelerators. The Large Hadron Collider is designed to reach a centre-of-mass energy of 14 TeV and will be able to produce and measure potential new particles in the TeV range. Two of its experiments (ATLAS and CMS) are specifically designed for these direct searches for new physics.

Alternatively one can study the effect of new particles on the properties of Standard Model particles which will be modified by virtual corrections. The advantage of this approach is that one does not necessarily have to make any assumptions on new physics models, instead they can be parametrised by adding additional higher order operators to the Standard Model Lagrangian. At the Large Hadron Collider the LHCb detector is specifically built for studying the properties of B mesons which will be produced in unprecedented quantities at the accelerator.

In addition to precise measurements this requires very exact theoretical predictions of the Standard Model processes, the latter is particularly challenging for strongly interacting particles. The aim of the HPQCD collaboration is the calculation of precise lattice matrix elements. The work presented in this thesis contributes to this programme by further improvement of the lattice action and decay currents used in the simulations.

Chapter 2

Physics of rare B-decays

Of particular interest for indirect new physics searches are processes which are known to be suppressed in the Standard Model. Rare B decays as $B \to K^*\gamma$ or $B \to K^{(*)}\ell^+\ell^-$ are mediated by flavour changing neutral currents and can only occur at the loop level in the Standard Model. Contributions from virtual new particles in the loop, such as in the SUSY diagram in Fig. 1.2, are expected to be of comparable size to the contribution from the Standard Model.

In the first part of this chapter I discuss the radiative decay $B \to K^*\gamma$. I focus on this decay as it is sensitive to the tensor current; I have calculated the perturbative renormalisation of this current in an effective nonrelativistic lattice theory for the first time. In the second part I describe how the large mass of the b quark can be exploited to treat heavy particles in an effective low energy theory.

2.1 Experimental results

Decays of B mesons have been measured extensively at the so called B factories at KEK in Japan and SLAC in the United States. At these asymmetric electron-positron colliders the centre of mass energy of the colliding particles is tuned to the unstable $\Upsilon(4s)$ resonance which subsequently decays into $B\overline{B}$ pairs. This way it is possible to accumulate a lot of statistics and the BaBar detector at SLAC and Belle at KEK have recorded a large number of events. As the colliding beams have different energies, the produced B-mesons are not at rest in the laboratory frame and time dependent CP asymmetries can be studied in addition to branching ratios.

2.1.1 Inclusive decay

As of April 2009 the world average from the Heavy Flavour Averaging Group for $E_\gamma > 1.6$ GeV is [19]

$$Br(\overline{B} \to X_s\gamma) = (3.52 \pm 0.23 \pm 0.09) \cdot 10^{-4} \tag{2.1}$$

where the first error is due to the statistical and systematic uncertainty, whereas the second uncertainty estimates nonperturbative corrections due to the Fermi motion of the b quark inside the decaying B meson. This number includes results from the BaBar and Belle experiments and a measurement of the CLEO-c detector at the Cornell Electron Storage Ring CESR.

2.1.2 Exclusive decays

The latest (preliminary) results for the branching ratios obtained at BaBar are [34]

$$\begin{aligned} Br(B^0 \to K^{*0}\gamma) &= (4.58 \pm 0.10(\text{stat.}) \pm 0.16(\text{sys.})) \cdot 10^{-5}, \\ Br(B^+ \to K^{*+}\gamma) &= (4.73 \pm 0.15(\text{stat.}) \pm 0.17(\text{sys.})) \cdot 10^{-5}. \end{aligned} \tag{2.2}$$

Over the last four years the collaboration has reduced both statistical and systematical errors by nearly a factor two and for both channels they are now smaller than 5% which has to be compared to the 7% error in the inclusive measurement (2.1). It should be noted that the new results differ significantly from the previous numbers in [35].

The corresponding results of the Belle collaboration are [36]

$$\begin{aligned} Br(B^0 \to K^{*0}\gamma) &= (4.01 \pm 0.21(\text{stat.}) \pm 0.17(\text{sys.})) \cdot 10^{-5}, \\ Br(B^+ \to K^{*+}\gamma) &= (4.25 \pm 0.31(\text{stat.}) \pm 0.24(\text{sys.})) \cdot 10^{-5}. \end{aligned} \tag{2.3}$$

The world average presented by the Heavy Flavour Averaging Group is [19]

$$\begin{aligned} Br(B^0 \to K^{*0}\gamma) &= (4.40 \pm 0.15) \cdot 10^{-5}, \\ Br(B^+ \to K^{*+}\gamma) &= (4.57 \pm 0.19) \cdot 10^{-5}. \end{aligned} \tag{2.4}$$

In the Standard Model this decay proceeds by transforming a left-handed bottom quark into a right-handed strange quark quark under emission of a right-handed photon. The transition with opposite helicities is strongly suppressed but might be sizable in some new physics models. Although direct measurements of the photon polarisation are difficult, one can constrain the size of the $b_R \to s_L\gamma_R$ transition by measuring the time dependent CP asymmetry for the decay to a hadronic CP eigenstate M^0 and a photon [37], see section 2.2.2 . M^0 can be realised by using the decay of K^{*0} to $K_{S,L}\pi^0$.. The asymmetry is parametrised as

$$\begin{aligned} A_{M^0\gamma}(t) &= \frac{\Gamma(B^0 \to M^0\gamma(t)) - \Gamma(\overline{B}^0 \to M^0\gamma(t))}{\Gamma(B^0 \to M^0\gamma(t)) + \Gamma(\overline{B}^0 \to M^0\gamma(t))} \\ &= C_{K^*\gamma}\cos(\Delta m_B t) + S_{K^*\gamma}\sin(\Delta m_B t). \end{aligned} \tag{2.5}$$

The (preliminary) results from the BaBar experiment are $S_{K^*\gamma} = -0.08 \pm 0.31(\text{stat.}) \pm 0.05(\text{sys.})$ and $C_{K^*\gamma} = -0.15 \pm 0.17(\text{stat.}) \pm 0.03(\text{sys.})$ [38]. These quantities have also been measured by the Belle collaboration who find $S_{K^{*0}\gamma} = -0.32^{+0.36}_{-0.33}(\text{stat.}) \pm 0.05(\text{sys.})$ [39].

In the future more results are expected from the LHCb detector and the planned Super B collider.

2.2 Effective Lagrangians for electroweak physics

Particles at the electroweak energy scale $\mu_W \sim m_W, m_t \sim 100$ GeV do not contribute directly to low energy matrix elements at the bottom quark scale $\mu_b \sim m_b \approx 5$ GeV. Due to the uncertainty principle virtual heavy particles can only travel distances of the order $\sim 1/\mu_W$ which is much shorter than the typical time $\sim 1/\mu_b$. This implies that fluctuations at the electroweak scale, which might include physics beyond the Standard Model, can be integrated out to obtain an effective theory with local, point-like interactions. The subsequent discussion follows the comprehensive overview in [40].

For the $\Delta B = 1$, $\Delta S = 1$ transition the effective Hamiltonian at leading order in m_b/m_W can be written as a linear combination of eight operators,

$$\mathscr{H}_{\text{eff}}(b \to s\gamma) = -\frac{4G_F}{\sqrt{2}} V_{tb}V_{ts}^* \sum_{j=1}^{8} C_j(\mu) Q_j. \tag{2.6}$$

Here G_F is the Fermi constant and the unitarity of the CKM matrix and the relation $V_{ub}V_{us}^*/(V_{tb}V_{ts}^*) \ll 1$ has been used to eliminate all but one combination of CKM matrix elements (this implies that operators, which can be obtained from Q_1 and Q_2 by replacing $c \mapsto u$, are suppressed and are not shown in (2.7)). I use the operator

basis in [41],

$$
\begin{aligned}
Q_1 &= (\overline{c}_{L\beta}\gamma^\mu b_{L\alpha})(\overline{s}_{L\alpha}\gamma_\mu c_{L\beta}), \\
Q_2 &= (\overline{c}_{L\alpha}\gamma^\mu b_{L\alpha})(\overline{s}_{L\beta}\gamma_\mu c_{L\beta}), \\
Q_3 &= (\overline{s}_{L\alpha}\gamma^\mu b_{L\alpha}) \sum_{q=u,d,c,s,b} (\overline{q}_{L\beta}\gamma_\mu q_{L\beta}), \\
Q_4 &= (\overline{s}_{L\alpha}\gamma^\mu b_{L\beta}) \sum_{q=u,d,c,s,b} (\overline{q}_{L\beta}\gamma_\mu q_{L\alpha}), \\
Q_5 &= (\overline{s}_{L\alpha}\gamma^\mu b_{L\alpha}) \sum_{q=u,d,c,s,b} (\overline{q}_{R\beta}\gamma_\mu q_{R\beta}), \\
Q_6 &= (\overline{s}_{L\alpha}\gamma^\mu b_{L\beta}) \sum_{q=u,d,c,s,b} (\overline{q}_{R\beta}\gamma_\mu q_{R\alpha}), \\
Q_7 &= \frac{e}{16\pi^2} m_b \overline{s}_{L\alpha} \sigma^{\mu\nu} b_{R\alpha} F_{\mu\nu} \qquad \text{with} \quad \sigma^{\mu\nu} = \frac{i}{2}[\gamma^\mu, \gamma^\nu], \\
Q_8 &= \frac{g}{16\pi^2} m_b \overline{s}_{L\alpha} \sigma^{\mu\nu} T^a_{\alpha\beta} b_{R\beta} G^a_{\mu\nu}.
\end{aligned}
\tag{2.7}
$$

$F_{\mu\nu}$ ($G^a_{\mu\nu}$) is the electromagnetic (chromodynamic) field strength tensor; α and β are colour indices. In the effective Hamiltonian the physics is factorised into two contributions: effects at the electroweak scale are encoded in the μ-dependent Wilson coefficients $C_j(\mu)$ and matrix elements of the operators Q_j are evaluated between low energy particle states. The dependence on the unphysical scale μ, which separates the two regimes, cancels in physical predictions. However, at a finite order in perturbation theory this cancellation is usually only approximate.

The first two operators arise from an electroweak current-current interaction, see Fig. 2.1 and in the Standard Model Q_2 is the only operator with a nonvanishing matrix element at tree level, Q_1 has a different colour structure which can only be generated by gluon exchange between the quark lines. The other four quark operators $Q_3, \ldots, Q_6$ and the (chromo-) magnetic tensor currents Q_7, Q_8 are generated by penguin diagrams, Figs. 2.2 and 2.3. In the Standard Model their Wilson coefficients are given at leading order by Inami-Lim functions [42] which depend on the ratio $x_t = m_t/m_W$. In other new physics models the Wilson coefficients will be different.

As photons and gluons can couple to internal charm quarks (Fig. 2.4) the one loop matrix elements of the four quark operators do not necessarily vanish. It turns out that they depend on the regularisation scheme and in particular on the treatment of γ_5 in d dimensions [43, 44]. This can be summarised as

$$
\langle Q_i \rangle_{\text{one-loop}} = y_i \langle Q_7 \rangle_{\text{tree}}, \qquad\qquad \langle Q_i \rangle_{\text{one-loop}} = z_i \langle Q_8 \rangle_{\text{tree}} \tag{2.8}
$$

where y_i and z_i are scheme dependent. To compensate for this the coefficients C_7 and

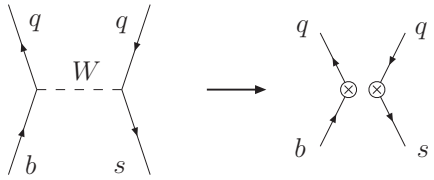

Figure 2.1: Electroweak current-current interaction and effective vertex. Diagrams of this type and QCD corrections, which can change the quark colour structure, generate the local operators Q_1 and Q_2.

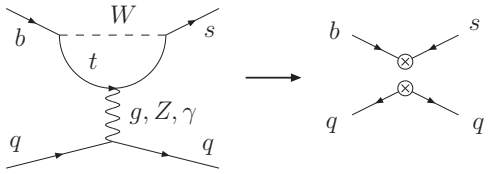

Figure 2.2: One loop penguin interaction and effective vertex. Diagrams of this type generate the local operators Q_3,. . . ,Q_6.

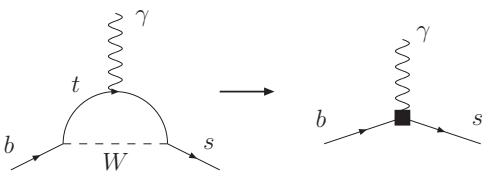

Figure 2.3: Magnetic penguin interaction and effective vertex. Diagrams of this type generate the local operator Q_7. The corresponding diagram for Q_8 can be obtained by replacing the external photon by a gluon.

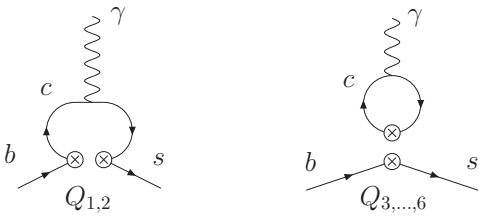

Figure 2.4: Loop diagrams of four quark operators that contribute to $b \to s\gamma$.

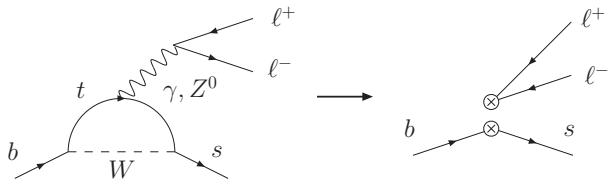

Figure 2.5: Effective operators in $b \to s\ell\ell$.

C_8 can be redefined in an regularisation scheme independent way by replacing

$$\begin{aligned} C_7(\mu) &\mapsto C_7^{\text{eff}}(\mu) = C_7(\mu) + \sum_{i=1}^{6} y_i C_i(\mu), \\ C_8(\mu) &\mapsto C_8^{\text{eff}}(\mu) = C_8(\mu) + \sum_{i=1}^{6} z_i C_i(\mu). \end{aligned} \tag{2.9}$$

In the following I will work with these coefficients but drop the superscript "eff" for simplicity.

2.2.1 Operators in $b \to s\ell^+\ell^-$

For the decay $B \to K^{(*)}\ell^+\ell^-$ two additional operators contribute with the leptonic current coupling to the hadronic heavy-light vector current, see Fig. 2.5,

$$Q_9 = e^2(\overline{s}_L\gamma_\mu b_L)\sum_\ell(\overline{\ell}\gamma^\mu\ell), \qquad Q_{10} = e^2(\overline{s}_L\gamma_\mu b_L)\sum_\ell(\overline{\ell}\gamma^\mu\gamma_5\ell). \tag{2.10}$$

2.2.2 Tensor operators with opposite chirality

In addition to Q_7 and Q_8, which change a left handed b-quark into a right-handed s-quark, there are corresponding operators with opposite chirality. In the Standard Model only left handed quarks couple to the electroweak gauge bosons and the chirality has to be flipped on one of the external quark lines. This is only possible by insertion of a mass term $m\overline{\psi}_L\psi_R + (h.c.)$ which will generate a factor of m_b for the $b_R \to s_L$ and a factor of m_s for the $b_L \to s_R$ transition. The strong interaction conserves chirality so even after including radiative corrections these additional operators are suppressed by a relative factor m_s/m_b. As argued in [37] this is not necessarily true for some new physics models. Even though it is difficult to measure the photon polarisation directly the size of these operators can be constrained by studying the time dependent

CP asymmetry

$$A_{M^0\gamma}(t) = \frac{\Gamma(B^0 \to M^0\gamma(t)) - \Gamma(\overline{B}^0 \to M^0\gamma(t))}{\Gamma(B^0 \to M^0\gamma(t)) + \Gamma(\overline{B}^0 \to M^0\gamma(t))} \tag{2.11}$$

where M^0 is a hadronic CP eigenstate, for example $K^{*0} \to K_{L,S}\pi^0$. This asymmetry is nonzero if both B^0 and $\overline{B}^0$ can decay to a common final state. As the photon polarisation can in principle be observed this is only possible if the transition $b_L \to s_R$ is allowed. Indeed one finds

$$A_{M^0\gamma}(t) \sim \sin(2\psi)\sin(\Delta m_B t) \tag{2.12}$$

where $\tan\psi$ is the relative strength of the $b_L \to s_R$ and the $b_R \to s_L$ operator.

2.3 Theoretical predictions

Using the Hamiltonian in (2.6) predictions for physical processes can now be obtained in three steps:

1. Matching at the electroweak scale. Compute an amplitude both in the full theory and in the effective theory and adjust the Wilson coefficients at the electroweak scale, $C_j(\mu_W)$ such that the amplitudes agree. To illustrate the procedure I first work in the leading log (LL) approximation and then comment on the current status of the next-to-next-to-leading-log (NNLL) $\mathcal{O}(\alpha_s^2)$ calculation in section 2.3.1.

At the lowest order QCD corrections are not taken into account in this step and only C_2, C_7 and C_8 are nonzero,

$$\begin{aligned} C_2(\mu_W) &= 1, \\ C_7(\mu_W) &= \frac{3x_t^3 - 2x_t^2}{4(x_t-1)^4}\log x_t + \frac{-8x_t^3 - 5x_t^2 + 7x_t}{24(x_t-1)^3}, \\ C_8(\mu_W) &= \frac{-3x_t^2}{4(x_t-1)^4}\log x_t + \frac{-x_t^3 + 5x_t^2 + 2x_t}{8(x_t-1)^3}. \end{aligned} \tag{2.13}$$

Here C_7 and C_8 are given by Inami-Lim functions [42] from integrating out the top quark and electroweak vector bosons. For $m_t = 170$ GeV, $m_W = 80.425$ GeV one has

$$C_7(m_W) = -0.193, \qquad C_8(m_W) = -0.096. \tag{2.14}$$

This is the only step which depends on physics at the electroweak scale; in extensions of the Standard Model with new particles in the loop the Wilson coefficients $C_i(\mu_W)$

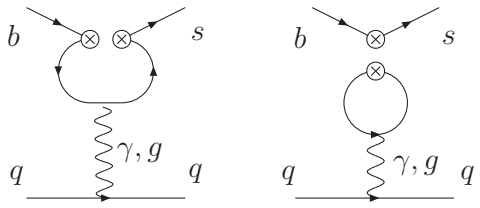

Figure 2.6: Penguin loop diagrams.

will be different.

For example, in [45] it is shown how $C_7(\mu_W)$ and $C_8(\mu_W)$ change in a two Higgs doublet model. The W boson in the loop in Fig. 1.2 can be replaced by a charged Higgs boson. The numerical size of these changes depends on the parameters of the specific model. In [45] it is reported that the inclusive decay rate $B \to X_s\gamma$, which in the LL approximation is proportional to $|C_7(\mu_b)|^2$, can be enhanced by about a factor of three compared to the Standard Model.

2. Renormalisation group running. As there is a huge separation between the electroweak scale and the mass of the b quark large logarithms of the form $\alpha_s^\ell \log^k(\mu_W^2/\mu_b^2))$ are resummed using the renormalisation group equations. The LL approximation corresponds to $\ell = k$. The scale dependence of the Wilson coefficients is described by the anomalous dimension matrix $\gamma(g)$,

$$\mu \frac{dC_i(\mu)}{d\mu} = \gamma_{ij}(g(\mu))C_j(\mu). \tag{2.15}$$

This can be solved for $C_i(\mu)$ with the initial conditions $C_i(\mu_W)$ in (2.13). At LL one only keeps the lowest order term in the expansion

$$\gamma(g) = \frac{\alpha_s}{4\pi}\gamma^{(0)} + \frac{\alpha_s^2}{(4\pi)^2}\gamma^{(1)} + \dots. \tag{2.16}$$

The matrix $\gamma^{(0)}$ is given explicitly in [43, 44]. It turns out that none of the other operators mixes into Q_1 and Q_2. This is because gluons do not change flavour and the mixing could only come from the penguin diagrams in Fig. 2.6. However, in these diagrams one has to sum over all flavours in the lowest quark line. The dimension five tensor operators do not mix into the dimension six quark operators, as expected in a mass independent renormalisation scheme. Schematically the anomalous dimension

μ_b	2.5 GeV	5.0 GeV	10.0 GeV
$C_1(\mu_b)$	0.019	0.016	0.013
$C_2(\mu_b)$	0.629	0.711	0.788
$C_3(\mu_b)$	−0.107	−0.078	−0.055
$C_4(\mu_b)$	0.125	0.093	0.066
$C_5(\mu_b)$	0.023	0.017	0.011
$C_6(\mu_b)$	0.013	0.009	0.006
$C_7(\mu_b)$	−0.336	−0.300	−0.269
$C_8(\mu_b)$	−0.158	−0.144	−0.131

Table 2.1: Wilson coefficients of the effective Lagrangian (2.6) at three different scales in the leading logarithmic approximation. I use $m_Z = 91.1876$ GeV, $m_W = \mu_W = 80.425$ GeV and $\alpha_s(m_Z) = 0.118$ in the numerical evaluation.

matrix can be written as

$$\gamma \;=\; \left(\begin{array}{ccc} \boxed{1,2 \;\; 1,2} & \boxed{1,2 \;\; 3-6} & \boxed{1,2 \;\; 7,8} \\ 0 & \boxed{3-6 \;\; 3-6} & \boxed{3-6 \;\; 7,8} \\ 0 & 0 & \boxed{7,8 \;\; 7,8} \end{array} \right) . \tag{2.17}$$

Solving the RG equations the contribution from C_2 to the tensor operators turns out to be particularly large. In [40] the coefficient C_7 is calculated for $m_t = 170$ GeV and $\alpha_s(M_Z) = 0.118$,

$$\begin{aligned} C_7(\mu_b = 5\text{ GeV}) &= 0.695\, C_7(\mu_W) + 0.085\, C_8(\mu_W) - 0.158\, C_2(\mu_W) \\ &= 0.695(-0.193) + 0.085(-0.096) - 0.158 = -0.300. \end{aligned} \tag{2.18}$$

For C_8 a similar enhancement by Q_2 is observed.

The leading order Wilson coefficients of all operators can be computed using the "magic numbers" in Tabs. 6 and 23 of [40] and are collected in Tab. 2.1. Note that, apart from $C_2(\mu_b)$, the Wilson coefficients of all four quark operators are small.

3. Matrix elements. Finally, using the effective Hamiltonian and the Wilson coefficients at a scale $\mu_b \sim m_b$ matrix elements for physical processes have to be computed. For inclusive decays this can be done using quark hadron duality and it is sufficient to consider the process on the quark level. However, for exclusive decays, where the quarks are bound within hadrons, this is much more challenging. Before I discuss the evaluation of exclusive matrix elements in more detail I review the status of the NNLL calculation.

2.3.1 NNLL calculation

The error on the experimental value of the inclusive $B \to X_s\gamma$ branching ratio is of the order of 7%. As the accuracy of the NLL calculation is known to be around 10% [46] this motivated a NNLL order calculation of this process which was completed in 2006 [47, 48]. The results of the matching calculation and the calculation of the anomalous dimension matrix are universal and can be used both for inclusive and exclusive processes.

In the NNLL approximation matching at the electroweak scale is carried out at $\mathcal{O}(\alpha_s^2)$. To compute the mixing between four quark operators it is necessary to evaluate three loop diagrams. As a photon (or gluon) can be attached to the internal charm line calculations of four loop diagrams are necessary for the mixing of four quark operators to the dipole operators.

Inclusive branching ratio

To complete the calculation of the decay width the operator product expansion

$$\Gamma(\overline{B} \to X_s\gamma) \quad = \quad \Gamma(b \to X_s^{\text{parton}}\gamma) + \Delta^{(\text{nonpert.})} \tag{2.19}$$

is used where nonperturbative corrections are suppressed by $(\Lambda_{\text{QCD}}/m_b)^2$. The partonic rate can be written as

$$\Gamma(b \to X_s^{\text{parton}})_{E_\gamma > E_0} \quad = \quad \frac{G_F^2 \alpha_{\text{em}} \overline{m}_{b,\overline{MS}}^2(\mu) m_{b,\text{pole}}^3}{32\pi^4} |V_{tb}V_{ts}^*|^2 \sum_{ij} C_i(\mu) C_j(\mu) G_{ij}(E_0, \mu). \tag{2.20}$$

Here $G_{ij}(\mu)$ denotes the contribution from (Q_i, Q_j) interference to the matrix element. G_{ij} can be calculated using the optical theorem which connects the imaginary part of the forward matrix element to the total cross section. To this end the imaginary parts of the heavy quark self-energy correction induced by the operators Q_i and Q_j are calculated, see Fig. 2.7.

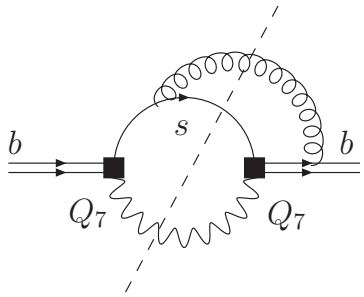

Figure 2.7: $\mathcal{O}(\alpha_s)$ correction to the inclusive matrix element arising from Q_7-Q_7 interference. The dashed line indicates one possible cut of the diagram.

So far only the dominant (C_7, C_7) part from the dipole operator is known which requires a two loop calculation. For the three loop matrix elements of four quark operators an approximation in the charm quark mass is necessary which introduces additional uncertainties.

To reduce systematic uncertainties, in particular to cancel the dependence on the fifth power of the bottom quark mass and on the largely unknown CKM factor $|V_{tb}V_{ts}^*|^2$, the branching ratio is normalised to $Br(\overline{B} \to X_c e\overline{\nu})$.

The final result for a lower cut of $E_0 = 1.6$ GeV on the photon spectrum is [47]

$$Br(\overline{B} \to X_s\gamma) \quad = \quad (3.15 \pm 0.23) \cdot 10^{-4} \tag{2.21}$$

which has to be compared to the experimental result in (2.1). The systematic error comes from nonperturbative corrections, uncertainties in the input parameters, higher order radiative corrections and the ambiguity in the m_c interpolation.

2.3.2 Exclusive matrix elements

As heavy quarks are bound within mesons the prediction of exclusive matrix elements is more difficult. The decay amplitude of $B \to K^*\gamma$ can be split into a local part, arising from the tensor operator Q_7, and nonlocal effects from Q_8 and four quark operators,

$$\begin{aligned} \mathcal{A}(B \to K^*\gamma) \quad = \quad & -\frac{4G_F}{\sqrt{2}} V_{tb}V_{ts}^* \Big[C_7(\mu) \langle K^*\gamma | Q_7(0) | B \rangle \\ & + \sum_{j \neq 7} C_j(\mu) \int \frac{d^4x}{(2\pi)^4} e^{-iq\cdot x} \langle K^*\gamma | T\{A_\mu(x) j_{\rm em}^\mu(x) Q_j(0)\} | B \rangle \Big] \end{aligned} \tag{2.22}$$

where $j_{\rm em}^\mu = e\sum_q Q_q \overline{q}\gamma^\mu q$ is the electromagnetic current (Q_q denotes the charge of quark q). Only the local contribution can be calculated directly on the lattice.

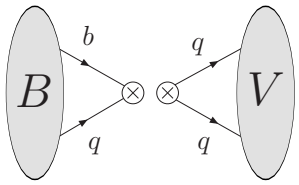

Figure 2.8: W annihilation diagram.

Calculating matrix elements of nonlocal operators is inherently difficult; several methods such as phenomenological models combined with perturbation theory [49, 50, 51], vector meson dominance [52] and operator product expansions in combination with QCD sum rules [53, 54, 55] have been used to estimate their size. In [56] these calculations are reviewed for the decay $B \to V\gamma$, where V is any vector meson such as ρ, ω, ψ or K^*. In this analysis the operators $Q_{3,\ldots,6}$ are neglected due to their small Wilson coefficients.

For a first, very rough estimate of the relative importance of the different operators in the electroweak Lagrangian consider the branching ratios from the local amplitude only. This is estimated in [56] as

$$Br(B^0 \to K^{*0}\gamma) = 4.5 \cdot 10^{-5}, \qquad Br(B^\pm \to K^{*\pm}\gamma) = 4.6 \cdot 10^{-5}. \tag{2.23}$$

Comparison with the central values of the latest world average of experimental measurements in (2.4) suggests that the nonlocal contributions are small.

In the following I describe the contributions from different operators in the effective Hamiltonian and finally outline the lattice calculation of the local tensor operator Q_7.

Weak annihilation

The weak annihilation amplitude in Fig. 2.8 is generated by four quark operators and can be calculated at leading order using factorisation. Note that, as the exchanged W boson is charged, this process does not contribute to the radiative decay of neutral mesons. More specifically, in [56] it is shown that for the decay $B \to \rho\gamma$ the amplitude can be written as the sum of two contributions,

$$A \;\sim\; -f_B p_\mu \langle \rho^-\gamma|(\overline{d}u)^\mu_{V-A}|0\rangle + m_{\rho^-} f_{\rho^-} (\epsilon^*_\rho)_\mu \langle \gamma|(\overline{u}b)^\mu_{V-A}|B^-\rangle \tag{2.24}$$

corresponding to the photon coupling to the ρ- and B-meson. f_B and f_{ρ^-} are the meson decay constants whereas ϵ^*_ρ is the polarisation vector of the vector meson. The first contribution can be calculated exactly in the chiral limit whereas the matrix element

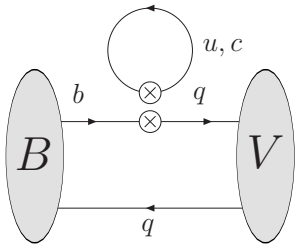

Figure 2.9: Penguin diagram with u- and c-loops.

$\langle\gamma|(\overline{u}b)^{\mu}_{V-A}|B^{-}\rangle$ can be expressed in terms of the two form factors which parametrise the decay $B \to \gamma e\nu$. At higher order gluons can connect the mesons in the initial and in the final state and the matrix element does not factorise as in (2.24). However, it is argued in [56] that these effects are small and factorisation remains a very good approximation.

The amplitude in the decay to a final state K^* is strongly CKM suppressed by $V_{ub}V^*_{us}/(V_{tb}V^*_{ts}) \sim 0.02$ relative to the contribution from the electromagnetic tensor operator. It is calculated in [51] in the framework of the quark model described in [57, 49]. The leading quark-antiquark Fock states inside the mesons are described by phenomenological ansatz and perturbative corrections to the decay amplitude from gluon exchange are calculated in perturbation theory. The relative size of the weak annihilation contribution to the branching ratio is relatively small, around 6%.

Long distance contributions from internal c-quark loops

The dominant contribution to the long distance amplitude induced by the $b \to s\overline{c}c$ operators (see Fig. 2.9) is usually assumed to come from the diagram where the photon couples to the charm quark loop. This is confirmed by the perturbative calculation combined with a quark model in [51] where it is found that the main contribution generated by Q_2 comes from diagrams where the photon couples to the $\overline{c}c$ loop and the gluon connects this loop to either the b or s quark. Only Q_7 contributes at tree level but in [51] it is found that the $\mathcal{O}(\alpha_s)$ contribution of the four quark operator is of the same order as the one loop correction to the electromagnetic tensor operator Q_7.

This process can be described as the decay $B \to V\psi_n$, where the ψ_n is a bound $\overline{c}c$ vector state, such as J/ψ, which subsequently decays into a photon, see Fig. 2.10. In this approximation the long-distance amplitude can be written as

$$A \;=\; Q_c e \sum_{n,\epsilon_n} \frac{(\epsilon^*_n)_\mu \langle 0|\overline{c}\gamma^\mu c|\psi_n\rangle \mathcal{A}(B \to V\psi_n)}{q^2 - M_n^2 + iM_n\Gamma_n}. \tag{2.25}$$

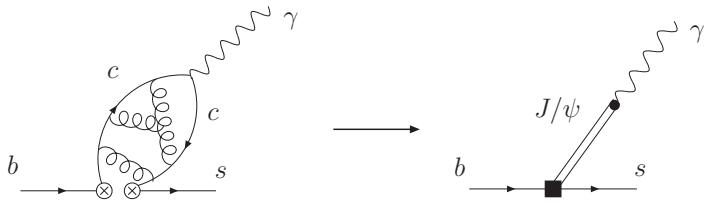

Figure 2.10: Resonant contribution to $b \to s\gamma$ from four quark operators.

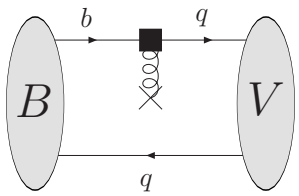

Figure 2.11: Chromomagnetic tensor diagram.

where ϵ_n is the polarisation of the vector meson ψ_n with mass M_n and width Γ_n. For real photons with $q^2 = 0$ the sum is dominated by the lowest lying resonances. The mass of the J/ψ is 3.097 GeV so that long distance effects from charm loops are expected to be suppressed.

This argument is supported by the explicit calculation in [53] where the charm quark is integrated out to obtain an effective $b\overline{s}g\gamma$ operator suppressed by $1/m_c^2$. The matrix element of this local operator is calculated using QCD sum rules and found to be small, contributing around 5% of the dominant amplitude from Q_7.

Note that the contribution from $\overline{c}c$ loops is not CKM suppressed for the decay to a K^* in a final state, whereas $\overline{u}u$ loops are. The latter is not necessarily the case for decays to other vector mesons, such as the ρ.

Chromomagnetic tensor operator

The contribution from the chromomagnetic tensor operator is shown in Fig. 2.11 where the photon can couple to any internal quark. The size of this contribution is estimated in [50]. There the decay amplitude is calculated for both the electromagnetic and the tensor operator in the framework of a quark model. The contribution of Q_8 is found to be suppressed relative to Q_7 by a factor $\Lambda_{\rm QCD}/m_B \times C_8/C_7 \approx 5\%$.

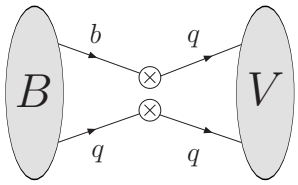

Figure 2.12: Four quark penguin operators ($Q_3 \dots Q_6$) and W exchange (Q_1 and Q_2) diagrams.

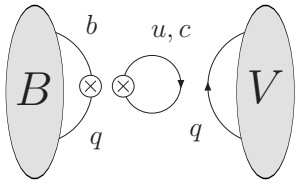

Figure 2.13: Penguin annihilation diagram (does not contribute to $B \to K^*\gamma$).

Four quark penguins, W-exchange and penguin annihilation

The contribution of four quark penguin operators $Q_3 \dots Q_6$ and W-exchange via Q_1, Q_2 is shown in Fig. 2.12. The contribution from Q_1- and Q_2-like operators with c replaced by u is strongly CKM suppressed for $B \to K^*\gamma$. The W-exchange diagram can be treated in a similar way to the weak annihilation process in Fig. 2.8. However, for $B \to K^*\gamma$ this process is suppressed by the small Wilson coefficients of the operators $Q_3, \dots, Q_6$. The penguin annihilation diagram in Fig. 2.13 only produces flavour singlets in the final state and is not relevant for the decay $B \to K^*\gamma$.

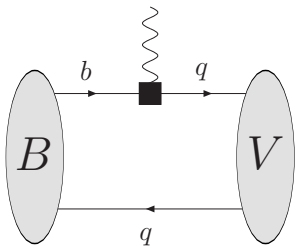

Figure 2.14: Electromagnetic tensor diagram

Local contribution from electromagnetic tensor operator

The local contribution to the decay $B \to K^*\gamma$ is given by the operator Q_7 in (2.7), see Fig. 2.14, and this contribution can be calculated in lattice QCD. One thus needs to calculate matrix elements of the tensor operator $T^{\mu\nu} = i\bar{s}\sigma^{\mu\nu}b$. If the momentum of the decaying meson is denoted by p and the momentum and polarisation of the final state vector particle by p' and ϵ then the matrix element can be parametrised by three form factors as

$$\langle K^*(p',\epsilon)|T^{\mu\nu}|B(p)\rangle \quad = \quad \epsilon_\alpha \mathcal{T}^{\alpha\mu\nu} \tag{2.26}$$

with

$$\begin{aligned}\mathcal{T}^{\alpha\mu\nu} \quad = \quad & \epsilon^{\alpha\mu\nu\beta}\Big[\left(p_\beta + p'_\beta - \frac{m_B^2 - m_{K^*}^2}{q^2}q_\beta\right)T_1(q^2) + \frac{m_B^2 - m_{K^*}^2}{q^2}q_\beta T_2(q^2) \\ & + \frac{2p^\alpha}{q^2}\epsilon^{\mu\nu\sigma\lambda}q_\sigma p'_\lambda\left(T_2(q^2) - T_1(q^2) + \frac{q^2}{m_B^2 - m_{K^*}^2}T_3(q^2)\right)\Big].\end{aligned} \tag{2.27}$$

For a physical photon with $(p-p')^2 = q^2 = 0$ the factor multiplying $T_3(0)$ is zero and $T_1(0) = T_2(0) \equiv T(0)$ as the matrix element is finite for all q^2.

2.3.3 Calculation with relativistic fermions

The authors of [58] calculate the tensor form factor on the lattice by simulating at unphysically light bottom quark masses m_H and then extrapolate in $1/m_H$ using heavy quark scaling laws. An $\mathcal{O}(a)$ improved Wilson action is used to discretise the quark fields. All gauge configurations in [58] are quenched.

They first simulate directly at large recoil and use soft collinear effective theory (SCET) [59] for the extrapolation in the heavy quark mass. At $q^2 = 0$ the momentum of the final state meson is close to the light cone. In SCET the collinear part of the light quark momentum is integrated out. This is similar to HQET, where the high energy fluctuations of the heavy quark do not appear in the effective theory. However, the light quark can emit both soft- and collinear gluons and stay near its mass shell; both gluonic degrees of freedom are kept as dynamic fields in SCET. A systematic power counting in λ, the ratio between the perpendicular and collinear part of the light quark momentum, can be established.

The result of the lattice calculation is

$$T(0) \quad = \quad 0.24(3)^{+0.04}_{-0.01}. \tag{2.28}$$

The first error is statistical/fitting whereas they estimate the systematical uncertainty by comparing to results on two lattices with coarser lattice spacing.

They also extrapolate to the physical quark mass while keeping q^2 fixed. The form factors T_1 and T_2 can then be extrapolated to zero using a phenomenological ansatz for their dependence on the momentum transfer,

$$T_1(q^2) = \frac{F}{(1-\tilde{q}^2)(1-\alpha\tilde{q}^2)}, \qquad T_2(q^2) = \frac{F}{1-\tilde{q}^2/\beta} \tag{2.29}$$

with $\tilde{q}^2 = q^2/m^2_{B^*_s}$. The results they obtain with this method are compatible with the result in (2.28).

An older study of $B \to K^*\gamma$ form factors using relativistic, $\mathcal{O}(a)$ improved Wilson fermions can be found in [60]. The authors calculate the form factors that parametrise the matrix elements $\langle P|\overline{q}\gamma^\mu b|B\rangle$, $\langle V|\gamma^\mu(1-\gamma^5)|B\rangle$ and $\langle V|q_\nu\sigma^{\mu\nu}\frac{1+\gamma_5}{2}|B\rangle$, where P and V denote pseudoscalar and vectors mesons respectively. For each q^2 they simulate at four values of the heavy quark mass around m_c and extrapolate to the physical value by fitting to an expansion in the inverse mass. This fit is constrained by using heavy quark symmetry to relate different form factors.

2.3.4 mNRQCD calculation

The HPQCD collaboration uses an effective action which is a systematic expansion in the inverse quark mass. Instead of approaching the physical heavy quark mass by extrapolating from unphysically light quark masses the leading term in this expansion corresponds to an infinitely heavy quark mass. The action includes corrections up to (and including) $\mathcal{O}(1/m^2)$ in heavy-light power counting. An additional advantage of this approach is that the heavy quark propagator in this nonrelativistic theory can be calculated very effectively by a single sweep through the lattice.

A drawback of the method is that the heavy quark expansion is only valid if the energies and momenta of the process under study are much smaller than the heavy quark scale. This is not the case at the physical, large recoil point $q^2 = 0$ where the energy of the light quark is of the order $m_B/2$. Instead, all our calculations are performed around the zero recoil point $q^2 = q^2_{\text{max}}$ where the final state meson is at rest. The lattice data is then extrapolated to the physical point using the phenomenological ansatz for the form factors in (2.29), this is described in more detail in section 2.3.5.

As q^2 decreases in the lattice calculation, the discretisation errors in the final state meson grow. Instead of using standard NRQCD, where the heavy quark is discretised in the rest frame of the decaying B meson, we discretise the effective heavy quark action in a moving frame. Although due to Lorentz invariance the two frames are equivalent

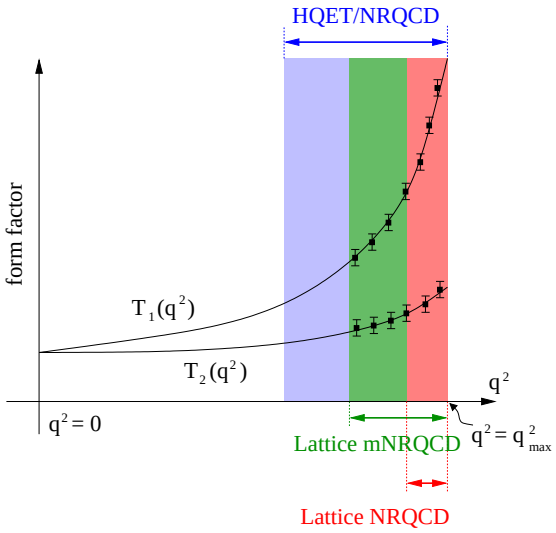

Figure 2.15: Schematic form of the form factors $T_{1,2}$ as a function of q. The shaded regions show the validity of the continuum heavy quark theory (blue) and the lattice discretisations, NRQCD (red) and mNRQCD (green).

in the continuum, this is not true on the lattice. Working in the moving frame extends the range of accessible q^2 and will improve the fit of form factors, see Fig. 2.15.

As discussed above the contribution of four quark operators to the matrix element in the transition $b \to s\gamma$ is small at $q^2 = 0$ (remember, however, that Q_2 has a large influence on the Wilson coefficient C_7). At larger q^2, especially near $\overline{c}c$ resonances, four quark operators are important and the lattice calculation with the chromomagnetic operator Q_7 only does not include these effects.

Matrix elements of the operator Q_7 in mNRQCD are currently being calculated by Stefan Meinel [61] and Zhaofeng Liu [30]. In chapter 7 I show how radiative corrections to these operators can be obtained in lattice perturbation theory. Using radiatively improved leading order operators in combination with tree level matrix elements of the $1/m$ currents will improve the accuracy of the form factor calculation.

2.3.5 Phenomenological form factors

To extrapolate the lattice results to $q^2 = 0$ a physically motivated ansatz for the tensor form factors $T_{1,2}(q^2)$, which is valid for the whole q^2 region, has to be made. In [62] a parametrisation for the form factors $f_0(q^2)$ and $f_+(q^2)$ in the vector current matrix element $\langle V(p')|\overline{u}\gamma_\mu b|B(p)\rangle$ is suggested. It is shown that after constraining the parameters with lattice data at large q^2 the results agree with those from light cone sum rules at small q^2. In [58] this analysis is extended to the tensor current.

The form factors have to fulfil the following conditions:

1. $T_1(0) = T_2(0)$. This follows from (2.27) as the matrix element has to be finite for $q^2 \to 0$.

2. At large $q^2 \approx q^2_{\text{max}} = (m_B - m_{K^*})^2$, where HQET is valid, the matrix element scales like $\sqrt{m_B}$ as the only dependence on the heavy quark mass comes from the normalisation of the B state. This implies

$$T_1(q^2 \approx q^2_{\text{max}}) \sim m_B^{1/2}, \qquad T_2(q^2 \approx q^2_{\text{max}}) \sim m_B^{-1/2}. \tag{2.30}$$

3. In the high recoil region $q^2 \to 0$ the additional scaling law $T_{1,2}(q^2 \to 0) \sim m_B^{-3/2}$ holds.

4. Dispersion relations relate the form factors to resonances R and multiparticle states above the cut at $t_{\text{cut}} = (m_B + m_{K^*})^2$,

$$T_{1,2}(q^2) \;=\; \sum_R \frac{\text{Res}_{q^2=m_R^2} T_{1,2}(q^2)}{m_R^2 - q^2} + \frac{1}{\pi}\int_{t_{\text{cut}}}^{\infty} dt\, \frac{\text{Im}\{T_{1,2}(t)\}}{t - q^2 - i\epsilon}. \tag{2.31}$$

   For T_1 the nearest resonance in the crossed channel $J^P = 1^-$ is at $m_{B_s^*} = 5.42$ GeV. Usually the multiparticle continuum and resonances well above $q^2_{\text{max}} = (m_B - m_{K^*})^2$ are modelled by a small number of resonances so that the form factors can be written as a sum of pole terms.

The authors of [62, 58] note that scaling laws can not be satisfied by using a single resonance structure for both $T_1(q^2)$ and $T_2(q^2)$ and that the pole at $q^2 = m^2_{B_s^*}$ should be included. They suggest the parametrisation

$$T_1(q^2) = \frac{C_1}{1 - \tilde{q}^2} + \frac{C_2}{1 - C_3\tilde{q}^2}, \qquad T_2(q^2) = \frac{C_1 + C_2}{1 - C_4\tilde{q}^2} \tag{2.32}$$

with $\tilde{q}^2 = q^2/m^2_{B_s^*}$.

The additional constraint $T_1(E) = m_B/(2E)T_2(E)$ in the high energy region $E \to \infty$, $m_B \to \infty$ (where E denotes the energy of the final state meson) can be used to reduce the number of parameters to three,

$$T_1(q^2) = \frac{F}{(1 - \tilde{q}^2)(1 - \alpha\tilde{q}^2)}, \qquad T_2(q^2) = \frac{F}{1 - \tilde{q}^2/\beta}. \tag{2.33}$$

The corresponding expressions for the vector form factors $f_{+,0}$ are obtained by replacing $T_1 \mapsto f_+$, $T_2 \mapsto f_0$ and $m_{B_s^*} \mapsto m_{B^*}$.

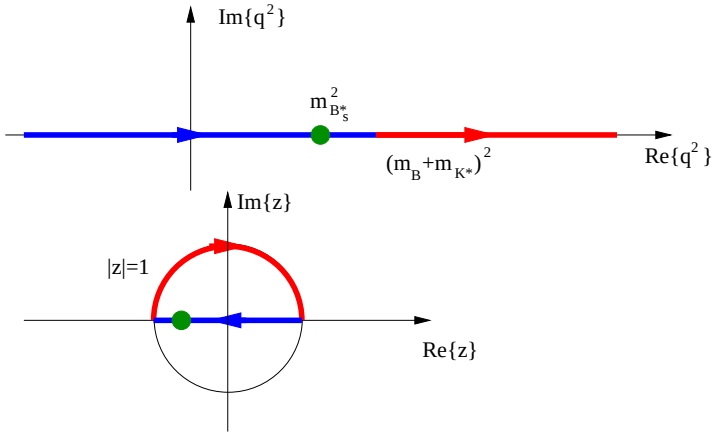

Figure 2.16: Analytical transformation to the z plane

Analyticity

The form factors are analytic functions of q^2 everywhere in the complex plane apart from poles and branch cuts. The transformation [20]

$$z(q^2, t_0) = \frac{\sqrt{1 - q^2/t_+} - \sqrt{1 - t_0/t_+}}{\sqrt{1 - q^2/t_+} + \sqrt{1 - t_0/t_+}} \tag{2.34}$$

maps the branch cut at $q^2 > (m_B + m_{K^*})^2$ onto the unit circle and the rest of the real axis onto the interval $[-1, +1]$ where it is legitimate to expand in a Taylor series in z, see Fig. 2.16. In the transformation t_0 is arbitrary and $t_\pm = (m_B \pm m_{K^*})^2$. The form factor can then be written as

$$T_{1,2}(q^2) = \frac{1}{P_{1,2}(q^2)\phi_{1,2}(q^2, t_0)} \sum_{k=0}^{\infty} a_k(t_0) z(q^2, t_0)^k. \tag{2.35}$$

The functions

$$P_{1,2}(q^2) = \prod_{p \in \{\text{poles of } T_{1,2}\}} (1 - q^2/m_p^2) \tag{2.36}$$

contain all poles of $T_{1,2}(q^2)$ and $\phi_{1,2}(q^2, t_0)$ is an arbitrary function which, guided by physical arguments, can be chosen such as to suppress higher order coefficients a_k. One furthermore has, due to the B_s^* pole in T_1:

$$P_1(q^2, t_0) = 1 - q^2/m_{B_s^*}^2, \qquad P_2(q^2, t_0) = 1. \tag{2.37}$$

The advantage of this parametrisation is that it does not make any assumptions, apart from analyticity and the presence of sub-threshold poles. I will use it to estimate the systematic uncertainty associated with the choice of a particular form factor parametrisation.

2.4 Heavy quark physics

Inside hadrons quarks are bound by the strong force which is described by a local $SU(3)$ gauge theory known as Quantum Chromodynamics (QCD). After briefly reviewing QCD I discuss how heavy quarks can be treated in the framework of an effective theory.

2.4.1 Quantum chromodynamics

Let $\Psi = (\psi_r, \psi_b, \psi_g)^T$ denote a three component quark spinor (r, b, g standing for the "colours" *red*, *blue* and *green*) representing a strongly interacting matter field. Under a local $SU(3)_c$ gauge transformation parametrised by $\alpha^a(x)$, $a = 1, \ldots, 8$ this field will transform as

$$\Psi(x) \quad \mapsto \quad e^{i\alpha(x)}\Psi(x) \qquad \text{with} \quad \alpha(x) = \alpha^a(x)T^a \tag{2.38}$$

where T^a are the generators of the group $SU(3)$. To keep the Lagrangian invariant under *local* transformations it is necessary to introduce a spin-one field A^a_μ in the adjoint representation and to use covariant instead of ordinary derivatives. Ignoring strong CP-violation the gauge invariant Lagrangian is given by

$$\mathscr{L} = \mathscr{L}_{\mathrm{G}} + \mathscr{L}_{\mathrm{F}} \quad = \quad -\frac{1}{2}\,\mathrm{tr}[F_{\mu\nu}F^{\mu\nu}] + \overline{\Psi}(i\not{D} - m)\Psi \tag{2.39}$$

with the covariant derivative[1] $D_\mu = \partial_\mu + igT^aA^a_\mu$. The first term, containing the field strength tensor $F_{\mu\nu} = F^a_{\mu\nu}T^a$ with $F^a_{\mu\nu} = \partial_\mu A^a_\nu - \partial_\nu A^a_\mu - gf^{abc}A^a_\mu A^b_\nu$, describes the kinetic energy and self interactions of the gauge bosons. The second term contains an expression of the form $\overline{\Psi}A^a_\mu\Psi$ which couples the gauge field to matter.

This theory is generally known as *Quantum Chromodynamics* (QCD). In the interacting theory the coupling constant g is scale dependent. It turns out that due to the self interactions in the non-Abelian case $\alpha_s = g^2/(4\pi)$ *decreases* for large energy scales, in particular one finds that at one loop order

$$\alpha_s(\mu) \quad = \quad \frac{1}{\beta_0 \log(\mu^2/\Lambda^2_{\mathrm{QCD}})} \tag{2.40}$$

[1] The sign convention for the coupling constant g is the one used in [63] which differs from the one in [3].

State	$^{2S+1}L_J$	Mass
$\eta_b(1S)$	$^1S_0$	9389 MeV
$\Upsilon(1S)$	$^3S_1$	9460 MeV
$\chi_{b0}(1P)$	$^3P_0$	9859 MeV
$\chi_{b1}(1P)$	$^3P_1$	9893 MeV
$\chi_{b2}(1P)$	$^3P_2$	9912 MeV
$\Upsilon(2S)$	$^3S_1$	10023 MeV
$\chi_{b0}(2P)$	$^3P_0$	10233 MeV
$\chi_{b1}(2P)$	$^3P_1$	10255 MeV
$\chi_{b2}(2P)$	$^3P_2$	10269 MeV
$\Upsilon(3S)$	$^3S_1$	10355 MeV

Table 2.2: Observed bottomonium states below the $B\overline{B}$ threshold. All data is taken from [5] except for the recent measurement of the $\eta_b(1S)$ ground state reported in [64]; see these references for a detailled analysis of errors.

with $\beta_0 = (33 - 2N_f)/(12\pi)$ and N_f the number of quark flavours. This also implies that at energies below $\Lambda_{\rm QCD} \sim 500$ MeV the perturbative expansion in the coupling constant breaks down and one has to resort to other methods. Today the most successful model-independent approaches either exploit the symmetries of the theory to construct an effective low energy expansion or rewrite the theory so that it can be simulated on a space time lattice. I discuss lattice field theory in chapter 3.

2.4.2 Separation of scales

The mass of the bottom quark is larger than the hadronic scale $\Lambda_{\rm QCD}$. This separation of scales has interesting consequences and can be used to explain a wide range of phenomena in heavy quark physics with simple arguments.

At leading order the heavy quark mass does not contribute to the dynamics inside mesons containing heavy quarks. This can be seen, for example, from the bottomonium spectrum in Tab. 2.2 where the mass splittings are of order of the hadronic scale. More precisely the mass of particles in the spectrum can be written as

$$M_{\{n\}} \;=\; 2m_b + a^{(0)}_{\{n\}}\Lambda_{\rm QCD} + a^{(1)}_{\{n\}}\frac{\Lambda^2_{\rm QCD}}{m_b} + \ldots . \tag{2.41}$$

The coefficients $a^{(k)}_{\{n\}}$ are group theoretical factors of order one and depend on the quantum numbers $\{n\}$ of the $\overline{b}b$ state, such as spin and orbital angular momentum.

Many aspects of heavy meson spectra, such as near-degeneracy of spin-states and

the weak quark mass dependence of energy splittings, can be explained by treating the heavy quark in an effective theory where the high energy excitations have been integrated out and new symmetries emerge.

2.4.3 Effective theories for heavy quarks

Originally Heavy Quark Effective Theory (HQET) was formulated in [12, 13, 14] and the subsequent derivation of the Lagrangian follows [65]. Consider a meson containing one heavy and one light quark. The field of a heavy quark with mass m moving with velocity v can be written as

$$\psi(x) \;=\; e^{-im\,v\cdot x}[h_v^+(x)+h_v^-(x)] \qquad \text{with} \tag{2.42}$$

$$P_+h_v^+=h_v^+, \qquad P_-h_v^+=0, \qquad P_+h_v^-=0, \qquad P_-h_v^-=h_v^- \tag{2.43}$$

where $P_\pm=\frac{1}{2}(1\pm\not{v})$. The heavy mass is much larger than the QCD scale and at lowest order in $1/m$ the quark acts as a static colour source. Interactions with the light degrees of freedom will only change its velocity at $\mathcal{O}(\Lambda_{\rm QCD}/m)$. The external momentum mv has been removed from h_v^+ so that the wavelength of typical fluctuations of this field is small. An effective theory for the infrared modes is now constructed by integrating out h_v^- and expanding in $1/m$.

The heavy quark action in QCD, $\int d^4x\,\overline{\psi}(x)(i\not{D}-m)\psi(x)$, can be written as

$$\int d^4x\,\left\{\overline{h}_v^+iv\cdot Dh_v^+-\overline{h}_v^-(iv\cdot D+2m)h_v^-+\overline{h}_v^+i\not{D}_\perp h_v^-+\overline{h}_v^-i\not{D}_\perp h_v^+\right\} \tag{2.44}$$

where $a_\perp^\mu=a^\mu-v^\mu(v\cdot a)$. In the path integral the fields h_v^- can be integrated out by completing the square and performing the Gaussian integral. The resulting Lagrangian is at tree level

$$\mathscr{L} \;=\; \overline{h}_v^+iv\cdot Dh_v^+-\overline{h}_v^+\not{D}_\perp\frac{1}{iv\cdot D+2m}\not{D}_\perp h_v^+. \tag{2.45}$$

By expanding to $\mathcal{O}(1/m)$ one finally obtains a set of local operators

$$\mathscr{L}^{(\rm HQET)} \;=\; \overline{h}_v^+iv\cdot Dh_v^+-\overline{h}_v^+\frac{D_\perp^2}{2m}h_v^+-g\overline{h}_v^+\frac{\sigma_{\mu\nu}G^{\mu\nu}}{4m}h_v^++\mathcal{O}(1/m^2). \tag{2.46}$$

$G^{\mu\nu}$ is the chromomagnetic field strength tensor and $\sigma_{\mu\nu}=\frac{i}{2}[\gamma_\mu,\gamma_\nu]$ a commutator of gamma matrices. Note that in the $v=0$ frame the kinetic operator reduces to $-\boldsymbol{D}^2/(2m)$ whereas the chromomagnetic operator can be written as $-g\boldsymbol{\sigma}\cdot\boldsymbol{B}/(2m)$. As

expected, the dispersion relation is nonrelativistic, $E(\boldsymbol{p}) = \boldsymbol{p}^2/(2m)$. The derivation can be extended to include higher order terms in the $1/m$ expansion without difficulty.

Beyond tree level the couplings receive radiative corrections. It can be shown, however, that some of the operators are protected from renormalisation by an additional symmetry of the heavy quark Lagrangian known as reparametrisation invariance [66]. If the total heavy quark momentum is written as $p = p_{\text{ext}} + p_{\text{res}} = mv + k$ then momenta of order Λ_{QCD} can be moved between the external momentum p_{ext} and the residual momentum p_{res} without changing the physics. This fixes the relative coefficient between the static term $v \cdot D$ and the kinetic term $D_\perp^2/(2m)$ to all orders in perturbation theory.

Alternatively the heavy quark effective Lagrangian can be derived by writing down all operators that are compatible with the symmetries of the system. The prefactors have then to be adjusted by on-shell matching. For this it is necessary to compute matrix elements both in full QCD and the effective theory. Although the theories agree for small momenta their short distance behaviour is completely different and the matching coefficients correct for this ultraviolet mismatch. As QCD is perturbative above the heavy quark scale the matching can be done perturbatively.

Finally it should be remarked that four quark operators in the heavy quark action are suppressed by additional powers of the strong coupling constant. They can only arise at loop level in full QCD.

Heavy Quark Effective Theory

The effective Lagrangian has an infinite number of terms and to make physical predictions one has to find a way of ordering the operators according to their relative importance. Power counting rules are not an inherent property of the effective Lagrangian but have to be derived from the physics of the system under study.

In mesons containing one heavy and one light quark there are only two energy scales, the dynamic scale Λ_{QCD} and the mass of the heavy quark. Any operator of dimension d will be suppressed by $(\Lambda_{\text{QCD}}/m)^{d-4}$ relatively to the leading order static operator $v \cdot D$. To make predictions with a given precision it is then sufficient to include only a finite number of operators.

For infinitely heavy quarks the symmetries of the HQET Lagrangian are different from those of finite mass QCD. The leading order term does not depend on the heavy quark spin and mass which has observable effects on the heavy-light meson spectrum. In particular one expects that to a good approximation the mass of any heavy-light meson is given by $m_H = m + \overline{\Lambda}$ with $\overline{\Lambda} \sim \Lambda_{\text{QCD}}$. Fine and hyperfine splittings are expected to be suppressed by an additional factor of Λ_{QCD}/m.

Experimentally one finds that the splitting between pseudoscalar and vector states

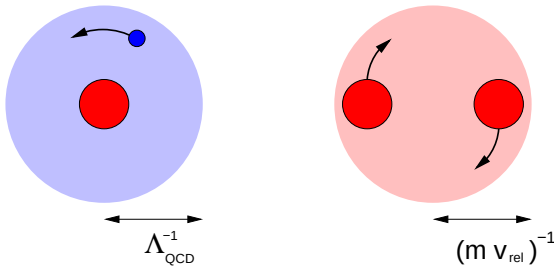

Figure 2.17: Schematic picture of heavy-light (left) and heavy-heavy (right) meson systems. The heavy degrees of freedom are coloured in red, the light quark in blue.

D, D^* as well as B, B^* is small and the mass differences $m_{B^*}^2 - m_B^2$ and $m_{D^*}^2 - m_D^2$ are of comparable size. At next order in the $1/m$ expansion the expectation values of the kinetic and the chromomagnetic operators can be parametrised by two additional numbers for each multiplet. Masses of different spin states can then be derived using simple group theoretical relations, see for example [67].

Nonrelativistic QCD

The situation is more complicated for mesons with two heavy quarks. Here the kinetic term can not be treated as a correction as it is essential for stabilising the bound state as a hydrogen-like system. Instead of expanding in $\Lambda_{\rm QCD}/m$ the relative velocity $v_{\rm rel}$ of the quark-antiquark pair plays a crucial role. Besides $\Lambda_{\rm QCD}$ and the hard scale m there are two additional scales in the problem: the heavy quark momentum is of the order of the soft scale $mv_{\rm rel}$ (the inverse of which determines the size of the meson due to the uncertainty principle) and its energy of the order of the ultrasoft scale $mv_{\rm rel}^2$.

The leading order Lagrangian in the rest frame is

$$\mathscr{L}_0^{(\rm NRQCD)} = \overline{h}_0^+ iD_0 h_0^+ - \overline{h}_0^+ \frac{\boldsymbol{D}^2}{2m} h_0^+ . \tag{2.47}$$

D_0 is a temporal derivative and scales like an energy $mv_{\rm rel}^2$, whereas the spatial derivative $\boldsymbol{D}$ scales as a momentum $mv_{\rm rel}$. Both terms in the leading Lagrangian have the same power in the relative velocity $v_{\rm rel}$. The size of m and $v_{\rm rel}$ can be estimated from the bottomonium spectrum, see Tab. 2.2. The heavy quark mass is given by half the energy of the $\Upsilon(1S)$ state from which one obtains $m \approx 4.7$ GeV. The spin independent energy splittings are of the order of $mv_{\rm rel}^2$. For the low-lying states radial excitations are of the order of $M(\Upsilon(2S)) - M(\Upsilon(1S)) \approx 560$ MeV and orbital-angular-momentum splittings of $M(\chi_{bJ}) - M(\Upsilon(1S)) \approx 430$ MeV. This gives an estimate of $mv_{\rm rel}^2 \approx 500$ MeV and $v_{\rm rel}^2 \approx 0.1$. Indeed it turns out that both for charmonium and

operator	
$\boldsymbol{D}$	mv_{rel}
D_0	mv_{rel}^2
gA_0 (Coulomb gauge)	mv_{rel}^2
$g\boldsymbol{A}$ (Coulomb gauge)	mv_{rel}^3
$g\boldsymbol{E}$	$m^2v_{\mathrm{rel}}^3$
$g\boldsymbol{B}$	$m^2v_{\mathrm{rel}}^4$

Table 2.3: NRQCD power counting rules derived in [68]. Rules for gauge-invariant operators are independent of the choice of gauge.

bottomonium mv_{rel}^2 is very close to Λ_{QCD} which suggest that in this range the ultrasoft scale is independent of the quark mass [68].

It is expected that systematic errors from the relativistic expansion are reduced to below the 1%-level by including terms of order v_{rel}^4 in the effective Lagrangian.

Power counting rules for other operators are derived in [68]. There it is shown how powers of v_{rel} can be assigned to the vector potential and the chromomagnetic field such that the field equations of the heavy quark and chromomagnetic field are self consistent, see Tab. 2.3.

2.4.4 Renormalisation

Due to the different power counting the renormalisation of HQET and NRQCD has to be discussed separately.

For HQET it turns out that the leading, static theory is renormalisable. When computing the radiative corrections to some operator $\mathcal{O}$ the $1/m$ terms will be treated as operator insertions in the path integral. Any divergences that arise from combinations of $\mathcal{O}$ and these insertions can be absorbed into the coefficients of operators of the same or lower order in $1/m$. This implies that the theory can be renormalised order by order, i.e. if one wants to make predictions with a given accuracy $\delta = (\Lambda_{\mathrm{QCD}}/m)^n$ only operators up to dimension $n+3$ [69] have to be taken into account. It has to be kept in mind, however, that the relation between bare and renormalised parameters is not necessarily finite. Higher order operators can "mix down" in a cutoff dependent renormalisation scheme, i.e. an operator of dimension n_+ can renormalise a lower dimensional operator with dimension n_- by terms proportional to $(\Lambda_{\mathrm{cutoff}}/m)^{n_+-n_-}$. If one only works with renormalised operators this is of course not a problem. However, in the lattice regularisation bare parameters are used which will diverge with some power of $\Lambda_{\mathrm{cutoff}} \sim 1/a$. This restricts the allowed range of accessible a and taking the

continuum limit becomes impossible. Although this is a drawback it should be noted that discretisation errors only form part of the error budget in a lattice calculation. Even if they can not be removed completely, they can be reduced by using improved actions and their size can be estimated and quoted together with the central value obtained in a lattice simulation.

For NRQCD the $1/m$ corrections are already contained in the propagator and the leading order theory is not renormalisable. Here there is an infinite number of divergences which can not be absorbed by low energy constants, so the desired order-by-order renormalisation of the theory seems to be impossible. It has to be kept in mind, though, that even an unrenormalisable theory is still predictive if the cutoff dependence of the coupling constants is taken into account properly. In principle the cutoff dependence of physical quantities can be reduced by going to a sufficiently high order in the perturbative expansion (or by fixing the couplings nonperturbatively). To avoid both power divergences in lattice perturbation theory and large discretisation errors one is restricted to work in the window of lattice spacings given by $1/m \lesssim a \lesssim 1/\Lambda_{\mathrm{QCD}}$. In the future sufficiently fine lattices with $am \ll 1$ might become available and a relativistic fermion action can be used.

After reviewing the lattice discretisation of QCD in the next chapter I describe how heavy quarks are discretised on a spacetime lattice in chapter 4.

Chapter 3

Lattice Field Theory

A very successful approach to quantising field theories was proposed by Feynman [70]. It is particularly useful when an expansion in a small parameter, such as the coupling constant, is not possible. Predictions from the full theory can be obtained by discretising it on a space time lattice and evaluating the remaining integrals numerically using Monte Carlo methods. This approach has been successfully applied to study the nonperturbative dynamics of strongly interacting particles as described by QCD. Since this idea was originally proposed in [71] a tremendous increase in available computing power, advanced algorithms and better understanding of conceptual problems have enabled the lattice community to make predictions of high accuracy at parameter values that are close to the physical ones.

"Gold plated" observables with at most one hadronic particle in the final state are of particular interest as these can be studied very reliably in lattice QCD, as has been reported in the proceedings of recent lattice conferences. In particular the HPQCD collaboration uses dynamical sea quarks and a highly improved light quark action and has recently calculated spectra and decay constants of mesons containing light and charm quarks [18, 72, 73, 74] as well as neutral B mixing matrix elements [32].

These calculations have now reached a level of precision that makes it possible to compare them to experimental data. In a recent update Davies et al. [74] reported a 3σ discrepancy between lattice predictions and experiment of the D_s decay constant f_{D_s}, which is proportional to V_{cs}, and good agreement for f_D. In a new experimental measurement of f_{D_s} [75] this discrepancy has been reduced but is still significant.

3.1 The Feynman path integral

The time ordered vacuum expectation value of a product of operators $\mathcal{O}_j(x)$ which depend on the fermion fields $\psi(x)$, $\overline{\psi}(x)$ and the gluon field $A_\mu(x)$ at the space time

point x can be written as a ratio of functional integrals

$$\langle 0|T\{\mathcal{O}_1(x_1)\dots\mathcal{O}_1(x_n)\}|0\rangle \;=\; \frac{\int \mathcal{D}\overline{\psi}\mathcal{D}\psi\mathcal{D}A_\mu\; \mathcal{O}_1(x_1)\dots\mathcal{O}_n(x_n)e^{-S[\psi,\overline{\psi},A_\mu]}}{\int \mathcal{D}\overline{\psi}\mathcal{D}\psi\mathcal{D}A_\mu\; e^{-S[\psi,\overline{\psi},A_\mu]}}. \tag{3.1}$$

The theory is formulated in Euclidean space where the Minkowski time coordinate t has been replaced by $-i\tau$ to avoid rapid oscillations in the integrand. $S[\psi,\overline{\psi},A_\mu]$ is the action which can be obtained by integrating the Euclidean version of the QCD Lagrangian (2.39) over space and time.

In the discretised version of the theory the fields are only defined at points of a hypercubic space time lattice $L \subset \mathbb{Z}^4$. The shortest distance between any two points is the lattice spacing a which naturally introduces an ultraviolet cutoff of π/a in momentum space and renders all predictions of the theory finite. The infinite dimensional functional integrals are replaced by products of ordinary integrals which can be evaluated numerically using stochastic methods. To this end Monte Carlo techniques are used to generate a set of statistically independent field configurations distributed according to e^{-S}. Expectation values of operators as in (3.1) can then be obtained as averages over these configurations.

3.2 Lattice QCD action

When discretising QCD on a lattice it is desirable not to break gauge invariance as otherwise a considerable amount of fine tuning is necessary to obtain the same renormalised coupling constant for all gluon vertices. This can be achieved by using the gauge invariant link variables $U_\mu(x)$ instead of the gluon fields. The quantities are related by

$$U_\mu(x) \;=\; P\left\{\exp\left[iag\int_x^{x+a\hat{\mu}} dz\; A_\mu(z)\right]\right\} \approx \exp\left[iagA_\mu(x+\frac{a}{2}\hat{\mu})\right] \tag{3.2}$$

where P stands for path-ordering. The links transform as $U_\mu(x) \mapsto e^{i\alpha(x)}U_\mu(x)e^{-i\alpha(x+a\hat{\mu})}$ under gauge transformations so that quantities such as $\overline{\psi}(x)U_\mu(x)\dots U_\nu(y-a\hat{\nu})\psi(y)$ or traced closed loops of links are gauge invariant and can be used in the construction of the action.

The simplest gluon action proposed in [71] is constructed from products of links around a 1×1 loop, usually called a *plaquette*,

$$U_P = U_\mu(x)U_\nu(x+a\hat{\mu})U_\mu^\dagger(x+a\hat{\nu})U_\nu^\dagger(x), \tag{3.3}$$

$$S_G = \beta \sum_P \left(1 - \frac{1}{6} \mathrm{tr}\left[U_P + U_P^\dagger\right]\right) \qquad \text{with} \quad \beta = 6/g^2. \tag{3.4}$$

By expanding in powers of a this can be shown to be identical to the continuum action up to discretisation errors of $\mathcal{O}(a^2)$.

The fermionic part of the action can be written as

$$S_F = a^4 \sum_x \overline{\psi}(x)(\gamma_\mu \Delta_\mu^\pm + m)\psi(x) \tag{3.5}$$

with the discrete version of the covariant derivative

$$\Delta_\mu^\pm \psi(x) = \frac{1}{2a}\left(U_\mu(x)\psi(x + a\hat{\mu}) - U_\mu^\dagger(x - a\hat{\mu})\psi(x - a\hat{\mu})\right). \tag{3.6}$$

Again it is straightforward to check that this is identical to the continuum expression up to errors quadratic in the lattice spacing.

3.3 Improved actions

Ultimately one is not interested in observables on the lattice but in those in the continuum limit $a \to 0$. Discretising the theory will introduce errors which (at leading order) scale with some power of the lattice spacing. The most naive way of removing these lattice artifacts would be to use finer lattice spacings.

Taking the lattice spacing to zero is equivalent to removing the cutoff in other regularisation schemes, the theory should become independent of the lattice structure and hence correlation functions (in lattice units) will diverge. If one would simply keep the number of lattice points constant the physical lattice size will eventually become smaller than the correlation length of the lightest particle in the theory leading to notable finite size effects. To avoid these problems the physical volume is kept constant and larger and larger lattices have to be used when approaching the continuum limit. In practice for a fixed physical lattice size the computational cost is proportional to approximately $1/a^6$. This is because in addition to the increase of lattice points proportional to $1/a^4$, standard Monte Carlo techniques produce highly autocorrelated configurations as long range correlations dominate when the continuum limit is approached [76, 77]. Finite size effects from the exchange of pseudoscalar particles of mass m_{PS} between copies of hadronic particles are proportional to $\exp[-m_{PS}L]$ where $L \gg 1/m_{PS}$ is the linear lattice size in physical units. As the quarks become more chiral m_{PS} decreases and L needs to be increased. Eventually the brute force reduction of lattice artifacts by using lattices with more and more points becomes computationally unfeasible.

Another way to overcome these difficulties is to include additional irrelevant operators in the Lagrangian which systematically remove discretisation errors at finite a. This process is called improvement.

For example, in (3.5) the improved derivative

$$\Delta_\mu^{\rm imp} \;=\; \Delta_\mu^{\pm} - \frac{a^2}{6}\Delta_\mu^{+}\Delta_\mu^{\pm}\Delta_\mu^{-} + \mathcal{O}(a^4) \tag{3.7}$$

could be used where the forward and backward derivatives Δ_μ^+ and Δ_μ^- are defined in (A.9).

An improved version of the gluonic part of the action with errors of $\mathcal{O}(a^4)$ is constructed by adding 2×1 gauge invariant Wilson loops to it

$$S_G \;=\; -\beta\sum_{x,\mu>\nu}\left(\frac{5}{3}P_{\mu\nu} - \frac{a^2}{12}(R_{\mu\nu}+R_{\nu\mu})\right) \tag{3.8}$$

where

$$\begin{aligned} P_{\mu\nu} &= \frac{1}{3}\,\mathrm{Re}\{\mathrm{tr}[U_\mu(x)U_\nu(x+a\hat{\mu})U_\mu^\dagger(x+a\hat{\nu})U_\nu^\dagger(x)]\} \qquad (3.9)\\ R_{\mu\nu} &= \frac{1}{3}\,\mathrm{Re}\{\mathrm{tr}[U_\mu(x)U_\mu(x+a\hat{\mu})U_\nu(x+2a\hat{\mu})U_\mu^\dagger(x+a\hat{\mu}+a\hat{\nu})U_\mu^\dagger(x+a\hat{\nu})U_\nu^\dagger(x)]\}. \end{aligned}$$

So far I have only described improvement at tree level: radiative corrections will reintroduce errors of $\mathcal{O}(\alpha_s a^2)$ and the coefficients in (3.8) have to be adjusted to account for this. This can be done nonperturbatively or in perturbation theory as the corrections come from highly energetic gluons and the strong coupling constant α_s is small at the scale of the lattice cutoff $1/a$.

3.3.1 Mean field improvement

It has turned out [78, 79], however, that a large amount of these corrections can be removed by dividing each link by its mean field value u_0. This is closely related to the problem of defining a sensible expansion parameter in the perturbative expansion of lattice quantities.

The bare coupling constant $\alpha_{\rm lat}$ receives large renormalisations which can be removed by partial resummation. The coefficients in the perturbative series of, for example, a small Wilson loop are much smaller if it is expressed in terms $\alpha_V(q)$ instead, where $\alpha_V(q)$ is defined via the static heavy quark potential,

$$V(q) \;=\; -\frac{4\pi C(r)\alpha_V(q)}{q^2}. \tag{3.10}$$

Here $C(r)$ is the Casimir operator in the fundamental representation. The lattice theory is formulated in terms of links $U_\mu = \exp[iagA_\mu]$ instead of the gauge potentials. Expanding U_μ in the strong coupling constant this generates additional quark-gluon vertices with an arbitrary number of gluons. Although these are suppressed by powers of the lattice spacing, the gluon lines can be connected to give tadpole diagrams which are ultraviolet divergent and proportional to some power of $1/a$, which leads to a constant shift at $\mathcal{O}(\alpha_s)$ between the bare coupling constant and α_V

$$\alpha_V(q) \quad = \quad \alpha_{\rm lat}\left(1+\alpha_{\rm lat}\left[\beta_0\log\left(\frac{\pi}{aq}\right)^2+(\text{large constant})\right]+\ldots\right). \qquad (3.11)$$

As these renormalisations are process independent they can be largely removed by dividing each link U_μ in the lattice action by its expectation value u_0. As the link is not gauge invariant u_0 is usually defined to be the fourth root of the mean plaquette or the expectation value of U_μ in Landau gauge. In this work I will always use the latter definition. Although there is no formal proof in practise this strategy of "tadpole"- or "mean-field" improvement is very successful.

A tadpole improved gluon action is therefore obtained from (3.8) by replacing $P_{\mu\nu} \mapsto P_{\mu\nu}/u_0^4$ and $R_{\mu\nu} \mapsto R_{\mu\nu}/u_0^6$ which will remove the majority of $\mathcal{O}(a^2\alpha_s)$ corrections. The leading power of u_0 can be absorbed in the inverse coupling constant, $\beta \mapsto \beta/u_0^4$.

3.4 Fermions on the lattice

A closer look at the naive action in (3.5) reveals that in addition to the physical fermion with on-shell momenta well below the lattice cutoff there are 15 additional spurious degrees of freedom. This can be seen by studying the dispersion relation of the free theory which has additional solutions near the boundary of the Brillouin zone. More generally the action is invariant under the set of transformations

$$\psi(x) \quad \mapsto \quad \prod_\rho (i\gamma_5\gamma_\rho)^{\zeta_\rho} e^{ix\cdot\zeta\,\pi/a}\psi(x) \qquad (3.12)$$

where the components of the vector ζ can be zero or one. Even if these doublers are projected out in external states they can be created in intermediate states by absorption of highly virtual gluons with momenta of the order π/a.

There are several ways of dealing with this problem. The original idea of Wilson was to add a higher order operator to the action to give the doublers a mass of the order of the lattice cutoff and decouple them from the theory in the continuum limit (see, for example [63]). The $\mathcal{O}(a)$ errors generated by this term can be removed by adding

an additional operator of the same dimension, the so called clover term [80]. A more serious drawback is that Wilson-type fermions explicitly break chiral symmetry which requires fine tuning of the mass that is not protected from additive renormalisation any more. Chiral symmetry is also often desirable as it prevents mixing of operators with different handedness. An additional problem of the Wilson Dirac operator is that it can have very small eigenvalues which can cause problems when inverting this operator to compute correlators.

To overcome these problems actions with a modified definition of chiral symmetry have been constructed. It can be shown that in this case the Dirac operator D has to fulfil the Ginsparg-Wilson relation $\gamma_5 D + D\gamma_5 = aD\gamma_5 D$ [81]. One realisation is Neuberger's operator [82] which is non-local and costly to simulate. Another way of designing an action with chiral symmetry is to formulate the theory in five dimensions. If the mass is a suitably chosen function of the fifth coordinate s, for example a sign function that is $+M$ for positive and $-M$ for negative s, there will be massless chiral solutions bound to the domain wall $s = 0$ in the effective four dimensional theory [83]. However, also this approach is computationally challenging.

3.4.1 Staggered fermions

The discretisation of relativistic fermions used in this work is the staggered formulation. Here, by using a local field transformation $\psi(x) \mapsto \psi'(x) = \Omega(x)\psi(x)$, the action is diagonalised in Dirac space. The transformation matrix is given by $\Omega(x) = \gamma_0^{x_0}\gamma_1^{x_1}\gamma_2^{x_2}\gamma_3^{x_3}$ and by using $\Omega(x)^\dagger \gamma_\mu \Omega(x + a\hat{\mu}) = (-1)^{x_0+x_1+\cdots+x_{\mu-1}} = \alpha_\mu(x)$ the action can be rewritten as

$$\begin{aligned} S &= \sum_x \overline{\psi}'(x)\alpha_\mu(x)\left(U_\mu(x)\psi'(x+a\hat{\mu}) - U_\mu(x-a\hat{\mu})^\dagger\psi'(x-a\hat{\mu})\right) \\ &\quad + m\sum_x \overline{\psi}'(x)\psi'(x). \end{aligned} \tag{3.13}$$

The four components of the new spinor field are independent and the number of degrees of freedom can be reduced to four by only simulating one component of the field.

Although the field transformation $\psi(x) \mapsto \Omega(x)\psi(x)$ complicates the construction of operators, an advantage of this formulation is that the action has a remnant chiral symmetry and it is easy to simulate as the spin degrees of freedom have been removed. This makes the generation of gauge configuration with dynamical sea quarks very cost efficient. This is particularly important when working at masses that are close to the physical ones to reduce systematic errors. The remaining four degrees of freedom are usually called *tastes*, they are not independent and can still transform into each other by the exchange of highly virtual gluons with momenta $p \sim \pi/a$. These unwanted taste

changing interactions are not present in the continuum, suppressing them by suitable modifications of the action will lead to a substantial reduction of discretisation errors.

3.4.2 Improved actions for fermions

As the exchange of gluons close to the boundary of the Brillouin zone is a highly ultraviolet process taste changing interactions can be suppressed by adding effective four quark operators to the action. However, a more efficient solution is to modify the high-energy behaviour of the quark-gluon vertex. In [84] it is shown how this can be achieved by smearing the gluon fields. Then lattice artifacts at $\mathcal{O}(a^2)$ can be removed by a further modification of the links and tree level improvement of the first order derivative as described in Section 3.3. The derivation starts with the naive fermion action

$$S = \sum_x \overline{\psi}(x) \left(\gamma_\mu \Delta_\mu^{\pm} + m\right) \psi(x). \tag{3.14}$$

To suppress taste changing interactions at tree level and remove $\mathcal{O}(a^2)$ errors one proceeds as follows:

Link smearing. Each link variable U_μ is replaced by $\mathcal{F}_\mu U_\mu$ with the "Fat7" smearing operator

$$\mathcal{F}_\mu = \prod_{\rho \neq \mu} \left(1 + \frac{a^2 \Delta_\rho^{(2)}}{4}\right) \Big|_{\text{symm.}} \tag{3.15}$$

where $\Delta_\rho^{(2)}$ is a second order covariant derivative acting on the link $U_\mu(x)$. By expanding the smeared link in gluon fields A_μ it can be shown that the exchange of taste-changing gluons with a momentum component of π/a is forbidden.

$\mathcal{O}(a^2)$ Symanzik improvement. The remaining $\mathcal{O}(a^2)$ errors in the action can be removed by an additional smearing of the link fields. This is done by modifying the smearing operator to

$$\mathcal{F}_\mu^{\text{ASQ}} = \mathcal{F}_\mu - \sum_{\rho \neq \mu} \frac{a^2 (\Delta_\rho)^2}{4} \tag{3.16}$$

where Δ_ρ is a first order derivative of the link field. Finally the derivative in the action (3.14) is improved by adding a third order derivative, usually called the "Naik"-term,

$$\Delta_\mu^{\pm} \;\mapsto\; \Delta_\mu^{\mathrm{ASQ}} = \Delta_\mu^{\pm(V)} - \frac{a^2}{6}\left(\Delta_\mu^{\pm}\right)^3. \tag{3.17}$$

The additional superscript V indicates that the smeared links $V_\mu = \mathcal{F}_\mu^{\mathrm{ASQ}} U_\mu$ are used instead of U_μ in the covariant derivative. In addition, the links are divided by u_0 to reduce mean field corrections,

$$\Delta_\mu^{\mathrm{ASQTad}} \;=\; \left(\Delta_\mu^{\mathrm{ASQ}}\right)_{U_\mu \mapsto U_\mu/u_0}. \tag{3.18}$$

The a^2 tadpole improved (ASQTad) action is given by

$$S_{\mathrm{ASQTad}} \;=\; \sum_x \overline{\psi}(x)\left(\gamma_\mu \Delta_\mu^{\mathrm{ASQTad}} + m\right)\psi(x). \tag{3.19}$$

This action has tree level errors of $\mathcal{O}(a^4)$; errors of $\mathcal{O}(\alpha_s a^2)$ are strongly reduced. As for the naive action the number of degrees of freedom can be reduced to four by staggering the fields.

Taste changing interactions can be suppressed even further by repeated smearing of the links. In [85] two levels of smearing with an intermediate reunitarisation

$$\mathcal{F}_\mu^{\mathrm{HISQ}} \;=\; \left(\mathcal{F}_\mu - \sum_{\rho\neq\mu} \frac{a^2\left(\Delta_\rho\right)^2}{2}\right)\mathcal{U}\mathcal{F}_\mu \tag{3.20}$$

are suggested. The operator $\mathcal{U}$ projects the smeared link back to $SU(3)$. By measuring mass splittings between the 16 different Goldstone bosons and other observable quantities the authors of [85] conclude that this reduces taste splitting by an additional factor of around three.

The derivative acting on the quark field is given by

$$\Delta_\mu^{\mathrm{HISQ}} \;=\; \Delta_\mu^{\pm(W)} - \frac{a^2}{6}(1+\epsilon)\left(\Delta_\mu^{\pm(X)}\right)^3. \tag{3.21}$$

In the first difference operator the HISQ-smeared link variables $W_\mu = \mathcal{F}_\mu^{\mathrm{HISQ}} U_\mu$ are used. In the Naik term only one level of smearing followed by reunitarisation is sufficient, the links used there are given by $X_\mu = \mathcal{U}\mathcal{F}_\mu U_\mu$. The ϵ - term can be tuned to remove $\mathcal{O}((am)^4)$ errors which are sizeable for charm quarks.

The Highly Improved Staggered Quark (HISQ) action has been used extensively for studies of the mesons containing charm quarks [73, 74]. Its relative simplicity and

low computational cost makes it possible to include the effects of fermionic vacuum polarisation at small values of the sea quark mass. In the staggered formulation the number of degrees of freedom is usually reduced to 2 or 1 by taking the square- or fourth root of the sea quark determinant that is obtained by integrating out the anticommuting Grassmann fields.

While this has lead to some debate on the validity of this method, this problem is not directly relevant for the perturbative calculations in this thesis. In perturbation theory the spurious degrees of freedom can be accounted for by dividing every (naive) closed fermion loop by 16. In addition, in the radiative corrections to the heavy quark self-energy and to heavy-light currents vacuum polarisation effects of light quarks only arise at two loop order.

Chapter 4

Heavy quarks on the lattice and perturbative renormalisation

In the previous chapter I always implicitly assumed that the quark mass is much smaller than the inverse lattice spacing. On lattices currently used with $a \sim 0.1$ fm this is the case for light quarks; for charm quarks sufficient accuracy can be reached by using the HISQ action described in section 3.4.2. Bottom quarks, however, have a Compton wavelength that is smaller than the lattice spacing and hence a direct simulation with a relativistic fermion action will not give meaningful results.

In this chapter I show how this problem can be solved by using a discretised version of the nonrelativistic quark action described in section 2.4.3. I discuss the methods for calculating radiative corrections to the effective action in lattice perturbation theory.

4.1 Lattice NRQCD

Nonrelativistic lattice actions for heavy quarks have been developed in [86, 87, 88] and were substantially improved in [89]. In the next section I present an alternative derivation of the nonrelativistic continuum action and show how the theory can be discretised on a lattice.

4.1.1 Derivation of lattice NRQCD

The following discussion follows [1, 90, 91]. In the first step, quark- and antiquark fields are decoupled by a Foldy-Wouthuysen-Tani (FWT) transformation. This method automatically generates the correct tree level couplings and is easily generalised to a moving frame of reference. Knowledge of the explicit relation between the QCD field and the corresponding quantity is also essential for the construction of heavy-light operators in chapter 7. In the continuum this transformation relates the relativistic

field $\Psi(x)$ to the field $\tilde{\Psi}(x)$ in the effective theory,

$$\Psi(x) \;=\; T_{FWT} e^{-imx^0\gamma^0}\tilde{\Psi}(x), \qquad \tilde{\Psi} = \begin{pmatrix}\psi\\ \chi\end{pmatrix}. \tag{4.1}$$

The factor $e^{-imx^0\gamma^0}$ removes the rest mass from the Lagrangian. In the Dirac basis γ^0 is diagonal so that ψ describes the quark and χ the antiquark field. The transformation can be constructed recursively order by order in inverse powers of the heavy quark mass. Up to corrections of $\mathcal{O}(1/m^4)$ it is given by

$$\begin{aligned} T_{FWT} \;&=\; \exp\left[\frac{1}{2m}\,(i\boldsymbol{\gamma}\cdot\boldsymbol{D})\right]\exp\left[\frac{1}{2m^2}\left(-\frac{ig}{2}\gamma^0\boldsymbol{\gamma}\cdot\boldsymbol{E}\right)\right] \\ &\quad\times\;\exp\left[\frac{1}{2m^3}\left(\frac{g}{4}\boldsymbol{\gamma}\cdot(D_0^{\mathrm{ad}}\boldsymbol{E}) + \frac{1}{3}(i\boldsymbol{\gamma}\cdot\boldsymbol{D})^3\right)\right] \end{aligned} \tag{4.2}$$

where $\boldsymbol{E}$ and $\boldsymbol{B}$ are the chromo-electric and -magnetic fields. The Lagrangian can be written as

$$\begin{aligned} \mathscr{L} \;&=\; \overline{\tilde{\Psi}}(x)\Big[i\gamma^0 D_0 + \frac{\boldsymbol{D}^2}{2m} + \frac{g}{2m}\boldsymbol{\Sigma}\cdot\boldsymbol{B} \\ &\quad+\;\frac{g}{8m^2}\gamma^0\left(\boldsymbol{D}^{\mathrm{ad}}\cdot\boldsymbol{E} + i\boldsymbol{\Sigma}\cdot(\boldsymbol{D}\times\boldsymbol{E} - \boldsymbol{E}\times\boldsymbol{D})\right)\Big]\tilde{\Psi}(x) + \mathcal{O}(1/m^3) \end{aligned} \tag{4.3}$$

with

$$\Sigma^j \;=\; \begin{pmatrix}\sigma^j & 0\\ 0 & \sigma^j\end{pmatrix}. \tag{4.4}$$

As expected particle- and antiparticle- fields decouple and the action can be written as a sum of two independent actions in the two-component spinor fields ψ and χ.

The Lagrangian in (4.3) is correct up to order $\Lambda_{\mathrm{QCD}}^2/m^2$ in heavy-light power counting. To include all terms of order v_{rel}^4 in heavy-light mesons an additional kinetic operator $\boldsymbol{D}^4/(8m^3)$ has to be added. This term can be derived by expanding the relativistic kinetic energy $E_{\mathrm{kin}} - m = \sqrt{\boldsymbol{k}^2 + m^2} - m = \frac{\boldsymbol{k}^2}{2m} - \frac{\boldsymbol{k}^4}{8m^3} + \frac{\boldsymbol{k}^6}{16m^5} + \ldots$.

Rotation to Euclidean space is achieved by making the replacements

$$\begin{aligned} x^0 \mapsto -ix_E^4 = -i\tau, \qquad & \boldsymbol{x} \mapsto \boldsymbol{x}_E, \\ \tilde{\Psi}(x) \mapsto \tilde{\Psi}(x_E), \qquad & \overline{\tilde{\Psi}}(x) \mapsto \overline{\tilde{\Psi}}(x_E), \\ A_0(x) \mapsto iA_4(x_E), \qquad & \boldsymbol{A}(x) \mapsto \boldsymbol{A}(x_E), \end{aligned} \tag{4.5}$$

so that the Lagrangian is given by

$$\begin{aligned}\mathscr{L} &= \overline{\tilde{\Psi}}(x)\Big[\gamma^0 D_4 - \frac{\boldsymbol{D}^2}{2m} - \frac{g}{2m}\boldsymbol{\Sigma}\cdot\boldsymbol{B} \\ &- \frac{g}{8m^2}\gamma^0\left(\boldsymbol{D}^{\mathrm{ad}}\cdot\boldsymbol{E} + \boldsymbol{\Sigma}\cdot(\boldsymbol{D}\times\boldsymbol{E} - \boldsymbol{E}\times\boldsymbol{D})\right) - \frac{1}{8m^3}\boldsymbol{D}^4\Big]\tilde{\Psi}(x) + \mathcal{O}(1/m^3).\end{aligned} \tag{4.6}$$

On the lattice the Hamiltonian is split into a leading order kinetic operator H_0 and a correction δH which contains interaction terms and higher order operators. In the past, various alternative discretisations have been suggested and in this work I follow the most recent convention in [92]. The action that describes the dynamics of particle solutions has the form

$$S = \sum_{\boldsymbol{x},\tau}\psi^+(\boldsymbol{x},\tau)\left[\psi(\boldsymbol{x},\tau) - K(\tau)\psi(\boldsymbol{x},\tau-1)\right] \tag{4.7}$$

with kernel

$$K(\tau) = \left(1-\frac{\delta H}{2}\right)\left(1-\frac{H_0}{2n}\right)^n U_4^\dagger(\boldsymbol{x},\tau-1)\left(1-\frac{H_0}{2n}\right)^n\left(1-\frac{\delta H}{2}\right). \tag{4.8}$$

The operators are

$$H_0 = -\frac{\Delta^{(2)}}{2m}, \tag{4.9}$$

$$\begin{aligned}\delta H &= -\frac{\left(\Delta^{(2)}\right)^2}{8m^3} - \frac{g}{2m}\boldsymbol{\sigma}\cdot\boldsymbol{B} - \frac{g}{8m^2}\boldsymbol{\sigma}\cdot\left(\tilde{\boldsymbol{\Delta}}^{(\pm)}\times\tilde{\boldsymbol{E}} - \tilde{\boldsymbol{E}}\times\tilde{\boldsymbol{\Delta}}^{(\pm)}\right) \\ &+ \frac{ig}{8m^2}\left(\tilde{\boldsymbol{\Delta}}^{(\pm)}\cdot\tilde{\boldsymbol{E}} - \tilde{\boldsymbol{E}}\cdot\tilde{\boldsymbol{\Delta}}^{(\pm)}\right) + \delta H_{\mathrm{corr.}}.\end{aligned}$$

The finite difference operators are defined in appendix A.2. Improved derivatives and fields are denoted by "$\sim$". In the continuum the Leibniz rule $\boldsymbol{D}^{\mathrm{ad}}\cdot\boldsymbol{E} = \boldsymbol{D}\cdot\boldsymbol{E} - \boldsymbol{E}\cdot\boldsymbol{D}$ holds but on the lattice the two discretisations of the adjoint derivative are not equivalent. The correction term $\delta H_{\mathrm{corr.}}$ reduces discretisation errors both in the spatial and the temporal direction. The first can be removed up to corrections of $\mathcal{O}(a^4p^4)$ by including the correction $-\frac{1}{12}\Delta^{(4)}$ to the kinetic operator $\Delta^{(2)}$. However, for performance reasons, it is advantageous to leave H_0 unchanged and include this correction in $\delta H_{\mathrm{corr.}}$ as well. The errors in the temporal direction can be reduced without introducing higher order time derivatives by fixing $\delta H_{\mathrm{corr.},t}$ such that

$$e^{-aH_0^*/2} = \left(1-\frac{aH_0}{2n}\right)^n\left(1-\frac{a\delta H_{\mathrm{corr.},t}}{2}\right). \tag{4.10}$$

where the improved kinetic operator H_0^* contains the improved second order derivative.

$\mathcal{O}(a^2E^2)$ errors can be removed by choosing

$$\delta H_{\text{corr.},t} = -\frac{aH_0^2}{4n} = -\frac{\left(\Delta^{(2)}\right)^2}{16nm^2}. \tag{4.11}$$

The full correction term is

$$\delta H_{\text{corr.}} = \frac{\Delta^{(4)}}{24m} - \frac{\left(\Delta^{(2)}\right)^2}{16nm^2}. \tag{4.12}$$

The stability parameter n is introduced to stabilise the time evolution of the propagator for small quark masses. It has to be chosen such that $\left|1 - \frac{H_0}{2n}\right| < 1$. In the free theory this can be shown to be equivalent to $n > 3/(2am)$; gluons are known to relax this bound slightly [89].

The heavy-quark Green function satisfies the simple evolution equation

$$G(\boldsymbol{x}, \tau; \boldsymbol{x}', \tau') = K(\tau) G(\boldsymbol{x}, \tau - 1; \boldsymbol{x}', \tau') \tag{4.13}$$

which can be solved recursively.

Mean field corrections

As the time derivative in (4.8) is realised by a backward finite difference there are no mean field corrections to wavefunction renormalisation. This can be seen by replacing all links in the momentum space propagator by u_0 [89],

$$G(p_0, \boldsymbol{p}) = \frac{1}{1 - u_0 e^{-ip_0} T(\boldsymbol{p})} \quad \text{with} \quad T(\boldsymbol{p}) = \left(1 - \frac{H_0(\boldsymbol{p})}{2n}\right)^{2n} \left(1 - \frac{\delta H(\boldsymbol{p})}{2}\right)^2. \tag{4.14}$$

After Fourier-transforming in the time coordinate,

$$G(\boldsymbol{p}; \tau, \tau') = (u_0 T(\boldsymbol{p}))^{\tau' - \tau} \equiv Z_\psi^{(\text{mf})} \exp\left[-(\tau' - \tau) E^{(\text{mf})}(\boldsymbol{p})\right] \tag{4.15}$$

the mean field wavefunction renormalisation $Z_\psi^{(\text{mf})} = 1$ and mean field energy $E^{(\text{mf})}(\boldsymbol{p}) = -\log[u_0 T(\boldsymbol{p})]$ can be read off.

4.1.2 Extension to a moving frame

In decays like $B \to \pi\ell\nu$, $B \to K^{(*)}\ell^+\ell^-$ or $B \to K^*\gamma$ the hadronic particles in the final state can have large momenta $\boldsymbol{p}_f$ in the rest frame of the B meson. This would introduce large discretisation errors which for $q^2 \to 0$ scale as some power of $\sim am/2$. It

is thus desirable to extend the formalism to a moving frame where $\boldsymbol{p}_f$ is reduced while still keeping the momentum fluctuations in the B meson small. As Lorentz boosts and the lattice discretisation do not commute, this will lead to an action which differs from the NRQCD action derived in the previous section.

The momentum of the b quark can parametrised as

$$p = mu + k \tag{4.16}$$

where u is usually chosen to be the velocity of the B meson, $u = p_B/m$. The four velocity is given by $u = (\gamma, \gamma\boldsymbol{v})$ with $\gamma = (1 - \boldsymbol{v}^2)^{-1/2}$. Only the residual momentum k is discretised on the lattice. The kinetic energy is then obtained by expanding

$$\begin{aligned} E_{\text{kin}} &= \sqrt{(m\gamma\boldsymbol{v} + \boldsymbol{k})^2 + m^2} - \gamma m \\ &= \boldsymbol{v}\cdot\boldsymbol{k} + \frac{\boldsymbol{k}^2 - (\boldsymbol{v}\cdot\boldsymbol{k})^2}{2\gamma m} + \ldots . \end{aligned} \tag{4.17}$$

From this the leading order "kinetic" part of the Hamiltonian in the moving frame can be read off as

$$H = -i\boldsymbol{v}\cdot\boldsymbol{D} - \frac{\boldsymbol{D}^2 - (\boldsymbol{v}\cdot\boldsymbol{D})^2}{2\gamma m}. \tag{4.18}$$

By choosing the frame velocity $\boldsymbol{v}$ antiparallel to the momentum $\boldsymbol{p}_f$ of the hadronic particle in the final state, the overall discretisation error can be minimised. When picking an optimal frame the following considerations have to be taken into account:

Discretisation errors. In the rest frame of the B the residual momentum $\boldsymbol{k}$ has a distribution with a width of order Λ_{QCD}. Due to momentum conservation the typical momentum of the light spectator quark is of the same order. The heavy quark is nonrelativistic and its energy has a distribution of width $\Lambda_{\text{QCD}}^2/(2m) \ll \Lambda_{\text{QCD}}$. In a moving frame the width of the momentum distribution is boosted to $\gamma\Lambda_{\text{QCD}}$. Both the NRQCD action used in this work and the ASQTad and HISQ actions have no discretisation errors of $\mathcal{O}(a^2\boldsymbol{k}^2)$ but there are $\mathcal{O}(\alpha_s a^2\boldsymbol{k}^2)$ errors due to radiative corrections. To get an estimate for the velocity of the optimal frame the momenta of all quarks are required to be of the same size. The *increase* in discretisation errors in the heavy meson is proportional to $\gamma^2\Lambda_{\text{QCD}}^2 - \Lambda_{\text{QCD}}^2$. Assuming that the two valence quarks in the final state meson share its momentum equally, each carrying $\boldsymbol{p}_f/2$, the increase in discretisation errors when going from zero momentum to $\boldsymbol{p}_f$ is proportional

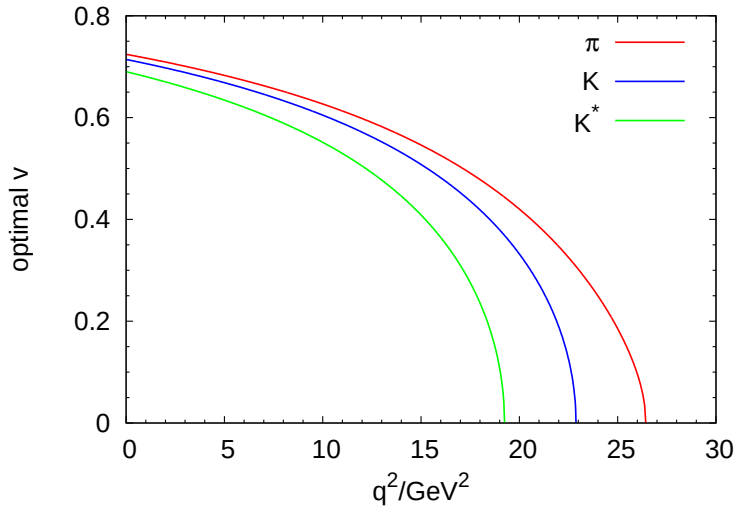

Figure 4.1: Optimal frame velocity as a function of q^2.

to $(|\boldsymbol{p}_f|/2)^2$. For a given q^2 the frame velocity v is chosen such that

$$(\gamma^2 - 1)\Lambda^2_{\rm QCD} \quad = \quad \frac{1}{4}|\boldsymbol{p}_f|^2. \tag{4.19}$$

In Fig. 4.1 I plot the optimal frame velocity as a function of q^2. At maximum recoil $v \approx 0.7$ will lead to minimal discretisation errors. It should be emphasised that this is only a very rough estimate, the optimal frame velocity depends on the details of the lattice calculation. I carry out all perturbative calculations in this thesis for a range of frame velocities.

Statistical errors. The precision of lattice calculations is also affected by statistical errors in the Monte Carlo evaluation of the path integral. Although in principle these can be made arbitrarily small by accumulating enough statistics they can be sizeable in practise due to limited computing power.

Consider the B meson two-point function $\langle B^\dagger(\boldsymbol{p}_B, 0)B(\boldsymbol{p}_B, \tau)\rangle$. For large τ this function decays like $\exp[-E_B(\boldsymbol{p}_B)\tau]$ where the energy $E_B(\boldsymbol{p}_B)$ increases with the frame velocity. The variance of the correlator is

$$\sigma^2(\tau) \quad = \quad \langle [B^\dagger(\boldsymbol{p}_B, 0)B(\boldsymbol{p}_B, \tau)][B^\dagger(\boldsymbol{p}_B, 0)B(\boldsymbol{p}_B, \tau)]^\dagger\rangle - \langle B^\dagger(\boldsymbol{p}_B, 0)B(\boldsymbol{p}_B, \tau)\rangle^2. \tag{4.20}$$

For large times τ this expression is dominated by the first term which can couple to a

combination of a heavy-heavy (HH) meson and a light-light meson (LL) at rest. The variance decays like $\exp[-(M_{HH}+M_{LL})\tau]$ and the signal-to-noise ratio is given by

$$\frac{\langle B^\dagger(\boldsymbol{p}_B,0)B(\boldsymbol{p}_B,\tau)\rangle}{\sigma(\tau)} \quad \propto \quad \exp\left[-\left(E_B(\boldsymbol{p}_B)-\frac{1}{2}M_{HH}-\frac{1}{2}M_{LL}\right)\tau\right] \tag{4.21}$$

which approaches zero for large τ. As $E_B(\boldsymbol{p}_B)$ increases with the frame velocity it will deteriorate more rapidly for large v. For the computation of B decay form factors statistical errors in the light meson two-point function and the three point function have to be taken into account as well.

The signal-to-noise ratio can be improved by constructing more elaborate sources which increase the overlap with the ground state. Zhaofeng Liu [30] uses random wall sources to reduce statistical errors in the two- and three-point functions.

Convergence of heavy quark expansion. The heavy quark expansion is only valid if the momentum scales in the final state are much smaller than the mass of the heavy quark. In particular the energy and the momentum of the final state meson with mass m_F are:

$$E' = \frac{p\cdot p'}{m_B} = \frac{m_B^2+m_F^2-q^2}{2m_B}, \qquad\qquad p' = \sqrt{E'^2-m_F^2}. \tag{4.22}$$

The energy and momentum are plotted as a function of the momentum transfer q^2 in Fig. 4.2. Hadronic form factors calculated at large q^2 have to be extrapolated to $q^2=0$ by using the phenomenological parametrisations discussed in section 2.3.5.

4.1.3 Derivation of the mNRQCD action

The derivation in section 4.1.1 can be extended to a moving frame of reference. This was first done by Kerryann Foley in her PhD thesis [90] and here I follow the analysis in [1]. An additional complication is that in a moving frame the FWT transformation introduces higher order time derivatives which would make the recursive calculation of heavy quark Greens functions impossible. These higher order derivatives can, however, be removed by an additional field transformation.

I work in two frames, one moving with velocity v and coordinates x and the rest frame of the B meson with coordinates x'. Quantities in the two frames are related by a Lorentz-transformation, $x=\Lambda x'$. The fields in full QCD are transformed by a spinorial boost, $\Psi(x)=S(\Lambda)\Psi'(x')$, $\overline{\Psi}(x)=\overline{\Psi}'(x')\overline{S}(\Lambda)$. In the rest frame the NRQCD action can be derived as above by a FWT transformation $\Psi'(x')=T'_{FWT}e^{-imx'^0\gamma^0}\tilde{\Psi}'(x')$. One arrives at the Lagrangian in (4.3) where all quantities are understood to be in the rest

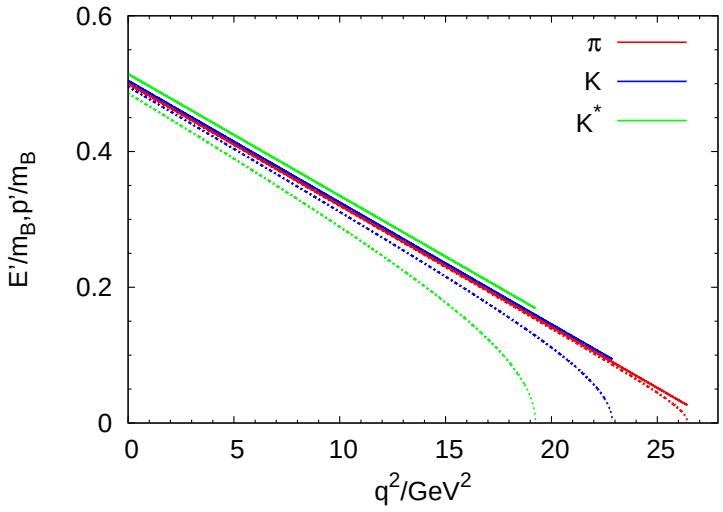

Figure 4.2: Energy E'/m_B (solid curves) and momentum p'/m_B (dashed) of the final state meson as a function of q^2.

frame, i.e. I replace $x \mapsto x'$, $\boldsymbol{E} \mapsto \boldsymbol{E}'$ etc.

I now express quantities in this frame by those in the moving frame where the action will be discretised. In this frame a new field $\tilde{\Psi}(x) \equiv \tilde{\Psi}'(x')$, $\overline{\tilde{\Psi}}(x) \equiv \overline{\tilde{\Psi}}'(x')$ is defined. This way the action kernel still commutes with γ^0. One finds

$$\begin{aligned} \mathscr{L} &= \overline{\tilde{\Psi}}(x)\Big[i\gamma^0 u\cdot D + \frac{(u\cdot D)^2 - D^2}{2m} + \frac{g}{2m}\boldsymbol{\Sigma}\cdot\boldsymbol{B}' \\ &\quad + \frac{g}{8m^2}\gamma^0\left(D^{\mathrm{ad}}_\mu u_\nu F^{\mu\nu} + i\epsilon_{jk\ell}\Sigma^j\Lambda^\mu{}_k\{D_\mu, E'_\ell\}\right)\Big]\tilde{\Psi}(x). \end{aligned} \tag{4.23}$$

For ease of notation not all chromodynamic fields have been expressed in the moving frame. Higher order time derivatives in the Lagrangian are removed by a set of field transformations. To this end the Lagrangian is written as

$$\mathscr{L} = \gamma\overline{\tilde{\Psi}}\left[\mathcal{O}_0 + \frac{1}{\gamma m}\mathcal{O}_1 + \frac{1}{(\gamma m)^2}\mathcal{O}_2\right]\tilde{\Psi} + \mathcal{O}(1/m^3) \tag{4.24}$$

with

$$\begin{aligned} \mathcal{O}_0 &= i\gamma^0(D_0 + \boldsymbol{v}\cdot\boldsymbol{D}), \\ \mathcal{O}_1 &= \frac{1}{2}\left((u\cdot D)^2 - D^2\right) + \frac{g}{2}\boldsymbol{\Sigma}\cdot\boldsymbol{B}', \\ \mathcal{O}_2 &= \frac{g}{2}\gamma\gamma^0\left(D^{\mathrm{ad}}_\mu u_\nu F^{\mu\nu} + i\epsilon_{jk\ell}\Sigma^j\Lambda^\mu{}_k\{D_\mu, E'_\ell\}\right). \end{aligned} \tag{4.25}$$

Time derivatives in $\mathcal{O}_1$ are removed by a field transformation

$$\tilde{\Psi} = \exp\left(\frac{1}{\gamma m}U\right)\tilde{\Psi}_{(1)}, \qquad \overline{\tilde{\Psi}} = \overline{\tilde{\Psi}}_{(1)}\exp\left(\frac{1}{\gamma m}U\right). \tag{4.26}$$

The Lagrangian in the new fields is

$$\gamma\overline{\tilde{\Psi}}_{(1)}\left[\mathcal{O}_0 + \frac{1}{\gamma m}\mathcal{O}_{(1)1} + \frac{1}{(\gamma m)^2}\mathcal{O}_{(1)2}\right]\tilde{\Psi}_{(1)} \tag{4.27}$$

with new operators

$$\begin{aligned}\mathcal{O}_{(1)1} &= \mathcal{O}_1 + \{U, \mathcal{O}_0\} \\ \mathcal{O}_{(1)2} &= \mathcal{O}_2 + \{U, \mathcal{O}_1\} + U\mathcal{O}_0 U + \frac{1}{2}\{U^2, \mathcal{O}_0\}.\end{aligned} \tag{4.28}$$

By choosing $U = \frac{i}{4}\gamma^0\left[(\gamma^2-1)D_0 + (\gamma^2+1)\boldsymbol{v}\cdot\boldsymbol{D}\right]$ all time derivatives are removed from $\mathcal{O}_{(1)1}$. Time derivatives can be removed from the $1/m^2$ terms in the Lagrangian by an additional higher order field transformation

$$\tilde{\Psi}_{(1)} = \exp\left(\frac{1}{(\gamma m)^2}V\right)\tilde{\Psi}_{(2)}, \qquad \overline{\tilde{\Psi}}_{(1)} = \overline{\tilde{\Psi}}_{(2)}\exp\left(\frac{1}{(\gamma m)^2}V\right). \tag{4.29}$$

The explicit expression of V can be found in [1].

Finally the fields are rescaled by a factor $1/\sqrt{\gamma}$ to normalise the coefficient of the leading order kinetic term to one,

$$\tilde{\Psi}_{(2)} = \frac{1}{\sqrt{\gamma}}\Psi_v, \qquad \overline{\tilde{\Psi}}_{(2)} = \frac{1}{\sqrt{\gamma}}\overline{\Psi}_v. \tag{4.30}$$

Again it turns out that a further kinetic operator has to be added to include all terms to $\mathcal{O}(v_{\text{rel}}^4)$ in heavy-heavy power counting. The missing term is obtained by expanding the relativistic dispersion relation

$$\begin{aligned}E_{\text{kin}} &= \sqrt{(\gamma m\boldsymbol{v}+\boldsymbol{k})^2 + m^2} - \gamma m \\ &= \boldsymbol{v}\cdot\boldsymbol{k} + \frac{1}{2\gamma m}\left(\boldsymbol{k}^2 - (\boldsymbol{v}\cdot\boldsymbol{k})^2\right) + \frac{1}{4\gamma^2 m^2}\left(-\{\boldsymbol{v}\cdot\boldsymbol{k}, \boldsymbol{k}^2\} + 2(\boldsymbol{v}\cdot\boldsymbol{k})^3\right) \\ &\quad + \frac{1}{8\gamma^3 m^3}\left(-\boldsymbol{k}^4 + 3\{\boldsymbol{k}^2, (\boldsymbol{v}\cdot\boldsymbol{k})^2\} - 5(\boldsymbol{v}\cdot\boldsymbol{k})^4\right) + \ldots.\end{aligned} \tag{4.31}$$

Some terms are written as anticommutators as this is how they would arise from a field transformation. The operator

$$\frac{1}{8\gamma^3 m^3}\left(\boldsymbol{D}^4 - 3\{\boldsymbol{D}^2, (\boldsymbol{v}\cdot\boldsymbol{D})^2\} + 5(\boldsymbol{v}\cdot\boldsymbol{D})^4\right) \tag{4.32}$$

has to be added to the Lagrangian. The continuum Lagrangian in Euclidean space is

$$\begin{aligned}
\mathscr{L} &= \overline{\Psi}_v \Big[\gamma^0 D_4 - i\gamma^0 \boldsymbol{v}\cdot\boldsymbol{D} - \frac{\boldsymbol{D}^2 - (\boldsymbol{v}\cdot\boldsymbol{D})^2}{2\gamma m} - \frac{g}{2\gamma m}\boldsymbol{\Sigma}\cdot\boldsymbol{B}' \\
&- \frac{i}{4\gamma^2 m^2}\gamma^0 \left(\{\boldsymbol{v}\cdot\boldsymbol{D}, \boldsymbol{D}^2\} - 2(\boldsymbol{v}\cdot\boldsymbol{D})^3 \right) \\
&+ \frac{g}{8m^2}\gamma^0 \Big(i\boldsymbol{D}^{\mathrm{ad}}\cdot\boldsymbol{E} + \boldsymbol{v}\cdot(\boldsymbol{D}^{\mathrm{ad}}\times\boldsymbol{B}) \Big) \\
&- \frac{g}{8\gamma m^2}\gamma^0 \boldsymbol{\Sigma}\cdot(\boldsymbol{D}\times\boldsymbol{E}' - \boldsymbol{E}'\times\boldsymbol{D}) \\
&+ \frac{g}{8(1+\gamma)m^2}\gamma^0 \{\boldsymbol{v}\cdot\boldsymbol{D}, \boldsymbol{\Sigma}\cdot(\boldsymbol{v}\times\boldsymbol{E}')\} \\
&- \frac{(2-\boldsymbol{v}^2)g}{16m^2}\gamma^0 (D_4^{\mathrm{ad}} + i\boldsymbol{v}\cdot\boldsymbol{D}^{\mathrm{ad}})(\boldsymbol{v}\cdot\boldsymbol{E}) \\
&- \frac{ig}{4\gamma^2 m^2}\gamma^0 \{\boldsymbol{v}\cdot\boldsymbol{D}, \boldsymbol{\Sigma}\cdot\boldsymbol{B}'\} \\
&- \frac{1}{8\gamma^3 m^3}\left(\boldsymbol{D}^4 - 3\{\boldsymbol{D}^2, (\boldsymbol{v}\cdot\boldsymbol{D})^2\} + 5(\boldsymbol{v}\cdot\boldsymbol{D})^4 \right) \Big] \Psi_v .
\end{aligned} \tag{4.33}$$

The action can be discretised as in the nonmoving case. Again the Hamiltonian is split into two parts and the kernel is written as in (4.8), with operators

$$H_0 = -i\boldsymbol{v}\cdot\boldsymbol{\Delta}^{\pm} - \frac{\Delta^{(2)} - \Delta_v^{(2)}}{2\gamma m}, \tag{4.34}$$

$$\begin{aligned}
\delta H &= -\frac{i}{4\gamma^2 m^2}\left(\left\{ \Delta^{(2)}, \boldsymbol{v}\cdot\boldsymbol{\Delta}^{\pm} \right\} - 2\Delta_v^{(3)} \right) \\
&- \frac{1}{8\gamma^3 m^3}\Big(\left(\Delta^{(2)}\right)^2 - 3\left\{ \Delta^{(2)}, \Delta_v^{(2)} \right\} + 5\Delta_v^{(4)} \Big) \\
&- \frac{g}{2\gamma m}\boldsymbol{\sigma}\cdot\tilde{\boldsymbol{B}}' \\
&- \frac{g}{8\gamma m^2}\boldsymbol{\sigma}\cdot\left(\tilde{\boldsymbol{\Delta}}^{\pm}\times\tilde{\boldsymbol{E}}' - \tilde{\boldsymbol{E}}'\times\tilde{\boldsymbol{\Delta}}^{\pm} \right) \\
&- \frac{ig}{4\gamma^2 m^2}\left\{ \boldsymbol{v}\cdot\tilde{\boldsymbol{\Delta}}^{\pm}, \boldsymbol{\sigma}\cdot\tilde{\boldsymbol{B}}' \right\} \\
&+ \frac{g}{8(\gamma+1)m^2}\left\{ \boldsymbol{v}\cdot\tilde{\boldsymbol{\Delta}}^{\pm}, \boldsymbol{\sigma}\cdot(\boldsymbol{v}\times\tilde{\boldsymbol{E}}') \right\} \\
&+ \frac{g}{8m^2}\Big(i(\boldsymbol{\Delta}^{\pm}\cdot\tilde{\boldsymbol{E}} - \tilde{\boldsymbol{E}}\cdot\boldsymbol{\Delta}^{\pm}) + \boldsymbol{v}\cdot(\boldsymbol{\Delta}^{\mathrm{ad}}\times\tilde{\boldsymbol{B}}) \Big) \\
&- \frac{(2-\boldsymbol{v}^2)g}{16m^2}\left(\Delta_4^{\mathrm{ad}} + i\boldsymbol{v}\cdot\boldsymbol{\Delta}^{\mathrm{ad}} \right)\left(\boldsymbol{v}\cdot\tilde{\boldsymbol{E}} \right) \\
&+ \delta H_{\mathrm{corr.}}.
\end{aligned} \tag{4.35}$$

$\delta H_{\text{corr.}}$ contains spatial and temporal correction terms which can be derived as for the NRQCD action. For $v \neq 0$ the first term in H_0 is of $\mathcal{O}(p)$ instead of $\mathcal{O}(p^2)$. It is thus necessary to expand up to order H_0^4 in (4.10). Neglecting operators of order 5 and higher one finally obtains the correction

$$\begin{aligned}
\delta H_{\text{corr.}} &= \tilde{H}_0 - H_0 \\
&- \frac{1}{4n}\Bigg(-(\boldsymbol{v}\cdot\boldsymbol{\Delta}^{\pm})^2 + \frac{\left\{i\boldsymbol{v}\cdot\boldsymbol{\Delta}^{\pm}, \Delta^{(2)}\right\} - 2i\Delta_v^{(3)}}{2\gamma m} \\
&\qquad + \frac{(\Delta^{(2)})^2 - \left\{\Delta^{(2)}, \Delta_v^{(2)}\right\} + \Delta_v^{(4)}}{4\gamma^2 m^2}\Bigg) \\
&- \frac{1}{12n^2}\Bigg(i\Delta_v^{(3)} + \frac{\left\{\Delta^{(2)}, \Delta_v^{(2)}\right\} - 3\Delta_v^{(4)}}{2\gamma m} \\
&\qquad + \frac{(\boldsymbol{v}\cdot\boldsymbol{\Delta}^{-})\Delta^{(2)}(\boldsymbol{v}\cdot\boldsymbol{\Delta}^{+}) + (\boldsymbol{v}\cdot\boldsymbol{\Delta}^{+})\Delta^{(2)}(\boldsymbol{v}\cdot\boldsymbol{\Delta}^{-})}{4\gamma m}\Bigg) \\
&- \frac{(2+n)}{64n^3}\Delta_v^{(4)}.
\end{aligned} \tag{4.36}$$

This concludes the derivation of the mNRQCD action on the lattice. It can be used both for heavy-heavy and heavy-light systems. This has the advantage of providing additional tests of the formalism. The heavy-quark propagator can be computed very efficiently in nonperturbative simulations so that the calculation of heavy-heavy meson spectra and decay constants gives more precise results which can be compared to experimental measurements (see also Figs. 5.8 and 5.9 for a comparison between heavy-heavy and heavy-light results).

The mNRQCD action derived above is correct up to $\mathcal{O}(\Lambda_{\text{QCD}}^2/m^2)$ in heavy-light- and to $\mathcal{O}(v_{\text{rel}}^4)$ in heavy-heavy power counting. Relative errors in the energy splitting of heavy-heavy systems are of $\mathcal{O}(v_{\text{rel}}^4)$ which is around 1% in the bottomonium system where $v_{\text{rel}}^2 \sim 0.1$. In [93] it is argued that the errors might be smaller for splittings between states with similar wave functions. Spin dependent terms enter at sub-leading order and spin dependent splittings have larger relative errors.

4.2 Radiative corrections

Beyond tree level the nonrelativistic lattice actions derived in the previous sections are modified by quantum corrections. The ultraviolet behaviour of the effective heavy quark action is different from relativistic QCD in the continuum which will introduce $\mathcal{O}(\alpha_s)$ errors when the action is used to calculate hadronic quantities. Knowing these systematic uncertainties is important for various reasons:

- Hadronic observables, as for example the Υ-spectrum [93], have reached very high accuracy and it is important to account for radiative corrections of the heavy quark action. In [93] a detailed error budget is presented, radiative corrections are of the same order as relativistic corrections. In chapter 5 I calculate these radiative corrections for the mNRQCD action.

- For the same reason radiative corrections to matrix elements in heavy-light decays, which are of the same size as $1/m$ corrections in the heavy quark expansion, need to be calculated. This is the subject of chapter 7.

- By relating the bare parameters in the lattice theory to those in continuum QCD, the fundamental parameters of QCD can be extracted from lattice simulations. This requires the calculation of renormalised quantities, as for example the heavy quark mass. This is discussed in more detail in section 4.2.2.

In principle the parameters of the heavy quark action can be tuned nonperturbatively by adjusting them such that they reproduce experimental results. This, however, can be very time consuming as it has to be done for each individual lattice and reduces the predictive power of the theory, in particular if the action contains a large number of operators as is the case for mNRQCD.

The RI-MOM scheme [94] can be used to calculate the renormalisation constants of transition operators by fixing the on-shell matrix elements to their value at tree level. The results can then be converted to the $\overline{MS}$ scheme with continuum perturbation theory.

In this work I use a perturbative method on the lattice and compute renormalisation constants order by order in the strong coupling constant. This is legitimate as it corrects for the mismatch in the ultraviolet at momenta $p \gtrsim \pi/a$ where QCD is perturbative; for typical lattices $a \lesssim 0.1$ fm so that $\pi/a \gtrsim 6$ GeV and the strong coupling constant is small, $\alpha_s(\pi/a) \approx 0.2$.

4.2.1 Perturbative matching

The perturbative matching procedure works as follows: Calculate the radiative corrections $1 + \alpha_s c_j^{(1),\mathrm{lat}} + \ldots$ to an on-shell quantity on the lattice. For example, corrections to the kinetic terms in the action can be extracted from the two-point function of the heavy quark, the coefficient of the chromomagnetic interaction term $\boldsymbol{\sigma} \cdot \boldsymbol{B}$ can be obtained from considering scattering off an external chromomagnetic field. For an external current, such as the heavy-light tensor current, compute an on-shell matrix element. The expansion of the same quantity in continuum perturbation theory is $1 + \alpha_s c_j^{(1),\mathrm{con}} + \ldots$. The coefficient of the corresponding operator in the lattice action

or the heavy-light current can then be corrected according to

$$c_j \;\mapsto\; c_j \left(1 + \alpha_s (c_j^{(1),\mathrm{con}} - c_j^{(1),\mathrm{lat}}) + \dots\right). \tag{4.37}$$

4.2.2 Renormalisation parameters from high-β simulations

In addition to calculating hadronic quantities lattice simulations can be used to extract the fundamental parameters of QCD. This has been done in [95] for the strong coupling constant. After tuning the bare lattice parameters an ultraviolet Wilson loop is measured. The same quantity can be calculated in lattice perturbation theory as a power series in the strong coupling constant and the series is well behaved if the coupling in the potential scheme [79] (see also (3.10)) is used instead of the bare lattice coupling. By inverting this relation α_V can be extracted from the simulation and converted to the $\overline{MS}$ scheme using conventional continuum perturbation theory. $\alpha_s^{\overline{MS}}(M_Z)$ obtained in this way agrees very well with the experimental measurement and has an error of comparable size.

In [74, 96, 97] the charm quark mass is calculated by relating the bare lattice mass to an on-shell mass which can then be converted to the mass in the $\overline{MS}$ scheme.

To achieve sufficient accuracy it is necessary to extend the perturbative calculation beyond one loop level. In the continuum this is straightforward and the bottleneck is the lattice calculation. As the gauge potential enters via the link $U_\mu = \exp[igaA_\mu]$ there are additional vertices with an arbitrary number of gluons which increases the number of diagrams that need to be evaluated (see for example Fig. 1 in [96]). For highly improved actions, such as HISQ, the Feynman rules are very complicated and evaluation of all these diagrams in diagrammatic perturbation theory is computationally very expensive. Instead, a different method has been suggested in [98]: by simulating in the weak coupling limit, which corresponds to high values of the parameter β, and fitting to a polynomial in the strong coupling constant, the coefficients in the perturbative expansion can be extracted. This has been done very successfully for a wide range of quantities, including Wilson loops [99, 100, 101], the expectation value of the mean link used for tadpole improvement [102], the additive mass renormalisation in HQET [103, 99, 100] and quark masses for simple lattice actions [98, 104, 105, 106].

Calculation of the two loop renormalisation parameters of the HISQ is under way [96, 97, 74]. Here a mixed strategy is used: The high-β simulations are carried out in the quenched limit. At $\mathcal{O}(\alpha_s)$ fermionic loops do not contribute, so the coefficient $c^{(1)}$ from the high-β fit will be the same as from diagrammatic perturbation theory which provides a very useful check of both methods. The two loop coefficients $c^{(2)}_{\mathrm{gluonic}}$ from high-β simulations contains gluonic contributions only. However, there are only

Figure 4.3: Fermionic two-loop contributions to the heavy quark self-energy

four diagrams with fermion loops, see Fig. 4.3, which can be readily evaluated in diagrammatic perturbation theory. In addition, if the one loop coefficient from diagrammatic perturbation theory is known for finite lattice size, it can be used as an input to stabilise the higher order fit of lattice data. This is usually done with a constrained fitting technique [107] as it is expected that higher order coefficients are of order one if a well behaved expansion parameter such as α_V is used.

In section 5.2 I calculate the one loop renormalisation coefficients of the mNRQCD action on a finite lattice. The results are used to stabilise the high-β fits from simulations by Horgan and Lee [108].

Nonperturbative tunnelling

Whereas the techniques in section 4.2.3 assume an infinite lattice with a gluon mass as an infrared regulator, nonperturbative high-β simulations are carried out on a lattice with finite extent $L^3 \times T$. In a small box the gluon action has an additional $Z(N)$ symmetry. If each link in a given lattice plane is multiplied by the same element $z = e^{i\pi n/N}$ from the centre of the gauge group closed paths of links remain unchanged. This transformation changes the value of the Polyakov line

$$P_\mu \quad = \quad \mathrm{tr}\{U_\mu(x)U_\mu(x+\hat{\mu})\ldots U_\mu(x+L\hat{\mu})\} \tag{4.38}$$

according to $P_\mu \mapsto zP_\mu$. Although the expectation value P_μ, averaged over a large number of gauge configurations, is zero, its effective potential will have N minima in the complex plane which are related by multiplication by $e^{i\pi/N}$. The perturbative expansion is around one of these minima and on a finite lattice there will be nonperturbative tunnelling between the vacua. If one wants to extract the perturbative expansion from high-β simulations it is desirable to suppress these effects. As demonstrated in [100] this can be achieved by using twisted boundary conditions [109, 110]. An additional advantage is that this introduces a lower momentum cutoff which acts as a regulator for infrared divergences in the perturbative calculation.

Twisted boundary conditions

Twisted boundary conditions are imposed on the gauge fields by requiring that the shifted link at $x + L\hat{\nu}$ satisfies

$$U_\mu(x + L\hat{\nu}) \quad = \quad \Omega_\nu U_\mu(x)\Omega_\nu^{-1} \qquad \text{with} \quad \nu = 1, 2. \tag{4.39}$$

As the order of shifts does not matter the two twist matrices have to satisfy

$$\Omega_1\Omega_2 \quad = \quad z\Omega_2\Omega_1 \qquad \text{with} \quad z = e^{2\pi i/N} \in \text{Centre}\{SU(N)\}. \tag{4.40}$$

As explained in appendix B this changes the spectrum of the chromodynamic field A_μ. In addition to the lattice momentum, which is a multiple of $2\pi/L$, an additional twisted component proportional to $2\pi/(NL)$ is introduced. The colour degrees of freedom are replaced by the twist vector.

4.2.3 Lattice perturbation theory

In principle, perturbative calculations on the lattice are not different from those in the continuum, in fact the lattice can just be seen as yet another regularisation scheme (which, however, breaks Lorentz invariance which is only restored in the continuum limit). As in the continuum the calculation proceeds in two steps:

1. Extract the Feynman rules from the action.

2. Integrate the Feynman diagrams over phase space.

In practise, however, the lattice calculation is more complicated. The lattice action is written in terms of the links variables U_μ instead of the gauge fields A_μ which generates additional vertices with an arbitrary number of gluons. As Lorentz symmetry is broken the Feynman rules, even for simple actions, are very complicated. Writing down the Feynman rules of state-of-the-art highly improved actions as ASQTad or HISQ by hand becomes an extremely tedious task. Due to the complicated structure of the integrand it is also usually impossible to solve the resulting integrals analytically.

These problems can be overcome by automating the extraction of Feynman rules and evaluating the resulting integrals numerically by using a Monte Carlo integrator such as Vegas [111].

Automated generation of Feynman rules

Originally the idea was laid out by Lüscher and Weisz [109] and in [112, 113] an implementation of the algorithm in Python is described; the package is commonly

known as HiPPy. I adapted the code to the actions that are needed for the perturbative calculations carried out in this work.

Due to gauge invariance all terms in the fermionic action can be written as a linear combination of fermion fields connected by a Wilson line, $\overline{\psi}(x)L(x,y;U)\psi(y)$. $L(x,y;U)$ is a product of link variables which can be expanded in the strong coupling constant g

$$U_\mu(x) \;=\; \exp\left[agA_\mu(x+\frac{a}{2}\hat{\mu})\right] = \sum_{r=0}^{\infty} \frac{\left[agA_\mu(x+\frac{a}{2}\hat{\mu})\right]^r}{r!} \tag{4.41}$$

where anti-Hermitian generators of $SU(N)$ are used. In momentum space the Wilson line is then given in terms of gluon fields as

$$\begin{aligned} L(x,y;U) \;=\; & \sum_r \frac{(ag)^r}{r!} \sum_{k_1,\mu_1,a_1} \cdots \sum_{k_r,\mu_r,a_r} \tilde{A}^{a_1}_{\mu_1}(k_1)\ldots\tilde{A}^{a_r}_{\mu_r}(k_r) \\ & \times\; V_r(k_1,\mu_1,a_1;\ldots;k_r,\mu_r,a_r). \end{aligned} \tag{4.42}$$

Inserting this in the action and using the Fourier expansion of the fermion fields with momenta p and q (and colour indices b and c) it can be shown that the Feynman rule for the emission of r gluons is $-g^r V_{F,r}$ where the vertex function $V_{F,r}$ is the symmetrised product of a colour factor $C_{F,r}$ and a reduced vertex function $Y_{F,r}$,

$$\begin{aligned} & V_{F,r}(p,b;q,c;k_1,\mu_1,a_1;\ldots;k_r,\mu_r,a_r) = \\ & \quad \frac{1}{r!}\sum_{\sigma\in\mathcal{S}_r} \sigma\cdot C_{F,r}(b,c;a_1,\ldots,c_r)\;\sigma\cdot Y_{F,r}(p,q;k_1,\mu_1;\ldots;k_r,\mu_r). \end{aligned} \tag{4.43}$$

$\mathcal{S}_r$ is the group of permutations of r objects. The reduced vertex function can always be written as an exponential

$$Y_{F,r}(p,q;k_1,\mu_1;\ldots;k_r,\mu_r) \;=\; \sum_{n=1}^{n_r} \Gamma_n f_n e^{\frac{i}{2}(p\cdot x+q\cdot y+k_1\cdot v_1^{(n)}+\cdots+k_r\cdot v_r^{(n)})} \tag{4.44}$$

where Γ_n is the Dirac structure and f_n the amplitude associated with a specific term. This implies that the Feynman rules can be encoded in a list of entities of the form $(\mu_1,\ldots,\mu_r;x,y;v_1,\ldots,v_r;f,\Gamma)$ which is generated by the Python code and stored in a file. As reduced vertex functions are always given as sums of exponentials, derivatives with respect to particle momenta can be obtained by algebraic manipulations. This avoids numerical instabilities which might arise when approximating derivatives by finite differences.

The entity list is generated by the HiPPy code by repeated application of the

convolution formulae in [114]: for an action of the form $\overline{\psi}AB\psi$ the Feynman rule for one gluon emission can be obtained as the Feynman rule for no gluon emission from A and one gluon emission from B plus the rule for one gluon from A and no gluon emission from B. For two gluons there are three cases: (1) both gluons come from A, (2) one gluon comes from A and the other from B or (3) both from B. The generalisation to an arbitrary number of gluons is obvious. These formulae translate into rules for adding and multiplying entity lists for simple blocks in the action. The advantage of carrying out the convolution in the HiPPy code is that the list is automatically compressed: if two entries differ only in their amplitudes, they can be replaced by a single entry with the sum of the amplitudes.

Sometimes it might also be advantageous to carry out the convolution in the numerical integration code, in this case the HiPPy code writes a set of vertex files for each factor in the action. For example, the kernel of the mNRQCD action is split into blocks as

$$1 - ABCBA \tag{4.45}$$

with $A = \left(1 - \frac{\delta H}{2}\right)$, $B = \left(1 - \frac{H_0}{2n}\right)^n$ and $C = U_4^\dagger$. Combining these factors in the Fortran code is advantageous if no further compression is possible. In the case of mNRQCD, AB and BA sit on different time slices. A and B are stored separately as the combined vertex file would be very large. In addition, as B mainly contains spin dependent terms, not much compression between A and B is expected. The colour structure is implicit and can be dealt with in the integration routine.

Extending the algorithm to gluonic actions is described in [112, 113].

Link smearing. The construction of highly improved actions often involves repeated smearing of the link variables; in particular the HISQ action is constructed from the "Fat7"-smeared, reunitarised links $\mathcal{UF}_\mu U_\mu$. Using the expansion algorithm described above will be practically impossible due to the large number of terms generated. Instead the expansion can be performed in two steps [115]. The reunitarised link $U_\mu^{\mathrm{Fat7R}}(x) \in U(3)$ is parametrised by fields $B_\mu(x)$ in the Lie algebra,

$$U_\mu^{\mathrm{Fat7R}}(x) \;=\; \mathcal{UF}_\mu U_\mu(x) = \exp\left[agB_\mu\left(x + \frac{a}{2}\hat{\mu}\right)\right] \tag{4.46}$$

and Wilson lines can be expanded in terms of these fields as in (4.42) with $\tilde{A}_\mu^a(k) \mapsto \tilde{B}_\mu^a(k)$. The Feynman rules for the emission of B_μ-fields can then be extracted from vertex functions $V_{F,r}^{(B)}$ as described above. To obtain the Feynman rules for the gluon-

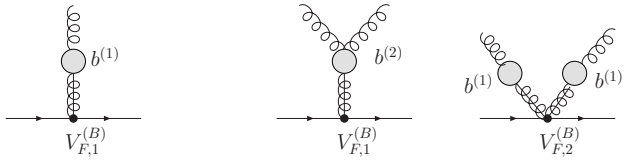

Figure 4.4: Diagrams for one- and two-gluon emission in actions with link smearing.

fields, $\tilde{B}_\mu$ has to be expressed in terms of the $\tilde{A}_\mu$,

$$\tilde{B}_\mu(k) \;=\; b_\rho^{(1)}(k)\tilde{A}_\rho(k) + \sum_{k_1+k_2=k} b^{(2)}_{\rho_1\rho_2}(k_1,k_2)\tilde{A}_{\rho_1}(k_1)\tilde{A}_{\rho_2}(k_2) + \ldots \qquad (4.47)$$

which introduces additional form factors $b_\rho^{(1)}$, $b^{(2)}_{\rho_1\rho_2}$, etc. This is represented graphically in Fig. 4.4. The rule for one-gluon-emission is given by the vertex function $V_{F,1}^{(B)}$ multiplied by the form factor $b^{(1)}$. Two gluons can either come from a two-gluon vertex $V_{F,2}^{(B)}$ multiplied by two form factors $b^{(1)}$ or by the emission of one B_μ gluon which is converted into an A_μ-field by $b^{(2)}$. In addition to the vertex files with the reduced vertices the PYTHON-code also writes an "algebra" file which contains the form factors $b^{(j)}$. In the numerical integration code these are then combined according to the rules outlined above. This procedure can be iterated for multiple levels of smearing.

Hard wired gluon propagator

To speed up the code I wrote a hard-wired version of the gluon propagator. The general form of the gauge action is [116]

$$S_g \;=\; -\beta \sum_{x,\mu>\nu} \left(c_0^G P_{\mu\nu} + c_1^G (R_{\mu\nu} + R_{\nu\mu}) \right) \qquad \text{with} \quad c_0^G + 8c_1^G = 0. \qquad (4.48)$$

where the 1×1 plaquette and 2×1 rectangle are given in (3.9). In particular $c_1^G = 0$ corresponds to the Wilson action, $c_1^G = -\frac{1}{12}$ is the tree level Symanzik improved action.

The action is expanded in terms of the gluon fields A_μ in momentum space. The quadratic term can only be inverted after adding a gauge fixing term $\xi^{-1}\sum_\mu(\hat{k}_\mu A_\mu(x))^2$ with $\hat{k}_\mu = 2\sin(k_\mu/2)$. Common choices are $\xi = 1$ (Feynman gauge) and $\xi = 0$ (Landau gauge). It is also possible to work in a noncovariant gauge by fixing the gauge with $\xi^{-1}\sum_j(\Delta_j^{(\pm)}A_j(x))^2$ where j runs over spatial values only, Coulomb gauge corresponds to $\xi = 0$. To regulate infrared singularities a gluon mass term $\lambda^2\delta_{\mu\nu}$ can be added.

The two-point function $M_\xi^{(0)}(k)$ is a 4×4 matrix whose entries are functions of the gluon momenta. This matrix can be inverted using a computer-algebra package such as MATHEMATICA but it turns out that it is advantageous to first write it as $M_\xi^{(0)} = M^{(0)} +$

$g_\xi(k)P$ where only $g_\xi(k)$ depends on the gauge fixing parameter. $P_{\mu\nu}(k) = \hat{k}_\mu \hat{k}_\nu / \hat{k}^2$ is a projector on a one-dimensional subspace. As P commutes with $M^{(0)}$ the propagator is given by

$$G_{\xi,\mu\nu}(k) = \left(\frac{1}{g_\xi(k)} - \frac{1}{g_{\xi=1}(k)} \right) P_{\mu\nu}(k) + \frac{f^{(N)}_{\mu\nu}(k)}{f^{(D)}(k)} \tag{4.49}$$

where the functions $f^{(N)}_{\mu\nu}(k)$ and $f^{(D)}(k)$ are obtained by inverting $M^{(0)}_{\xi=1}(k)$.

A similar decomposition is possible in Coulomb gauge.

For the Symanzik improved gluon action hard wiring leads to a speed up of a factor 5 in the gluon propagator if no derivatives of the propagator need to be calculated. With derivatives up to second order there is no difference in speed. It should be noted that by suitable routing of the external momentum through the diagram it is often not necessary to know derivatives of the gluon propagator.

4.3 Numerical evaluation of Feynman diagrams

A set of FORTRAN routines is used to evaluate the Feynman integrals. Specific modules read the vertex files written by the HIPPY code and construct Feynman rules for fundamental vertices according to (4.44).

For example, the function `vert_qqg(k,lorentz,colour)` will return the vertex $(T^c)_{ba} V_\mu(k_2, k_1; k_3)$ for emission of a gluon with momentum k_3, colour c and Lorentz index μ by a quark with initial momentum k_1 and final momentum k_2. The colour of the quark changes from a to b. `k=(/`k_1, k_2, k_3`/)`, `lorentz=(/`μ`/)` and `colour=(/`a, b, c`/)` are FORTRAN arrays.

The colour structure is dealt with in the FORTRAN integration routines and the same reduced vertex files, generated by the HIPPY code, can be used for both periodic and twisted boundary conditions. In the first case the Clebsch Gordon coefficient is given by a combination of colour matrices. On a twisted lattice a small twist vector is added to the lattice momentum and the colour factors are replaced by traces over the Γ_n matrices introduced in appendix B. For example, the gluon r-point function will have a Clebsch Gordon coefficient of

$$C_r(k_1, \ldots, k_r) = \frac{1}{N} \left(\mathrm{tr}\{\Gamma_{n_1} \ldots \Gamma_{n_r}\} + (-1)^r \, \mathrm{tr}\{\Gamma_{n_r} \ldots \Gamma_{n_1}\} \right). \tag{4.50}$$

The function `tayl_vert_qqg(k,lorentz,colour)` returns a TAYLUR object [117] which, in addition to the value of the vertex, also stores its derivatives with respect to the particle momenta. To this end each momentum vector object has a field `route` that stores the fraction of this momentum which will be differentiated. If, for example,

one is interested in $V_\mu(k+p/2, k-p/2; -k)$ and derivatives with respect to p one would set `k%route=0`, `p%route=1` and call the vertex routine with `(k-p/2,k+p/2,-k)`. The Leibniz rule is implemented by overloading multiplication of TaylUR objects.

Finally, the integral over momentum space is carried out by the stochastic integration algorithm described in the following section.

4.3.1 Stochastic integration

Without loss of generality, consider the following integral over the n-dimensional unit volume $\Omega = [0,1]^n$

$$I = \int_\Omega d^n\boldsymbol{x} f(\boldsymbol{x}), \tag{4.51}$$

where $f(\boldsymbol{x})$ is an arbitrary, not necessarily analytical or even continuous function.

If the points $\boldsymbol{x}_1, \ldots, \boldsymbol{x}_M$ are randomly chosen from Ω according to the probability density $p(\boldsymbol{x})$ with $p(\boldsymbol{x}) > 0$, $\int_\Omega p(\boldsymbol{x}) = 1$ the integral I can be approximated by the sum

$$S = \frac{1}{M}\sum_{i=1}^{M} \frac{f(\boldsymbol{x}_i)}{p(\boldsymbol{x}_i)} \overset{M\to\infty}{\longrightarrow} I. \tag{4.52}$$

The variance of S depends on the choice of $p(\boldsymbol{x})$ and, for nonnegative f, can be minimised by choosing p similar to f. Of course the choice of $p(\boldsymbol{x})$ is limited by the requirement that it has to be possible to generate points distributed according to $p(\boldsymbol{x})$. In practise the construction of a suitable $p(\boldsymbol{x})$ may be difficult. The Vegas-algorithm, invented by G. P. Lepage [118, 111], recursively constructs a suitable distribution $p(\boldsymbol{x})$ for arbitrary $f(\boldsymbol{x})$ and is applicable under very general circumstances.

In one dimension the algorithm works a follows:

Initialise. Divide $[0,1]$ into N intervals by choosing a number of points $0 = x_0 < x_1 < \cdots < x_{N-1} < x_N = 1$ and construct a density $p(x)$ as

$$p(x) = \frac{1}{N\Delta x_i} \qquad x_{i-1} \le x < x_i \qquad \text{where } \Delta x_i = x_i - x_{i-1}. \tag{4.53}$$

In the beginning the points will usually be distributed uniformly in $[0,1]$.

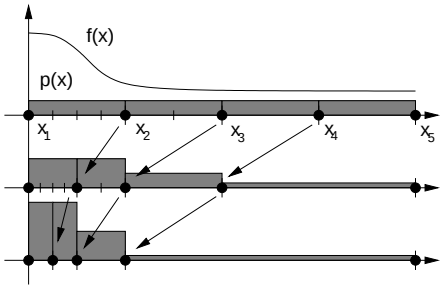

Figure 4.5: VEGAS grid refinement in one dimension.

Step 1. Now, choose N_{eval} points x distributed according to this density[1] and evaluate S according to (4.52) using $p(x)$. Also, for each interval, compute

$$\overline{f}_i \;=\; \sum_{x\in[x_{i-1},x_i)} |f(x)| \approx \frac{1}{\Delta x_i}\int_{x_{i-1}}^{x_i} dx\;|f(x)|. \tag{4.54}$$

Step 2. Divide each interval Δx_i into $m_i + 1$ subintervals where

$$m_i \;=\; K\frac{\overline{f}_i \Delta x_i}{\sum_j \overline{f}_j \Delta x_j}. \tag{4.55}$$

K is typically about 1000.

Step 3. To keep the same number of intervals in each iteration subintervals have to merged so that there are N intervals in the end. Using this new division of the unit interval construct a new $p(x)$ and continue with Step 1.

In this way the probability distribution $p(x)$ is constructed iteratively. $p(x)$ will be large where $f(x)$ is large and the sampling points for the evaluation of the integral are concentrated there.

Steps 1 to 3 are iterated N_{iter} times. In each iteration the integrand is evaluated N_{eval} times. A combined estimate $\overline{S}$ of the integral with error $\sigma_{\overline{S}}$ can be obtained from the individual evaluations S_k, σ_k in each iteration

$$\overline{S} = \sigma_{\overline{S}}^2 \sum_{k=1}^{N_{\text{iter}}} \frac{S_k}{\sigma_k^2}, \qquad\qquad \frac{1}{\sigma_{\overline{S}}^2} = \sum_{k=1}^{N_{\text{iter}}} \frac{1}{\sigma_k^2}. \tag{4.56}$$

Before recording S_k and σ_k, usually $N_{\text{iter}}^{(\text{warm})}$ thermalisation steps are performed, each with $N_{\text{eval}}^{(\text{warm})}$ evaluations of the integrand to allow $p(x)$ to converge against the

[1] This can be done by generating points y uniformly distributed in the interval $[0,1]$ and mapping them to x by $y \in \left[\frac{i-1}{N}, \frac{i}{N}\right) \to x_{i-1} + \Delta x_i(Ny + 1 - i)$.

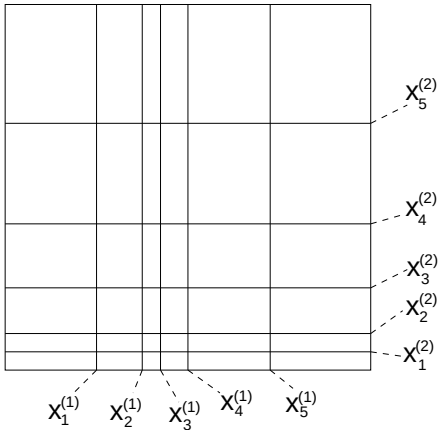

Figure 4.6: VEGAS grid in two dimensions.

optimal density.

In n dimensions the unit interval in each dimension is divided into N subintervals, i.e. the following product ansatz for $p(\boldsymbol{x})$ is used

$$p(\boldsymbol{x}) \quad = \quad p_1(x_1)\dots p_n(x_n). \tag{4.57}$$

By varying the $p_k(x_k)$ subject to the condition that the probability distribution is normalised it can be shown that the variance is minimised if

$$p_k(x_k) \quad \sim \quad \left(\widehat{\int_\Omega} d^{n-1}\boldsymbol{x}\frac{f^2(\boldsymbol{x})}{\widehat{p(\boldsymbol{x})}}\right)^{1/2} \tag{4.58}$$

is chosen. $\widehat{\int_\Omega}$ denotes an integral over all variables except x_k and $\widehat{p(\boldsymbol{x})}$ is the product in (4.57) without the factor $p_k(x_k)$.

Hence the same algorithm as above can be used in each dimension if $\overline{f}_i^{(k)}$ is defined as follows

$$\begin{aligned}\left(\overline{f}_i^{(k)}\right)^2 \quad &= \quad \sum_{x_k\in[x_{i-1}^{(k)},x_i^{(k)})} \widehat{\sum_{\boldsymbol{x}}}\frac{f^2(\boldsymbol{x})}{\widehat{p^2(\boldsymbol{x})}} \\ &\approx \quad \frac{1}{\Delta x_i^{(k)}}\int_{x_{i-1}^{(k)}}^{x_i^{(k)}} dx_k \widehat{\int_\Omega} d^{n-1}\boldsymbol{x}\frac{f^2(\boldsymbol{x})}{\widehat{p(\boldsymbol{x})}}\end{aligned} \tag{4.59}$$

where the $x_i^{(k)}$ divide the unit interval in dimension k , see Fig. 4.6, and $\widehat{\sum_{\boldsymbol{x}}}$ stands for summation in all dimensions except k. $\boldsymbol{x} = (x_1,\dots,x_k,\dots,x_n)$ denotes the points generated according to the distribution $p(\boldsymbol{x})$ in each iteration step.

By using the product ansatz in (4.57) for the probability density integrands with peaks or ridges parallel to a coordinate axis can be sampled very efficiently by adjusting the VEGAS grid. This is not possible for integrands with, for example, a diagonal ridge as in this case the points would still be distributed uniformly on each coordinate axis. Sometimes this problem can be solved by changing the coordinate system. In my implementation of the integration code both spherical and cartesian coordinates can be used for the spatial loop momentum.

Peaked integrands

In perturbative lattice calculations the integrand can be very peaked if the integration contour passes close to poles in a propagator. In principle VEGAS will adapt to this by adjusting the grid and sampling around this peak. However, often this problem only arises in the infrared region of the integrand where the integration contour is pinched by the gluon poles. For small momenta the lattice integrand reduces to the continuum expression whose IR behaviour can be calculated analytically. It is then possible to construct a subtracted integrand where the peaks cancel point by point and the errors in the VEGAS integral are reduced:

$$\begin{aligned} I &= \underbrace{\int \frac{d^4k}{(2\pi)^4} f(k)}_{\text{IR divergent}} \\ &= \underbrace{\int \frac{d^4k}{(2\pi)^4} \left(f(k) - f^{(\text{sub})}(k) \right)}_{\text{IR finite, VEGAS}} + \underbrace{\int \frac{d^4k}{(2\pi)^4} f^{(\text{sub})}(k)}_{\text{IR divergent, analytical}} \\ &= \overline{I} + I^{(\text{sub})}. \end{aligned} \tag{4.60}$$

The subtraction integrand satisfies $f^{(\text{sub})}(k) \to f(k)$ for $k \to 0$ and $I^{(\text{sub})}$ can be calculated analytically.

Parallelisation

Due to the complexity of lattice Feynman rules the function evaluations in perturbative calculations can be computationally very expensive. To accumulate sufficient statistics for the perturbative integrals I use a parallel version of the VEGAS algorithm where the workload is shared between a large number of processors[2]. To minimise communications the processors are divided into farms, see Fig. 4.7. The layout is chosen such that nodes

[2]By processor I mean a fundamental unit which can run a single process. This is not to be confused with an individual node in a cluster or a CPU which can have multiple cores, each of which might accommodate a process.

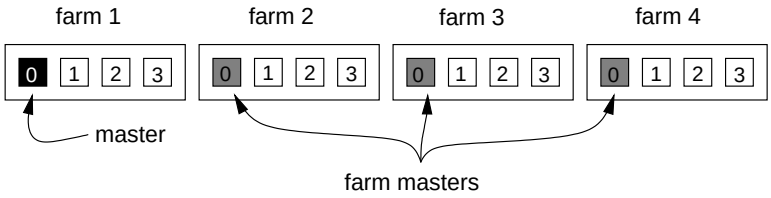

Figure 4.7: Processor layout in parallel VEGAS. Each farm has a master processor (grey) and the final result is accumulated by the global master (black).

within a farm can communicate with each other much faster than with nodes in other farms. This can for example be the case if they are located on the same physical chip. The integral is evaluated independently by each farm and the results are finally combined and collected on the master node.

The calculations for this work were carried out on the "Eddie" cluster of the Edinburgh Compute and Data Facility [119]. In its original setup this high performance cluster consists of 128 worker nodes, each with two dual core CPUs. The nodes are standard IBM x3550 servers with 3.0 GHz Intel Xeon processors and 8 MB of RAM. In the beginning of 2008 the system was upgraded with 118 additional worker nodes with two quad core CPUs each, giving 1456 cores in total. The nodes are connected by a gigabit Ethernet network. 60 dual core nodes are in addition equipped with a faster Infiniband interconnect with a latency of 2.11ns and bandwith of 956MB/s which is about eight times the bandwith of the ethernet connection. In its current setup the total computing power of the cluster is around 10 TFlops [119].

4.3.2 Mode summation

On a finite lattice with twisted boundary conditions the integral over the loop momentum is replaced by a discrete momentum sum,

$$\int \frac{d^4k}{(2\pi)^4} f(\boldsymbol{k}, k_4) \quad \mapsto \quad \frac{1}{L^3 T} \sum_{j_1,\ldots,j_3=0}^{L-1} \sum_{j_4=0}^{T-1} f\left((j_1, j_2, j_3)\frac{2\pi}{L}, j_4 \frac{2\pi}{T}\right). \tag{4.61}$$

Instead of summing over colour indices an additional sum over the twisted part of the momentum vector has to be performed. This is most conveniently done within each individual diagram routine for a given untwisted momentum. I adapted the mode summation (4.61) for parallel machines by splitting the sum between processors.

For very large lattices performing the mode summation directly can be computationally very expensive. The sum has an exact representation as an integral over a

piecewise defined function,

$$\frac{1}{L}\sum_{j=1}^{L-1} f\left(\frac{2\pi j}{L}\right) \;=\; \int_{-\pi}^{\pi}\frac{dk}{2\pi}\overline{f}(k) \tag{4.62}$$

with

$$\overline{f}(k) \;=\; f\left(\frac{2\pi j}{L}\right) \quad \text{for} \quad \frac{2\pi j}{L} \le k < \frac{2\pi(j+1)}{L},\;\; 0 \le j \le L-1. \tag{4.63}$$

This integral can then be evaluated in VEGAS.

Chapter 5

Heavy quark renormalisation parameters

As argued in section 4.2 renormalisation of the operators in the heavy quark action is important to predict the properties of heavy mesons to high accuracy. In this chapter I show how the renormalisation constants can be obtained in lattice perturbation theory. I give results for the leading kinetic terms in the mNRQCD action.

Horgan and Lee [108] calculate renormalisation parameters at higher loop order by simulations in the weak coupling regime of the lattice theory. To suppress nonperturbative tunnelling between equivalent $Z(3)$ vacua they use twisted boundary conditions [109, 110]. These have the additional advantage of introducing a lower momentum cutoff and thus regulate potential infrared singularities in a gauge invariant way. Adapting the perturbative calculation for twisted boundary conditions is straightforward. I compare my results to those from high-β simulations and find good agreement. In addition, my one loop results are used as an input for the fitting of high-β results as a polynomial in the strong coupling constants to stabilise the fit and extract higher order terms.

5.1 Leading order kinetic terms in mNRQCD

Beyond tree level the coefficients of the operators in H_0, the kinetic part of the Hamiltonian (see (4.34)), deviate from unity. They can be expanded in the strong coupling constant $c_j = 1 + \alpha_s c_j^{(1)} + \ldots$ where the c_j are adjusted such that the heavy quark dispersion relation agrees with the continuum expression. This requires the calculation of renormalisation parameters $Z_j = 1 + \alpha_s \delta Z_j + \ldots$ both in the continuum and on the lattice.

5.1.1 Renormalisation parameters

I calculate the renormalisation parameters of the heavy quark action on the lattice to $\mathcal{O}(\alpha_s)$ in mean field improved lattice perturbation theory.

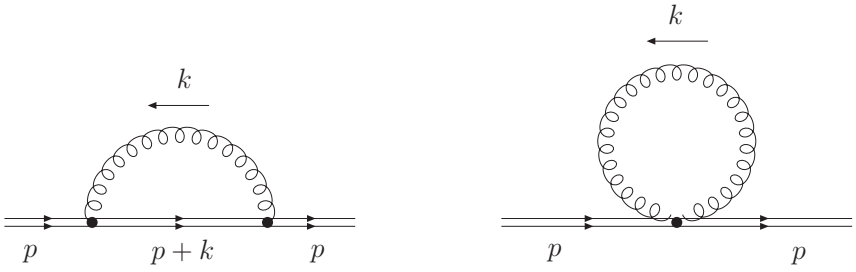

Figure 5.1: One loop corrections to the heavy quark self-energy.

In particular I discuss the following quantities:

- heavy quark wavefunction renormalisation Z_ψ,
- zero point energy shift E_0,
- renormalisation of the frame velocity Z_v and
- mass renormalisation Z_m.

In the continuum the frame velocity is a symmetry parameter and does not get renormalised. On the lattice there exists a separate theory for each choice of the frame velocity, which can now be interpreted as a coupling constant in the action that is renormalised by quantum fluctuations. The zero point energy, which vanishes in the continuum due to Lorentz invariance, is nonzero on the lattice and indeed diverges like $1/a$ for dimensional reasons. Of particular interest is the renormalisation Z_p of the external momentum $\boldsymbol{P} = \gamma M \boldsymbol{v}$ as this quantity is not renormalised in the continuum due to reparametrisation invariance [66, 67, 120].

On the lattice all renormalisation parameters can be extracted from the corrections to the heavy quark self-energy Σ. At $\mathcal{O}(\alpha_s)$ this quantity is given by the one loop diagrams in Fig. 5.1 and counterterms that come from mean field improving the action by replacing $U_\mu \mapsto U_\mu/u_0$. The derivation in the following sections was laid out in [90, 121] and has been taken from [1].

Wavefunction renormalisation. The wavefunction renormalisation, Z_ψ, can be computed as follows: At tree-level the heavy quark propagator is

$$G_0(z) = \frac{z}{z - z_0}\,, \tag{5.1}$$

where $z = e^{ip_4}$ and

$$z = z_0 \equiv \left(1 - \frac{H_0(\boldsymbol{p})}{2n}\right)^{2n} \left(1 - \frac{\delta H(\boldsymbol{p})}{2}\right)^2 \tag{5.2}$$

is the on-shell (tree-level) value. At one loop the propagator is

$$G^{-1}(z) = G_0^{-1}(z) - \alpha_s \Sigma(z) = Z_\psi^{-1} \frac{z - z_1}{z}$$

where $\alpha_s\Sigma(z)$ is the self-energy (to order α_s), containing both rainbow and tadpole diagrams. Let the new "one-loop" on-shell value be z_1, which is the solution of

$$G^{-1}(z_1) = G_0^{-1}(z_1) - \alpha_s \Sigma(z_1) = 0\,. \tag{5.3}$$

Expanding $\Sigma(z)$ around the new on-shell value and using $z_1 - z_0 = \mathcal{O}(\alpha_s)$ the wavefunction renormalisation is, at one-loop,

$$Z_\psi \simeq 1 + \alpha_s \Big[\Sigma + z\,\frac{\partial \Sigma}{\partial z}\Big]_{z=z_0} \;=\; 1 + \alpha_s \Big[\Sigma - i \frac{\partial \Sigma}{\partial p_4}\Big]_{\text{on shell}}. \tag{5.4}$$

Other renormalisation parameters. To derive expressions for the other renormalisation parameters I use the following argument from [122].

At tree level one has in momentum space (up to $\mathcal{O}(p^2)$):

$$\begin{aligned} H_0(\boldsymbol{p}) &= \boldsymbol{v}\cdot\boldsymbol{p} + \frac{\boldsymbol{p}^2 - (\boldsymbol{v}\cdot\boldsymbol{p})^2}{2\gamma m} + \ldots, \\ \delta H(\boldsymbol{p}) &= -\frac{1}{4n}(\boldsymbol{v}\cdot\boldsymbol{p})^2 + \ldots. \end{aligned} \tag{5.5}$$

By combining this with (5.2) and expanding in $\boldsymbol{p}$ I find that the pole in the tree level propagator (5.1) is given by

$$\omega = \omega_0(\boldsymbol{p}) = \boldsymbol{v}\cdot\boldsymbol{p} + \frac{\boldsymbol{p}^2 - (\boldsymbol{v}\cdot\boldsymbol{p})^2}{2\gamma m} \tag{5.6}$$

where $\omega = -ip_4$ is the energy in Minkowski space. At one loop the inverse propagator is

$$G(\boldsymbol{p},\omega)^{-1} \;=\; 1 - e^{\omega - \omega_0(\boldsymbol{p})} - \alpha_s \Sigma(\boldsymbol{p}, \omega_0(\boldsymbol{p}))$$

so that

$$\begin{aligned} \omega(\boldsymbol{p}) &= \omega_0(\boldsymbol{p}) - \alpha_s \Sigma(\boldsymbol{p}, \omega_0(\boldsymbol{p})) \\ &\equiv \boldsymbol{v}_R \cdot \boldsymbol{p} + \frac{\boldsymbol{p}^2 - (\boldsymbol{v}_R \cdot \boldsymbol{p})^2}{2\gamma_R m_R} - \alpha_s \delta\omega(\boldsymbol{p}) \end{aligned} \tag{5.7}$$

with $\boldsymbol{v}_R = Z_v \boldsymbol{v}$, $\gamma_R = (1 - \boldsymbol{v}_R^2)^{-1/2}$, $m_R = Z_m m$ and $\alpha_s \delta\omega(\boldsymbol{p}) = E_0 + \ldots$. Here and in the following I assume that the boost velocity points in one of the lattice directions, which guarantees that only the magnitude of $\boldsymbol{v}$ is renormalised. The self energy can now be expanded in small momenta

$$\Sigma(\boldsymbol{p}, \omega) = \Sigma_0(\omega) + \Sigma_v(\omega)\ \boldsymbol{v} \cdot \boldsymbol{p} + \Sigma_1(\omega) \frac{\boldsymbol{p}^2}{2\gamma m} + \ldots$$

and the renormalisation constants can be expressed in terms of the coefficients $\Sigma_j^{(\ell)}$ in the expansion

$$\Sigma_j(\omega) = \sum_{\ell=0}^{\infty} \Sigma_j^{(\ell)} \omega^\ell.$$

I find

$$\begin{aligned} E_0 &= \alpha_s \Sigma_0^{(0)}, \\ Z_v &= 1 - \alpha_s (\Sigma_0^{(1)} + \Sigma_v^{(0)}), \\ Z_m &= 1 + \alpha_s ((\Sigma_0^{(1)} + \Sigma_1^{(0)}) + \gamma^2 \boldsymbol{v}^2 (\Sigma_v^{(0)} + \Sigma_0^{(1)})), \end{aligned} \tag{5.8}$$

and have for the renormalisation of the external momentum $\boldsymbol{p}_{\mathrm{ext},R} = \gamma_R m_R \boldsymbol{v}_R \equiv Z_p \boldsymbol{p}_{\mathrm{ext}}$ with

$$Z_p = 1 + \alpha_s (\Sigma_1^{(0)} - \Sigma_v^{(0)}). \tag{5.9}$$

In actual calculations I consider the real parts of parameters $\Sigma_j^{(\ell)}$. It is convenient to

define

$$\begin{aligned}
\Omega_0 &= \mathrm{Re}\,\Sigma_0^{(0)} = \Sigma(0), \\
\Omega_1 &= -\mathrm{Re}\,\Sigma_0^{(1)} = \mathrm{Im}\,\frac{\partial\Sigma}{\partial p_4}\bigg|_{p=0}, \\
\Omega_2 &= \mathrm{Re}\,\Sigma_1^{(0)} = \gamma m \mathrm{Re}\,\frac{\partial^2\Sigma}{\partial p_z^2}\bigg|_{p=0}, \\
\Omega_v &= \mathrm{Re}\,\Sigma_v^{(0)} = \frac{1}{v}\mathrm{Re}\,\frac{\partial\Sigma}{\partial p_x}\bigg|_{p=0},
\end{aligned} \tag{5.10}$$

taking the frame velocity $\boldsymbol{v}$ to point in the x-direction. The renormalisation parameters are then expressed as

$$\begin{aligned}
Z_\psi &= 1 + \alpha_s(\Omega_0 + \Omega_1), \\
E_0 &= \alpha_s\Omega_0, \\
Z_v &= 1 - \alpha_s(\Omega_v - \Omega_1), \\
Z_m &= 1 + \alpha_s(\Omega_2 - \Omega_1) + \alpha_s(\Omega_v - \Omega_1)\boldsymbol{v}^2\gamma^2\,, \\
Z_p &= 1 - \alpha_s(\Omega_v - \Omega_2).
\end{aligned} \tag{5.11}$$

Dispersion relation and energy shift. The renormalised dispersion relation in mNRQCD is given by

$$\omega(\boldsymbol{k}) \;=\; \boldsymbol{v}_R\cdot\boldsymbol{k} + \frac{\boldsymbol{k}^2 - (\boldsymbol{v}_R\cdot\boldsymbol{k})^2}{2\gamma_R m_R} - \delta\omega(\boldsymbol{k}) + \ldots \tag{5.12}$$

with

$$\delta\omega(\boldsymbol{k}) \;=\; E_0 + A\frac{(\boldsymbol{v}_R\cdot\boldsymbol{k})^2}{2\gamma_R m_R}. \tag{5.13}$$

This has to be compared to the corresponding expression in QCD

$$\begin{aligned}
\omega^{(\mathrm{QCD})}(\boldsymbol{k}) &= \sqrt{(\gamma_R m_R \boldsymbol{v}_R + \boldsymbol{k})^2 + m_R^2} \\
&= \gamma_R m_R + \boldsymbol{v}_R\cdot\boldsymbol{k} + \frac{\boldsymbol{k}^2 - (\boldsymbol{v}_R\cdot\boldsymbol{k})^2}{2\gamma_R m_R} + \ldots
\end{aligned} \tag{5.14}$$

from which one obtains a shift in the zero point energy of a heavy quark of

$$\begin{aligned}
C_v &= \omega^{(\mathrm{QCD})}(\boldsymbol{k}=0) - \omega(\boldsymbol{k}=0) \\
&= \gamma_R m_R + E_0.
\end{aligned} \tag{5.15}$$

I write $C_v = \gamma m(1 + \alpha_s \delta C_v + \dots)$ and the one loop correction is given by

$$\delta C_v \quad = \quad \Omega_2 - \Omega_1 + \frac{\Omega_0}{\gamma m}. \tag{5.16}$$

The shift C_v and the renormalisation of the external momentum can be obtained nonperturbatively by computing the energy $E_v(\boldsymbol{k})$ of a heavy-heavy system which can be written as

$$E_v(\boldsymbol{k}) + 2C_v \quad = \quad \sqrt{(2Z_p \gamma m \boldsymbol{v} + \boldsymbol{k})^2 + M_{\text{kin}}^2} + \dots. \tag{5.17}$$

Perturbative and nonperturbative results are compared in section 5.1.7.

5.1.2 One loop integrals

The one loop integrals in Fig. 5.1 are evaluated using automated perturbation theory as described in section 4.2.3. The two integrands for the self-energy are

$$\begin{aligned} f^{(\text{lat})}_{\text{rainbow}} &= 4\pi \; wh^{(1)a}_{\mu}(k+p,-p,k) D^{(0)}_h(k+p) wh^{(1)a}_{\nu}(p,-k-p,k) D^{(0)}_{g,\mu\nu}(k), \\ f^{(\text{lat})}_{\text{tadpole}} &= 4\pi \; wh^{(2)}_{\mu\nu}(p,-p,k,-k) D^{(0)}_{g,\mu\nu}(k). \end{aligned} \tag{5.18}$$

Here $wh^{(1)a}_{\mu}(k_1,k_2;q_1)$ and $wh^{(2)ab}_{\mu\nu}(k_1,k_2;q_1,q_2)$ denote the one- and two-gluon vertices. $D^{(0)}_h(k)$ is the heavy quark propagator and $D^{(0)}_{g,\mu\nu}(k)$ the gluon propagator.

Derivatives with respect to external momenta, which are needed for the calculation of the Ω_j, are implemented in the TaylUR code by overloading the Leibniz rule.

Contour shift

On an infinite Euclidean lattice the energy integral is over the unit circle $|z| = 1$ with $z = e^{ip_4}$. As can be seen from Fig. 5.2 the heavy quark pole can move outside the unit circle and the integration contour has to be deformed to ensure that no poles are crossed when Wick rotating back to Minkowski space. For certain momentum configurations it will be necessary to integrate over the circle $|z| = R$ with

$$1 < \max\{z_-, |z_h|\} < R < z_+. \tag{5.19}$$

To satisfy this condition I shift the integration contour to $z \to Rz$ with $R = \sqrt{|z_h z_+|}$ for $z_- < |z_h|$. As a precaution, the code stops in case a loop momentum with $|z_h| \geq z_+$ is encountered and Wick rotation to Minkowski space is not possible. However, in all integrals I calculated this has never been the case. Keeping the contour as far away

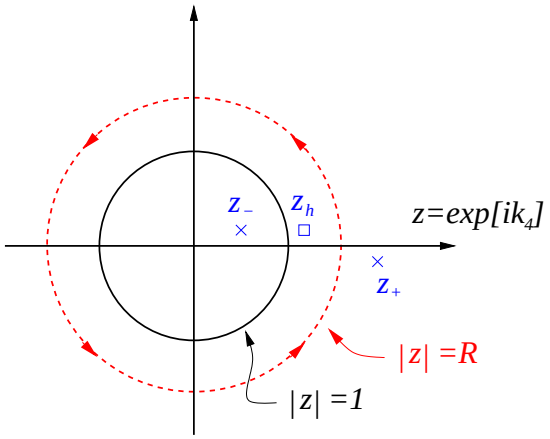

Figure 5.2: Poles in the complex z plane and integration contour (dashed circle). If $|z_h| > z_-$ I shift the contour halfway between the heavy quark- and larger gluon pole according to $z \mapsto Rz$ with $R = \sqrt{|z_h z_+|}$.

from the poles as possible avoids large peaks in the integrand which potentially spoil the convergence of the VEGAS integration.

The heavy quark action contains no higher order time derivatives and it is easy to obtain an explicit expression for the position of the pole in the propagator

$$D_h^{(0)}(v,k) \;=\; \frac{1}{1 - z^{-1}\left(1 - \frac{H_0(v,\boldsymbol{k})}{2n}\right)^{2n}\left(1 - \frac{\delta H(v,\boldsymbol{k})}{2}\right)^2}.$$

The denominator vanishes for

$$z = z_h \;\equiv\; \left(1 - \frac{H_0(v,\boldsymbol{k})}{2n}\right)^{2n}\left(1 - \frac{\delta H(v,\boldsymbol{k})}{2}\right)^2. \tag{5.20}$$

For unimproved Wilson gluons the propagator in Feynman gauge is

$$D_{g,\mu\nu}^{(0)}(k) \;=\; \delta_{\mu\nu}\left(4\sum_{\rho=0}^{3}\sin^2\frac{k_\rho}{2} + \lambda^2\right)^{-1} = \delta_{\mu\nu}\left(2 - z - z^{-1} + \hat{\boldsymbol{k}}^2 + \lambda^2\right)^{-1} \tag{5.21}$$

with $\hat{\boldsymbol{k}}^2 \equiv 4\sum_{j=1}^{3}\sin^2\frac{k_j}{2}$.

From this the two gluon poles can be obtained

$$z_\pm \;=\; \frac{1}{2}\left(2 + \hat{\boldsymbol{k}}^2 + \lambda^2 \pm \sqrt{(\hat{\boldsymbol{k}}^2 + \lambda^2)(\hat{\boldsymbol{k}}^2 + \lambda^2 + 4)}\right) \in \mathbb{R}. \tag{5.22}$$

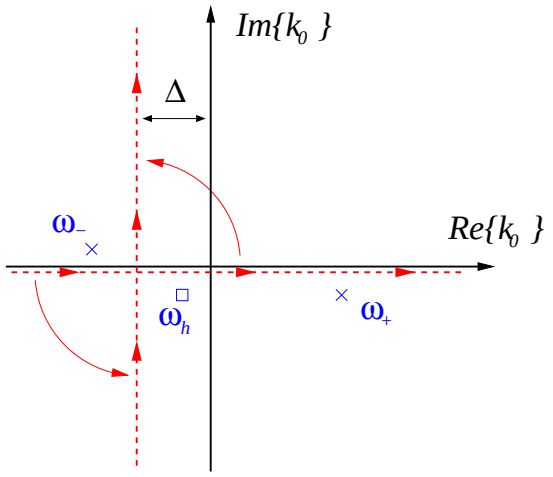

Figure 5.3: Wick rotation to Euclidean space for HQET in the continuum. If the heavy quark pole ω_h lies to the left of the imaginary axis the contour has to be rotated around $-\Delta = \boldsymbol{v}\cdot\boldsymbol{k} - \delta$.

In particular these poles satisfy $z_+ z_- = 1$ and it is not necessary to shift the contour for the tadpole diagram.

For improved gluon actions there are additional poles $z_\pm^{(\mathrm{imp})}$ but, as argued in appendix C.1 they always satisfy $|z_-^{(\mathrm{imp})}| < z_-$ and $z_+ < |z_+^{(\mathrm{imp})}|$ so that even in this case it is sufficient to satisfy the condition (5.19).

The additional contour shift which is necessary in Euclidean space has been discussed in the literature [123, 124]. As can be seen from Fig. 5.3 it is possible to rotate the deformed contour back to Minkowski space in a way that preserves causality. For negative $\boldsymbol{v}\cdot\boldsymbol{k}$ the heavy quark pole lies to the left of the imaginary axis and it is necessary to rotate around $-\Delta = \boldsymbol{v}\cdot\boldsymbol{k} - \delta$ instead of the origin of the k_0 plane.

Infrared divergences

The constants Ω_j are potentially infrared divergent. In all gauge invariant renormalisation parameters such as Z_v, Z_m and E_0 these divergences cancel. However, it turns out that Ω_1, Ω_2 and Ω_v itself and the wavefunction renormalisation in Feynman gauge are logarithmically divergent. To deal with these divergences note that any lattice theory has the same infrared behaviour as the corresponding continuum theory. It is therefore easier to analyse the corresponding continuum integrals. After performing the integral over the temporal momentum as a contour integral it can be shown that the tadpole diagram and all its derivatives are infrared finite. The same is true for the rainbow diagram, however, its derivatives behave for low momentum as $\sim \int \frac{dk}{k}$ and are thus

logarithmically divergent. To regulate this divergence I introduce a finite gluon mass λ. The advantage of this approach is that the same method can be used to regulate the continuum QCD integral. It is crucial to use the same regulator to ensure that infrared divergences cancel in the matching coefficients. The infrared divergent part of $\Omega_{j\neq 0}$ is then

$$\Omega_{j\neq 0} \quad = \quad -\frac{2}{3\pi}\log a^2\lambda^2. \tag{5.23}$$

For wavefunction renormalisation in Feynman gauge I find the same IR divergence in continuum QCD (see (D.11)) and the matching coefficients are well defined in the limit $\lambda \to 0$.

The calculations in section 5.2 are carried out in a finite volume with twisted boundary conditions. This introduces a lower momentum cutoff and it is not necessary to use a finite gluon mass to regulate infrared divergences.

IR subtraction function for δZ_ψ

The infrared divergence will manifest itself in large peaks in the integrand which can potentially spoil the convergence of the VEGAS integration. To deal with the remaining infrared divergence in the wavefunction renormalisation I construct a suitable subtraction function. Note that in principle $f^{(\mathrm{sub})}$ is arbitrary as long as it: agrees with the lattice integrand for small loop momenta k; is ultraviolet-finite in $d = 4$ dimensions; and can be evaluated analytically. The resulting integral (which is *not* restricted to the Brillouin zone) is evaluated in appendix J.1 and gives

$$\delta Z_\psi^{(\mathrm{sub})} = -\frac{2}{3\pi}\log \lambda^2/m^2 + \mathcal{O}(\lambda/m). \tag{5.24}$$

This corresponds exactly to the logarithmic divergence found in (5.23). The subtracted integral $\delta\overline{Z}_\psi$ is evaluated numerically,

$$\begin{aligned} \delta Z_\psi \quad &= \quad \int \frac{d^4k}{(2\pi)^4}\left(\theta_{\mathrm{BZ}}(k) f^{(\mathrm{lat})}(k) - f^{(\mathrm{sub})}(k)\right) + \delta Z_\psi^{(\mathrm{sub})} \\ &\equiv \quad \delta\overline{Z}_\psi - \frac{2}{3\pi}\log a^2\lambda^2 \end{aligned} \tag{5.25}$$

where $\theta_{\mathrm{BZ}}(k)$ is equal to 1 inside the Brillouin zone and vanishes for any $|k_\mu| > \pi/a$.

Direct calculation for different gluon masses

The alternative way of isolating the IR divergent behaviour is to perform the integration for different values of λ and then obtain the desired $\log\lambda^2$ behaviour by numerically

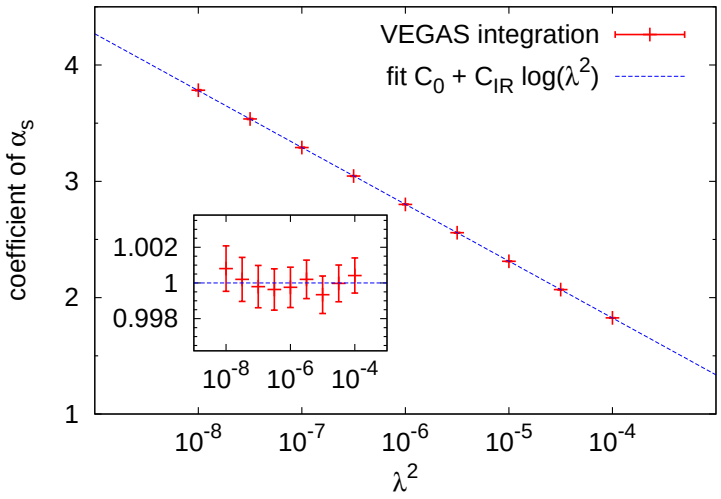

Figure 5.4: Wavefunction renormalisation (in Feynman gauge) for different values of the infrared regulator λ. I show a linear fit $C_0 + C_{\mathrm{IR}} \log \lambda^2$ with $\chi^2/\mathrm{dof} = 0.17$. The slope is $C_{\mathrm{IR}} = -0.21220(14) \approx -\frac{2}{3\pi}$ and in agreement with (5.23). In the inset I show the results normalised to the linear fit function. I use the simple heavy quark action defined in (5.26); the frame velocity is $v = 0.3$.

fitting a line through the points. In Fig. 5.4 I show the wavefunction renormalisation for λ^2 varying from 10^{-8} to 10^{-4}. Using a logarithmic scale on the horizontal axis I find a very clear linear behaviour, which demonstrates the desired dependence on $\log \lambda^2$. After fitting to $C_0 + C_{\mathrm{IR}} \log \lambda^2$, I obtain $C_0 = -0.1291(18)$ and $C_{\mathrm{IR}} = -0.21220(14)$. The coefficient of the logarithmic term is in excellent agreement with the analytical result $C_{\mathrm{IR}} = -2/(3\pi) = -0.21221$. The constant term has to be compared to the infrared finite part of the wavefunction renormalisation in Tab. 5.6.

This method can only be applied if VEGAS is able to cope with divergences of the integrand in the infrared region. For simple integrals, such as the wavefunction renormalisation in mNRQCD, this seems to be the case. As discussed in chapter 6, more severe infrared peaks prohibit the direct evaluation of other renormalisation parameters. Even for formally IR finite integrals subtraction functions need to be introduced. In addition, the evaluation of the integrand for different gluon masses and the subsequent fit requires additional computational resources and complicates the analysis. In this work I will not pursue this approach and always use a subtraction function where necessary.

5.1.3 Mean field corrections

As discussed in section 3.3.1 mean field corrections can be included by dividing each link in the action by its expectation value u_0. I work in Landau gauge and expand the link in a power series in the strong coupling constant, $u_0 = 1 - \alpha_s u_0^{(2)} + \ldots$. For the Wilson gluon action the first order coefficient has been evaluated to $u_0^{(2)} = 0.9735$ [102], for the Symanzik improved action the authors of [125] find $u_0^{(2)} = 0.750$. In perturbation theory mean field corrections are included as counterterms to the two-point function. I use the computer algebra package FORM [126] to replace each link in the kinetic part of the heavy quark action according to $U_\mu \mapsto U_\mu/u_0$, $U_\mu^\dagger \mapsto U_\mu^\dagger/u_0$ taking care to cancel adjacent links in the opposite direction, $U_\mu U_\mu^\dagger \mapsto 1$. Ideally this cancellation should be carried out after expanding the entire action kernel $K = 1 - \left(1 - \frac{\delta H}{2}\right)\left(1 - \frac{H_0}{2n}\right)^n U_4^\dagger \left(1 - \frac{H_0}{2n}\right)^n \left(1 - \frac{\delta H}{2}\right)$, I refer to this as "complete" cancellation. In the lattice simulation code for evaluating nonperturbative matrix elements this turns out to be prohibitively difficult. As it is important to use the same convention in both calculations, I choose to cancel adjacent links only within H_0 and δH separately, which I call "partial" cancellation. This does not imply that in this case mean field improvement is incomplete in any sense as it has to be understood as a prescription for improving the convergence of the perturbative series. Numerically the difference in the size of perturbative mean field improvement corrections between "complete" and "partial" cancellation is never more than around 10%, see for example Tab. 5.5.

After expanding $u_0 = 1 - \alpha_s u_0^{(2)} + \ldots$ and collecting the $\mathcal{O}(\alpha_s)$ terms in the action kernel, links are replaced according to $U_\mu \mapsto e^{ik_\mu}$, $U_\mu^\dagger \mapsto e^{-ik_\mu}$ and the constants $\Omega_j^{(\text{tadpole})}$ can be obtained by taking appropriate derivatives as in (5.10).

5.1.4 Results

Heavy quark actions

In addition to the full $\mathcal{O}(1/m^2, v_{\text{rel}}^4)$ mNRQCD action derived in section 4.1.3 I adapted the HIPPY code to generate Feynman rules for various other actions of varying complexity. In particular I use the following simple action with no interaction term δH. The Hamiltonian is defined by

$$H_0 = -i\boldsymbol{v}\cdot\boldsymbol{\Delta}^{\pm} - \frac{\Delta^{(2)} - \Delta_v^{(2)}}{2\gamma m}, \qquad \delta H = 0, \tag{5.26}$$

where all derivatives are unimproved. Note that this action differs from the one in [90, 121] by a more local discretisation of the $(\boldsymbol{v}\cdot\boldsymbol{D})^2$ term.

I calculate renormalisation constants both for the simple action in (5.26) and for

the full $\mathcal{O}(1/m^2, v_{\rm rel}^4)$ mNRQCD action. In the first case I work with the unimproved Wilson action whereas in the second case the gluon action is Symanzik improved. In both calculations I use $m = 2.8$, $n = 2$; the heavy quark mass corresponds to the one on coarse MILC lattices [93].

In appendix F I summarise additional results for an improved action which contains all $\mathcal{O}(1/m)$ terms.

Mean field corrections

I find the following analytical expressions for mean field corrections: for the simple action in (5.26) and "partial" cancellation they are

$$\begin{aligned}
\Omega_0^{(\rm tadpole)} &= -\Omega_1^{(\rm tadpole)} = u_0^{(2)}\Big(1+\frac{3-v^2}{\gamma m}\Big), \\
\Omega_2^{(\rm tadpole)} &= \Omega_v^{(\rm tadpole)} = -u_0^{(2)}\Big(2+\frac{2n-1}{2n}\ \frac{3-v^2}{\gamma m}\Big).
\end{aligned} \tag{5.27}$$

For the full $\mathcal{O}(1/m^2, v_{\rm rel}^4)$ mNRQCD action I obtain

$$\begin{aligned}
\Omega_0^{(\rm tadpole)} &= -\Omega_1^{(\rm tadpole)} \\
&= u_0^{(2)}\Bigg[1+7\frac{3-v^2}{6\gamma m}-\frac{3-6v^2+5v^4}{2\gamma^3 m^3}+\frac{1}{4n}\left(-v^2+\frac{-3+2v^2-v^4}{\gamma^2 m^2}\right) \\
&\qquad +\frac{1}{6n^2}\frac{-5v^2+3v^4}{\gamma m}-\frac{n+2}{16n^3}v^4\Bigg],
\end{aligned}$$

$$\begin{aligned}
\Omega_2^{(\rm tadpole)} &= -u_0^{(2)}\Bigg[\frac{5}{3}+7\frac{3-v^2}{6\gamma m}+\frac{3-3v^2}{\gamma^2 m^2}-\frac{3-6v^2+5v^4}{2\gamma^3 m^3} \\
&\qquad +\ \frac{1}{4n}\left(-v^2+\frac{-3+2v^2-v^4}{\gamma^2 m^2}\right)+\frac{1}{6n^2}\left(2v^2+\frac{-5v^2+3v^4}{\gamma m}\right) \\
&\qquad -\frac{n+2}{16n^3}v^4\Bigg],
\end{aligned}$$

$$\Omega_v^{(\rm tadpole)} = \Omega_2^{(\rm tadpole)} - u_0^{(2)}\left[\frac{2v^2}{\gamma^2 m^2}-\frac{v^2}{6n^2}\right].$$

For $v = 0$ these expressions reduce to the ones obtained in [92]. In both cases the difference between $\Omega_2^{(\rm tadpole)}$ and $\Omega_v^{(\rm tadpole)}$, which defines the renormalisation of the external momentum, is small. In appendix E I present the corresponding expressions for "complete" cancellation. As an additional check of my derivation I verified that I

λ^2	E_0	$\delta\overline{Z}_\psi$	δZ_m
10^{-12}	$-0.9436(22)$	$-0.13285(48)$	$0.4981(15)$
10^{-9}	$-0.9431(22)$	$-0.13284(48)$	$0.4980(15)$
10^{-6}	$-0.9438(22)$	$-0.13297(48)$	$0.5000(15)$
10^{-3}	$-0.9250(20)$	$-0.12636(44)$	$0.4917(14)$

λ^2	δZ_v	δZ_p	δC_v
10^{-12}	$-0.4401(16)$	$0.0187(14)$	$0.1331(35)$
10^{-9}	$-0.4388(16)$	$0.0186(13)$	$0.1333(36)$
10^{-6}	$-0.4387(15)$	$0.0182(13)$	$0.1351(36)$
10^{-3}	$-0.4327(14)$	$0.0184(13)$	$0.1338(33)$

Table 5.1: Heavy quark renormalisation parameters for different gluon masses λ^2. An infrared subtraction function has been used to calculate $\delta\overline{Z}_\psi$. The heavy quark action is the simple action defined in (5.26), the frame velocity $v = 0.3$. Mean field corrections for "partial" cancellation are included.

can reproduce the results in [121].

Tab. 5.4 shows numerical values for the simple action defined in (5.26) with $m = 2.8$ and $n = 2$ both for "partial" and "complete" cancellation, the corresponding numbers for the full $\mathcal{O}(1/m^2, v_{\text{rel}}^4)$ action are collected in Tab. 5.5. I conclude that the difference between the two cancellation schemes is small.

Gluon mass dependence

After introducing a suitable subtraction function for wavefunction renormalisation in Feynman gauge all renormalisation parameters should be independent of the gluon mass if λ^2 is sufficiently small. I demonstrate this in Tab. 5.1 and Fig. 5.5 where I show results for λ^2 between 10^{-12} and 10^{-3}. Within errors they are independent of the gluon mass for $\lambda^2 < 10^{-6}$ and I conclude that an extrapolation to $\lambda^2 = 0$ is not necessary, in the following I will work with $\lambda^2 = 10^{-6}$.

Vegas integration

To test both the automated generation of Feynman rules and the numerical integration routine I also compare to results reported in [90, 121][1] with $m = 2.0$, $n = 2$ and find perfect agreement within errors.

[1] I would like to thank Christine Davies for providing me with updated values for the renormalisation parameter Ω_v in [90].

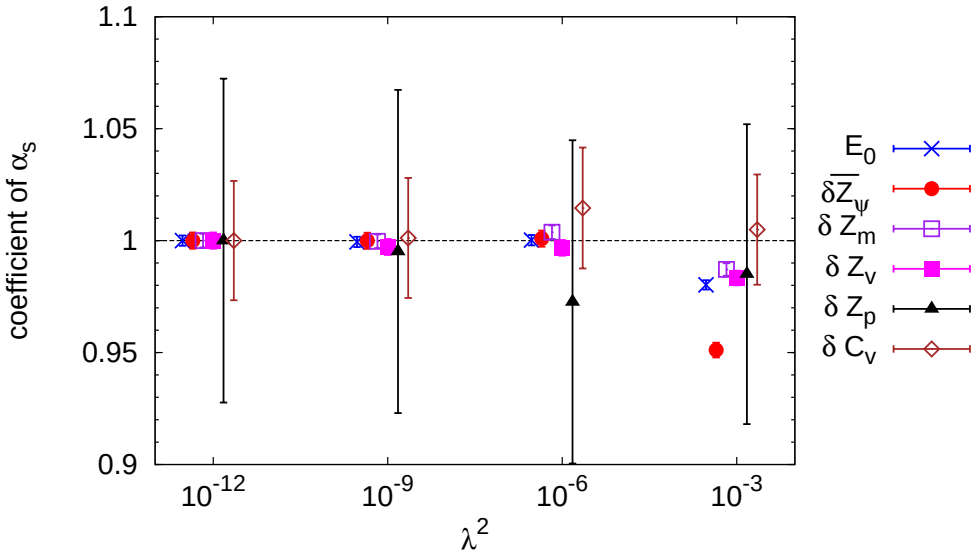

Figure 5.5: Heavy quark renormalisation parameters for different gluon masses λ^2, normalised to the values at $\lambda^2 = 10^{-12}$. An infrared subtraction function has been used to calculate $\delta\overline{Z}_\psi$. The points are offset horizontally for better legibility. The heavy quark action is the simple action defined in (5.26), the frame velocity $v = 0.3$. Mean field corrections for "partial" cancellation are included.

In Tabs. 5.2 and 5.3 I list values for the Ω_j without mean field corrections. I only show the infrared finite part of Ω_j without the infrared divergence $-2/(3\pi)\log\lambda^2$. All results are obtained in Feynman gauge with a subtraction function for the wavefunction renormalisation.

The renormalisation parameters (including mean field corrections for "partial" cancellation of $U_\mu U_\mu^\dagger$) are given in Tabs. 5.6 and 5.7 and plotted in Figs. 5.6 and 5.7. For the simple action I perform 5 iterations of $200,000$ function evaluations each both for thermalisation and measurement. The renormalisation parameters of the full action are evaluated with 10 iterations of $200,000$ function evaluations each. The calculations were carried out on the Eddie cluster [119]; on 64 processors this took about 4 hours wallclock time.

5.1.5 Observations

As can be seen by comparing Tabs. 5.2 and 5.4 the inclusion of mean field corrections reduces the size of the renormalisation parameters significantly: for not too large frame velocities they are all of order one, as expected for a well behaved perturbative expansion. The same can be observed for the full action, see Tabs. 5.3 and 5.5. It is interesting to compare Fig. 5.6 to the corresponding results in Fig. F.1 in appendix F. I checked explicitly that the chromomagnetic interaction term has neglegible influence on the renormalisation parameters. Improving the action reduces the size of some renormalisation constants, in particular it halves the renormalisation of the heavy quark mass. The dependence on the frame velocity is smaller for all radiative corrections except E_0. I explain this by the fact that improvement reduces the size of Lorentz symmetry breaking for all parameters which are also present in the continuum. For dimensional reasons E_0 diverges as $1/a$ in the continuum limit and is not reduced by improvement of the action. The additional terms in the full $\mathcal{O}(1/m^2, v_{\text{rel}}^4)$ action introduce further breaking of Lorentz invariance and increase the v dependence again. As discussed in more detail in the following section, the renormalisation of the external momentum is small for the simplest action but increases with the frame velocity for actions of increasing complexity.

v	Ω_0	Ω_1	Ω_2	Ω_v
0.00	−2.9851(24)	2.8619(24)	3.9967(29)	—
0.01	−2.9879(24)	2.8645(24)	3.9987(29)	4.003(23)
0.10	−2.9721(24)	2.8483(25)	3.9889(29)	3.9741(39)
0.20	−2.9299(23)	2.8033(24)	3.9567(29)	3.9474(31)
0.30	−2.8564(23)	2.7252(24)	3.9022(29)	3.8826(29)
0.40	−2.7490(22)	2.6092(23)	3.8218(29)	3.7898(28)
0.50	−2.6085(22)	2.4540(22)	3.7104(30)	3.6702(27)
0.60	−2.4260(20)	2.2462(21)	3.5651(33)	3.5087(27)
0.70	−2.2057(18)	1.9859(20)	3.3833(39)	3.3157(25)
0.75	−2.0832(18)	1.8335(20)	3.2742(45)	3.2110(26)
0.80	−1.9371(17)	1.6482(19)	3.1333(57)	3.0851(26)
0.85	−1.7790(16)	1.4343(20)	3.0029(80)	2.9447(26)
0.90	−1.5992(15)	1.1742(22)	2.820(13)	2.7790(29)
0.95	−1.3887(13)	0.8223(29)	2.480(29)	2.5639(36)

Table 5.2: Infrared finite part of Ω_j for the simple mNRQCD action defined in (5.26). Mean field corrections are not included.

v	Ω_0	Ω_1	Ω_2	Ω_v
0.00	−2.36685(40)	2.03045(62)	3.0487(13)	—
0.01	−2.36672(39)	2.03042(62)	3.0470(13)	3.039(18)
0.10	−2.35534(40)	2.02033(62)	3.0276(13)	3.0192(24)
0.20	−2.32049(39)	1.98900(62)	2.9668(13)	2.9695(16)
0.30	−2.26205(38)	1.93675(62)	2.8646(14)	2.8857(14)
0.40	−2.17678(37)	1.86081(61)	2.7199(14)	2.7636(13)
0.50	−2.06318(35)	1.75964(61)	2.5330(15)	2.6023(12)
0.60	−1.91598(33)	1.62928(62)	2.3020(17)	2.4059(12)
0.70	−1.72666(31)	1.46150(63)	2.0220(20)	2.1623(11)
0.75	−1.61272(30)	1.36128(65)	1.8614(24)	2.0247(11)
0.80	−1.48224(28)	1.24847(69)	1.6828(29)	1.8794(11)
0.85	−1.33083(27)	1.12528(82)	1.4925(41)	1.7275(12)
0.90	−1.15125(25)	1.0118(11)	1.2930(68)	1.5972(15)
0.95	−0.92738(24)	1.0698(21)	1.236(19)	1.6559(25)

Table 5.3: Infrared finite part of Ω_j for the full $\mathcal{O}(1/m^2, v_{\rm rel}^4)$ mNRQCD action. Mean field corrections are not included.

v	$\Omega_0^{(\mathrm{tadpole})}/u_0^{(2)}$	$\Omega_2^{(\mathrm{tadpole})}/u_0^{(2)}$
0.00	2.07143	−2.80357
0.01	2.07134	−2.80350
0.10	2.06250	−2.79688
0.20	2.03578	−2.77684
0.30	1.99142	−2.74356
0.40	1.92961	−2.69721
0.50	1.85056	−2.63792
0.60	1.75429	−2.56571
0.70	1.64018	−2.48013
0.75	1.57581	−2.43185
0.80	1.50571	−2.37929
0.85	1.42848	−2.32136
0.90	1.34093	−2.25570
0.95	1.23391	−2.17543

v	$\hat{\Omega}_0^{(\mathrm{tadpole})}/u_0^{(2)}$	$\hat{\Omega}_2^{(\mathrm{tadpole})}/u_0^{(2)}$
0.00	2.0236	−2.77966
0.01	2.0235	−2.77959
0.10	2.01422	−2.77273
0.20	1.98607	−2.75198
0.30	1.93913	−2.71742
0.40	1.87337	−2.66909
0.50	1.78867	−2.60697
0.60	1.6847	−2.53092
0.70	1.56055	−2.44032
0.75	1.49021	−2.38905
0.80	1.41349	−2.33317
0.85	1.32898	−2.27161
0.90	1.23351	−2.20199
0.95	1.11797	−2.11746

Table 5.4: Mean field improvement correction for the simple mNRQCD action defined in (5.26) and both "partial" ($\Omega_j^{(\mathrm{tadpole})}$) and "complete" ($\hat{\Omega}_j^{(\mathrm{tadpole})}$) cancellation of $U_\mu U_\mu^\dagger$. I do not show $\Omega_1^{(\mathrm{tadpole})} = -\Omega_0^{(\mathrm{tadpole})}$, $\hat{\Omega}_1^{(\mathrm{tadpole})} = -\hat{\Omega}_0^{(\mathrm{tadpole})}$, $\Omega_v^{(\mathrm{tadpole})} = \Omega_2^{(\mathrm{tadpole})}$ and $\hat{\Omega}_v^{(\mathrm{tadpole})} = \hat{\Omega}_2^{(\mathrm{tadpole})}$ explicitly.

v	$\Omega_0^{(\mathrm{tadpole})}/u_0^{(2)}$	$\Omega_2^{(\mathrm{tadpole})}/u_0^{(2)}$	$\Omega_v^{(\mathrm{tadpole})}/u_0^{(2)}$
0.00	2.13384	−3.18316	—
0.01	2.13375	−3.18300	−3.18302
0.10	2.12459	−3.16713	−3.16923
0.20	2.09650	−3.11915	−3.12728
0.30	2.04863	−3.03967	−3.05682
0.40	1.97963	−2.92963	−2.95725
0.50	1.88797	−2.79071	−2.82813
0.60	1.77221	−2.62561	−2.66939
0.70	1.63091	−2.43793	−2.48127
0.75	1.54999	−2.33677	−2.37612
0.80	1.46143	−2.23103	−2.26313
0.85	1.36379	−2.12013	−2.14118
0.90	1.25365	−2.00163	−2.00714
0.95	1.12074	−1.86625	−1.85110

v	$\hat{\Omega}_0^{(\mathrm{tadpole})}/u_0^{(2)}$	$\hat{\Omega}_2^{(\mathrm{tadpole})}/u_0^{(2)}$	$\hat{\Omega}_v^{(\mathrm{tadpole})}/u_0^{(2)}$
0.00	2.10610	−3.14336	—
0.01	2.10600	−3.14319	−3.14321
0.10	2.09592	−3.12639	−3.12898
0.20	2.06507	−3.07557	−3.08573
0.30	2.01267	−2.99112	−3.01321
0.40	1.93722	−2.87358	−2.91083
0.50	1.83666	−2.72404	−2.77787
0.60	1.70836	−2.54438	−2.61351
0.70	1.54900	−2.33743	−2.41672
0.75	1.45625	−2.22476	−2.30557
0.80	1.35355	−2.10633	−2.18513
0.85	1.23910	−1.98182	−2.05402
0.90	1.10911	−1.84923	−1.90880
0.95	0.95262	−1.70037	−1.73901

Table 5.5: Mean field improvement correction for the full $\mathcal{O}(1/m^2, v_{\mathrm{rel}}^4)$ mNRQCD action and both "partial" ($\Omega_j^{(\mathrm{tadpole})}$) and "complete" ($\hat{\Omega}_j^{(\mathrm{tadpole})}$) cancellation of $U_\mu U_\mu^\dagger$. I do not show $\Omega_1^{(\mathrm{tadpole})} = -\Omega_0^{(\mathrm{tadpole})}$ and $\hat{\Omega}_1^{(\mathrm{tadpole})} = -\hat{\Omega}_0^{(\mathrm{tadpole})}$ explicitly.

v	E_0	$\delta\overline{Z}_\psi$	δZ_m
0.00	−0.9686(24)	−0.12323(49)	0.4221(15)
0.01	−0.9715(24)	−0.12348(50)	0.4215(15)
0.10	−0.9642(24)	−0.12379(50)	0.4299(16)
0.20	−0.9481(23)	−0.12657(50)	0.4496(16)
0.30	−0.9178(23)	−0.13124(52)	0.4869(16)
0.40	−0.8705(22)	−0.13984(54)	0.5479(17)
0.50	−0.8070(22)	−0.15447(58)	0.6398(20)
0.60	−0.7182(20)	−0.17982(63)	0.7948(23)
0.70	−0.6090(18)	−0.21983(74)	1.0719(30)
0.75	−0.5492(18)	−0.24972(83)	1.3070(35)
0.80	−0.4713(17)	−0.28893(95)	1.6772(45)
0.85	−0.3884(16)	−0.3446(12)	2.3686(63)
0.90	−0.2938(15)	−0.4250(16)	3.800(10)
0.95	−0.1875(13)	−0.5664(26)	8.377(21)

v	δZ_v	δZ_p	δC_v
0.00	—	—	0.0761(17)
0.01	−0.425(23)	−0.029(23)	0.0745(18)
0.10	−0.4109(30)	−0.0000(28)	0.0831(18)
0.20	−0.4227(21)	0.0082(18)	0.1002(18)
0.30	−0.4252(18)	0.0177(15)	0.1321(18)
0.40	−0.4334(16)	0.0288(13)	0.1804(19)
0.50	−0.4497(16)	0.0433(13)	0.2403(21)
0.60	−0.4726(16)	0.0553(12)	0.3237(25)
0.70	−0.5122(16)	0.0660(11)	0.4245(34)
0.75	−0.5442(16)	0.0671(11)	0.4776(41)
0.80	−0.5864(17)	0.0599(11)	0.5337(54)
0.85	−0.6411(18)	0.0476(11)	0.6262(78)
0.90	−0.7142(19)	0.0210(11)	0.709(13)
0.95	−0.8250(21)	−0.0353(11)	0.720(29)

Table 5.6: Infrared finite renormalisation parameters for the simple mNRQCD action defined in (5.26), including mean field corrections for "partial" cancellation.

v	E_0	$\delta\overline{Z}_\psi$	δZ_m
0.00	−0.76647(40)	−0.33639(48)	0.2313(12)
0.01	−0.76641(39)	−0.33630(47)	0.2297(12)
0.10	−0.76190(40)	−0.33501(47)	0.2275(12)
0.20	−0.74812(39)	−0.33149(48)	0.2194(12)
0.30	−0.72558(38)	−0.32530(48)	0.2037(12)
0.40	−0.69206(37)	−0.31597(49)	0.1789(13)
0.50	−0.64720(35)	−0.30354(50)	0.1421(13)
0.60	−0.58682(33)	−0.28670(52)	0.0910(15)
0.70	−0.50349(31)	−0.26516(55)	0.0158(17)
0.75	−0.45023(30)	−0.25144(58)	−0.0337(19)
0.80	−0.38616(28)	−0.23377(63)	−0.0901(24)
0.85	−0.30798(27)	−0.20554(77)	−0.1502(32)
0.90	−0.21101(25)	−0.1395(11)	−0.1933(51)
0.95	−0.08682(24)	0.1425(21)	−0.038(14)

v	δZ_v	δZ_p	δC_v
0.00	—	—	−0.0425(12)
0.01	−0.221(18)	−0.002(18)	−0.0441(12)
0.10	−0.2154(23)	0.0061(20)	−0.0454(12)
0.20	−0.2074(15)	0.0025(12)	−0.0510(12)
0.30	−0.1928(12)	−0.0087(10)	−0.0626(12)
0.40	−0.1696(11)	−0.02131(89)	−0.0799(13)
0.50	−0.1376(10)	−0.04175(86)	−0.1039(14)
0.60	−0.1037(10)	−0.06974(87)	−0.1350(16)
0.70	−0.06305(91)	−0.10943(92)	−0.1731(19)
0.75	−0.04380(89)	−0.1394(10)	−0.1964(23)
0.80	−0.02967(90)	−0.1746(11)	−0.2256(29)
0.85	−0.01915(93)	−0.2235(11)	−0.2580(40)
0.90	−0.0203(10)	−0.2966(13)	−0.3127(67)
0.95	−0.0383(13)	−0.4374(16)	−0.402(18)

Table 5.7: Infrared finite renormalisation parameters for the full $\mathcal{O}(1/m^2, v_{\rm rel}^4)$ mNRQCD action, including mean field corrections.

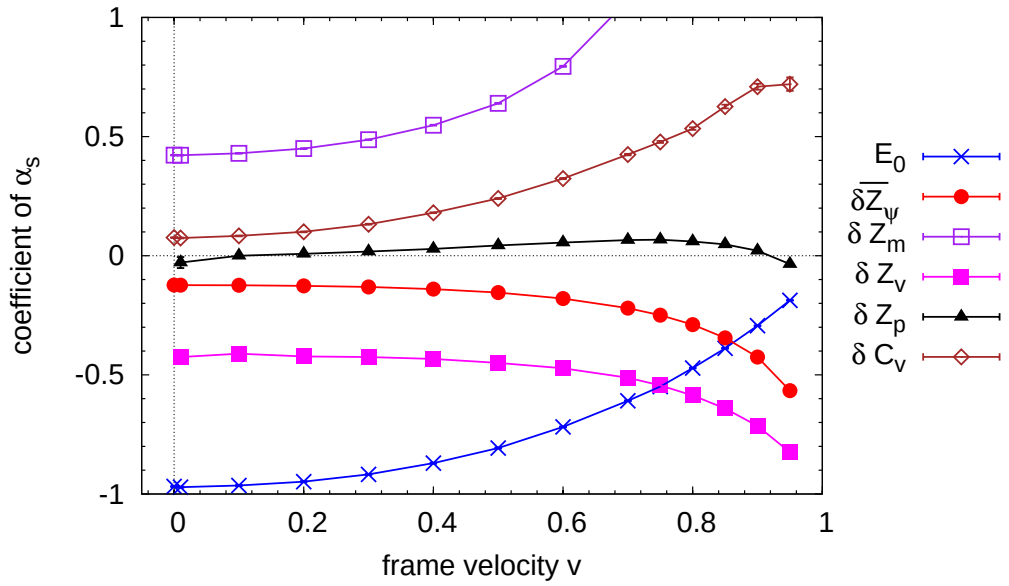

Figure 5.6: Infrared finite renormalisation parameters for the simple mNRQCD action defined in (5.26), including mean field corrections.

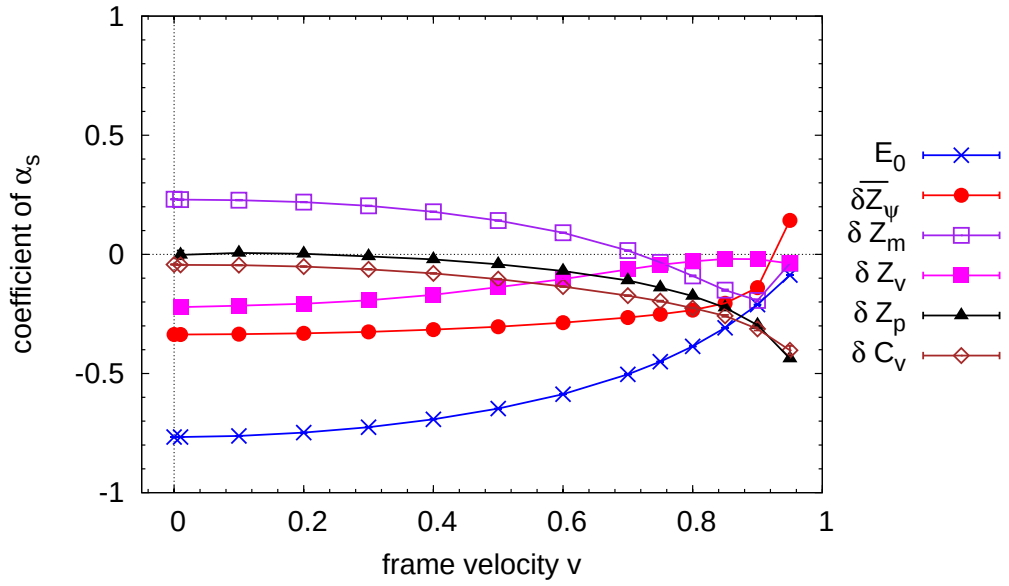

Figure 5.7: Infrared finite renormalisation parameters for the full $\mathcal{O}(1/m^2, v_{\rm rel}^4)$ mNRQCD action, including mean field corrections.

5.1.6 Reparametrisation invariance

In the continuum

There is some ambiguity in how the heavy quark momentum $p = mu + k$ is split into mu and a residual momentum k. Choosing

$$u \mapsto u + \epsilon/m, \qquad\qquad k \mapsto k - \epsilon \tag{5.28}$$

instead should give the same physical results if $2u \cdot \epsilon + \epsilon^2 = 0$ is chosen to preserve $u^2 = 1$. In the continuum the HQET Lagrangian

$$\mathscr{L}_{\mathrm{HQET}} \;=\; \overline{\psi}\left(iu \cdot D - \frac{D^2 - (v \cdot D)^2}{2m}\right)\psi \tag{5.29}$$

is invariant under (5.28) accompanied by a field transformation $\psi \mapsto e^{i\epsilon \cdot x}\left(1 + \frac{\not{\epsilon}}{2m}\right)\psi$ [66, 67, 120]. As this is a symmetry of the renormalised Lagrangian the relative coefficients of the leading order term and the $\mathcal{O}(1/m)$ kinetic operator in (5.29) are fixed to all orders in perturbation theory.

In [1] the discussion is extended to actions written in noncovariant form. The action in section 4.1.3 is not covariant so consider a transformation of the spatial part of the four momentum $\boldsymbol{p} = \gamma m \boldsymbol{v} + \boldsymbol{k}$ instead. For simplicity I consider the simple Hamiltonian

$$H_0 \;=\; -i\boldsymbol{v} \cdot \boldsymbol{D} - \frac{\boldsymbol{D}^2}{2\gamma m}. \tag{5.30}$$

It is easy to see that the transformation

$$\boldsymbol{v} \mapsto \boldsymbol{v} + \boldsymbol{\epsilon}, \qquad\qquad \psi \mapsto e^{-i\gamma m \boldsymbol{v} \cdot \boldsymbol{\epsilon}}\psi \tag{5.31}$$

leaves the theory invariant if one requires $2\boldsymbol{v} \cdot \boldsymbol{\epsilon} + \boldsymbol{\epsilon}^2 = 0$ to preserve the length of the frame velocity $\boldsymbol{v}$. This implies that the external momentum $\boldsymbol{p} = \gamma m \boldsymbol{v}$ is not renormalised as the relative coefficient between the two terms in (5.30) is fixed to all orders in perturbation theory.

On the lattice

The discretised version of (5.30) reads

$$H_0^{(\mathrm{lat})} \;=\; -i\boldsymbol{v} \cdot \boldsymbol{\Delta}^{(\pm)} - \frac{\Delta^{(2)}}{2\gamma m}. \tag{5.32}$$

Under the transformation (5.31) this transforms to

$$H_0^{(\mathrm{lat})} \mapsto H_0^{(\mathrm{lat})} + \frac{1}{2}\gamma m a^2 \sum_j v_j \epsilon_j \Delta_j^{(+)} \Delta_j^{(-)} \psi + \mathcal{O}(a^2\epsilon^2). \tag{5.33}$$

If the frame velocity points in a lattice direction, $v_j\epsilon_j$ can be replaced by $-\frac{1}{2}\boldsymbol{\epsilon}^2$ and it can be seen that the breaking of reparametrisation invariance is of $\mathcal{O}(a^2\epsilon^2)$. Using an improved derivative operator instead one finds that

$$H_0^{(\mathrm{lat})} \mapsto H_0^{(\mathrm{lat})} + \frac{1}{6}\gamma m a^4 \sum_j v_j \epsilon_j \Delta_j^{(+)} \Delta_j^{(-)} \Delta_j^{(+)} \Delta_j^{(-)} \psi + \mathcal{O}(a^4\epsilon^2). \tag{5.34}$$

and with the same argument as above the breaking of reparametrisation invariance is of $\mathcal{O}(a^4\epsilon^2)$. I calculated the renormalisation of the external momentum both with unimproved and improved derivatives for $am = 2.8$, $n = 2$ and $v = 0.75$ and find $\delta Z_p = -0.067(1)$ (unimproved) and $\delta Z_p = -0.039(1)$ (improved).

Additional terms in the action will break reparametrisation invariance which will also be affected by the fact that the kinetic operator always appears in the form $\left(1 - \frac{aH_0}{2n}\right)^n$.

I study the influence of $(\boldsymbol{v}\cdot\boldsymbol{D})^2/(2\gamma m)$ by simulating with the same parameters as above ($m = 2.8$, $n = 2$ and $v = 0.75$) now including $\Delta_v^{(2)}/(2\gamma m)$ in the action (with unimproved derivatives) and find $\delta Z_p = 0.066$. The effect of this term is about twice the size and of different sign as the breaking of the symmetry due to lattice artifacts. I also expect the breaking to be proportional to $v^2/(2\gamma m)$, i.e. it should rise quadratically for small v, reach a maximum at $v = \sqrt{2/3} \approx 0.8$ and then drop to zero for $v \to \infty$. Quantitatively this is exactly the behaviour observed in Fig. 5.6. For the full action in 5.7 the renormalisation of the external momentum is small for small frame velocities but becomes sizable for $v \to 1$. I explain this increased breaking of reparametrisation invariance by the presence of additional operators in the full action.

5.1.7 Comparison to nonperturbative calculations

The renormalisation Z_p of the external momentum and the energy shift C_v can be obtained from nonperturbative calculations by measuring the two-point function of heavy-heavy and heavy-light mesons for different residual momenta. For each $\boldsymbol{p}$ the energy $E_v(\boldsymbol{p})$ is obtained by fitting a sum of exponentials to the correlator. Z_p, C_v and the meson mass M_{kin} are then extracted as described in [1, 90].

Value of the strong coupling constant

To compare to these results a value for the strong coupling constant has to be chosen. I use the strong coupling constant defined in the potential scheme [79]. A typical momentum scale q^* in a perturbative integral can be defined by [79, 127]

$$\alpha_V(q^*_{\rm loop})I_{\rm loop} = \alpha_V(q^*_{\rm loop})\int \frac{d^4k}{(2\pi)^4} I(k) \quad = \quad \int \frac{d^4k}{(2\pi)^4} I(k)\alpha_V(k). \tag{5.35}$$

Using the one-loop running of $\alpha_V(q^2) = \frac{\alpha_V(\overline{q}^2)}{1+\alpha_V\beta_0\log q^2/\overline{q}^2} \approx \alpha_V - \beta_0\alpha_V^2 \log q^2/\overline{q}^2$ this reduces to

$$\log(q^*_{\rm loop})^2 \quad = \quad \frac{\int \frac{d^4k}{(2\pi)^4} I(k)\log k^2}{\int \frac{d^4k}{(2\pi)^4} I(k)}. \tag{5.36}$$

This value has to be combined with the one from mean field improvement. I calculate the typical momentum scale of the one loop correction to $\frac{1}{3}\,\mathrm{tr}\,[U_\mu] \propto \mathrm{tr}\,[A_\mu^2]$ and find $aq^*_{\rm tadpole} = 2.64319(17)$ for the Symanzik improved gluon action. For the Wilson gluon action I obtain $aq^*_{\rm tadpole} = 2.77368(16)$ which agrees with [128].

The two values are combined according to [129],

$$\log(q^*) \quad = \quad \frac{I_{\rm loop}\log(q^*_{\rm loop}) + I_{\rm tadpole}\log(q^*_{\rm tadpole})}{I_{\rm loop} + I_{\rm tadpole}}. \tag{5.37}$$

In Tab. 5.8 I give aq^* for the infrared finite renormalisation parameters. For $v < 0.4$ it was not possible to obtain a clean signal for the external momentum renormalisation, here I choose $q^* = 2/a$. For the values where $q^*(Z_p)$ can not be calculated reliably the external momentum renormalisation is extremely small. The same problem arises for the mass renormalisation at some velocities where δZ_m is small.

After including mean field corrections the scales for E_0, Z_m and Z_v are relatively small, corresponding to a large value of α_s. Qualitatively the same result was found in [114]. The integrals have substantial contributions from the infrared region of the one loop integral and their perturbative series is not very well behaved. On the other hand, the scale for the physical parameters Z_p and C_v which can also be measured in nonperturbative simulations, is typically larger than $2/a$, corresponding to $\alpha_V(q^*) \lesssim 0.3$.

The running of the strong coupling constant has been calculated in [95] by measuring short distance observables on the lattice. I use their value of $\alpha_0 = \alpha_V(7.5\ \mathrm{GeV})$ and

v	$aq^*(E_0)$	$aq^*(\delta Z_m)$	$aq^*(\delta Z_v)$	$aq^*(\delta Z_p)$	$aq^*(\delta C_v)$
0.00	0.794(11)	0.597(17)	—	—	3.48(36)
0.01	0.754(11)	0.634(19)	0.41(19)	—	2.74(26)
0.10	0.751(11)	0.598(18)	0.292(19)	—	2.73(27)
0.20	0.751(11)	0.564(17)	0.408(17)	—	2.91(25)
0.30	0.727(10)	0.546(18)	0.461(17)	—	2.68(18)
0.40	0.731(11)	0.481(19)	0.518(20)	1.82(41)	2.32(13)
0.50	0.708(10)	0.327(16)	0.473(21)	2.39(27)	2.60(11)
0.60	0.739(12)	0.133(12)	0.392(21)	2.26(15)	2.452(82)
0.70	0.670(11)	—	0.441(35)	2.31(10)	2.297(64)
0.75	0.654(11)	—	0.340(37)	2.317(82)	2.159(54)
0.80	0.597(11)	—	0.314(49)	2.237(64)	2.356(55)
0.85	0.503(11)	5.90(64)	0.324(77)	2.132(52)	2.113(44)
0.90	0.3201(88)	3.05(37)	0.50(11)	2.180(43)	2.166(51)
0.95	0.1097(67)	—	1.64(21)	2.069(28)	2.180(83)

Table 5.8: Values of aq^* for various IR finite renormalisation parameters

integrate the evolution equation

$$q^2 \frac{d\alpha_V(q)}{dq^2} = -\beta_0 \alpha_V^2 - \beta_1 \alpha_V^3 - \beta_2 \alpha_V^4 + \mathcal{O}(\alpha_V^5) \tag{5.38}$$

numerically to obtain α_V at a specific scale. On the coarse MILC configurations the inverse lattice spacing is $a^{-1} = 1.6$ GeV. [93].

Numerical results

In Figs. 5.8 and 5.9 I show both perturbative and nonperturbative results for the renormalisation of the external momentum and the energy shift between QCD and mNRQCD. The nonperturbative results have been calculated by Stefan Meinel [91]. I estimate the part of the two loop correction, which comes from the running of α_V in the loop integral, by varying the scale q^* in the range $q^*/2, \ldots, 2q^*$. This is shown as a grey error band on the perturbative numbers in the plot. Note that this is only part of the two loop uncertainty. The discrepancy between the nonperturbative and perturbative results suggests that there are additional higher order corrections, to quantify these a two loop calculation is necessary. This calculation is currently carried out by a combination of high-β simulations and diagrammatic perturbation theory, see section 5.2.

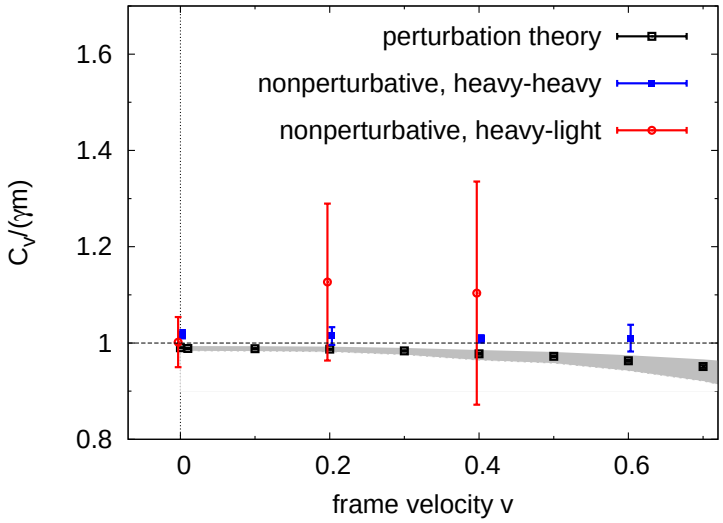

Figure 5.8: Energy shift $C_v/(\gamma m)$ from perturbation theory and nonperturbative simulations for the full $\mathcal{O}(1/m^2, v_{\mathrm{rel}}^4)$ mNRQCD action with $m = 2.8$, $n = 2$.

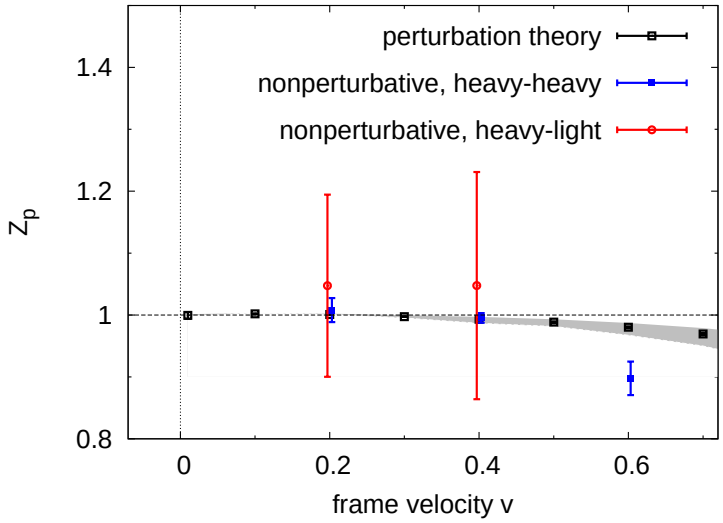

Figure 5.9: External momentum renormalisation Z_p from perturbation theory and nonperturbative simulations for the full $\mathcal{O}(1/m^2, v_{\mathrm{rel}}^4)$ mNRQCD action with $m = 2.8$, $n = 2$.

5.2 Finite lattice with twisted boundary conditions

I calculate the heavy quark self-energy on a finite lattice with twisted boundary conditions. As in the high-β calculations in [108] I use two different heavy quark actions: The simple action in (5.26) with $m = 2.0$ and $n = 2$, and the full $\mathcal{O}(1/m^2, v_{\rm rel}^4)$ action with the same stability parameter and $m = 2.8$. In both cases I use a Symanzik improved gluon action. At the time of writing results from high-β fits were available for the zero point energy shift of the simple mNRQCD action. Below I show results both for unconstrained and constrained polynomial fits of the α_s dependence of this renormalisation parameter. In the latter case the one loop coefficient is fixed by my calculation in diagrammatic perturbation theory. I also computed the $\mathcal{O}(\alpha_s)$ radiative corrections for other renormalisation parameters on a finite lattice with twisted boundary conditions, results for both the simple and the full mNRQCD action are collected in appendix G.

To check my calculations for internal consistency I first verify that I can reproduce the numbers in the infinite volume limit by extrapolation in the inverse lattice size.

Infinite volume extrapolation

On an infinite lattice the integration contour has to be deformed in the k_0 plane such that no poles are crossed when Wick rotating back to Minkowski space. On a finite lattice the integral is replaced by a sum over discrete momenta and it is not obvious how the residue theorem can be applied. However, the difference between the mode summation and the integral only introduces finite volume errors which vanish in the infinite volume limit and I conclude that the same contour shift can be applied in both cases.

I compare results on a finite lattice of size $T \times L^3$ (with $T = 3L$) to the infinite volume, $T = L = \infty$ result in Fig. 5.10 where I show the zero point energy for the full action and a range of frame velocities. I extrapolate the finite volume result assuming a quadratic dependence on the inverse linear lattice size $1/L$,

$$E_0 \quad = \quad E_0(L=\infty) + \frac{1}{L} E_0^{(1)} + \frac{1}{L^2} E_0^{(2)}. \tag{5.39}$$

The results are shown in Tab. 5.9 and Fig. 5.10. To estimate the parametrisation errors on $E_0(L = \infty)$ and $E_0^{(1)}$ I perform an additional linear fit leaving out the $L = 4$ point. The difference between the linear and quadratic fit parameters is the error quoted in the third and fourth column of Tab. 5.9. I also show the infinite volume result. The results from the infinite volume calculation and the extrapolation to $L = \infty$ agree within errors, as expected.

v	$E_0(L=\infty)$	$E_0(L=\infty)$ [fit]	$E_0^{(1)}$ [fit]	$E_0^{(2)}$ [fit]
0.0	−0.76647(40)	−0.7684(39)	0.743(61)	0.2277(13)
0.2	−0.74812(39)	−0.7504(39)	0.720(61)	0.227615(71)
0.4	−0.69206(37)	−0.6944(40)	0.644(62)	0.23034(68)
0.6	−0.58682(33)	−0.5887(42)	0.502(65)	0.24154(29)
0.8	−0.38616(28)	−0.3869(47)	0.234(74)	0.2732(10)

Table 5.9: Result from infinite volume perturbation theory (second column) and quadratic fit to the finite volume results. The parametrisation error in the third and fourth column is estimated by comparing the fit parameters from a linear fit without the $L = 4$ point to the central values of the quadratic fit. Mean field corrections are included.

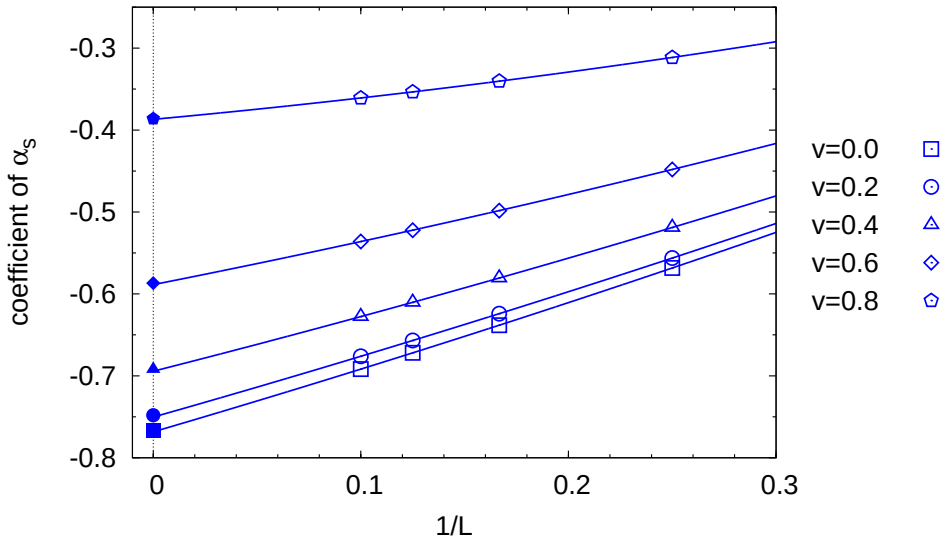

Figure 5.10: Infinite volume extrapolation of the zero point energy E_0 obtained on a $L^3 \times T$ lattice (empty symbols). I also show a quadratic fit in the inverse linear lattice size $1/L$ and the infinite volume result (filled symbols). I use the full $\mathcal{O}(1/m^2, v_{\mathrm{rel}}^4)$ action with $m = 2.8$ and $n = 2$. All mean field corrections are included in the plot.

5.2.1 High-β simulations

Nonperturbative calculations are carried out by Ron Horgan and Andrew Lee [108]. They generate quenched gauge configurations for different values of the inverse coupling constant β. For sufficiently large β the results can be expanded in the strong coupling constant α_s as nonperturbative effects are suppressed by twisted boundary conditions. For each value of β the heavy quark propagator is measured for a range of lattice momenta and fitted to a suitable function after fixing to Landau gauge. For the simple mNRQCD action described in (5.26) the functional dependence is assumed to be

$$\begin{aligned} G(\tau; \boldsymbol{p}^2, \boldsymbol{v}\cdot\boldsymbol{p}, (\boldsymbol{v}\cdot\boldsymbol{p})^2) &= (1 + a_1 + a_6\boldsymbol{p}^2 + a_7\boldsymbol{v}\cdot\boldsymbol{p})e^{(a_2-a_3)\tau} \\ &\times \left[1 - a_4\frac{\boldsymbol{v}\cdot\boldsymbol{p}}{2n} - \frac{\boldsymbol{p}^2 - a_5(\boldsymbol{v}\cdot\boldsymbol{p})^2}{2na_3}\right]^{2n\tau}. \end{aligned} \tag{5.40}$$

By expanding in small momenta it can be shown that

$$C_v = a_2, \qquad m_R\gamma_R = a_3, \qquad Z_v = a_4, \qquad E_0 = a_2 - a_3. \tag{5.41}$$

To reach sufficiently small momenta generalised boundary conditions are applied for the external quark fields [130],

$$\psi(x + L\hat{j}) = e^{2\pi i\theta_j}\psi(x), \qquad \overline{\psi}(x + L\hat{j}) = e^{-2\pi i\theta_j}\overline{\psi}(x) \qquad \text{for} \quad j = 1, 2, 3. \tag{5.42}$$

The real numbers θ_j are arbitrary parameters which can be used to tune the lattice momenta. Combining this with the twist described in section 4.2.2 the spatial lattice momenta are

$$p_j = \frac{2\pi}{L}\left(m_j + \theta_j + \frac{n_j}{3}\right) \tag{5.43}$$

with $m_j \in 0, \ldots, L-1$, $\theta_j \in \mathbb{R}$ and $n_j \in \{0, 1, 2\}$. The restrictions on the twist vector n_j are described in section 4.2.2.

Finally, the results for each renormalisation parameter are fitted to a polynomial in the strong coupling constant.

5.2.2 Numerical results

Tab. 5.10 shows the coefficients of a polynomial fit in α_s to the zero point energy shift from high-β simulations [108]. In Tab. 5.11 I present results from a constrained fit where the one loop results are taken from diagrammatic lattice perturbation theory. In both cases the simple mNRQCD action in (5.26) is used in combination with a Symanzik improved gluon action.

lattice		$v = 0.0$	$v = 0.2$	$v = 0.4$	$v = 0.8$
$4^3 \times 12$	1 loop	$-2.5186(27)$	$-2.4703(27)$	$-2.3231(28)$	$-1.7161(32)$
	2 loops	0.10(14)	0.13(15)	0.20(15)	$-0.22(15)$
	3 loops	-8.9 ± 1.2	-9.4 ± 1.2	-10.6 ± 1.1	-8.8 ± 1.1
$6^3 \times 18$	1 loop	$-2.5901(18)$	$-2.5387(17)$	$-2.3827(14)$	$-1.7706(69)$
	2 loops	$-0.25(11)$	$-0.35(11)$	$-0.653(92)$	$-0.83(36)$
	3 loops	-11.0 ± 1.0	-10.2 ± 1.0	-7.33 ± 0.91	-8.9 ± 3.0
$8^3 \times 24$	1 loop	$-2.6321(69)$	$-2.5797(67)$	$-2.4146(64)$	$-1.812(16)$
	2 loops	$-0.24(36)$	$-0.33(36)$	$-0.93(34)$	$-0.01(67)$
	3 loops	-15.1 ± 3.3	-14.8 ± 3.3	-8.9 ± 3.3	-20.0 ± 5.2

Table 5.10: Zero point energy shift E_0 for the simple action defined in (5.26) [108]. I show results from an unconstrained fit in the strong coupling constant. Each entry contains (from top to bottom): one loop coefficient, two loop coefficient and the three loop coefficient. Mean field corrections are not included.

In Fig. 5.11 I compare the $\mathcal{O}(\alpha_s)$ results from diagrammatic perturbation theory and the linear coefficient in an unconstrained fit to high-β simulations.

Comparison of fit models

The two different fits have been analysed by an F-test [131, 108]. This statistical tool is used to compare two "nested"[2] models with different numbers of parameters; it makes a quantitative statement about whether extending a simple model with more free parameters significantly improves the fit to the same data. In our case, the simple model corresponds to the constrained fit, it can be extended by keeping the one loop coefficient as an independent parameter. For each lattice size and frame velocity the value of the statistic $F = F_{\text{fit}}$ is calculated from the fit results. This quantity is distributed according to a known probability density which depends on the degrees of freedom. The null hypothesis is that the fit is not significantly improved by adding more free parameters to the model, i.e. that the unconstrained fit does not give better results than the constrained fit. For each calculated value of F_{fit} one can then look up the probability that F is larger than F_{fit}. The null hypothesis is rejected if this probability is smaller than a given threshold. In Tab. 5.12 I show this probablity as calculated from the fits in Tabs. 5.10 and 5.11.

[2]Model 1 is nested in model 2 if any regression curve in model 1 can be reproduced by some choice of parameters in model 2.

lattice		$v = 0.0$	$v = 0.2$	$v = 0.4$	$v = 0.8$
$4^3 \times 12$	1 loop	-2.5175	-2.4682	-2.3184	-1.6785
	2 loops	$0.051(71)$	$0.038(76)$	$-0.003(86)$	$-1,61(26)$
	3 loops	$-8.58(80)$	$-8.73(82)$	$-9.17(83)$	0.2 ± 2.3
$6^3 \times 18$	1 loop	-2.5906	-2.5393	-2.3832	-1.7126
	2 loops	$-0.228(52)$	$-0.312(52)$	$-0.625(46)$	$-3.41(42)$
	3 loops	$-11.19(67)$	$-10.44(68)$	$-7.58(60)$	9.7 ± 4.3
$8^3 \times 24$	1 loop	-2.6254	-2.5732	-2.4140	-1.7284
	2 loops	$-0.55(17)$	$-0.63(17)$	$-0.96(15)$	$3.06(59)$
	3 loops	-12.7 ± 2.1	-12.4 ± 2.3	-8.6 ± 2.1	0.3 ± 5.9

Table 5.11: Zero point energy shift E_0 for the simple action defined in (5.26). I show results from an constrained fit in the strong coupling constant [108]. Each entry contains (from top to bottom): one loop coefficient from diagrammatic perturbation theory, two loop coefficient and the three loop coefficient. Mean field corrections are not included.

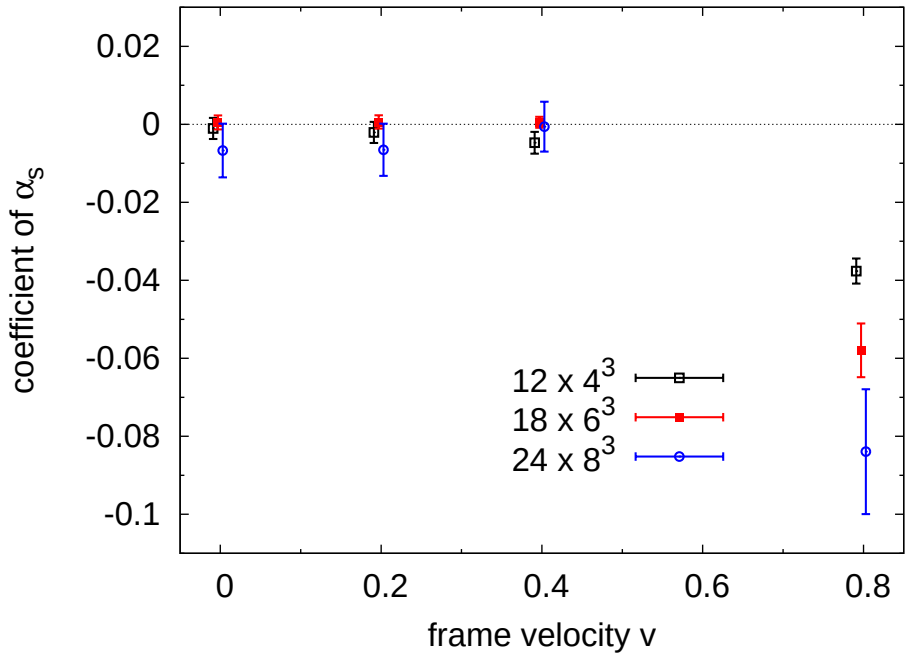

Figure 5.11: $\mathcal{O}(\alpha_s)$ correction to the zero point energy shift: I plot the difference between one-loop diagrammatic perturbation theory and the linear coefficient of a fit to high-β simulations. Mean field corrections are not included.

lattice	$v = 0.0$	$v = 0.2$	$v = 0.4$	$v = 0.8$
$4^3 \times 12$	72.14%	49.98%	14.67%	0.00%
$6^3 \times 18$	81.12%	75.15%	75.18%	0.00%
$8^3 \times 24$	39.29%	39.08%	93.17%	0.02%

Table 5.12: Probability of obtaining an F value equal or larger than that calculated from the two fits in Tabs. 5.10 and 5.11.

5.2.3 Observations

For velocities up to $v = 0.4$ the results for the one loop coefficients in Tabs. 5.10 and 5.11 agree within statistical errors. Using an F-test with 5% rejection level, the unconstrained fit to the lattice data only gives significantly better results for the largest considered frame velocity of $v = 0.8$. This agrees with the previous statement about the equality of one loop coefficients. The two loop coefficients in the unconstrained fit are small on all lattices except the largest, their values change, in some cases significantly, especially at large frame velocities, if the one loop coefficient is constrained by diagrammatic perturbation theory. Their errors are reduced if the value of the one loop coefficient is fixed. In all cases the three loop coefficients are very large with errors of the order of 10% and larger.

Chapter 6

Kinetic terms in the NRQCD action

In the following I discuss the perturbative renormalisation of kinetic terms in the nonmoving NRQCD action up to $\mathcal{O}(p^4)$; this is the first order where terms breaking rotational symmetry can enter the dispersion relation. This work was motivated by numerical simulations carried out Iain Kendall in Glasgow who found that the energy splitting between heavy-heavy mesons with identical $\boldsymbol{p}^2$ but different $\sum_{j=1}^{3} p_j^4$ is relatively large [132]. One of the possible explanations are large renormalisations of terms in the NRQCD action that break rotational invariance. Indeed it was found empirically in the same nonperturbative study that a matching coefficient of $c_5 = 2.6$ removes the energy splitting between mesons with different $\sum_j p_j^4$. In this chapter I compare this to my results from perturbative calculations.

6.1 Heavy quark action

Full NRQCD action. The heavy quark action I use in this section is the full $\mathcal{O}(1/m^2, v_{\mathrm{rel}}^4)$ NRQCD action defined in (4.8), (4.9) and (4.12); the kinetic terms in the action are

$$H_0 = -\frac{\Delta^{(2)}}{2m}, \qquad \delta H = -c_1 \frac{\left(\Delta^{(2)}\right)^2}{8m^3} + c_5 \frac{\Delta^{(4)}}{24m} - c_6 \frac{1}{4n} \frac{\left(\Delta^{(2)}\right)^2}{4m^2}. \tag{6.1}$$

As both c_1 and c_6 multiply the operator $\left(\Delta^{(2)}\right)^2$ one of these coefficients is redundant. I define

$$\tilde{c}_1 \equiv \left(c_1 + \frac{m}{2n} c_6\right) / \left(1 + \frac{m}{2n}\right) \tag{6.2}$$

so that the tree level values $c_1 = c_6 = 1$ correspond to $\tilde{c}_1 = 1$.

In some simulations I also include an additional correction $-\Delta^{(6)}/(180m)$ in δH which removes $\mathcal{O}(a^6)$ discretisation errors at tree level.

Morningstar's action. To verify my results I compare my matching coefficients for the action setup in [122]. There the kernel is

$$K = u_0 U_4(\boldsymbol{x},\tau) - \left(1-\frac{H_0}{2n}\right)^n (1-\delta H)\left(1-\frac{H_0}{2n}\right)^n. \tag{6.3}$$

Note that the time derivative is realised by a forward finite difference. For the simple setup used there the interaction term is given by

$$\begin{aligned}\delta H &= -c_1\frac{\left(\Delta^{(2)}\right)^2}{8m^3}\left(1+\frac{m}{2n}\right) + c_2\frac{a^2\Delta^{(4)}}{24m} + c_3\frac{ig}{8m^2}\left(\boldsymbol{\Delta}^{(\pm)}\cdot\boldsymbol{E} - \boldsymbol{E}\cdot\boldsymbol{\Delta}^{(\pm)}\right)\\ &\quad - c_4\frac{g}{8m^2}\boldsymbol{\sigma}\cdot\left(\boldsymbol{\Delta}^{(\pm)}\times\boldsymbol{E} - \boldsymbol{E}\times\boldsymbol{\Delta}^{(\pm)}\right) - c_5\frac{g}{2m}\boldsymbol{\sigma}\cdot\boldsymbol{B}.\end{aligned} \tag{6.4}$$

In this expression the non rotationally-invariant fourth order derivative is mean field improved as

$$\Delta^{(4)} = \sum_{k=1}^{3}\left(u_0^{-1}(U_k + U_k^\dagger) - 2\right)^2. \tag{6.5}$$

Compared to (6.1) the coefficients are ordered slightly differently. In particular my $\tilde{c}_1$ corresponds to c_1 and my c_5 is equivalent to c_2 used by Morningstar.

The unimproved Wilson gluon action is used with this NRQCD action.

6.2 Derivation of renormalisation parameters

This section is an extension of the derivation in section 5.1.1 to higher order kinetic terms in NRQCD. I adapted the calculation in [122] to my action setup.

The (naive) derivative operators $\Delta^{(2)}$ and $\Delta^{(4)}$ can be written in momentum space as

$$\Delta^{(2)} \mapsto -\boldsymbol{p}^2 + \frac{a^2\boldsymbol{p}^4}{12} + \mathcal{O}((ap)^6), \qquad \Delta^{(4)} \mapsto \boldsymbol{p}^4 + \mathcal{O}((ap)^6) \tag{6.6}$$

with $\boldsymbol{p}^{2n} = \sum_{j=1}^{3} p_j^{2n}$. Note that for $n > 1$ this term breaks rotational invariance. In the following I will always work up to (and including) terms of $\mathcal{O}((ap)^4)$.

The position of the renormalised pole $\omega(\boldsymbol{p})$ is found by identifying the zeros of the inverse propagator

$$D_h^{-1}(\omega,\boldsymbol{p}) = 1 - e^{\omega(\boldsymbol{p})}\Gamma_n(\boldsymbol{p})^{2n}\Lambda_n(\boldsymbol{p}) - \alpha_s\Sigma(\omega_0(\boldsymbol{p}),\boldsymbol{p}). \tag{6.7}$$

One finds

$$\omega(\boldsymbol{p}) \;=\; \omega_0(\boldsymbol{p}) - \alpha_s \Sigma(\omega_0(\boldsymbol{p}), \boldsymbol{p}) \tag{6.8}$$

with

$$\omega_0(\boldsymbol{p}) \;=\; \frac{\boldsymbol{p}^2}{2m} - \frac{(\boldsymbol{p}^2)^2}{8m^3} + \alpha_s \left\{ -\tilde{c}_1^{(1)} \left(\frac{1}{2n} + \frac{1}{m} \right) \frac{(\boldsymbol{p}^2)^2}{8m^2} + c_5^{(1)} \frac{\boldsymbol{p}^4}{24m} \right\}. \tag{6.9}$$

The self-energy is written as in [122]

$$\Sigma(\omega, \boldsymbol{p}) \;=\; \Sigma_0(\omega) + \Sigma_1(\omega) \frac{\boldsymbol{p}^2}{2m} + \Sigma_2(\omega) \frac{(\boldsymbol{p}^2)^2}{8m^2} + \Sigma_3(\omega) \boldsymbol{p}^4. \tag{6.10}$$

The functions $\Sigma_j(\omega)$ can be extracted by taking suitable combinations of partial derivatives,

$$\begin{aligned} &\Sigma_0(\omega) = \Sigma(\boldsymbol{p}=0), && \Sigma_1(\omega) = m \frac{\partial^2 \Sigma}{\partial p_z^2}\Big|_{\boldsymbol{p}=0}, \\ &\Sigma_2(\omega) = m^2 \frac{\partial^4 \Sigma}{\partial p_y^2 \partial p_z^2}\Big|_{\boldsymbol{p}=0}, && \Sigma_3(\omega) = \frac{1}{24} \left(\frac{\partial^4 \Sigma}{\partial p_z^4} - 3 \frac{\partial^4 \Sigma}{\partial p_y^2 \partial p_z^2} \right)_{\boldsymbol{p}=0}. \end{aligned} \tag{6.11}$$

They can be further expanded in a Taylor-series in ω as $\Sigma_m(\omega) = \sum_{\ell=0}^{\infty} \Sigma_m^{(\ell)} \omega^\ell$. From this one obtains

$$\omega(\boldsymbol{p}) \;=\; \frac{\boldsymbol{p}^2}{2m_R} - \frac{(\boldsymbol{p}^2)^2}{8m_R^3} - \alpha_s \delta\omega(\boldsymbol{p}).$$

The renormalised mass is $m_R = Z_m m$ with

$$Z_m \;=\; 1 + \alpha_s \left(\Sigma_0^{(1)} + \Sigma_1^{(0)} \right) \tag{6.12}$$

and the correction term

$$\begin{aligned} \delta\omega(\boldsymbol{p}) &= W_0 + \left(W_1 + \tilde{c}_1^{(1)} \left(\frac{1}{2n} + \frac{1}{m} \right) \right) \frac{(\boldsymbol{p}^2)^2}{8m^2} + \left(W_2 - \frac{c_5^{(1)}}{24m} \right) \boldsymbol{p}^4 \\ W_0 &= \Sigma_0^{(0)} \\ W_1 &= \frac{2\Sigma^{(1)}}{m} + 2\Sigma_0^{(2)} + \frac{3\Sigma_1^{(0)}}{m} + 2\Sigma_1^{(1)} + \Sigma_2^{(0)} \\ W_2 &= \Sigma_3^{(0)} \end{aligned} \tag{6.13}$$

In particular the $\mathcal{O}(\alpha_s)$ corrections to $\tilde{c}_1$ and c_5, which cancel the radiative corrections, can be obtained,

$$\tilde{c}_1^{(1)} = -\left(\frac{1}{2n}+\frac{1}{m}\right)^{-1} W_1, \qquad\qquad c_5^{(1)} = 24mW_2. \tag{6.14}$$

The corresponding expressions for Morningstar's action described in (6.3) and (6.4) can be found in [122].

6.2.1 Mean field improvement

I calculate the mean field corrections to $\tilde{c}_1^{(1)}$ and $c_5^{(1)}$ for "partial" cancellation of $U_\mu U_\mu^\dagger$ as described in detail in section 5.1.3 and find

$$\begin{aligned}
\tilde{c}_1^{(1)(\text{tadpole})}/u_0^{(2)} &= -\frac{1}{8}\left(1+\frac{m}{2n}\right)^{-1}\Big[\frac{12}{n^2}-\frac{1}{n}+\frac{1}{2m}\left(\frac{3}{n^2}-4\right) \\
&\quad + \frac{6}{m^2}\left(\frac{1}{n}-12\right)+\frac{6}{m^3}\Big], \\
c_5^{(1)(\text{tadpole})}/u_0^{(2)} &= -\frac{4}{3}+\frac{1}{4m}+\frac{3}{m^2}-\frac{3}{8nm^2}-\frac{3}{4m^3}.
\end{aligned} \tag{6.15}$$

I also checked that I can reproduce the analytical expressions in [122].

If I include the $\Delta^{(6)}$ operator in the action the latter expression changes to

$$c_5^{(1)(\text{tadpole})}/u_0^{(2)} = -\frac{3}{5}+\frac{7}{20m}+\frac{3}{m^2}-\frac{3}{8nm^2}-\frac{3}{4m^3}. \tag{6.16}$$

Numerical results for several masses and stability parameters are collected in Tab. 6.1.

6.3 Implementation of derivatives

To extract W_1 and W_2 using (6.13) I implement the higher order derivatives using two different approaches:

Analytical mixed derivatives. The TaylUR code can handle higher order mixed derivatives of the form $(\partial/\partial x_j)^n(\partial/\partial x_k)^m$ for $(n+m) \leq$ `Max_Taylor_order`. However, derivatives up to $n+m=4$ need to be calculated and this slows down the code significantly. To improve the performance, unnecessary mixed derivatives can be "switched off" and the Leibniz rule is not overloaded for these.

Numerical derivatives. Alternatively I implement higher order mixed derivatives using finite differences. For this I compute the second order derivative with respect

m	n	$\Delta^{(6)}$?	$\tilde{c}_1^{(1)(\text{tadpole})}/u_0^{(2)}$	$c_5^{(1)(\text{tadpole})}/u_0^{(2)}$
2.3	2	—	0.8537	−0.7546
2.8	2	—	0.4859	−0.9195
1.95	4	—	1.8300	−0.5420
2.8	4	—	0.8241	−0.9075
3.4	4	—	0.5269	−1.0275
1.95	4	✓	—	0.2426
2.8	4	✓	—	−0.1385
3.4	4	✓	—	−0.2647

Table 6.1: Mean field corrections to $\tilde{c}_1^{(1)}$ and $c_5^{(1)}$ for the full NRQCD action for different masses and stability parameters. The last three rows show results with $\Delta^{(6)}$ included in the action.

to p_z analytically by using a TaylUR object. Additional higher order derivatives are realised by finite differences, for example

$$(\partial/\partial p_z)^2(\partial/\partial p_y)^2\Sigma(p) \quad = \quad \frac{\partial_z^2\Sigma(p+\delta p\cdot\hat{y})+\partial_z^2\Sigma(p-\delta p\cdot\hat{y})-2\partial_z^2\Sigma(p)}{(\delta p)^2} \tag{6.17}$$

where $\partial_z = \partial/\partial p_z$ etc.

I analysed the speed of the code depending on which realisation of mixed higher order derivatives is used. Masking unwanted derivatives leads to a speedup of roughly one order of magnitude but the code is still about a factor of ten slower than for numerical derivatives, so these should be used if possible, i.e. if the function to be integrated is sufficiently smooth.

In appendix H I demonstrate that large peaks in the infrared region of the rainbow integral lead to numerical instabilities when using finite differences. It is thus mandatory to use analytical mixed derivatives in the calculation of this particular diagram.

On the other hand the integrand of the numerically more expensive tadpole diagram is much smoother in the infrared. This is because this diagram does not contain a heavy quark propagator whose power can be raised by derivatives with respect to the external momentum. Here it is sufficient to use finite differences to represent higher order mixed derivatives.

6.4 Numerical results

6.4.1 VEGAS integrals

The integrals I evaluate are

$$W_1 = \int \frac{d^4k}{(2\pi)^4} D_1 f^{(\mathrm{lat})} \qquad\qquad W_2 = \int \frac{d^4k}{(2\pi)^4} D_2 f^{(\mathrm{lat})} \tag{6.18}$$

where $f^{(\mathrm{lat})} = f^{(\mathrm{lat})}_{\mathrm{rainbow}} + f^{(\mathrm{lat})}_{\mathrm{tadpole}}$ is the lattice integrand as given explicitly in (5.18).

As can be seen from (6.11) and (6.13) the derivative operators D_1 and D_2 are defined as

$$\begin{aligned} D_1 f &= -\frac{2}{m}\frac{\partial}{\partial p_0}\mathrm{Im}\{f\} - 2\frac{\partial^2}{\partial p_0^2}\mathrm{Re}\{f\} + 3\frac{\partial^2}{\partial p_z^2}\mathrm{Re}\{f\} \\ &\quad - 2m\frac{\partial^3}{\partial p_z^2 \partial p_0}\mathrm{Im}\{f\} + m^2\frac{\partial^4}{\partial p_y^2 \partial p_z^2}\mathrm{Re}\{f\}, \\ D_2 f &= \frac{1}{24}\left(\frac{\partial^4}{\partial p_z^4}\mathrm{Re}\{f\} - 3\frac{\partial^4}{\partial p_y^2 \partial p_z^2}\mathrm{Re}\{f\}\right) \end{aligned} \tag{6.19}$$

where all derivatives are evaluated at $p = 0$.

Although both W_1 and W_2 are infrared finite quantities the integrand of the rainbow diagram has large peaks in the infrared region. Convergence of the VEGAS integration can be improved significantly by introducing suitable subtraction functions $D_1 f^{(\mathrm{sub})}$ and $D_2 f^{(\mathrm{sub})}$ which are discussed in appendix J.2. I thus write the lattice integrals as a sum of a subtracted lattice integral and the integral over the subtraction function

$$W_1 = I_1^{(\mathrm{lat-sub})} + I_1^{(\mathrm{sub})}, \qquad\qquad W_2 = I_2^{(\mathrm{lat-sub})}. \tag{6.20}$$

Note that for W_2 the integral over the subtraction function vanishes due to rotational invariance in the continuum. The integrand of the subtraction integral for W_1 is simple so evaluation of this integral is numerically inexpensive and can be carried out to very high accuracy.

Evaluation of the two-gluon vertex is expensive and it turns out that around 2/3 of the time is spent on evaluating the tadpole diagram. On the other hand the integrand is relatively smooth as the external derivatives only act on the two-gluon vertex and do not generate higher powers of the quark propagator. It is thus legitimate to use numerical derivatives when evaluating this diagram. This leads to a further speedup of

	results from [122]	my calculation
$-A = E_0 = \Omega_0$	$-3.44(5)$	$-3.389(3)$
$B = \delta Z_m = \Omega_0 - \Omega_1 + \Omega_2$	$1.92(5)$	$1.897(8)$
$c_1^{(2)}$	$-0.90(5)$	$-0.947(3)$
$c_2^{(2)}$	$1.10(5)$	$1.075(2)$

Table 6.2: Heavy quark renormalisation parameters from [122] and my calculation. The heavy quark action is defined in [122] with heavy quark mass $m = 2.0$ and stability parameter $n = 2$, the gluon action is the unimproved Wilson action and mean field corrections are not included.

the code if I split up the first integral in (6.20) as

$$\begin{aligned} W_1 &= I_{1,\text{rainbow}}^{(\text{lat}-\text{sub})} + I_{1,\text{tadpole}}^{(\text{lat})} + I_1^{(\text{sub})} \\ &= \int \frac{d^4k}{(2\pi)^4} \left[D_1 f_{\text{rainbow}}^{(\text{lat})} - D_1 f^{(\text{sub})} \right] + \int \frac{d^4k}{(2\pi)^4} D_1 f_{\text{tadpole}}^{(\text{lat})} \\ &\quad + \int \frac{d^4k}{(2\pi)^4} D_1 f^{(\text{sub})} \end{aligned} \tag{6.21}$$

where numerical derivatives are used in $I_{\text{tadpole}}^{(\text{lat})}$. The corresponding expression for W_2 is

$$\begin{aligned} W_2 &= I_{2,\text{rainbow}}^{(\text{lat}-\text{sub})} + I_{2,\text{tadpole}}^{(\text{lat})} \\ &= \int \frac{d^4k}{(2\pi)^4} \left[D_2 f_{\text{rainbow}}^{(\text{lat})} - D_2 f^{(\text{sub})} \right] + \int \frac{d^4k}{(2\pi)^4} D_2 f_{\text{tadpole}}^{(\text{lat})}. \end{aligned} \tag{6.22}$$

Comparison to the literature

To verify my code I reproduce the results for E_0, δZ_m, $c_1^{(2)}$ and $c_2^{(2)}$ given in [122]. I use the simple action setup described there with the Wilson gluon action. The results (without inclusion of mean field corrections) are shown in Fig. 2 of [122] (I estimate the errors from reading off the exact numbers from the plot to be 0.05). For E_0 and δZ_m I use a gluon mass of $\lambda^2 = 10^{-6}$. The calculation of the higher order kinetic terms $c_1^{(2)}$ and $c_2^{(2)}$ is discussed in detail in appendix H.3 where I also demonstrate that the results are numerically stable for $\lambda \to 0$ and an extrapolation in the gluon mass is not necessary. The results in Tab. 6.2 are obtained by averaging results for $\lambda^2 = 10^{-6}$, 10^{-9} and 10^{-12}. In the following I will work with $\lambda^2 = 10^{-6}$. Within errors I find perfect agreement with the results in [122].

m	n	gluons	$I^{(\mathrm{lat-sub})}_{1,\mathrm{rainbow}}$	$I^{(\mathrm{lat})}_{1,\mathrm{tadpole}}$	$I^{(\mathrm{sub})}_{1}$	W_1
2.3	2	Wilson	1.035(12)	0.4455(30)	−1.4603(37)	0.020(13)
2.8	2	Symanzik	0.820(12)	0.1176(16)	−1.1974(31)	−0.260(12)
1.95	4	Symanzik	1.225(12)	0.8801(28)	−1.7234(41)	0.382(13)
2.8	4	Symanzik	0.830(12)	0.2065(15)	−1.1974(31)	−0.161(13)
3.4	4	Symanzik	0.653(12)	0.1031(14)	−0.9891(26)	−0.233(12)

Table 6.3: The integrals $I^{(\mathrm{lat-sub})}_{1,\mathrm{rainbow}}$, $I^{(\mathrm{lat})}_{1,\mathrm{tadpole}}$, $I^{(\mathrm{sub})}_{1}$ and their sum W_1 for different action parameters and the full $\mathcal{O}(1/m^2, v^4_{\mathrm{rel}})$ NRQCD action.

m	n	$\Delta^{(6)}$?	gluons	$10^2 \times I^{(\mathrm{lat-sub})}_{2,\mathrm{rainbow}}$	$10^2 \times I^{(\mathrm{lat})}_{2,\mathrm{tadpole}}$	$10^2 \times W_2$
2.3	2	—	Wilson	0.253(27)	1.9968(81)	2.250(28)
2.8	2	—	Symanzik	−0.069(16)	1.7338(60)	1.665(17)
1.95	4	—	Symanzik	0.494(36)	1.2120(56)	1.706(36)
2.8	4	—	Symanzik	−0.051(16)	1.6678(59)	1.617(17)
3.4	4	—	Symanzik	−0.142(11)	1.6321(60)	1.490(13)
1.95	4	✓	Symanzik	0.8836(80)	−1.2362(21)	−0.3526(83)
2.8	4	✓	Symanzik	0.2195(38)	0.0206(10)	0.2400(39)
3.4	4	✓	Symanzik	0.0614(26)	0.2613(9)	0.3227(28)

Table 6.4: The integrals $I^{(\mathrm{lat-sub})}_{2,\mathrm{rainbow}}$, $I^{(\mathrm{lat})}_{2,\mathrm{tadpole}}$ and their sum W_2 for different action parameters and the full heavy quark action. The results in the last three rows are obtained with a NRQCD action which contains the $\Delta^{(6)}$ improvement term that removes tree level discretisation errors in the kinetic terms at $\mathcal{O}(p^6)$.

6.4.2 Results for the full NRQCD action

I compute $\tilde{c}^{(1)}_1$ and $c^{(1)}_5$ for the full $\mathcal{O}(1/m^2, v^4_{\mathrm{rel}})$ NRQCD action defined by (6.1) both with Wilson gluons and Symanzik improved glue and the masses chosen in the nonperturbative simulations carried out by Stefan Meinel and Iain Kendall, see section 6.5.

The values of the individual integrals $I^{(\mathrm{lat-sub})}_{1,\mathrm{rainbow}}$, $I^{(\mathrm{lat})}_{1,\mathrm{tadpole}}$, $I^{(\mathrm{sub})}_{1}$ and W_1 are given in Tab. 6.3; the corresponding results for W_2 can be found in Tab. 6.4.

Both for W_1 and W_2 the dominant uncertainty comes from the subtracted rainbow diagram, $I^{(\mathrm{lat-sub})}_{\mathrm{rainbow}}$. After adding on the value of the subtraction integral, the rainbow diagram is of comparable magnitude but different sign as the tadpole diagram for W_1 whereas $I^{(\mathrm{lat-sub})}_{2,\mathrm{rainbow}}$ is usually significantly smaller than $I^{(\mathrm{lat})}_{2,\mathrm{tadpole}}$ for W_2.

In Tab. 6.6 I list values for $\tilde{c}_1^{(1)}$ and $c_5^{(1)}$. For Wilson gluons I use $u_0^{(2)} = 0.9735$ from [102] and for the improved gluon action $u_0^{(2)} = 0.750$ (see [125]). I also plot my results, together with those I obtained using Morningstar's action in Fig. 6.1.

m	n	gluons	$\tilde{c}_1^{(1)}$[VEGAS only]	$\tilde{c}_1^{(1)}$
2.3	2	Wilson	−0.029(19)	0.802(19)
2.8	2	Symanzik	0.428(20)	0.793(20)
1.95	4	Symanzik	−0.599(21)	0.774(21)
2.8	4	Symanzik	0.333(26)	0.951(26)
3.4	4	Symanzik	0.556(30)	0.952(30)

Table 6.5: Results for the coefficient $\tilde{c}_1^{(1)}$ for different action parameters and the full heavy quark action. The numbers in the fourth column do not include the mean field corrections. In the last column I give the final results.

m	n	$\Delta^{(6)}$?	gluons	$c_5^{(1)}$[VEGAS only]	$c_5^{(1)}$
2.3	2	—	Wilson	1.242(15)	0.507(15)
2.8	2	—	Symanzik	1.119(12)	0.429(12)
1.95	4	—	Symanzik	0.799(17)	0.392(17)
2.8	4	—	Symanzik	1.087(11)	0.406(11)
3.4	4	—	Symanzik	1.216(10)	0.445(10)
1.95	4	✓	Symanzik	−0.1650(39)	0.0170(39)
2.8	4	✓	Symanzik	0.1613(26)	0.0574(26)
3.4	4	✓	Symanzik	0.2633(23)	0.0648(23)

Table 6.6: Results for the coefficient $c_5^{(1)}$ for different action parameters and the full $\mathcal{O}(1/m^2, v_{\rm rel}^4)$ heavy quark action. The numbers in the fifth column do not include mean field corrections. In the last column I give the final results. The results in the last three rows are obtained with a NRQCD action which contains the $\Delta^{(6)}$ improvement term that removes tree level discretisation errors in the kinetic terms at $\mathcal{O}(p^6)$.

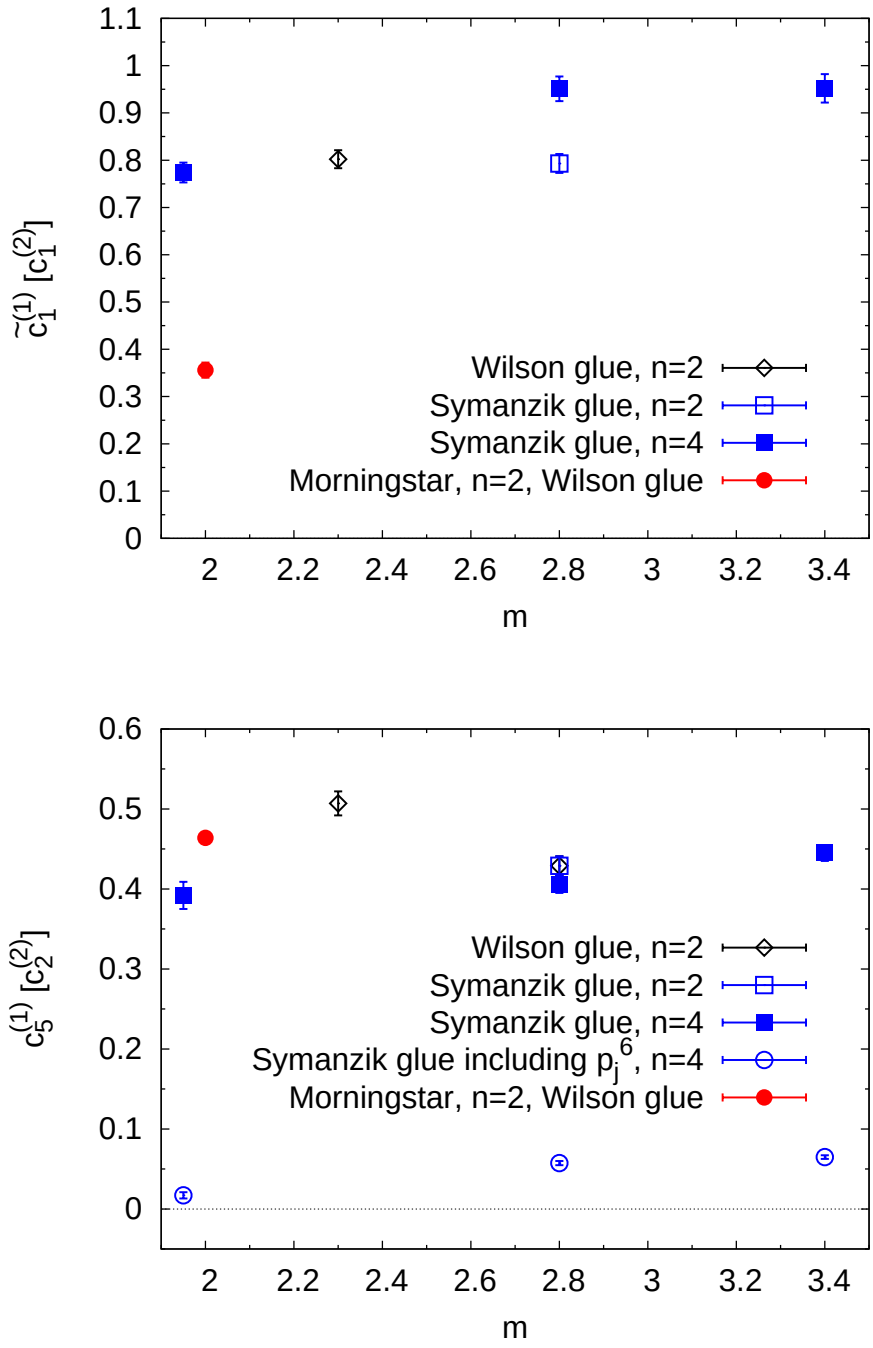

Figure 6.1: Results for the coefficient $\tilde{c}_1^{(1)}$ (top) and $c_5^{(1)}$ (bottom) for different action parameters, including mean field corrections. Note that including the $\mathcal{O}(p^6)$ improvement term $\Delta^{(6)}$ changes the coefficients significantly. I also show the numbers I obtained for $c_1^{(2)}$ and $c_2^{(2)}$ with the Morningstar action [122], in this case I use the one loop value of $u_0^{(2)} = \pi/3$ given there.

lattice	$E(2,2,1) - E(3,0,0)$
$16^3 \times 32$ lattice, Wilson glue	0.00094(38)
$20^3 \times 64$ coarse MILC lattice	0.00082(78)
$16^3 \times 48$ super coarse MILC lattice	0.00133(10)

Table 6.7: Energy splittings between mesons with different $\sum_j p_j^4$ from numerical simulations.

6.5 Nonperturbative results

The presence of rotationally noninvariant terms in the Lagrangian leads to a splitting between the energies of mesons with three-momentum $\boldsymbol{p} = (2,2,1)\frac{2\pi}{L}$ and $\boldsymbol{p} = (3,0,0)\frac{2\pi}{L}$. Iain Kendall [132] and Stefan Meinel [61] have computed this energy difference for different lattices:

- $16^3 \times 32$ lattice, $\beta = 6/g^2 = 5.8$, Wilson gluons (quenched). The heavy quark mass is $m = 2.3$, stability parameter $n = 2$ [Stefan Meinel, using gauge configurations described in [133]].
- $16^3 \times 48$ super coarse MILC lattice with $\beta = 10/g^2 = 6.458$, $2+1$ flavours of rooted staggered quarks, $m = 3.4$, $n = 4$ [Iain Kendall].
- $20^3 \times 64$ coarse MILC lattice with $\beta = 10/g^2 = 6.76$, $2+1$ flavours of rooted staggered quarks, $m = 2.8$, $n = 2$ [Stefan Meinel].

The heavy quark action is always the full $\mathcal{O}(1/m^2, v_{\text{rel}}^4)$ NRQCD action. The results are summarised in Tab. 6.7. In all cases, except for the coarse MILC lattice with Symanzik gluons, the splitting is significantly different from zero.

It turns out that the energy splitting on the super coarse MILC lattice can be set to zero by choosing $c_5 = 2.6$ [132].

6.6 Observations

After including mean field corrections the $\mathcal{O}(\alpha_s)$ coefficients are of the order of one. For the full $\mathcal{O}(1/m^2, v_{\text{rel}}^4)$ NRQCD action with stability parameter $n = 4$ they do not show a strong heavy quark mass dependence. The choice of stability parameter has only a very small influence on $c_5^{(1)}$ and a slightly larger impact on $\tilde{c}_1^{(1)}$

Including the $\mathcal{O}(a^6)$ improvement term $\Delta^{(6)}/(180m)$ reduces the size of the renormalisation of the rotationally noninvariant term $\sum_j p_j^4$ by a factor of $5 - 10$. This indicates that this term significantly reduces discretisation errors which break

	without $\Delta^{(6)}$	with $\Delta^{(6)}$
E_0	$-0.76647(40)$	$-0.73290(40)$
$\delta\overline{Z}_\psi$	$-0.77338(48)$	$-0.79006(47)$
δZ_m	$0.2313(12)$	$0.2347(12)$

Table 6.8: Leading order renormalisation parameters with and without the $\Delta^{(6)}/(180m)$ term in the NRQCD action. I use the full $\mathcal{O}(1/m^2, v_{\mathrm{rel}}^4)$ NRQCD action with $m = 2.8$ and $n = 2$. The gluon action is Symanzik improved. Mean field corrections for "partial" cancellation of $U_\mu U_\mu^\dagger$ are included.

rotational invariance. Note that although the term is of $\mathcal{O}(a^6)$ is is only suppressed by two powers of the lattice spacing relative to the fourth order renormalisation parameters which I calculate. In the continuum, where the theory is rotationally invariant, the coefficient $c_5^{(1)}$ vanishes. I checked that the influence of $\Delta^{(6)}/(180m)$ on the leading order renormalisation parameters is small, see Tab. 6.8.

The nonperturbative results obtained by Iain Kendall predict a strong correction to the $\Delta^{(4)}$ term. This does not agree with I find in my perturbative calculations. One explanation for this discrepancy are large two-loop effects. However, the NRQCD action is not the only ingredient of the lattice calculation where rotational symmetry is broken. The simulations were carried out on relatively coarse lattices and the effect might be reduced on finer configurations where the dispersion relation can be probed for smaller, nonrelativistic lattice momenta; more work is needed to clarify this. The results in Tab. 6.7 suggest that the energy splitting is reduced on the coarse MILC lattice, however, the errors on this number still need to be reduced significantly. In my perturbative calculations I also see a strong influence of the $\mathcal{O}(a^6)$ improvement term which was included with the tree level coefficient in nonperturbative simulations. Instead of fixing this term to its classical value and tuning the $\Delta^{(4)}$ nonperturbatively it might be better to fit both the $\mathcal{O}(a^4)$ and $\mathcal{O}(a^6)$ coefficients simultaneously to avoid a spurious minimum of χ^2. An alternative approach would be to fix the $\mathcal{O}(a^4)$ term to the perturbative result and adjust the coefficient of the $\mathcal{O}(a^6)$ term by nonperturbative tuning.

Chapter 7

Matching of heavy-light currents

In this chapter I match the heavy-light vector and tensor currents to the effective heavy quark theory on the lattice. The vector current

$$Q_0^{(V)\mu} \quad = \quad \overline{q}\gamma^\mu\Psi \tag{7.1}$$

arises in the $b \to q$ transition of the semileptonic decay $B \to \pi\ell\nu$, see (1.6). The heavy quark field is denoted by $\Psi(x)$ and the light quark by $q(x)$. Hadronic matrix elements of this current are also needed for predictions of the rare decay $B \to K^{(*)}\ell^+\ell^-$; in the operators Q_9 and Q_{10} (see section 2.2.1) the heavy-light current $\overline{s}\gamma^\mu P_L b$ is coupled to the leptonic (axial-) vector current. I set the light quark mass, which is much smaller than the hadronic scale $\Lambda_{\rm QCD}$, to zero throughout the matching calculation. Then it is legitimate to drop chiral projectors $P_{R/L} = \frac{1\pm\gamma_5}{2}$ as the matching coefficients do not depend on them.

The electromagnetic tensor operator $Q_0^{(T)\mu\nu}$, coupled to the field strength $F_{\mu\nu}$, appears in the $b \to s$ Hamiltonian and is defined as

$$Q_7 \equiv Q_0^{(T)\mu\nu}F_{\mu\nu} \quad = \quad \frac{e}{16\pi^2}m(\overline{q}\sigma^{\mu\nu}\Psi)F_{\mu\nu} \tag{7.2}$$

where I have already dropped the chiral projector. In the following I use the notation

$$Q_0^{(\Gamma)} \quad = \quad \rho^{(\Gamma)}\overline{q}\Gamma\Psi \tag{7.3}$$

with

$$\rho^{(V)} = 1 \quad \text{(vector)}, \qquad\qquad \rho^{(T)} = \frac{e}{16\pi^2}m \quad \text{(tensor)}. \tag{7.4}$$

For the matching calculation it is necessary to calculate one loop matrix elements $\langle q|Q_0^{(\Gamma)}|b\rangle$ both in the continuum and on the lattice. In the continuum this is done between an on-shell heavy quark with momentum p and a light quark with momentum p' in the final state. In the following I perform this calculation as an expansion in

$p^\mu_{\rm res}/m$, p'^μ/m, s/m^2 where $s/m = 2p\cdot p'/m = 2E'$ is (twice) the energy of the final state quark in the rest frame of the decaying meson. The heavy quark momentum is $p = mu + p_{\rm res}$.

7.1 Continuum calculation

Due to Lorentz invariance the matrix element can be written as

$$\langle q|Q_0^{(\Gamma)}|b\rangle_{\rm con} = \sum_j Z_j^{(\Gamma,{\rm con})}\langle q|Q_j^{(\Gamma)}|b\rangle_{\rm tree} \tag{7.5}$$

where the operators $Q_j^{(\Gamma)}$ are defined by their Dirac structure:

- Vector:

$$Q_0^{(V)\mu} = \overline{q}\gamma^\mu\Psi, \qquad Q_1^{(V)\mu} = \frac{p^\mu}{m}\overline{q}\Psi, \qquad Q_2^{(V)\mu} = \frac{p'^\mu}{m}\overline{q}\Psi. \tag{7.6}$$

  As $p^\mu = mu^\mu + p^\mu_{\rm res}$ the second operator contributes at leading order in $1/m$ where it can be written as $Q_1^{(V)\mu} = u^\mu\overline{q}\Psi$.

- Tensor:

$$\begin{aligned} Q_0^{(T)\mu\nu} &= \rho^{(T)}\left(\overline{q}\sigma^{\mu\nu}\Psi\right), \\ Q_1^{(T)\mu\nu} &= \frac{2i\rho^{(T)}}{m}\left(\overline{q}\left(\gamma^\mu p^\nu - \gamma^\nu p^\mu\right)\Psi\right), \\ Q_2^{(T)\mu\nu} &= \frac{2i\rho^{(T)}}{m}\left(\overline{q}\left(\gamma^\mu p'^\nu - \gamma^\nu p'^\mu\right)\Psi\right), \\ Q_3^{(T)\mu\nu} &= \frac{2i\rho^{(T)}}{m}\left(\overline{q}\left(p^\mu p'^\nu - p^\nu p'^\mu\right)\Psi\right). \end{aligned} \tag{7.7}$$

  Again, both $Q_0^{(T)\mu\nu}$ and $Q_1^{(T)\mu\nu}$ are leading order in $1/m$.

The mixing matrix can be expanded in the strong coupling constant

$$Z_j^{(\Gamma,{\rm con})} = \delta_{0j} + \alpha_s\delta Z_j^{(\Gamma,{\rm con})} + \ldots \tag{7.8}$$

and the one loop coefficients are computed order by order in the heavy quark expansion. In particular I find for the one loop matrix element in the static limit, where $1/m$ corrections are ignored,

- Vector:

$$\begin{aligned} \delta Z_0^{(V,\mathrm{con})} &= \frac{\alpha_s}{3\pi}\left(-\frac{11}{4}-\frac{3}{2}\log\lambda^2/m^2\right), \\ \delta Z_1^{(V,\mathrm{con})} &= \frac{2}{3\pi}. \end{aligned} \tag{7.9}$$

- Tensor:

$$\begin{aligned} \delta Z_0^{(T,\mathrm{con})} &= \frac{1}{3\pi}\left(-\frac{27}{4}-\frac{3}{2}\log\lambda^2/m^2+4\log m^2/\mu^2\right), \\ \delta Z_1^{(T,\mathrm{con})} = \delta Z_2^{(T,\mathrm{con})} = \delta Z_3^{(T,\mathrm{con})} &= 0. \end{aligned} \tag{7.10}$$

Details of the calculation can be found in appendix I where I also include $\mathcal{O}(1/m)$ corrections and compare my expressions to the literature.

Note that for the tensor current the $\overline{MS}$ mass is used. The on-shell mass is defined perturbatively both in the continuum and on the lattice so in principle the following matching calculation should be carried out in the on-shell scheme and then converted to an $\overline{MS}$ mass (see (D.14)). In (7.10) this conversion is understood to be carried out implicitly at the end of the calculation.

In contrast to the vector operator, which is protected from renormalisation by gauge invariance, the tensor operator is not conserved and its anomalous dimension does not vanish. Indeed I find in appendix I.3:

$$\gamma_T^{(\mathrm{con})} = \frac{8\alpha_s}{3\pi}+\ldots \tag{7.11}$$

which agrees with what is reported in [45].

7.2 Matching to lattice mNRQCD

On the lattice I construct operators $Q_0^{(\Gamma,\mathrm{lat})}$ which have the same on-shell matrix elements as the continuum operators $Q_0^{(\Gamma)}$,

$$\langle q|Q_0^{(\Gamma,\mathrm{lat})}|b\rangle_{\mathrm{lat}} = \langle q|Q_0^{(\Gamma)}|b\rangle_{\mathrm{con}}. \tag{7.12}$$

In this section I construct these operators at leading order in the heavy quark expansion and show how one loop coefficients can be adjusted such that (7.12) holds at $\mathcal{O}(\alpha_s)$.

7.2.1 Operators

At tree level the operator in the effective theory is obtained from (7.1) and (7.2) by applying the field transformation

$$\Psi(x) = \Lambda_{1/2}\tilde{T}(\tilde{x})e^{-im\gamma^0 u\cdot x}A_{D_t}\frac{1}{\sqrt{\gamma}}\tilde{\Psi}_v^{(+)} \tag{7.13}$$

where in $\tilde{\Psi}_v^{(+)} = (\psi_v, 0)^T$ I only keep the positive energy, particle component. Up to corrections of $\mathcal{O}(1/m^2)$ the Foldy-Wouthuysen transformation T and the field transformation A_{D_t} are given by

$$\begin{aligned} T &= 1 + \frac{i\not{D}}{2m} - i\frac{\not{u}\,(u\cdot D)}{2m}, \\ A_{D_t} &= 1 + \frac{i\gamma \boldsymbol{v}^2 D_0}{4m} + \frac{i\gamma(1-\boldsymbol{v}^2/2)\boldsymbol{v}\cdot\boldsymbol{D}}{2m}. \end{aligned} \tag{7.14}$$

These expressions can be simplified using the leading order equation of motion, $u\cdot D\tilde{\Psi}_v^{(+)} = 0$ and one finally finds for the field transformation

$$\Psi(x) = \frac{1}{\sqrt{\gamma}}\Lambda_{1/2}\left(1 - \frac{i\gamma_0\boldsymbol{v}\cdot\boldsymbol{D}}{2m} + \frac{i\boldsymbol{\gamma}\cdot\boldsymbol{D}}{2m} + \frac{i\boldsymbol{v}\cdot\boldsymbol{D}}{2\gamma m}\right)\tilde{\Psi}_v^{(+)}. \tag{7.15}$$

By inserting this into (7.6) and (7.7) the tree level currents in the effective theory to $\mathcal{O}(1/m)$ can be read off. The coefficients of the different operators in the $1/m$ expansion will get renormalised by radiative corrections. Matrix elements of the $1/m$ operators are only calculated at tree level; they are expected to give corrections of $\mathcal{O}(\Lambda_{\rm QCD}/m) \sim 10\%$ relative to the leading order. This is smaller than the naive estimate of radiative corrections to leading order operators which is expected to be $\mathcal{O}(\alpha_s) \sim 30\%$.

At leading order in the $1/m$ expansion both the Foldy-Wouthuysen transformation $\tilde{T}(\tilde{x})$ and the field transformation A_{D_t} are equal to the identity and can be dropped. The Lorentz boost matrix is (in Minkowski space)

$$\Lambda_{1/2} = \frac{1}{\sqrt{2(1+\gamma)}}\left((1+\gamma) - \gamma v\hat{\boldsymbol{v}}\cdot\boldsymbol{\gamma}\gamma^0\right). \tag{7.16}$$

In the continuum the operator basis $Q_0^{(\Gamma)}$, $Q_1^{(\Gamma)}$ is used (see, for example, [67] where the matching calculation between QCD and continuum HQET is performed at leading order in the heavy quark expansion). On the lattice Lorentz invariance is broken and another operator basis is used. First, consider the operator $Q_0^{(\Gamma)}$ which is split into the

sum of two operators with different Dirac structure, $Q_0^{(\Gamma)} = Q_{0,1}^{(\Gamma)} + Q_{0,2}^{(\Gamma)}$ with

$$\begin{aligned} Q_{0,1}^{(\Gamma)} &= \rho^{(\Gamma)} f_1(v) \overline{q}(x) \Gamma \tilde{\Psi}_v^{(+)}, \\ Q_{0,2}^{(\Gamma)} &= -\rho^{(\Gamma)} f_2(v) \overline{q}(x) \Gamma \hat{\boldsymbol{v}} \cdot \boldsymbol{\gamma} \gamma^0 \tilde{\Psi}_v^{(+)}. \end{aligned} \tag{7.17}$$

The velocity dependence has been absorbed in the functions

$$f_1(v) = \sqrt{\frac{1+\gamma}{2\gamma}}, \qquad f_2(v) = v\sqrt{\frac{\gamma}{2(1+\gamma)}} \tag{7.18}$$

and $\hat{\boldsymbol{v}}$ is a unit vector in the direction of the frame velocity, which is chosen to be parallel to a lattice axis.

The other leading order tree level matrix elements of operators with $\Gamma = \gamma^\mu$ replaced by $\tilde{\Gamma} = u^\mu$ (vector) and $\Gamma = \sigma^{\mu\nu}$ replaced by $\tilde{\Gamma} = 2(\gamma^\mu u^\nu - \gamma^\nu u^\mu)$ (tensor) can always be expressed as linear combinations of $Q_{0,1}^{(\Gamma)}$ and $Q_{0,2}^{(\Gamma)}$, for example

$$\begin{aligned} Q_{0,1}^{(\tilde{V})0} &= \gamma Q_{0,1}^{(V)0}, & Q_{0,2}^{(\tilde{V})0} &= -\gamma Q_{0,2}^{(V)0}, \\ Q_{0,1}^{(\tilde{V})\parallel} &= (1+\gamma) Q_{0,2}^{(V)\parallel}, & Q_{0,2}^{(\tilde{V})\parallel} &= (1-\gamma) Q_{0,1}^{(V)\parallel}. \end{aligned} \tag{7.19}$$

The Lorentz index can be timelike (0), parallel ($\parallel$) or orthogonal ($\perp$) to the frame velocity. Clearly, the decomposition in (7.19) is not Lorentz invariant.

On the lattice the two operators in (7.17) mix under renormalisation,

$$\langle q | Q_{0,j}^{(\Gamma)} | b \rangle_{\text{lat}} = \sum_k \left(\delta_{jk} + \alpha_s \delta Z_{jk}^{(\Gamma,\text{lat})} + \dots \right) \langle q | Q_{0,k}^{(\Gamma)} | b \rangle_{\text{tree}} \tag{7.20}$$

It is convenient to work in the basis $Q_{0,\pm}^{(\Gamma)} = Q_{0,1}^{(\Gamma)} \pm Q_{0,2}^{(\Gamma)}$ as only the operator $Q_{0,+}^{(\Gamma)}$ contributes at tree level. In the continuum the one loop matrix element is (see section (7.1))

$$\langle q | Q_{0,+}^{(\Gamma)} | b \rangle_{\text{con}} = (1 + \alpha_s \delta Z_+^{(\Gamma,\text{con})}) \langle q | Q_{0,+}^{(\Gamma)} | b \rangle_{\text{tree}} + \alpha_s \delta Z_-^{(\Gamma,\text{con})} \langle q | Q_{0,-}^{(\Gamma)} | b \rangle_{\text{tree}}. \tag{7.21}$$

- Vector: One has to distinguish whether the Lorentz index of the current is timelike, parallel or perpendicular to the frame velocity. (7.19) is used to calculate

the mixing matrix elements $Z_{\pm}^{(\Gamma,\mathrm{con})}$:

$$\begin{aligned}
\delta Z_{+}^{(V,\mathrm{con})0} &= \delta Z_{0}^{(V,\mathrm{con})}, & \delta Z_{-}^{(V,\mathrm{con})0} &= \gamma \delta Z_{1}^{(V,\mathrm{con})}, \\
\delta Z_{+}^{(V,\mathrm{con})\parallel} &= \delta Z_{0}^{(V,\mathrm{con})} + \delta Z_{1}^{(V,\mathrm{con})}, & \delta Z_{-}^{(V,\mathrm{con})\parallel} &= -\gamma \delta Z_{1}^{(V,\mathrm{con})}, \\
\delta Z_{+}^{(V,\mathrm{con})\perp} &= \delta Z_{0}^{(V,\mathrm{con})}, & \delta Z_{-}^{(V,\mathrm{con})\perp} &= 0.
\end{aligned} \tag{7.22}$$

- Tensor: Here $\delta Z_{1}^{(T,\mathrm{con})}$ is zero, so there is no dependence on the Lorentz indices

$$\delta Z_{+}^{(T,\mathrm{con})} = \delta Z_{0}^{(T,\mathrm{con})}, \qquad \delta Z_{-}^{(T,\mathrm{con})} = 0. \tag{7.23}$$

Combining (7.20) and (7.21) the lattice operator which has the same one loop matrix elements as the continuum operator is

$$Q_{0}^{(\Gamma,\mathrm{lat})} \;=\; \left(1 + \alpha_s c_{+}^{(\Gamma)}\right) Q_{0,+}^{(\Gamma)} + \alpha_s c_{-}^{(\Gamma)} Q_{0,-}^{(\Gamma)} \tag{7.24}$$

with

$$c_{+}^{(\Gamma)} = \delta Z_{+}^{(\Gamma,\mathrm{con})} - \delta Z_{++}^{(\Gamma,\mathrm{lat})}, \qquad c_{-}^{(\Gamma)} = \delta Z_{-}^{(\Gamma,\mathrm{con})} - \delta Z_{+-}^{(\Gamma,\mathrm{lat})}. \tag{7.25}$$

Mixing matrix

In the $(1,2)$ basis of operators the mixing matrix can be split into a diagonal part and a contribution $\xi_{jk}^{\mu\nu}$ from one particle irreducible (1PI) diagrams,

$$\delta Z_{jk}^{(\Gamma,\mathrm{lat})} \;=\; \left(\delta Z_{\mathrm{mult}}^{(\Gamma)} - \delta Z_{f_j}\right) \delta_{jk} + \xi_{jk}^{(\Gamma)}. \tag{7.26}$$

For the vector current the multiplicative renormalisation contains the wavefunction renormalisations only, $\delta Z_{\mathrm{mult}}^{(V)} = \frac{1}{2}\left(\delta Z_q + \delta Z_\psi\right)$ whereas for the tensor current there is an additional contribution from mass renormalisation, $\delta Z_{\mathrm{mult}}^{(T)} = \frac{1}{2}\left(\delta Z_q + \delta Z_\psi\right) - \delta Z_m$. The relation between renormalised and bare parameters is $\boldsymbol{v}_R = Z_v v$, $\gamma_R = (1-\boldsymbol{v}_R^2)^{-1/2}$, $m_R = Z_m m$ and $q = \sqrt{Z_q} q_R$, $\Psi = \sqrt{Z_\psi}\Psi_R$ where all renormalisation constants can be expanded in the strong coupling constant as $Z_x = 1 + \alpha_s \delta Z_x + \ldots$. The renormalisation of the velocity functions $f_{1,2}$ is $f_{j,R} = Z_{f_j} f_j$ with

$$\delta Z_{f_1} = \frac{1-\gamma}{2}\delta Z_v, \qquad \delta Z_{f_2} = \frac{1+\gamma}{2}\delta Z_v. \tag{7.27}$$

I then find

$$\begin{aligned} \delta Z_{++}^{(\Gamma,\mathrm{lat})} &= \delta Z_{\mathrm{mult}}^{(\Gamma)} - \frac{1}{2}\delta Z_v + \xi_{++}^{(\Gamma)}, \\ \delta Z_{+-}^{(\Gamma,\mathrm{lat})} &= \frac{\gamma}{2}\delta Z_v + \xi_{+-}^{(\Gamma)}. \end{aligned} \tag{7.28}$$

Even though I use only the leading order heavy-light operators I still include $1/m$ corrections in the action. Next I isolate infrared divergences in the renormalisation constants and find (in Feynman gauge)

$$\begin{aligned} \delta Z_q &= \frac{1}{3\pi}\log a^2\lambda^2 + F_q, \\ \delta Z_\psi &= -\frac{2}{3\pi}\log a^2\lambda^2 + F_\psi(v, am), \\ \delta Z_m &= F_m(v, am), \\ \delta Z_v &= F_v(v, am), \\ \xi_{++}^{(\Gamma)} &= -\frac{1}{3\pi}\log a^2\lambda^2 + F_{\xi_{++}}^{(\Gamma)}(v, am), \\ \xi_{+-}^{(\Gamma)} &= F_{\xi_{+-}}^{(\Gamma)}(v, am). \end{aligned} \tag{7.29}$$

The infrared divergence of $\xi_{++}^{(\Gamma)}$ is independent of the Dirac structure Γ due to heavy quark symmetry and and can be inferred from the subtraction integral discussed in section 7.2.1. The functions F_x are infrared finite and can be expanded in powers of the inverse heavy quark mass on the lattice,

$$F_x(v, am) = F_x^{(0)}(v) + \frac{1}{am}F_x^{(1)}(v) + \frac{1}{a^2m^2}F_x^{(2)}(v) + \ldots. \tag{7.30}$$

This gives the final expressions for the matching coefficients $c_\pm^{(\Gamma)}$,

- Vector:

$$\begin{aligned}
c_+^{(V)0}(v,am) &= -\frac{11}{12\pi} - \frac{1}{2}\left(F_q + F_\psi(v,am)\right) + \frac{1}{2}F_v(v,am) \\
&\quad + \frac{1}{2\pi}\log a^2m^2 - F_{\xi_{++}}^{(V)0}(v,am), \\
c_+^{(V)\parallel}(v,am) &= -\frac{1}{4\pi} - \frac{1}{2}\left(F_q + F_\psi(v,am)\right) + \frac{1}{2}F_v(v,am) \\
&\quad + \frac{1}{2\pi}\log a^2m^2 - F_{\xi_{++}}^{(V)\parallel}(v,am), \\
c_+^{(V)\perp}(v,am) &= -\frac{11}{12\pi} - \frac{1}{2}\left(F_q + F_\psi(v,am)\right) + \frac{1}{2}F_v(v,am) \\
&\quad + \frac{1}{2\pi}\log a^2m^2 - F_{\xi_{++}}^{(V)\perp}(v,am), \\
c_-^{(V)0}(v,am) &= \frac{2\gamma}{3\pi} - \frac{\gamma}{2}F_v(v,am) - F_{\xi_{+-}}^{(V)0}(v,am), \\
c_-^{(V)\parallel}(v,am) &= -\frac{2\gamma}{3\pi} - \frac{\gamma}{2}F_v(v,am) - F_{\xi_{+-}}^{(V)\parallel}(v,am), \\
c_-^{(V)\perp}(v,am) &= -\frac{\gamma}{2}F_v(v,am) - F_{\xi_{+-}}^{(V)\perp}(v,am).
\end{aligned} \tag{7.31}$$

For $v = 0$ there is only one operator $\overline{q}\gamma^\mu\tilde{\Psi}_v^{(+)}$ with matching coefficients

$$\begin{aligned}
c^{(V)0}(am) &= -\frac{1}{4\pi} - \frac{1}{2}\left(F_q + F_\psi(am)\right) + \frac{1}{2\pi}\log a^2m^2 - F_\xi^{(V)0}(am), \\
c^{(V)j}(am) &= -\frac{11}{12\pi} - \frac{1}{2}\left(F_q + F_\psi(am)\right) + \frac{1}{2\pi}\log a^2m^2 - F_\xi^{(V)j}(am).
\end{aligned} \tag{7.32}$$

The matching coefficient of the zero component of the (axial-) vector current at $v = 0.0$ has been calculated in [92].

- Tensor:

$$\begin{aligned}
c_+^{(T)\mu\nu}(\mu/m,v,am) &= -\frac{9}{4\pi} - \frac{1}{2}\left(F_q + F_\psi(v,am)\right) + F_m(v,am) \\
&\quad + \frac{1}{2}F_v(v,am) - F_{\xi_{++}}^{(T)\mu\nu}(v,am)) \\
&\quad + \frac{1}{2\pi}\log a^2m^2 + \frac{4}{3\pi}\log m^2/\mu^2, \\
c_-^{(T)\mu\nu}(v,am) &= -\frac{\gamma}{2}F_v(v,am) - F_{\xi_{+-}}^{(T)\mu\nu}(v,am).
\end{aligned} \tag{7.33}$$

For $v = 0$ there is only one operator $\frac{e}{16\pi^2} m\, \overline{q}\sigma^{\mu\nu}\tilde{\Psi}_v^{(+)}$ with matching coefficient

$$\begin{aligned} c^{(T)\mu\nu}(\mu/m, am) &= -\frac{9}{4\pi} - \frac{1}{2}\left(F_q + F_\psi(am)\right) + F_m(am) - F_\xi^{(T)\mu\nu}(am) \\ &\quad + \frac{1}{2\pi}\log a^2m^2 + \frac{4}{3\pi}\log m^2/\mu^2. \end{aligned} \tag{7.34}$$

The ultraviolet behaviour of the lattice theory is described by the logarithmic terms in (7.31) and (7.33), in particular the $\log a^2m^2$ term is a UV divergence which is independent of the Dirac structure of the renormalised operator due to heavy quark symmetry. As the short distance behaviour of the effective theory is different from continuum QCD its coefficient differs from the one of the $\log m^2/\mu^2$ term in (7.33). The anomalous dimension of the lattice operator can be obtained by noting that the renormalised operator is related to the bare operator by multiplication with $Z_\Gamma^{(\mathrm{lat})}$, i.e.

$$Q_{0,+}^{(\Gamma,\mathrm{ren})} = \left(Z_\Gamma^{(\mathrm{lat})}\right)^{-1} Q_{0,+}^{(\Gamma)}. \tag{7.35}$$

The counterterm has to be chosen such that is absorbs the logarithmic UV divergence in $\delta Z_{++}^{(\Gamma,\mathrm{lat})}$,

$$Z_\Gamma^{(\mathrm{lat})} = 1 - \frac{\alpha_s}{2\pi}\left[\log a^2\mu_{\mathrm{lat}}^2 + (\text{finite terms})\right] + \ldots \tag{7.36}$$

where μ_{lat} is an arbitrary scale which has to cancel in physical results. I find

$$\gamma_\Gamma^{(\mathrm{lat})} = \frac{1}{Z_\Gamma^{(\mathrm{lat})}}\frac{dZ_\Gamma^{(\mathrm{lat})}}{d\log\mu_{\mathrm{lat}}} = -\frac{\alpha_s}{\pi} + \ldots.$$

In [67] the anomalous dimension of a heavy-light operator with arbitrary Dirac structure is derived in HQET with dimensional regularisation. The expression quoted in (3.24) of [67] agrees with my result.

The heavy quark renormalisation parameters have been calculated in chapter 5. Wavefunction renormalisation of massless ASQTad quarks is given in [92] and I calculate it for HISQ quarks in the following section. Finally the one particle irreducible matrix elements can be found by evaluating the one loop diagram in Fig. 7.1.

Light quark wavefunction renormalisation

The inverse renormalised propagator for massless ASQTad/HISQ quarks is

$$G^{-1}(p) = G_0^{-1}(p) - \alpha_s\Sigma(p) \tag{7.37}$$

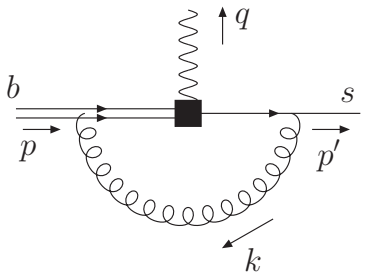

Figure 7.1: One particle irreducible diagram at one loop

with the inverse tree level propagator

$$G_0^{-1}(p) = \sum_\mu i\gamma_\mu \sin p_\mu \left(1 - \frac{1}{6}\sin^2 p_\mu\right) \tag{7.38}$$

and the self-energy at one loop,

$$\Sigma(p) = \sum_\mu i\gamma_\mu \sin p_\mu B_\mu(p). \tag{7.39}$$

There is no term proportional to the unit matrix at all orders. This is due to Chiral symmetry of the massless quark action which is invariant under the transformation $\psi \mapsto e^{i\epsilon\gamma_5}\psi$, $\overline{\psi} \mapsto \overline{\psi}e^{i\epsilon\gamma_5}$. This also implies that the dispersion relation starts with a linear term, for three momentum $\boldsymbol{p} = (p_x, 0, 0)$ the pole of the propagator is at $-ip_0 = E = E(p_x) = (\text{const.}) \times p_x + \ldots$.

The wavefunction renormalisation is then given by the residue of the pole in the propagator,

$$\begin{aligned} G(p) &= \frac{\gamma_0 E(1-\alpha_s B_0) - i\gamma_x p_x(1-\alpha_s B_x)}{-E^2(1-\alpha_s B_0)^2 + p_x^2(1-\alpha_s B_x)^2} + \ldots \\ &\equiv -\frac{\gamma_0 - i\gamma_x}{2}\,\frac{Z_q}{E - E(p_x)} + \ldots . \end{aligned} \tag{7.40}$$

It follows that

$$\delta Z_q = 1 + \alpha_s B_0(0), \qquad E(p_x) = \left[1 + \alpha_s(B_0(0) - B_x(0))\right] p_x = p_x \tag{7.41}$$

where the second relation follows from hypercubic invariance of the lattice.

The rainbow diagram which contributes to δZ_q is IR divergent in Feynman gauge, so as for heavy quarks I split the wavefunction renormalisation into an IR finite part

	$I^{(\mathrm{lat-sub})} + \overline{I}^{(\mathrm{sub})}$	$I^{(\mathrm{tad})}$	$I^{(\mathrm{MF})}$	$\delta\overline{Z}_q$
ASQ (my results)	$-0.79815(39)$	$1.60004(16)$	-1.726	$-0.92411(42)$
ASQ from [92]	$-0.798(3)$	$1.600(1)$	-1.726	$-0.924(3)$
HISQ	$-0.8155(12)$	$0.4250(10)$	—	$-0.3905(16)$

Table 7.1: Light quark wavefunction renormalisation. I only show the IR finite parts of the result.

and a logarithmic divergence (the latter agrees with the one found in the continuum, see (D.6) in appendix D),

$$\delta Z_q \;=\; \delta\overline{Z}_q + \frac{1}{3\pi}\log a^2\lambda^2 \tag{7.42}$$

I evaluate the IR finite contribution by constructing a suitable subtraction function which is needed to guarantee the convergence of the integrals, see section J.4.

The tadpole diagram is slightly more expensive to evaluate but as the integrand is smoother it can be evaluated with lower statistics. As a useful check I first obtain results for the ASQTad action, which have been published in [92]. I choose to evaluate the subtract rainbow integral $I^{(\mathrm{lat-sub})}$ with $1,000,000$ function evaluations and 20 VEGAS iterations which took 1.8h on 64 processors. Although the tadpole integral $I^{(\mathrm{tad})}$ was only evaluated with $200,000$ function evaluations (taking 0.6h) the error on results is a factor of approximately three smaller. There is an additional contribution of $I^{(\mathrm{MF})} = -\frac{9}{4}u_0^{(2)}$ from mean field improvement, which is -1.726 if the fourth root of the plaquette is used to extract $u_0^{(2)} = 0.767$ [92]. I summarise my findings in Tab. 7.1 where I also show the results in [92] which are in perfect agreement with what I find.

I then repeat the calculation for the HISQ action, the results are collected in the last row of Tab. 7.1. Note that in this case there is no mean field improvement as the links in the HISQ action are reunitarised.

One particle irreducible matrix elements

The $\mathcal{O}(\alpha_s)$ one particle irreducible (1PI) correction to the operators $Q_{0,j}^{(\Gamma)} = \rho^{(\Gamma)} f_j \overline{q} \Gamma S_j \tilde{\Psi}_v^{(+)}$ (with $S_1 = \mathrm{Id}$, $S_2 = -\boldsymbol{\gamma} \cdot \hat{\boldsymbol{v}} \gamma_0$) is given by

$$\begin{aligned} \langle q | Q_{0,j}^{(\Gamma)} | b \rangle_{\mathrm{lat,1PI}} &= \alpha_s \rho^{(\Gamma)} f_j \overline{u}_s(p') \Sigma_j^{(\Gamma)} U \\ &= \alpha_s \sum_{k=1,2} \xi_{jk}^{(\Gamma)} \langle q | Q_{0,k}^{(\Gamma)} | b \rangle_{\mathrm{tree}} \\ &= \alpha_s \rho^{(\Gamma)} \sum_{k=1,2} \xi_{jk}^{(\Gamma)} f_k \overline{u}_s(p') \Gamma S_k U \end{aligned} \tag{7.43}$$

where the heavy-quark four spinor is

$$U^{(\sigma)} = \begin{pmatrix} \chi^{(\sigma)} \\ 0 \end{pmatrix}, \qquad \text{with} \quad \chi^{(\sigma)} \in \left\{ \begin{pmatrix} 1 \\ 0 \end{pmatrix}, \begin{pmatrix} 0 \\ 1 \end{pmatrix} \right\}. \tag{7.44}$$

To extract $\xi_{jk}^{(\Gamma)}$ replace the spinors by Euclidean on-shell projection operators,

$$\sum_{\sigma=\uparrow,\downarrow} u_s^{(\sigma)}(p') \overline{u}_s^{(\sigma)}(p') = -i \not{p}\,' \equiv \Pi_s(p') \qquad \sum_{\sigma=\uparrow,\downarrow} U^{(\sigma)} U^{(\sigma)T} = \frac{1}{2}(1 + \gamma_0) \equiv \Pi_b \tag{7.45}$$

and take traces

$$T_j = \mathrm{Tr}\left[\Pi_s(p') \Sigma_j^{(\Gamma)} \Pi_b \Pi^{(\Gamma)} \right]. \tag{7.46}$$

In this expression $\Sigma_j^{(\Gamma)}$ is given by the integrand of the 1PI diagram and $\Pi^{(\Gamma)}$ is a suitable projection operator which depends on the Dirac structure of $\Sigma_j^{(\Gamma)}$. I tested the integration algorithm and correct implementation of the projection operators in (7.46) by reproducing the analytical results of the subtraction integral in (7.48).

Infrared subtraction function

I use a gluon mass to regulate the infrared divergence in the 1PI integral. As for the heavy quark wavefunction renormalisation I construct an appropriate subtraction function $f^{(\mathrm{sub})}$ to smoothen the VEGAS integrand, the 1PI matrix elements can be written as

$$\begin{aligned} \xi_{jk}^{(\Gamma)} &= \int \frac{d^4k}{(2\pi)^4} \left(f_{jk}^{(\Gamma,\mathrm{lat})} - f_{jk}^{(\mathrm{sub})} \right) + \int \frac{d^4k}{(2\pi)^4} f_{jk}^{(\mathrm{sub})} \\ &= \xi_{jk}^{(\Gamma,\mathrm{lat})} + \xi_{jk}^{(\mathrm{sub})} \end{aligned} \tag{7.47}$$

As discussed in detail in appendix J.3, the value of the subtraction integral is

$$\xi_{jk}^{(\mathrm{sub})} = \int \frac{d^4k}{(2\pi)^4} f_{jk}^{(\mathrm{sub})} \quad = \quad -\frac{\delta_{jk}}{3\pi}\left(1 + \log \lambda^2/m^2\right) + \mathcal{O}(\lambda/m). \tag{7.48}$$

7.2.2 Numerical results

In the following I show results for the matching coefficients both for the simple heavy quark action defined in (5.26) and for the full $\mathcal{O}(1/m^2, v_{\mathrm{rel}}^4)$ action. In both cases I use a heavy mass of $m = 2.8$ and a stability parameter $n = 2$. The gluon action is the Wilson action for the simple mNRQCD action and Symanzik improved for the full $\mathcal{O}(1/m^2, v_{\mathrm{rel}}^4)$ action. For the simple action I show results obtained with the ASQTad light quark action whereas for the full $\mathcal{O}(1/m^2, v_{\mathrm{rel}}^4)$ action I use both the ASQTad and the HISQ action.

The heavy quark renormalisation parameters δZ_ψ, δZ_m and δZ_v are taken from Tabs. 5.6 and 5.7. The wavefunction renormalisation of the massless light quark is $-0.92411(42)$ for ASQTad quarks and $-0.3905(16)$ for HISQ quarks (see Tab. 7.1). In Tabs. 7.2 to 7.7 I list results both for the vector- and tensor current matching coefficients.

For the vector current I calculate the matching coefficients for three different Lorentz indices:

1. μ points in the temporal direction, $\mu = 0$
2. μ is parallel to the frame velocity, $\mu = \parallel$
3. μ is orthogonal to the frame velocity, $\mu = \perp$

For $v = 0.0$ I consider $\mu = 0$, $\mu = 1$ and $\mu = 2$. For the tensor current there are four different cases:

1. μ points in the temporal direction and ν is parallel to the frame velocity, $(\mu, \nu) = (0, \parallel)$
2. μ points in the temporal direction and ν is orthogonal to the frame velocity, $(\mu, \nu) = (0, \perp)$
3. μ is parallel and ν orthogonal to the frame velocity, $(\mu, \nu) = (\parallel, \perp)$
4. both μ and ν are orthogonal to the frame velocity, $(\mu, \nu) = (\perp, \perp)$

For $v = 0.0$ I choose $(\mu, \nu) = (0, 1)$, $(\mu, \nu) = (0, 2)$, $(\mu, \nu) = (1, 2)$ and $(\mu, \nu) = (2, 3)$.

As the light quark is massless and because of $\sigma_{01} = -\gamma_5 \sigma_{23}$ the matching coefficients for $(0, \|)$ and $(\perp, \perp)$ are identical. The same holds for $(0, \perp)$ and $(\|, \perp)$ because of $\sigma_{02} = \gamma_5 \sigma_{13}$. For $v = 0$ this implies that the matching coefficients for all combinations of (μ, ν) are identical as there is no preferred direction.

The renormalisation scale of the tensor current is $\mu = m$.

v	$c^{(V)0}$	$c^{(V)1}$	$c^{(V)2}$
0.00	0.26575(41)	0.05410(41)	0.05379(41)

v	$c_+^{(V)0}$	$c_+^{(V)\parallel}$	$c_+^{(V)\perp}$
0.10	−0.1259(23)	0.0865(23)	−0.1748(23)
0.20	−0.1268(14)	0.0846(14)	−0.1816(15)
0.30	−0.1217(12)	0.0899(11)	−0.1840(12)
0.40	−0.1145(10)	0.0961(10)	−0.1886(11)
0.50	−0.1049(10)	0.1060(10)	−0.1957(11)
0.60	−0.0876(10)	0.1238(10)	−0.2036(11)
0.70	−0.0604(10)	0.1510(10)	−0.2175(11)
0.75	−0.0407(11)	0.1708(11)	−0.2285(12)
0.80	−0.0139(11)	0.1980(11)	−0.2430(13)
0.85	0.0283(13)	0.2402(13)	−0.2597(15)
0.90	0.0966(15)	0.3084(15)	−0.2828(18)
0.95	0.2321(20)	0.4438(20)	−0.3158(25)

v	$c_-^{(V)0}$	$c_-^{(V)\parallel}$	$c_-^{(V)\perp}$
0.10	0.3950(21)	−0.0314(21)	0.2315(21)
0.20	0.4059(13)	−0.0272(13)	0.2425(13)
0.30	0.4164(11)	−0.0287(11)	0.2522(11)
0.40	0.4352(10)	−0.0283(10)	0.2697(10)
0.50	0.4662(10)	−0.0242(10)	0.2982(10)
0.60	0.5149(11)	−0.0161(11)	0.3413(11)
0.70	0.5999(12)	0.0055(12)	0.4142(12)
0.75	0.6700(13)	0.0285(13)	0.4730(13)
0.80	0.7738(14)	0.0660(14)	0.5570(14)
0.85	0.9358(17)	0.1295(17)	0.6839(17)
0.90	1.2234(22)	0.2493(22)	0.9015(22)
0.95	1.9150(34)	0.5553(34)	1.4063(34)

Table 7.2: Vector current matching coefficients for the simple heavy quark action defined in (5.26). The ASQTad action is used to discretise the light quark.

v	$c^{(T)0,1}$	$c^{(T)0,2}$	$c^{(T)1,2}$	$c^{(T)2,3}$
0.00	0.0512(16)	0.0518(16)	0.0514(16)	0.0513(16)

v	$c_+^{(T)0,\parallel}$	$c_+^{(T)0,\perp}$	$c_+^{(T)\parallel,\perp}$	$c_+^{(T)\perp,\perp}$
0.10	−0.1726(27)	−0.1203(27)	−0.1215(27)	−0.1721(27)
0.20	−0.1604(21)	−0.1029(21)	−0.1028(21)	−0.1578(21)
0.30	−0.1238(20)	−0.0598(20)	−0.0600(20)	−0.1223(20)
0.40	−0.0669(20)	0.0083(20)	0.0081(20)	−0.0652(20)
0.50	0.0181(22)	0.1095(22)	0.1098(22)	0.0202(22)
0.60	0.1653(25)	0.2825(25)	0.2823(25)	0.1670(25)
0.70	0.4287(32)	0.5870(31)	0.5864(31)	0.4300(32)
0.75	0.6529(37)	0.8420(37)	0.8408(37)	0.6544(37)
0.80	1.0086(46)	1.2390(46)	1.2379(46)	1.0101(46)
0.85	1.6821(64)	1.9725(64)	1.9716(64)	1.6842(64)
0.90	3.092(10)	3.472(10)	3.471(10)	3.093(10)
0.95	7.635(21)	8.184(21)	8.183(21)	7.639(21)

v	$c_-^{(T)0,\parallel}$	$c_-^{(T)0,\perp}$	$c_-^{(T)\parallel,\perp}$	$c_-^{(T)\perp,\perp}$
0.10	0.2311(21)	0.1810(21)	0.1811(21)	0.2332(21)
0.20	0.2423(13)	0.1886(13)	0.1887(13)	0.2429(13)
0.30	0.2524(11)	0.1932(11)	0.1933(11)	0.2527(11)
0.40	0.2702(10)	0.2030(10)	0.2032(10)	0.2703(10)
0.50	0.2990(10)	0.2205(10)	0.2209(10)	0.2987(10)
0.60	0.3424(11)	0.2487(11)	0.2495(11)	0.3418(10)
0.70	0.4156(12)	0.3020(12)	0.3028(12)	0.4148(12)
0.75	0.4741(13)	0.3488(13)	0.3496(13)	0.4735(13)
0.80	0.5581(15)	0.4196(15)	0.4204(15)	0.5572(15)
0.85	0.6852(17)	0.5323(17)	0.5334(17)	0.6841(17)
0.90	0.9026(22)	0.7362(22)	0.7372(22)	0.9014(22)
0.95	1.4067(34)	1.2349(34)	1.2358(34)	1.4060(34)

Table 7.3: Tensor current matching coefficients for the simple heavy quark action defined in (5.26). The ASQTad action is used to discretise the light quark.

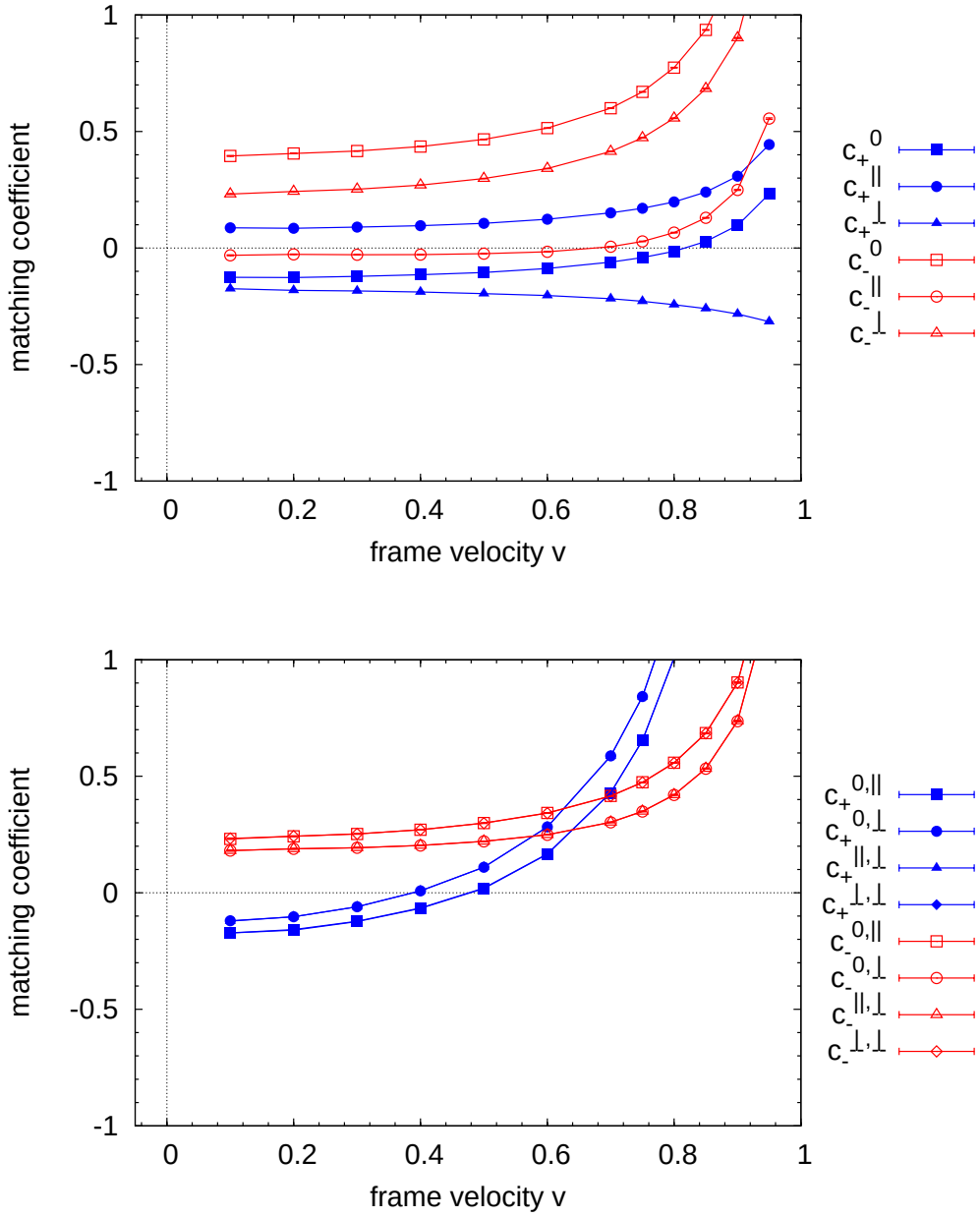

Figure 7.2: Matching coefficients for the simple heavy quark action defined in (5.26), vector current (top) and tensor current (bottom). The ASQTad action is used to discretise the light quark.

v	$c^{(V)0}$	$c^{(V)1}$	$c^{(V)2}$
0.00	0.04293(52)	0.26970(40)	0.26929(39)

v	$c_+^{(V)0}$	$c_+^{(V)\parallel}$	$c_+^{(V)\perp}$
0.10	0.1945(21)	−0.0553(22)	0.1384(18)
0.20	0.1965(12)	−0.0500(13)	0.1411(12)
0.30	0.2005(10)	−0.0419(11)	0.1444(10)
0.40	0.20708(84)	−0.0293(10)	0.15071(88)
0.50	0.21660(77)	−0.01038(88)	0.15972(84)
0.60	0.22620(73)	0.01358(85)	0.16775(85)
0.70	0.24297(71)	0.05349(80)	0.17817(87)
0.75	0.25596(72)	0.08412(80)	0.18243(91)
0.80	0.27674(77)	0.12920(85)	0.1862(10)
0.85	0.3201(13)	0.2078(13)	0.1917(12)
0.90	0.4258(16)	0.3633(17)	0.1981(15)
0.95	0.6340(19)	0.6496(19)	0.2002(23)

v	$c_-^{(V)0}$	$c_-^{(V)\parallel}$	$c_-^{(V)\perp}$
0.10	−0.1533(22)	0.3227(22)	0.1301(17)
0.20	−0.1547(13)	0.3220(13)	0.1274(10)
0.30	−0.1598(10)	0.3183(10)	0.12224(81)
0.40	−0.16838(86)	0.31106(85)	0.11325(72)
0.50	−0.18137(81)	0.29887(80)	0.09967(67)
0.60	−0.19460(80)	0.28291(80)	0.08532(68)
0.70	−0.21033(81)	0.25390(80)	0.06649(69)
0.75	−0.21513(84)	0.23150(83)	0.05808(73)
0.80	−0.21139(91)	0.20128(91)	0.05445(80)
0.85	−0.1934(11)	0.1530(12)	0.0561(10)
0.90	−0.1348(13)	0.0713(14)	0.0774(12)
0.95	0.0615(23)	−0.0848(23)	0.1354(22)

Table 7.4: Vector current matching coefficients for the full $\mathcal{O}(1/m^2, v_{\rm rel}^4)$ heavy quark action. The ASQTad action is used to discretise the light quark.

v	$c^{(T)0,1}$	$c^{(T)0,2}$	$c^{(T)1,2}$	$c^{(T)2,3}$
0.00	0.0762(12)	0.0761(12)	0.0763(12)	0.0761(12)

v	$c_+^{(T)0,\parallel}$	$c_+^{(T)0,\perp}$	$c_+^{(T)\parallel,\perp}$	$c_+^{(T)\perp,\perp}$
0.10	−0.0507(24)	−0.0159(21)	−0.0157(22)	−0.0463(24)
0.20	−0.0559(17)	−0.0206(16)	−0.0214(16)	−0.0526(17)
0.30	−0.0675(16)	−0.0325(15)	−0.0321(15)	−0.0652(16)
0.40	−0.0861(15)	−0.0496(15)	−0.0497(15)	−0.0846(15)
0.50	−0.1148(16)	−0.0748(15)	−0.0750(15)	−0.1136(16)
0.60	−0.1605(17)	−0.1135(16)	−0.1136(16)	−0.1595(17)
0.70	−0.2302(19)	−0.1666(18)	−0.1668(18)	−0.2295(19)
0.75	−0.2791(21)	−0.1984(21)	−0.1992(21)	−0.2782(21)
0.80	−0.3379(26)	−0.2280(25)	−0.2292(25)	−0.3368(26)
0.85	−0.3997(34)	−0.2381(34)	−0.2385(34)	−0.3995(34)
0.90	−0.4468(53)	−0.1653(53)	−0.1682(53)	−0.4454(53)
0.95	−0.296(14)	0.209(14)	0.209(14)	−0.297(14)

v	$c_-^{(T)0,\parallel}$	$c_-^{(T)0,\perp}$	$c_-^{(T)\parallel,\perp}$	$c_-^{(T)\perp,\perp}$
0.10	0.1184(20)	0.0849(18)	0.0871(18)	0.1189(20)
0.20	0.1147(11)	0.0839(11)	0.0855(11)	0.1149(11)
0.30	0.10781(85)	0.07967(86)	0.08054(86)	0.10774(85)
0.40	0.09607(74)	0.07144(76)	0.07214(77)	0.09583(74)
0.50	0.07857(69)	0.05896(72)	0.05912(72)	0.07848(69)
0.60	0.05889(69)	0.04414(72)	0.04412(72)	0.05860(69)
0.70	0.03355(70)	0.02162(73)	0.02142(73)	0.03332(70)
0.75	0.02163(74)	0.00812(77)	0.00787(76)	0.02131(74)
0.80	0.01460(82)	−0.00494(84)	−0.00522(84)	0.01425(82)
0.85	0.0143(10)	−0.0198(10)	−0.0199(10)	0.0140(10)
0.90	0.0366(13)	−0.0321(13)	−0.0316(13)	0.0365(13)
0.95	0.0999(22)	−0.0122(22)	−0.0118(22)	0.0999(22)

Table 7.5: Tensor current matching coefficients for the full $\mathcal{O}(1/m^2, v_{\rm rel}^4)$ heavy quark action. The ASQTad action is used to discretise the light quark.

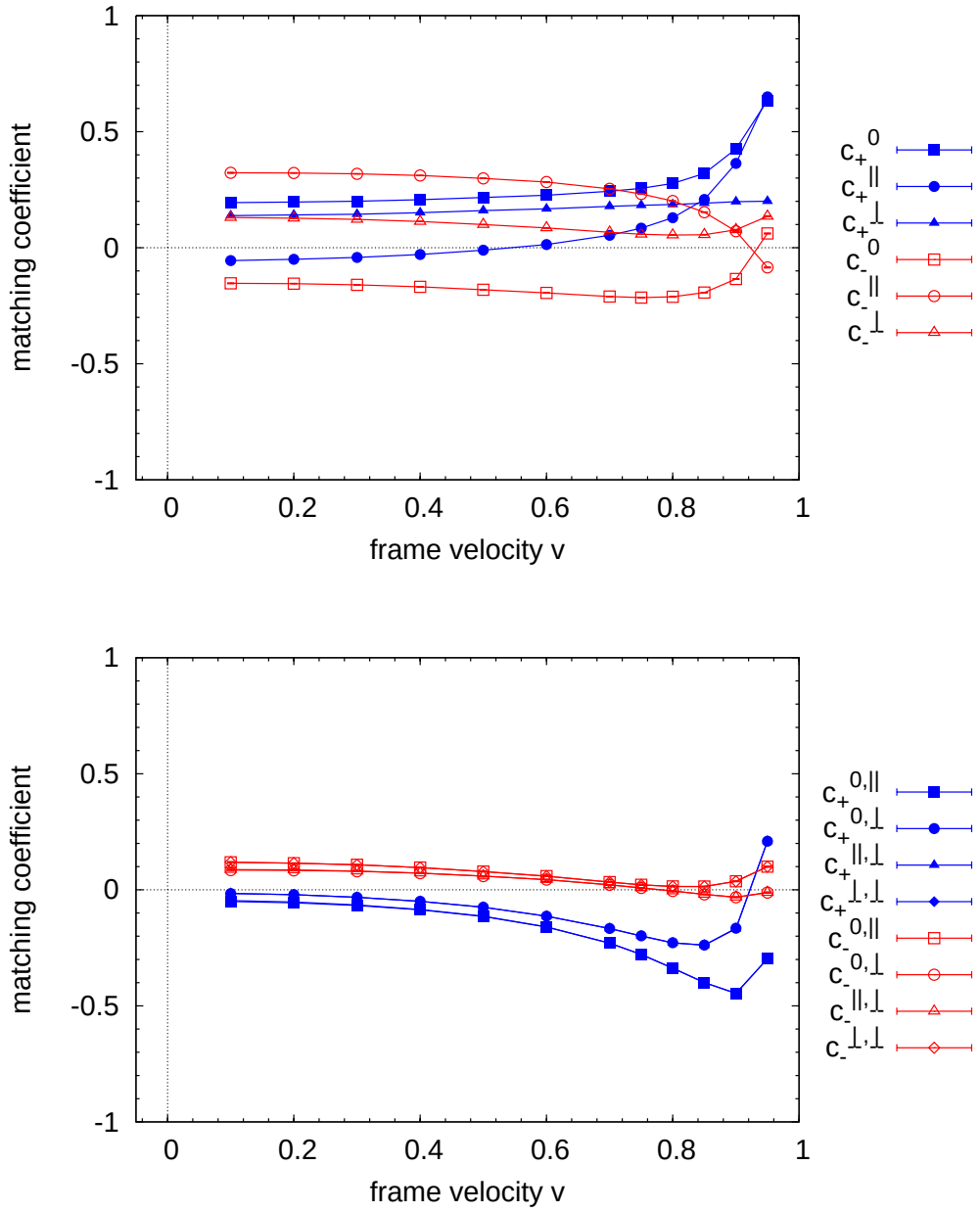

Figure 7.3: Matching coefficients for the full $\mathcal{O}(1/m^2, v_{\mathrm{rel}}^4)$ heavy quark action, vector current (top) and tensor current (bottom). The ASQTad action is used to discretise the light quark.

v	$c^{(V)0}$	$c^{(V)1}$	$c^{(V)2}$
0.00	−0.10157(94)	−0.03847(88)	−0.03876(88)

v	$c_+^{(V)0}$	$c_+^{(V)\parallel}$	$c_+^{(V)\perp}$
0.10	−0.1348(27)	−0.1963(27)	−0.1601(23)
0.20	−0.1337(16)	−0.1930(17)	−0.1573(15)
0.30	−0.1301(13)	−0.1887(14)	−0.1517(13)
0.40	−0.1243(12)	−0.1824(13)	−0.1422(12)
0.50	−0.1162(12)	−0.1726(12)	−0.1283(12)
0.60	−0.1103(11)	−0.1623(12)	−0.1123(12)
0.70	−0.1005(11)	−0.1447(12)	−0.0898(12)
0.75	−0.0925(11)	−0.1301(12)	−0.0765(12)
0.80	−0.0791(11)	−0.1056(12)	−0.0621(13)
0.85	−0.0474(12)	−0.0573(13)	−0.0430(15)
0.90	0.0262(14)	0.0430(14)	−0.0176(17)
0.95	0.1850(22)	0.2445(22)	0.0017(27)

v	$c_-^{(V)0}$	$c_-^{(V)\parallel}$	$c_-^{(V)\perp}$
0.10	0.0324(25)	0.1545(25)	0.1211(20)
0.20	0.0318(14)	0.1542(14)	0.1175(12)
0.30	0.0285(10)	0.1515(10)	0.11148(89)
0.40	0.02201(90)	0.14535(90)	0.10092(77)
0.50	0.01214(84)	0.13517(83)	0.08499(71)
0.60	0.00259(83)	0.12285(83)	0.06640(70)
0.70	−0.00797(84)	0.09962(83)	0.04179(70)
0.75	−0.01022(87)	0.08223(86)	0.02974(73)
0.80	−0.00477(93)	0.05912(93)	0.02228(81)
0.85	0.0120(11)	0.0203(11)	0.02032(94)
0.90	0.0648(13)	−0.0454(13)	0.0367(12)
0.95	0.2400(23)	−0.1828(23)	0.0936(22)

Table 7.6: Vector current matching coefficients for the full $\mathcal{O}(1/m^2, v_{\rm rel}^4)$ heavy quark action. The HISQ action is used to discretise the light quark.

v	$c^{(T)0,1}$	$c^{(T)0,2}$	$c^{(T)1,2}$	$c^{(T)2,3}$
0.00	−0.2296(17)	−0.2305(17)	−0.2325(17)	−0.2315(17)

v	$c_+^{(T)0,\parallel}$	$c_+^{(T)0,\perp}$	$c_+^{(T)\parallel,\perp}$	$c_+^{(T)\perp,\perp}$
0.10	−0.3677(64)	−0.3385(58)	−0.3391(59)	−0.3642(65)
0.20	−0.3662(38)	−0.3432(35)	−0.3416(35)	−0.3640(37)
0.30	−0.3734(30)	−0.3541(28)	−0.3524(28)	−0.3727(30)
0.40	−0.3892(27)	−0.3712(25)	−0.3709(25)	−0.3885(28)
0.50	−0.4127(26)	−0.4002(23)	−0.4001(23)	−0.4114(26)
0.60	−0.4492(27)	−0.4419(24)	−0.4427(24)	−0.4484(27)
0.70	−0.5045(30)	−0.5065(25)	−0.5059(25)	−0.5059(29)
0.75	−0.5408(32)	−0.5477(27)	−0.5441(27)	−0.5438(32)
0.80	−0.5834(38)	−0.5873(31)	−0.5857(31)	−0.5885(38)
0.85	−0.6306(48)	−0.6155(41)	−0.6112(41)	−0.6308(47)
0.90	−0.6541(68)	−0.5801(59)	−0.5765(60)	−0.6593(68)
0.95	−0.479(16)	−0.254(15)	−0.242(15)	−0.492(16)

v	$c_-^{(T)0,\parallel}$	$c_-^{(T)0,\perp}$	$c_-^{(T)\parallel,\perp}$	$c_-^{(T)\perp,\perp}$
0.10	0.1367(65)	0.0982(57)	0.0936(54)	0.1167(63)
0.20	0.1253(33)	0.0936(31)	0.0920(30)	0.1156(32)
0.30	0.1138(23)	0.0895(22)	0.0891(22)	0.1085(22)
0.40	0.1007(17)	0.0833(18)	0.0831(18)	0.0964(17)
0.50	0.0826(14)	0.0726(16)	0.0726(16)	0.0787(14)
0.60	0.0607(12)	0.0620(15)	0.0608(15)	0.0578(12)
0.70	0.0318(12)	0.0458(14)	0.0433(14)	0.0288(12)
0.75	0.0171(12)	0.0359(14)	0.0339(15)	0.0140(12)
0.80	0.0070(13)	0.0287(16)	0.0245(15)	0.0049(13)
0.85	0.0023(14)	0.0161(17)	0.0148(16)	−0.0005(14)
0.90	0.0154(17)	0.0099(20)	0.0090(19)	0.0144(17)
0.95	0.0760(26)	0.0301(28)	0.0281(28)	0.0752(26)

Table 7.7: Tensor current matching coefficients for the full $\mathcal{O}(1/m^2, v_{\mathrm{rel}}^4)$ heavy quark action. The HISQ action is used to discretise the light quark.

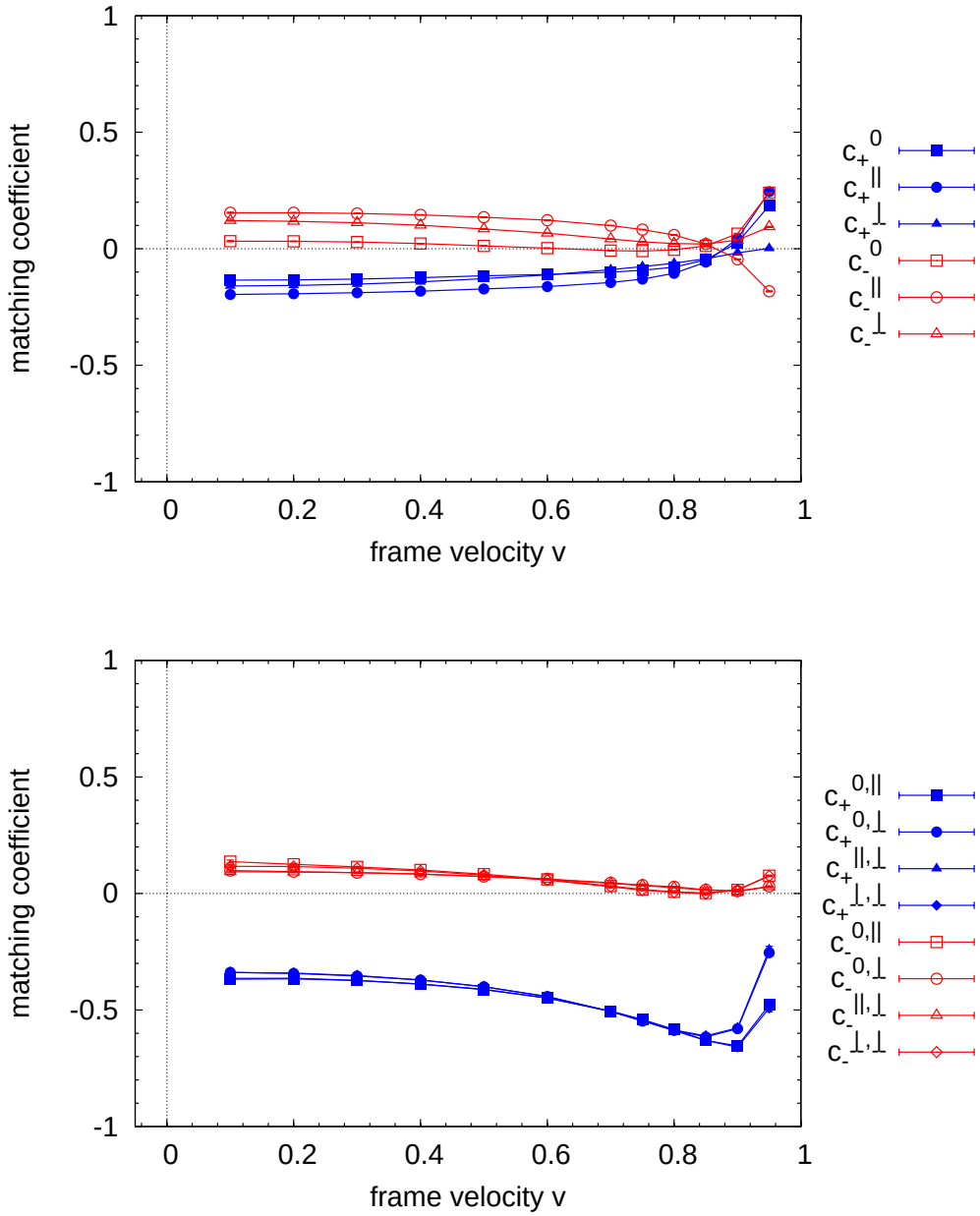

Figure 7.4: Matching coefficients for the full $\mathcal{O}(1/m^2, v_{\rm rel}^4)$ heavy quark action, vector current (top) and tensor current (bottom). The HISQ action is used to discretise the light quark.

7.2.3 Observations

The magnitude of all matching coefficients is reduced by including mean field corrections, for the full $\mathcal{O}(1/m^2, v_{\text{rel}}^4)$ mNRQCD action the dependence on the frame velocity is weak and all matching coefficients are of order one or smaller. Compared to the simple mNRQCD action the divergence for $v \to 1$ is suppressed.

Vector current

At vanishing frame velocity the matching coefficient for the zero component of the vector current, $c^{(V)0} = 0.04293(52)$ in Tab. 7.4, is in perfect agreement with the corresponding value $\tilde{\rho}_0 = 0.043(2)$ in Tab. III of [92]. For $v = 0$ I find that the matching coefficients $c^{(V)1}$ and $c^{(V)2}$ agree within errors as expected from rotational invariance (or, more precisely, the subgroup of $O(3)$ that corresponds to the interchange of spatial lattice directions).

When the full $\mathcal{O}(1/m^2, v_{\text{rel}}^4)$ mNRQCD action is used the splitting between the different Lorentz components of the matching coefficients is reduced. This reduction is more pronounced if the HISQ action is used for the light quark. Improving the action should reduce this splitting as the results are closer to those in the continuum limit where the theory is Lorentz invariant. However, this reduction is not as pronounced as in the case of the tensor current (see below).

Tensor current

For the tensor current I find that the splitting between the $(0, \|)$ and $(0, \perp)$ as well as the $(\|, \perp)$ and $(\perp, \perp)$ matching coefficients is reduced by using the full $\mathcal{O}(1/m^2, v_{\text{rel}}^4)$ mNRQCD action and becomes even smaller when the HISQ action is used to discretise the light quark. The matching coefficients $c_+^{(T)\mu\nu}$ depend on the continuum renormalisation scale μ. For ASQTad light quarks and $\mu = m$ I find that these coefficients are very small. Their magnitude is increased by using the HISQ action to discretise the light quark.

7.3 Nonperturbative calculation of form factors

Nonperturbative form factors have been computed by Stefan Meinel [29] for the decay of a B meson to pseudoscalar and vector mesons in the final state F using a simple mNRQCD action which is correct to $\mathcal{O}(1/m)$. These calculations are currently repeated by Zhaofeng Liu [30] with the full $\mathcal{O}(1/m^2, v_{\text{rel}}^4)$ mNRQCD action used in this thesis. In the new calculation $\mathcal{O}(1/m)$ corrections to the heavy-light currents will be included.

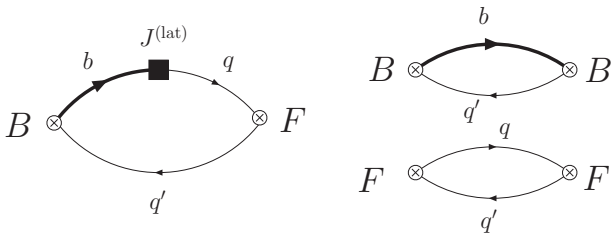

Figure 7.5: Two- and three-point functions on the lattice

7.3.1 Methods

To extract matrix elements and form factors two- and three point functions (see Fig. 7.5) are measured,

$$\begin{aligned} C_{F\Gamma B}(\boldsymbol{k}_{(p)},\boldsymbol{k}_{(q)};x_0,y_0,z_0) &= \sum_{\boldsymbol{y},\boldsymbol{z}}\langle 0|\Phi_F(x)J^{(\mathrm{lat})\Gamma}(y)\Phi_B^\dagger(z)|0\rangle e^{-i(\boldsymbol{p}'\cdot\boldsymbol{x}+\boldsymbol{k}_{(q)}\cdot\boldsymbol{y}-\boldsymbol{k}_{(p)}\cdot\boldsymbol{z})} \\ C_{BB}(\boldsymbol{k}_{(p)};x_0,y_0) &= \sum_{\boldsymbol{x}}\langle 0|\Phi_B(x)\Phi_B^\dagger(y)|0\rangle e^{-i\boldsymbol{k}_{(p)}\cdot(\boldsymbol{x}-\boldsymbol{y})} \\ C_{FF}(\boldsymbol{p}';x_0,y_0) &= \sum_{\boldsymbol{x}}\langle 0|\Phi_F(x)\Phi_F^\dagger(y)|0\rangle e^{-i\boldsymbol{p}'\cdot(\boldsymbol{x}-\boldsymbol{y})} \end{aligned} \tag{7.49}$$

$J^{(\mathrm{lat})\Gamma}$ is the vector- or tensor- current, expanded in terms of mNRQCD operators. $\Phi_B(z)$ and $\Phi_F(x)$ are local interpolating operators with the quantum number of the initial- and final state meson. To increase the overlap with the ground state smeared wavefunctions can be used after gauge fixing. The residual momenta $\boldsymbol{k}_{(p)}$, $\boldsymbol{k}_{(q)}$ are defined by

$$\boldsymbol{p}=\boldsymbol{k}_{(p)}+Z_p\gamma m\boldsymbol{v} \qquad\qquad \boldsymbol{q}=\boldsymbol{k}_{(q)}+Z_p\gamma m\boldsymbol{v} \tag{7.50}$$

where the external momentum renormalisation is $Z_p\approx 1$ (see section 5.1.7). Setting $t=|x_0-y_0|$ and $T=|x_0-z_0|$ the correlators are then fitted to sums of exponentials,

$$\begin{aligned} C_{F\Gamma B}(\boldsymbol{k}_{(q)},\boldsymbol{k}_{(p)};t,T) &\rightarrow \sum_{k=0}^{K-1}\sum_{\ell=0}^{L-1}A_{k\ell}^{(FJB)}(-1)^{kt}(-1)^{\ell(T-t)}e^{-E'_k t}e^{-E_\ell(T-t)}, \\ C_{BB}(\boldsymbol{k}_{(p)};t) &\rightarrow \sum_{\ell=0}^{L-1}A_\ell^{(BB)}(-1)^{\ell(t+1)}e^{-E_\ell t}, \\ C_{FF}(\boldsymbol{p}';t) &\rightarrow 16\sum_{k=0}^{K-1}(-1)^{k(t+1)}e^{-E'_k t} \end{aligned} \tag{7.51}$$

(the oscillating minus signs arise from the use of the ASQTad light quark action [20]). As a constrained curve fitting technique [107] is used, a relatively large number of exponentials can be included and one is not restricted to using data at large t and $T-t$ only.

By inserting a complete set of states in (7.49) it can be shown that the ground state fit parameters are related to field renormalisation of the mesons and the decay matrix element to pseudoscalar (P) or vector mesons (V),

$$\begin{aligned} A_{00}^{(PVB)} &= \frac{\sqrt{Z_P}}{2E_P}\frac{\sqrt{Z_B}}{2E_B}\langle P(p')|J^{(\mathrm{lat})V}|B(p)\rangle, \\ A_{00}^{(VTB)} &= \frac{\sqrt{Z_V}}{2E_V}\frac{\sqrt{Z_B}}{2E_B}\sum_s \epsilon_j(p',s)\langle V(p',\epsilon(p',s))|J^{(\mathrm{lat})T}|B(p)\rangle. \end{aligned} \tag{7.52}$$

For the two point function one finds

$$\begin{aligned} A_0^{(BB)} &= \frac{Z_B}{2E_B}, \\ A_0^{(PP)} &= \sum_s \frac{Z_P}{2E_P}, \\ A_0^{(VV)} &= \sum_s \frac{Z_V}{2E_V}\epsilon_j^*(p',s)\epsilon_j(p',s). \end{aligned} \tag{7.53}$$

Finally, form factors f_+, f_0 and T_1, T_2, T_3 can be extracted from the matrix elements in (7.52) by using the parametrisations in (1.6) and (2.27).

7.3.2 Results

The calculations were performed on 400 coarse MILC gauge configurations [134] of size $20^3 \times 64$. These configurations include the vacuum polarisation effects of $2+1$ flavours of light sea quarks with masses of $am_u = am_d = 0.007$ and $am_s = 0.05$. The ASQTad action is used for discretising the sea quarks and the one loop Symanzik improved gauge action, which reduces to (3.8) at tree level, for the gluons. The pion mass on these ensembles is around 300 MeV and the inverse lattice spacing $a^{-1} = 1.6$ GeV [93, 134]. The light valence quark masses are chosen to be $am_u = am_d = 0.007$, $am_s = 0.04$. As in the perturbative calculations the heavy quark mass is $am = 2.8$ and the stability parameter $n = 2$.

Extrapolation in q^2

In Fig. 7.6 I show results for the vector form factors f_+ and f_0. The solid curve is the simultaneous fit to the phenomenological ansatz in (2.33).

The error bands on the curves are estimated from propagation of the errors as described in [135]. The optimal fit parameters are

$$F = 0.277, \qquad \alpha = 0.569, \qquad \beta = 1.293 \tag{7.54}$$

with the covariance matrix

$$\mathrm{cov}(F,\alpha,\beta) \;=\; \begin{pmatrix} 0.0053 & -0.0159 & 0.0158 \\ & 0.0512 & -0.0475 \\ & & 0.0480 \end{pmatrix}. \tag{7.55}$$

From this I obtain the value at $q^2 = 0$ as

$$f_+(q^2=0) = f_0(q^2=0) \;=\; 0.277(73). \tag{7.56}$$

This error is statistical only. There is also an uncertainty associated with the choice of a specific phenomenological form factor parametrisation. Quantifying this ambiguity is not a well defined problem as the "correct" analytical dependence of f_+ and f_0 on q^2 is not known. I estimate the parametric uncertainty by making minimal assumptions about the form factors and comparing different parametrisations. As remarked in section 2.3.5 f_+ and f_0 are analytical functions of q^2 everywhere in the complex plane, apart from poles and branch cuts. After transforming variable from q^2 to

$$z \;=\; \frac{\sqrt{1-q^2/t_+}-\sqrt{1-t_0/t_+}}{\sqrt{1-q^2/t_+}+\sqrt{1-t_0/t_+}} \tag{7.57}$$

they can be expanded in a Taylor series in z

$$f_+(q^2)P(q^2) \equiv g_+(z) = \sum_{k=0}^{\infty} a_k^{(+)} z^k, \qquad f_0(q^2) \equiv g_0(z) = \sum_{k=0}^{\infty} a_k^{(0)} z^k \tag{7.58}$$

I perform two fits to g_+ and g_0, truncating at different orders in the polynomial expansion:

- fit$_1$: constant $g_0(z) = a_0^{(0)}$, linear $g_+(z) = a_0^{(+)} + a_1^{(+)} z$. I leave out the data point with largest q^2 for both f_0 and f_+.
- fit$_2$: linear $g_0(z) = a_0^{(0)} + a_1^{(+)} z$, quadratic $g_+(z) = a_0^{(+)} + a_1^{(+)} z + a_2^{(+)} z^2$.

In both cases I impose the constraint $f_+(0) = f_0(0)$. I choose $t_0 = 0.65 t_-$ as in [20]. In Fig. 7.7 I show the data in the variable z and the two polynomial fits to $g_+(z)$ and $g_0(z)$ in the range $[z(q^2_{\mathrm{max}}, t_0), z(0, t_0)]$. Due to the large statistical errors it is not easy

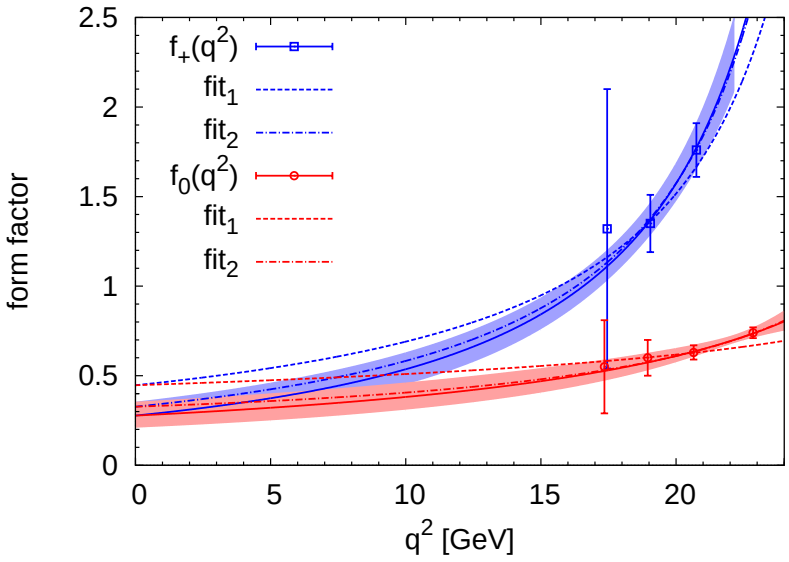

Figure 7.6: Vector form factors $f_+(q^2)$, $f_0(q^2)$ from [29]. I show both the fit to the BK parametrisation [62] and two parametrisations of different order in the analytical z expansion.

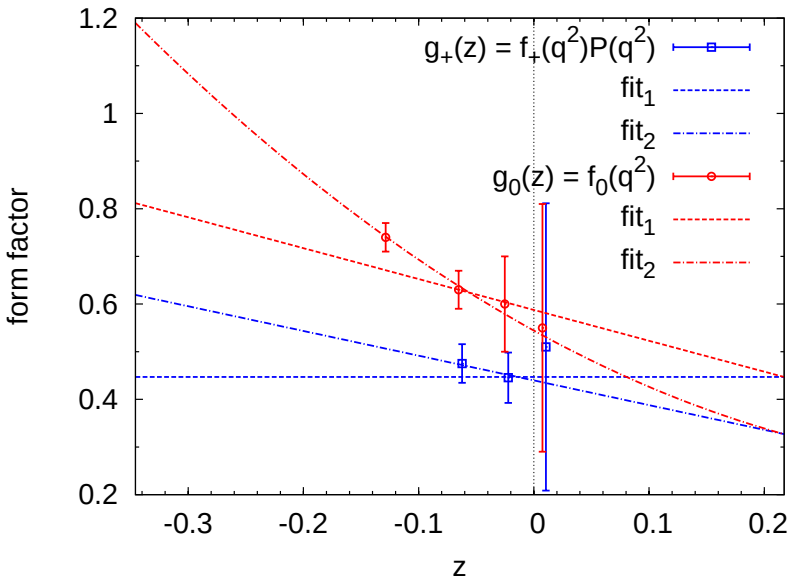

Figure 7.7: Polynomial fit to the vector form factor as a function of z.

to constrain the series coefficients and this should be regarded as an exploratory study; the results will refined once more higher statistics are available. The χ^2/(d.o.f.) is 0.02 for fit_1 and 0.05 for fit_2.

The difference between the two fit results is an estimate for the uncertainty in the parametrisation, see Fig. 7.6. I find

$$f_{+,0}(0) = 0.447 \quad (\text{fit}_1), \qquad f_{+,0}(0) = 0.327 \quad (\text{fit}_2). \tag{7.59}$$

The result from the higher order fit lies within the statistical error band. The error is of the same order as the statistical error.

In [18] the vector form factor has been calculated by the MILC collaboration in nonmoving NRQCD (see this paper for further references to older studies on unquenched gauge configurations[1]). Using the Becirevic-Kaidalov ansatz it is given at $q^2 = 0$

$$f_{+,0}(0) \;=\; 0.27(2)(4) \qquad \text{(Dalgic et al., [18])}. \tag{7.60}$$

The first error is due to statistics and the chiral extrapolation whereas the second estimates other systematic uncertainties.

The results in [136] have been obtained on the MILC gauge configurations and the Fermilab action for the heavy quarks. The value reported there is

$$f_{+,0}(0) \;=\; 0.23(2) \qquad \text{(Okamoto et al. [136])}. \tag{7.61}$$

Tensor form factor

I perform the same analysis for the tensor form factors T_1 and T_2. Here I find

$$F = 0.281, \qquad \alpha = 0.641, \qquad \beta = 1.364 \tag{7.62}$$

with the covariance matrix

$$\text{cov}(F, \alpha, \beta) \;=\; \begin{pmatrix} 0.0183 & -0.0628 & 0.0954 \\ & 0.2180 & -0.3265 \\ & & 0.5030 \end{pmatrix}. \tag{7.63}$$

[1] Note that the result in [62] where the Becirevic Kaidalov parametrisation was originally introduced is obtained on quenched configurations. The value of $f_{+,0}(0) = 0.38(8)$ given there does not agree very well with the recent, unquenched results.

From this I obtain the value at $q^2 = 0$

$$T_{1,2}(q^2 = 0) \quad = \quad \begin{cases} 0.28(13) & \text{BK parametrisation} \\ 0.221 & \text{fit}_1 \\ 0.152 & \text{fit}_2. \end{cases} \tag{7.64}$$

The corresponding plots are shown in Figs. 7.9 and 7.8. The results for the tensor form factor have to be compared to the results by Becirevic et al., who find

$$T(q^2 = 0) \quad = \quad 0.24(3)^{+0.04}_{-0.01} \qquad \text{(Becirevic et al. [58])} \tag{7.65}$$

where the errors are statistical/systematic.

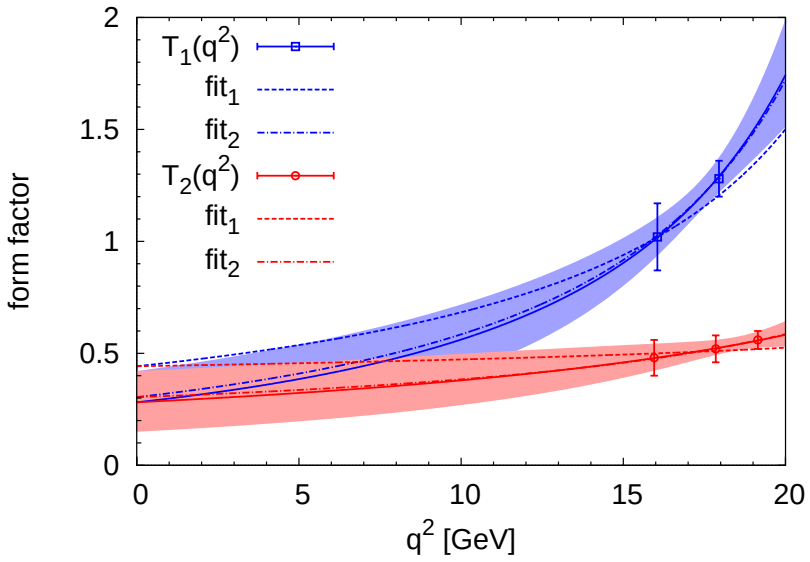

Figure 7.8: Vector form factors $T_1(q^2)$, $T_2(q^2)$ from [29]. I show both the fit to the BK parametrisation [62] and two parametrisations of different order in the analytical z expansion.

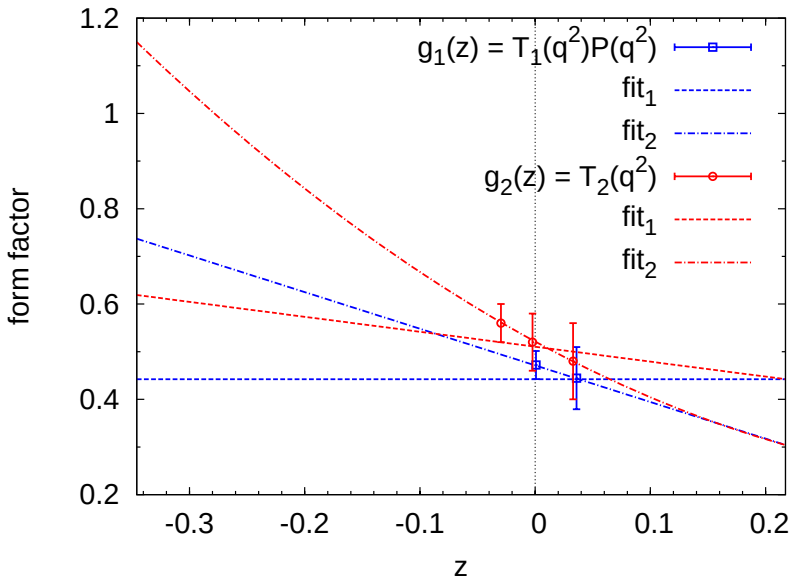

Figure 7.9: Polynomial fit to the tensor form factor as a function of z.

Chapter 8

Discussion

In this chapter I briefly review the methods used in this work, summarise my results and discuss systematic uncertainties of the approach. I finally outline possible further developments.

8.1 Summary of methods and results

In the first chapter I argue that heavy-light decays can be used to constrain the entries of the CKM matrix. In addition, rare decays of B mesons are loop suppressed in the Standard Model and offer an excellent opportunity to test new physics models. The prediction of exclusive decays requires the evaluation of hadronic matrix elements. After integrating out the physics at the electroweak scale these decays are described by an effective theory in the continuum. I review the contribution of various operators in the low energy Hamiltonian to heavy-light matrix elements and analyse their relative importance. Lattice QCD can be used to calculate matrix elements of local operators in a model independent way. This calculation is independent of the physics at the TeV scale which only changes the value of the Wilson coefficients. In the Standard Model the Wilson coefficients are now known at next-to-next-to-leading-log precision.

On presently available configurations the inverse lattice spacing is of the order of or smaller than the bottom quark mass. High energy fluctuations of the heavy quark field at this scale are integrated out to obtain an effective theory which can be discretised on a lattice. It is important to calculate hadronic form factors in the large recoil region where most experimental data can be found; for the decay $B \to K^*\gamma$ only the point $q^2 = 0$ is physical. A very successful approach for extending the calculation to smaller q^2 is to discretise the theory in a moving frame of reference. Over the last years the m(oving)NRQCD action has been developed and extensively tested by the HPQCD collaboration. The recent increase in precision of experimental results, which is expected to improve in the future, justifies work on further reducing systematic errors in this approach.

The heavy quark action can be systematically improved to reduce both nonpertur-

bative errors in the heavy quark expansion and discretisation artifacts. Beyond tree level the effective theory differs from full QCD at momentum scales of the order of the heavy quark mass where a perturbative treatment of radiative corrections is justified by the small value of the strong coupling constant. I calculate one loop corrections to the action and heavy-light lattice operators in perturbation theory. In particular, the calculation of radiative corrections to the tensor current is a new result which will help to increase the precision in theoretical predictions of hadronic form factors for the rare decay $B \to K^*\gamma$. As the operators in the lattice action are very complicated I use a PYTHON code to automatically generate Feynman rules and perform the integrals over phase space with the adaptive Monte Carlo integrator VEGAS. Wherever possible I have verified the correctness of my calculations by comparing to published results for simpler setups. I also report on results from nonperturbative lattice simulations obtained by other members of the HPQCD collaboration and discuss how heavy-light form factors of the vector- and tensor-current can be extrapolated to the large recoil region.

The results of my perturbative calculations are summarised in the following two sections:

8.1.1 Heavy quark renormalisation parameters

I calculate the one loop radiative corrections of the leading order coefficients in the moving NRQCD action. I find that, after including mean field corrections, all renormalisation parameters are of order one and smaller. In particular the renormalisation of the external momentum is small for not too large frame velocities, as is expected from approximate reparametrisation invariance on the lattice. Care has to be taken when choosing the integration contour to ensure that it can be Wick rotated to Minkowski space. The heavy quark wavefunction renormalisation is infrared divergent in Feynman gauge. I use a gluon mass to regulate the logarithmic divergence and repeat the continuum calculation with this infrared regulator. As the effective theory and full QCD agree in the infrared regime this artificial dependence on the gluon mass cancels in the matching coefficients. By comparing to published results for simple lattice setups I verify that my calculations are correct. I discuss the setting of the typical scale in loop integrals and compare my results to nonperturbative calculations of renormalisation parameters. The small mismatch might be explained by higher order radiative corrections or nonperturbative effects and further work is necessary to resolve this discrepancy.

In addition, I also present results obtained on a finite lattice. Twisted boundary conditions suppress nonperturbative tunnelling in numerical simulations and serve as an

infrared regulator by introducing a lower momentum cutoff. My results are compared to high-β simulations on quenched gluon configurations. I find agreement between the two methods and my one loop results from diagrammatic perturbation theory are used to constrain the polynomial fit of high-β data. This reduces the errors on the two loop coefficients.

Motivated by nonperturbative studies I also calculate the renormalisation of higher order kinetic terms for the NRQCD action in a nonmoving frame. Care has to be taken in the phase space integration as large peaks in the infrared region can spoil the convergence of the Vegas integral. I demonstrate the infrared stability of my results by varying the gluon mass and test my approach by reproducing results for other heavy quark actions in the literature. The perturbative matching coefficient of the $\mathcal{O}(a^4)$ term, which breaks rotational invariance, is of the order one. Although my results are of the same order of magnitude as those in previous perturbative studies with similar actions, they are not compatible with the large correction that is found by nonperturbative tuning of this term. However, these simulations have only been carried out on relatively coarse lattices and with large momenta. Other ingredients of the simulation, such as the gluon action, can have large discretisation errors. Further nonperturbative calculations are needed to reach a definitive conclusion. I find that including a further $\mathcal{O}(a^6)$ correction to the lowest order kinetic term reduces the size of radiative corrections substantially but has only a small impact on the lowest order renormalisation parameters. Including this term also reduces the size of the matching coefficient obtained in nonperturbative simulations; however, the reduction is only about a factor two and the discrepancy persists.

8.1.2 Renormalisation of heavy-light currents

I calculate the perturbative one loop matching coefficients of the leading order heavy-light vector and tensor currents. The continuum integrals are expanded in powers of the inverse heavy quark mass. After constructing suitable operators the one particle irreducible three point functions on the lattice are evaluated numerically with Vegas. Infrared subtraction functions are introduced to stabilise the Monte Carlo integration. An additional ingredient of the matching calculation is the light quark wavefunction renormalisation. After verifying that I can reproduce published results for the ASQTad action I calculate the wavefunction renormalisation of massless HISQ quarks at one loop.

I show results for different heavy quark actions, using both the ASQTad and the HISQ action to discretise the light quark. If the full $\mathcal{O}(1/m^2, v_{\text{rel}}^4)$ mNRQCD action and ASQTad quarks are used the matching coefficients are around $0.4\alpha_s$ for the vector

current and even smaller, around $0.2\alpha_s$ for the tensor current at the renormalisation scale $\mu = m$ and not too large frame velocities. With $\alpha_s = \alpha_V(2/a) \approx 2/a$ I conclude that the size of the leading order radiative corrections is around 12% for the vector current and around 6% for the tensor current. This is the same order as $1/m$ nonperturbative corrections but smaller than the naive estimate of $\mathcal{O}(\alpha_s) \approx 30\%$. In a nonmoving frame I find agreement with published results for the renormalisation of the zero component of the vector current. The splitting between the matching coefficients for different Lorentz indices of the current is reduced by using the full $\mathcal{O}(1/m^2, v_{\text{rel}}^4)$ mNRQCD action in combination with the HISQ light quark action. This reduction is much more pronounced for the tensor current. I interpret this as partial restoration of Lorentz invariance by improvement of the action.

8.1.3 Nonperturbative form factor calculation

Finally, I report on the calculation of nonperturbative heavy-light form factors carried out within the HPQCD collaboration. So far these calculations have been performed with a simplified mNRQCD action which is correct at $\mathcal{O}(1/m)$. Currently the simulations are repeated for the full $\mathcal{O}(1/m^2, v_{\text{rel}}^4)$ mNRQCD with tree level $1/m$ corrections to the currents. Eventually these matrix elements will be combined with my results for the radiative corrections to the leading order operators. Lattice data at high momentum transfer q^2 is extrapolated to the large recoil region $q^2 \approx 0$ using a phenomenological ansatz for the form factors, systematic uncertainties in this ansatz are estimated. I compare to results obtained in the literature. The nonperturbative results presented in this thesis should be seen as preliminary and will be updated with new data.

8.2 Discussion of uncertainties

As in every theoretical prediction it is important to quantify all uncertainties. In the lattice calculation discretisation errors are reduced by using improved actions. As mNRQCD is an effective action this introduces additional uncertainties, both from the heavy quark expansion and the renormalisation of operators. In the following I estimate the sources of errors and give a breakdown of all uncertainties in Tab. 8.1.

8.2.1 Finite volume effects

On a periodic lattice hadronic states can interact with their copies in a shifted lattice volume. The lightest particle in the theory is the pseudoscalar meson with mass m_{PS}. Over the size of the lattice volume its wavefunction decays as $\exp[-m_{PS}L]$ where L is

the linear size of the lattice, so this exchange process is suppressed by an exponential factor. Finite volume errors increase as the quark mass becomes more chiral. For the "coarse" MILC configurations used in the numerical simulation the authors of [134] find $am_{PS} \approx 0.19$ on the $20^3 \times 64$ lattice with $am_\ell/am_s = 0.007/0.05$, so a naive estimate of finite volume errors would be

$$\exp[-m_{PS}L] \sim e^{-4} \quad \approx \quad 2\%. \tag{8.1}$$

The authors of [20] calculate the vector form factors f_+, f_0 on MILC lattices with a Fermilab heavy quark and ASQTad light quarks. They estimate the finite volume error on the form factors in finite volume heavy meson staggered perturbation theory (HMSχPT) and conclude that the uncertainty on $f_+(q^2)$ does not exceed 0.5%. In the following I estimate the error from finite volume effects to be of the order of 1%.

8.2.2 Discretisation errors

Gluon action. The simple Wilson gluon action has errors of $\mathcal{O}(a^2)$. In the Symanzik improved action these are removed at tree level and one loop [78] and the discretisation errors in this action are of $\mathcal{O}(a^4, \alpha_s^2 a^2)$.

Light quark action. The ASQTad action does not have $\mathcal{O}(a^2)$ errors at tree level. $\mathcal{O}(\alpha_s a^2)$ errors from highly virtual taste-changing gluon interactions are suppressed by smearing of link variables. Taste breaking effects are reduced by a further factor of $3-4$ in the HISQ action; the authors of [85] conclude that the remaining errors from taste changing interactions are around 1%.

Heavy quark action. For the nonrelativistic heavy quark action discretisation errors in the different lattice directions have to be discussed separately. Errors in the spatial directions are reduced by using improved derivatives and chromodynamic fields in the leading Hamiltonian. The corresponding errors in the temporal direction are reduced by an improved time evolution, as discussed at the end of section 4.1.1. The remaining errors are of $\mathcal{O}(a^4)$ at tree level. In the higher order terms of the action unimproved derivatives are used, however, as they are multiplied by higher powers of the inverse quark mass they are $\mathcal{O}(a^2/m^2) \lesssim \mathcal{O}(a^4)$ as $am \gtrsim 1$; on the coarse MILC lattices the heavy quark mass is $am = 2.8$.

Radiative corrections will introduce errors of $\mathcal{O}(\alpha_s a^2)$. In numerical simulations a tadpole improved, tree level action has been used. As demonstrated in this work, tadpole improvement reduces the size of radiative corrections.

The nonrelativistic heavy quark theory is constructed such that the fluctuations both in the light and heavy quark within the B meson are of order $\Lambda_{\rm QCD}$. By discretising the theory in a moving frame the same is true for the quarks in the final state meson.

I conclude that the leading discretisation errors from the actions are $\mathcal{O}(\alpha_s(a\Lambda_{\rm QCD})^2)$. On the coarse lattices with $a^{-1} = 1.6$ GeV and using $\alpha_V(2/a) \approx 0.3$ and $\Lambda_{\rm QCD} \approx 500$ MeV I estimate the leading discretisation errors to be $\mathcal{O}(3\%)$. As remarked above, this is probably a conservative estimate as radiative corretions are reduced by tadpole improvement and $\mathcal{O}(\alpha_s a^2)$ errors from the exchange of high energetic gluon are small in the ASQTad and HISQ actions. To obtain a more realistic quantitative estimate of discretisation errors would require simulation at different lattice volumes to measure the coefficients of $\alpha_s^n a^m$ dependent terms.

Heavy-light operators. As the derivatives in the $\mathcal{O}(1/m)$ heavy-light operators are unimproved this introduces discretisation errors of $\mathcal{O}(a^2/m)$. On the coarse lattice with $am = 2.8$ these errors are $\mathcal{O}((a\Lambda_{\rm QCD})^2/(am)) = \mathcal{O}(3.5\%)$ and comparable to those from the actions.

8.2.3 Heavy quark expansion

At tree level the heavy quark action is correct up to (and including) $\mathcal{O}(1/m^2, v_{\rm rel}^4)$. Errors in heavy meson energy splittings are then $\mathcal{O}((\Lambda_{\rm QCD}/m)^2, v_{\rm rel}^4) \sim 1\%$. Radiative corrections will renormalise the operators in the action, leading to corrections of $\mathcal{O}(\alpha_s/m, \alpha_s v_{\rm rel}^2)$. However, some terms in the $1/m$ action are protected from renormalisation by reparametrisation invariance and it is found that this symmetry is only broken by higher order lattice artifacts in the discretised theory. In the mNRQCD action used in nonperturbative simulations all coefficients in the action were set to their tree level values. The errors are expected to be $\mathcal{O}(\alpha_s\Lambda_{\rm QCD}/m, \alpha_s v_{\rm rel}^2) \sim 3\%$, where I assume $v_{\rm rel}^2 \approx 0.1$.

For the calculation of meson masses and form factors the relevant hadronic scale is $\Lambda_{\rm QCD}$. As discussed in section 4.1.2 additional scales enter in heavy-light decays. Here the energy E' and momentum $\boldsymbol{p}'$ of the final state meson have to be small compared to the heavy quark mass. By including $1/m$ operators for the calculation of the decay matrix element these errors are reduced to $\mathcal{O}(\alpha_s E'/m, E'^2/m^2) \sim 8\%$. As can be seen from Fig. 4.2 one has $E' \lesssim 0.25$ for the smallest q^2 in the form factor calculation.

8.2.4 Higher order radiative corrections

In this work the renormalisation constants of operators in the heavy quark action and the matching coefficients have been calculated at the one loop order in lattice

perturbation theory. Higher order corrections enter at $\mathcal{O}(\alpha_s^2) \sim 9\%$. Again, this is a conservative estimate as radiative corrections are reduced by tadpole improvement of the action. Further work on renormalising the heavy quark action to two loop order, using a combination of lattice perturbation theory and high-β simulations is currently carried out [108, 137].

Mixing down

As the lattice introduces a momentum cutoff, higher order operators can mix down to lower order operators under renormalisation. This can be seen immediately from dimensional arguments: An operator $Q_j^{(1)}$ with a derivative operator will generate corrections proportional to $\alpha_s/(am)$ to the leading order operator $Q^{(0)}$. As $am \gtrsim 1$ this seems to violate the power counting in $1/m$. However, if instead one changes basis and works with subtracted higher order operators,

$$Q_j^{(1)\text{sub}} \quad = \quad Q_j^{(1)} - \alpha_s \xi_{j0} Q^{(0)}, \tag{8.2}$$

these will not mix down to the leading operator at $\mathcal{O}(\alpha_s)$. Nonperturbative matrix elements of $Q_j^{(1)\text{sub}}$ are suppressed by $1/m$ as expected from power counting.

8.2.5 Form factor extrapolation

To extrapolate the lattice data for heavy-light form factors requires a phenomenological ansatz for its functional dependence on the momentum transfer q^2. The uncertainties can be estimated by comparing results using different functional forms, see discussion in section 7.3.2. There I find that, for currently available data, this uncertainty is comparable to that from statistical/fitting errors.

8.2.6 Chiral extrapolation

The light quark masses used in the simulations are unphysically heavy, the lightest pseudoscalar particle on the most chiral ensemble of coarse lattices has a mass of $m_{PS} \approx 300$ MeV which has to be compared to that of a physical pion, $m_\pi \approx 140$ MeV. Chiral perturbation theory, an expansion in the light quark masses and small meson momenta, is used to extrapolate to the physical point. In [18] the chiral extrapolation is carried out for the vector form factors. As can be seen from Figs. 10 to 12 in [18] the difference between the most chiral data point (which corresponds to the quark masses used in our simulations) and the physical point never exceeds 10%. I take this as a naive upper limit on corrections from the chiral corrections to our results. To extrapolate to the chiral limit more calculations with different light quark masses are necessary.

Source of error	estimate
Finite volume effects	$\sim 1\%$
Discretisation [actions]	$\mathcal{O}(\alpha_s(a\Lambda_{\rm QCD})^2) \lesssim 3\%$
Discretisation [operators]	$\mathcal{O}((a\Lambda_{\rm QCD})^2/(am)) \sim 3.5\%$
Heavy quark expansion [action]	$\mathcal{O}(\alpha_s\Lambda_{\rm QCD}/m, \alpha_s v_{\rm rel}^2) \sim 3\%$
Heavy quark expansion [operators]	$\mathcal{O}(\alpha_s E'/m, E'^2/m^2) \sim 8\%$ (at $q^2 \approx 16$ GeV^2)
Radiative corrections	$\mathcal{O}(\alpha_s^2) \lesssim 9\%$
Chiral extrapolation	$\lesssim 10\%$

Table 8.1: Summary of uncertainties

8.2.7 Statistical/fitting errors

Statistical errors are still relatively large and increase with the frame velocity. They can be reduced by using more elaborate sources. Currently, calculations with random wall sources are carried out by Zhaofeng Liu [30].

8.3 Outlook

There are several ways of extending the work presented in this thesis. Using an improved heavy quark action which includes radiative corrections to the operators has a wide impact on the precision of predictions both for heavy-heavy and heavy-light mesons. Recent experimental discoveries, such as that of the $\eta_b(1s)$ meson [64] justify further development and improvement of the lattice heavy quark action.

To achieve sufficient precision it is necessary to renormalise other operators in the action. The chromomagnetic $\boldsymbol{\sigma} \cdot \boldsymbol{B}$ term is of particular interest as it determines the hyperfine splitting between the $\Upsilon(1s)$ state and the $\eta_b(1s)$ meson. The perturbative calculation has to be carried out in background field gauge as only in this gauge the one loop effective potential has the same symmetries as the tree level action. While so far the radiative corrections have only been calculated for higher order kinetic terms in the nonmoving NRQCD action, it is straightforward to extend this to the corresponding operators in the mNRQCD action.

Precise knowledge of the heavy quark mass renormalisation, which is obtained from radiative corrections to the self-energy, will help to constrain this fundamental parameter of the Standard Model. High-β simulations for extracting higher order loop corrections are carried out on quenched gauge configurations and only include gluonic contributions to the heavy quark self-energy. To complement these calculations it is necessary to include the effects of fermionic vacuum polarisation. This can be done in

diagrammatic perturbation theory, at two loop order only a small number of diagrams needs to be evaluated. Calculating higher order loop corrections will also help to understand the current, small discrepancy between perturbative calculations of leading order renormalisation constants and results from nonperturbative lattice simulations.

Naively, two loop radiative corrections to the leading order (in the $1/m$ expansion) heavy light currents are expected to be around 9% and of the same order as $1/m$ corrections, so it is necessary to calculate the coefficients at next order in the α_s expansion.

Clearly, the statistics of nonperturbative heavy-light form factor calculations need to be increased to improve the extrapolation to physical momenta transfers q^2.

As long as the lattice spacing of available configurations is larger than the Compton wavelength of the heavy quark it is justified to work with the effective, nonrelativistic discretisation used in this work. In the future, when sufficiently fine lattices might become available, it is desirable to use a relativistic quark action instead. For charm quarks with a mass of around 1.2 GeV first results have been obtained by the HPQCD collaboration. The HISQ action is used for the valence quarks. The finest ASQTad configurations generated by the MILC collaboration have $a = 0.045$ fm [138], so that am is about one. Note that the cost of a simulation scales with a high power of the inverse lattice spacing. For analysing experimental results expected within the next few years it is clearly necessary to use an effective lattice action for heavy quarks to achieve sufficient accuracy.

It should be stressed that the form factor calculations I present in this thesis only give the local contribution to the rare decays $B \to K^*\gamma$ and $B \to K^{(*)}\ell\ell$. As discussed in detail in 2.3.2 there are other, nonlocal contributions which can not be calculated in lattice QCD. Although there are indications that these contributions are small in the Standard Model, the size of these effects is hard to quantify. To make complete predictions for these processes, the lattice approach has to be combined with other methods.

Appendix A

Conventions

In this appendix I summarise some conventions and notation used in this work.

A.1 Euclidean space ↔ Minkowski space

The following conventions are used to relate quantities in Minkowski space (labelled by (M)) with metric $g_{\mu\nu} = \mathrm{diag}(+1,-1,-1,-1)$ to the corresponding expressions in Euclidean space with metric $\delta_{\mu\nu} = \mathrm{diag}(+1,+1,+1,+1)$.

A.1.1 Four-vectors and derivatives

$$\begin{aligned} x_0 = x^0 = ix^0_{(M)} = ix_0^{(M)} \qquad & x_j = x^j = x^j_{(M)} = -x_j^{(M)} \\ \partial_0 = \partial^0 = -i\partial^0_{(M)} = -i\partial_0^{(M)} \qquad & \partial_j = \partial^j = -\partial^j_{(M)} = \partial_j^{(M)} \end{aligned} \tag{A.1}$$

A.1.2 Gauge fields

As the covariant derivative $D_\mu = \partial_\mu + igA_\mu$ transforms as ∂_μ the gauge field A_μ is defined in Euclidean space as follows:

$$A_0 = A^0 = -iA^0_{(M)} = -iA_0^{(M)} \qquad A_j = A^j = -A^j_{(M)} = A_j^{(M)} \tag{A.2}$$

The chromoelectric field $\boldsymbol{E}$ and the chromomagnetic field $\boldsymbol{B}$ are thus

$$E_k = \boldsymbol{E}_k = iE^i_{(M)} \qquad \text{and} \qquad B_k = \boldsymbol{B}_k = B^i_{(M)}. \tag{A.3}$$

where they are defined by

$$E_k = -F_{0k} = -(\partial_0 A_k - \partial_k A_0) \qquad \text{and} \qquad B_k = -\frac{1}{2}\epsilon_{k\ell m}F_{\ell m}. \tag{A.4}$$

$\epsilon_{k\ell m}$ is completely antisymmetric with $\epsilon_{123} = +1$.

In Euclidean space the chromodynamic fields in the rest frame ($\boldsymbol{E}'$, $\boldsymbol{B}'$) and lattice frame ($\boldsymbol{E}$, $\boldsymbol{B}$) are related by

$$\begin{aligned} \boldsymbol{E}' &= \gamma\left(\boldsymbol{E} + i\boldsymbol{v}\times\boldsymbol{B} - \frac{\gamma}{1+\gamma}\boldsymbol{v}(\boldsymbol{v}\cdot\boldsymbol{E})\right), \\ \boldsymbol{B}' &= \gamma\left(\boldsymbol{B} + i\boldsymbol{v}\times\boldsymbol{E} - \frac{\gamma}{1+\gamma}\boldsymbol{v}(\boldsymbol{v}\cdot\boldsymbol{B})\right). \end{aligned} \tag{A.5}$$

A.1.3 Dirac matrices

To ensure that the Dirac matrices in Euclidean space satisfy $\{\gamma_\mu, \gamma_\nu\} = 2\delta_{\mu\nu}$ define

$$\gamma_0 = \gamma^0 = \gamma^0_{(M)} = \gamma_0^{(M)}, \qquad \gamma_j = \gamma^j = -i\gamma^j_{(M)} = i\gamma_j^{(M)}. \tag{A.6}$$

Thus $\gamma_5 = \gamma_0\gamma_1\gamma_2\gamma_3 = i\gamma^0_{(M)}\gamma^1_{(M)}\gamma^2_{(M)}\gamma^3_{(M)} = \gamma_5^{(M)}$. The definition of γ_5 in $d \neq 4$ dimension can cause problems. For the continuum calculation a completely anticommuting γ_5 is used; this corresponds to the naive dimensional regularisation (NDR) scheme [40].

I also define in Euclidean space

$$\sigma_{\mu\nu} = \frac{1}{2}[\gamma_\mu, \gamma_\nu]. \tag{A.7}$$

The Pauli-Dirac representation for gamma matrices in Minkowski space is

$$\gamma^0_{(M)} = \begin{pmatrix} I & 0 \\ 0 & -I \end{pmatrix} \quad \gamma^j_{(M)} = \begin{pmatrix} 0 & \sigma^j \\ -\sigma^j & 0 \end{pmatrix} \quad \gamma_5^{(M)} = i\gamma^0\gamma^1\gamma^2\gamma^3 = \begin{pmatrix} 0 & I \\ I & 0 \end{pmatrix} \tag{A.8}$$

where σ^j are the Pauli matrices.

A.2 Lattice derivatives and field strength

I give explicit expressions for the discretised derivatives I use in the lattice action. All expressions are constructed from the elementary forward-, backward- and symmetric difference operators

$$\begin{aligned} \Delta^+_\mu\psi(x) &= U_\mu(x)\psi(x+\hat{\mu}) - \psi(x), \\ \Delta^-_\mu\psi(x) &= \psi(x) - U_{-\mu}(x)\psi(x-\hat{\mu}), \\ \Delta^\pm_\mu\psi(x) &= \frac{1}{2}\left[U_\mu(x)\psi(x+\hat{\mu}) - U_{-\mu}(x)\psi(x-\hat{\mu})\right]. \end{aligned} \tag{A.9}$$

For performance reasons, a maximally local discretisation of higher-order operators is used by balancing the occurrence of these three types. All expressions are symmetrised.

Unimproved derivatives

$$\begin{aligned}
\Delta^{(2n)} &= \sum_{j=1}^{3}(\Delta_j^+\Delta_j^-)^n \qquad (A.10)\\
\Delta_v^{(2)} &= \frac{1}{2}\sum_{j,k=1}^{3} v^j v^k \left(\Delta_j^+\Delta_k^- + \Delta_j^-\Delta_k^+\right)\\
\Delta_v^{(3)} &= \frac{1}{2}\sum_{j,k,\ell=1}^{3} v^j v^k v^\ell \left(\Delta_j^+\Delta_k^\pm\Delta_\ell^- + \Delta_j^-\Delta_k^\pm\Delta_\ell^+\right)\\
\Delta_v^{(4)} &= \frac{1}{2}\sum_{j,k,\ell,m=1}^{3} v^j v^k v^\ell v^m \left(\Delta_j^+\Delta_k^-\Delta_\ell^+\Delta_m^- + \Delta_j^-\Delta_k^+\Delta_\ell^-\Delta_m^+\right)
\end{aligned}$$

Improved derivatives

$$\begin{aligned}
\tilde{\Delta}_j^\pm &= \Delta_j^\pm - \frac{1}{6}\Delta_j^+\Delta_j^\pm\Delta_j^- \qquad (A.11)\\
\tilde{\Delta}^{(2)} &= \Delta^{(2)} - \frac{1}{12}\sum_{j=1}^{3}\Delta_j^+\Delta_j^-\Delta_j^+\Delta_j^-\\
\tilde{\Delta}_v^{(2)} &= \Delta_v^{(2)} + \frac{1}{4}\sum_{j,k=1}^{3} v^j v^k \Delta_j^+\Delta_j^-\Delta_k^+\Delta_k^-\\
&\quad - \frac{1}{12}\sum_{j,k=1}^{3} v^j v^k \Big(\Delta_j^+\Delta_j^-\Delta_j^+\Delta_k^- + \Delta_j^-\Delta_j^+\Delta_j^-\Delta_k^+\\
&\qquad\qquad +\Delta_j^+\Delta_k^-\Delta_k^+\Delta_k^- + \Delta_j^-\Delta_k^+\Delta_k^-\Delta_k^+\Big)
\end{aligned}$$

Unimproved adjoint derivative

$$\Delta_\mu^{\mathrm{ad}}\tilde{F}_{\rho\sigma}(x) = \frac{1}{2}\left(U_\mu(x)\tilde{F}_{\rho\sigma}(x+\hat{\mu})U_\mu^\dagger(x) - U_{-\mu}(x)\tilde{F}_{\rho\sigma}(x-\hat{\mu})U_{-\mu}^\dagger(x)\right) \qquad (A.12)$$

Improved field strength tensor

$$\begin{aligned}
\tilde{F}_{\mu\nu}(x) &= \frac{5}{3}F_{\mu\nu}(x) - \frac{1}{6}\Big(U_\mu(x)F_{\mu\nu}(x+\hat{\mu})U_\mu^\dagger(x) \qquad (A.13)\\
&\qquad + \; U_{-\mu}(x)F_{\mu\nu}(x-\hat{\mu})U_{-\mu}^\dagger(x) - (\mu\leftrightarrow\nu)\Big)
\end{aligned}$$

$$
\begin{aligned}
F_{\mu\nu}(x) &= \frac{-i}{2g}\left(\Omega_{\mu\nu}(x) - \Omega^{\dagger}_{\mu\nu}(x)\right) \qquad \text{(A.14)}\\
\Omega_{\mu\nu}(x) &= \frac{1}{4}\sum_{\{(\alpha,\beta)\}_{\mu\nu}} U_{\alpha}(x)U_{\beta}(x+\hat{\alpha})U_{\text{-}\alpha}(x+\hat{\alpha}+\hat{\beta})U_{\text{-}\beta}(x+\hat{\beta})
\end{aligned}
$$

with

$$
\{(\alpha,\beta)\}_{\mu\nu} = \{(\mu,\nu),(\nu,\text{-}\mu),(\text{-}\mu,\text{-}\nu),(\text{-}\nu,\mu)\} \quad \text{for} \quad \mu \neq \nu \qquad \text{(A.15)}
$$

Appendix B

Twisted boundary conditions

In the following I summarise some technical details on twisted boundary conditions [109, 110] which are used for the high-β simulations discussed in section 4.2.2.

B.1 Basic formalism

Consider a four dimensional lattice with finite spatial extent L and temporal extent T. The latter can be infinite as I will only consider twist in up to three (spatial) directions. In [109] the formalism is outlined for twist in two directions.

B.1.1 Gauge fields

For a gauge link $U_\mu(x)$ the shifted field at $x + L\hat{\nu}$ is given by

$$U_\mu(x + L\hat{\nu}) \quad = \quad \Omega_\nu U_\mu(x) \Omega_\nu^{-1} \qquad \text{with} \quad \nu = 1, 2. \tag{B.1}$$

As the order of shifts does not matter the two twist matrices have to satisfy

$$\Omega_1 \Omega_2 \quad = \quad z \Omega_2 \Omega_1 \qquad \text{with} \quad z = e^{2\pi i/N} \in \text{Centre}\{SU(N)\}. \tag{B.2}$$

It is not necessary to know the explicit form of the matrices Ω_ν; they have the following properties:

- The Ω_ν are fixed up to unitary transformations.
- Any matrix which commutes with Ω_1 and Ω_2 is a multiple of the unit matrix.
- $\Omega_\nu^N = (-1)^{N-1}\text{Id}$.

In perturbative calculations the gauge potential $A_\mu(x)$ is used which is related to the links by $U_\mu(x) = e^{g a A_\mu(x)}$. $A_\mu(x)$ is traceless, antihermitian and satisfies the same periodicity condition as the links,

$$A_\mu(x + L\hat{\nu}) \quad = \quad \Omega_\nu A_\mu(x) \Omega_\nu^{-1}. \tag{B.3}$$

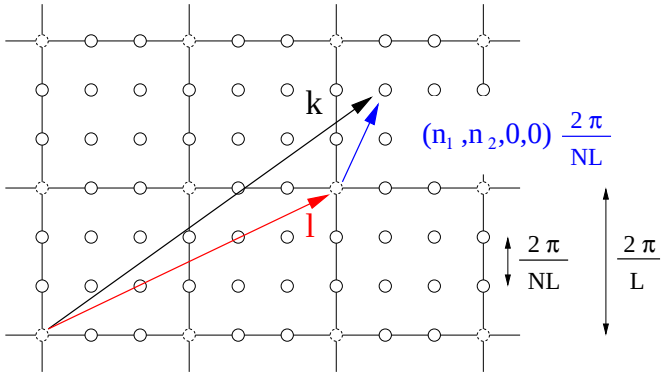

Figure B.1: The total lattice momentum k is split into an untwisted contribution ℓ which is a multiple of $\frac{2\pi}{L}$ and a twisted part $\frac{2\pi}{NL}n$. For twist in two directions the integer valued twist vector is $n = (n_1, n_2, 0, 0)$ with $0 \leq n_1, n_2 \leq N-1$.

In momentum space the gauge potential can be expanded in plane waves

$$A_\mu(x) \quad = \quad \frac{1}{L^3TN} \sum_k \Gamma_k e^{ikx} e^{\frac{i}{2}k_\mu a} \tilde{A}_\mu(k), \tag{B.4}$$

and Γ_k is a complex $N \times N$ matrix which satisfies the condition

$$\Omega_\nu \Gamma_k \Omega_\nu^{-1} \quad = \quad e^{ik_\nu L} \Gamma_k. \tag{B.5}$$

Using $\Omega_\nu^N = (-1)^{N-1}\mathrm{Id}$ this implies that k_ν is a multiple of $\frac{2\pi}{LN}$. It is convenient to split the momentum in a untwisted component ℓ, which is a multiple of $\frac{2\pi}{L}$, and a twisted component $\frac{2\pi}{LN}n$. For twist in two directions the integer valued twist vector is $n = (n_1, n_2, 0, 0)$ with $0 \leq n_1, n_2 \leq N-1$, see Fig. B.1. It turns out that Γ_k only depends on the twisted part of the momentum, so in the following I write Γ_n instead. The solution of (B.5) is unique up to a phase which can be chosen such that

$$\Gamma_n \quad = \quad \Omega_1^{-n_2} \Omega_2^{n_1} z^{\frac{1}{2}(n_1+n_2)(n_1+n_2-1)}. \tag{B.6}$$

Again, it is not necessary to know an explicit representation of the Γ_n as they will only appear in traces (for the gluonic action) or between quark spinors (in the fermionic

action). The following properties can be used to evaluate these traces:

$$\begin{aligned} \Gamma_{n=0} &= \mathrm{Id}, && \text{(B.7)} \\ \mathrm{tr}\{\Gamma_n\} &= 0 \qquad \text{unless} \quad n = 0, && \text{(B.8)} \\ \Gamma_n^\dagger &= z^{-\frac{1}{2}(n,n)}\Gamma_{-n}, && \text{(B.9)} \\ \Gamma_{n'}\Gamma_n &= \Gamma_{n'+n} z^{\frac{1}{2}(\langle n',n\rangle - (n',n))}. && \text{(B.10)} \end{aligned}$$

Here the symmetric and antisymmetric products are defined as

$$\begin{aligned} (n',n) &= n_1'n_1 + n_2'n_2 + (n_1' + n_2')(n_1 + n_2), && \text{(B.11)} \\ \langle n',n\rangle &= n_1'n_2 - n_2'n_1. \end{aligned}$$

As the vector potential has to be traceless, condition (B.8) implies that $\tilde{A}_\mu(k) = 0$ if the twisted part of k vanishes. For every momentum ℓ there are $N^2 - 1$ degrees of freedom which are characterised by their twist vector $n = (n_1, n_2, 0, 0)$ with $0 \leq n_1, n_2 \leq N - 1$ and $(n_1, n_2) \neq (0, 0)$. In particular this implies that there is an infrared cutoff as the momentum can not be smaller than $\frac{2\pi}{NL}$. Note that the number of degrees of freedom has not changed: the sum over colour indices $a = 1, ..., N^2 - 1$ has been replaced by a sum over twist vectors.

The formalism can be extended to more than two twisted directions. In general the twist matrices satisfy

$$\Omega_\mu\Omega_\nu = z_{\mu\nu}\Omega_\nu\Omega_\mu \qquad \text{with} \quad z_{\mu\nu} = e^{2\pi i n_{\mu\nu}/N} \in \mathrm{Center}\{SU(N)\}. \qquad \text{(B.12)}$$

The antisymmetric tensor $n_{\mu\nu}$ completely defines the nature of the boundary conditions. In [102] explicit expressions are given for the QCD gauge group $SU(3)$ and up to four twisted directions. All relations in the previous section, in particular the expressions for Clebsch Gordon coefficients, remain unchanged. The only difference is that the third and fourth component of the twist vector are nonzero. They are however constrained by (B.5) and one finds $n = (n_1, n_2, -(n_1 + n_2), 0)$ in three and $n = (n_1, n_2, -(n_1 + n_2), n_1 - n_2)$ in four dimensions [102]. All calculations in section 5.2 were carried out with three twisted directions.

B.1.2 Fermionic variables

Fermionic variables can be introduced by replacing $SU(N)$ quark spinors by $N \times N$ matrices which transform in colour-smell space [139].

Appendix C

Poles of improved propagators

For certain loop momenta the integration contour in a given one loop diagram has to be deformed to ensure that it can be Wick rotated back to Minkowski space without violating causality. For this it is essential to know the position of poles of all propagators. It is straightforward to find an analytic expression for these poles for the naive gluon and light fermion actions. However, this is not true any more for the Symanzik improved gluon action or the improved relativistic light quark actions, ASQTad and HISQ.

C.1 Symanzik improved gluons

I first analyse the poles of the Symanzik improved gluon propagator discussed in [116]. The gluon two-point function is in Feynman gauge

$$M_{\mu\nu} = \left(\sum_{\rho} q_{\mu\rho} \hat{k}_{\rho}^2 + \lambda^2 \right) \delta_{\mu\nu} + (1 - q_{\mu\nu}) \hat{k}_{\mu} \hat{k}_{\nu} \tag{C.1}$$

where $q_{\mu\nu} = 1 + \frac{1}{12}(\hat{k}_{\mu}^2 + \hat{k}_{\nu}^2)$ and $\hat{k}_{\mu} = 2\sin(k_{\mu}/2)$.

To find the poles of the propagator, I first compute the determinant of this matrix which is a polynomial in $\hat{k}_j^2$ and $\omega = \hat{k}_0^2$. For a given three momentum $k_j \in [-\pi, \pi]$ the zeros of this expression in the $z = e^{ik_0}$ plane can be obtained by solving $\det M(\omega) = 0$ and then using $\omega = 2 - z - 1/z$.[1] Note that the solutions come in pairs, (z_+, z_-) with $z_+ z_- = 1$ so that one of them lies inside, the other outside the unit circle.

It turns out that for a given three momentum there are 14 solutions. In Fig. C.1 these are plotted in the complex z-plane for 1,000 randomly chosen k_j. For the gluon mass a value of $\lambda^2 = 10^{-6}$ was chosen. To compare the poles in the improved propagator to the naive poles, their absolute value is computed and it is compared to that of the

[1] It turns out, that the determinant can be factored as $\det M(\omega) = (\omega + \sum_{j=1}^{3} \hat{k}_j^2 + \lambda^2) \det \tilde{M}(\omega)$ so that one solution coincides with the root of the naive propagator. Numerically, for small λ^2 one of the solutions of $\det \tilde{M}(\omega) = 0$ is very close to the naive solution.

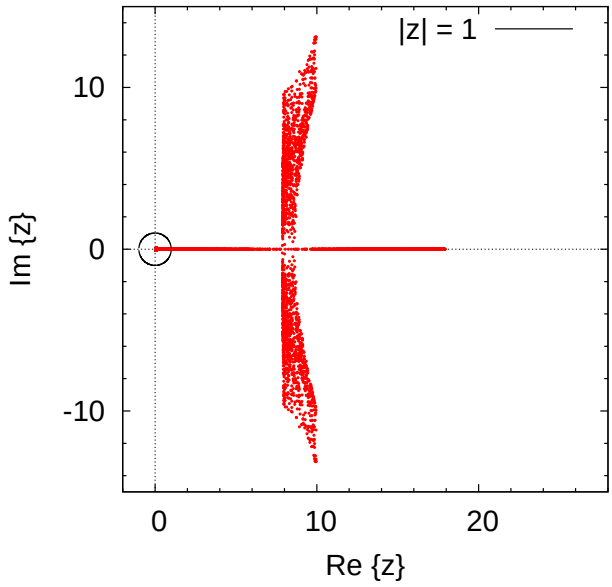

Figure C.1: Poles of the Symanzik improved gluon propagator in the complex plane

naive poles given by

$$z_{\pm}^{(\mathrm{naive})} = \frac{1}{2}\left(2+\hat{\boldsymbol{k}}^2+\lambda^2 \pm \sqrt{(\hat{\boldsymbol{k}}^2+\lambda^2)(\hat{\boldsymbol{k}}^2+\lambda^2+4)}\right) \tag{C.2}$$

with $\hat{\boldsymbol{k}}^2 = 4\sum_{j=1}^{3}\sin^2(k_j/2)$.

In Fig. C.2 these absolute values are plotted for the same random three momenta. As can be seen from this plot the absolute value of an improved pole is either larger than $z_+^{(\mathrm{naive})}$ or smaller than $z_-^{(\mathrm{naive})}$ but it never lies between these values.

I performed a similar analysis for the propagator in Coulomb gauge and find that also in this case the poles of the Symanzik improved propagator always lie outside the band defined by $z_-^{(\mathrm{naive})} < |z| < z_+^{(\mathrm{naive})}$.

C.2 Improved relativistic fermions

The same analysis can be performed for the poles of the ASQ/HISQ propagator. The denominator for massless quarks

$$D = \sum_{\nu}\sin^2(k_\nu)\left(1+\frac{1}{6}\sin^2(k_\nu)\right)^2 \tag{C.3}$$

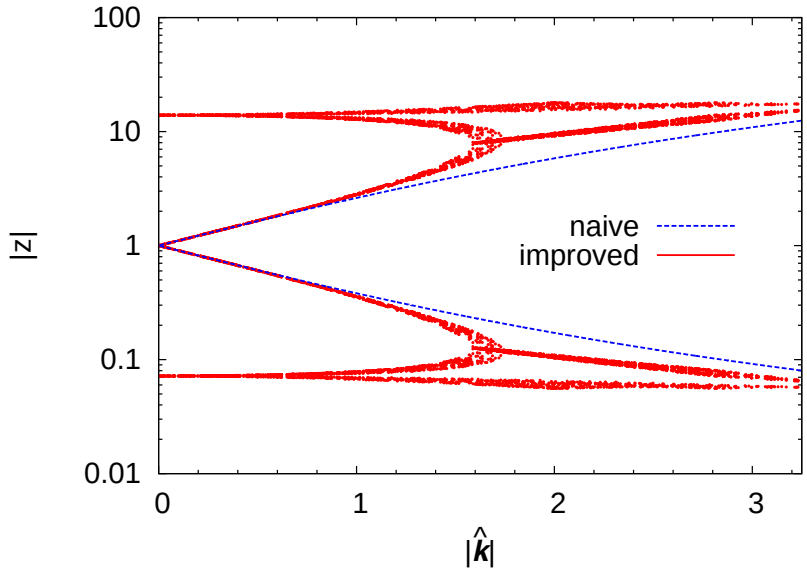

Figure C.2: Absolute value of poles in the naive and Symanzik improved gluon propagator as a function of $|\hat{\boldsymbol{k}}| = 2\sqrt{\sum_{j=1}^{3} \sin^2(k_j/2)}$.

can be written as a function of $\omega = \sin^2(k_0)$. For a given three momentum $k_j \in [-\pi, \pi]$ the cubic equation $D(\omega) = 0$ can be solved by writing it in standard form

$$y^3 - 12y + 36\overset{\circ}{\boldsymbol{k}}^2 - 16 \;=\; 0 \qquad \text{with} \quad y = \omega + 4 \tag{C.4}$$

where I use the notation $\overset{\circ}{\boldsymbol{k}}^2 = \sum_{j=1}^{3} \sin^2(k_j)$. Defining

$$q = 18\overset{\circ}{\boldsymbol{k}}^2 - 8, \qquad D = q^2 - 64, \qquad P = 2\,\mathrm{sgn}\, q \tag{C.5}$$

this cubic equation with real coefficients has either three real or one real and a pair of complex solutions depending on the sign of the discriminant D [131].

- $D \leq 0 \Leftrightarrow \overset{\circ}{\boldsymbol{k}}^2 \leq 8/9$:

$$y_1 = -2P\cos\beta, \quad y_{2,3} = 2P\cos\left(\beta \pm \frac{\pi}{3}\right) \qquad \text{with} \quad \beta = \frac{1}{3}\arccos\frac{q}{P^3}. \tag{C.6}$$

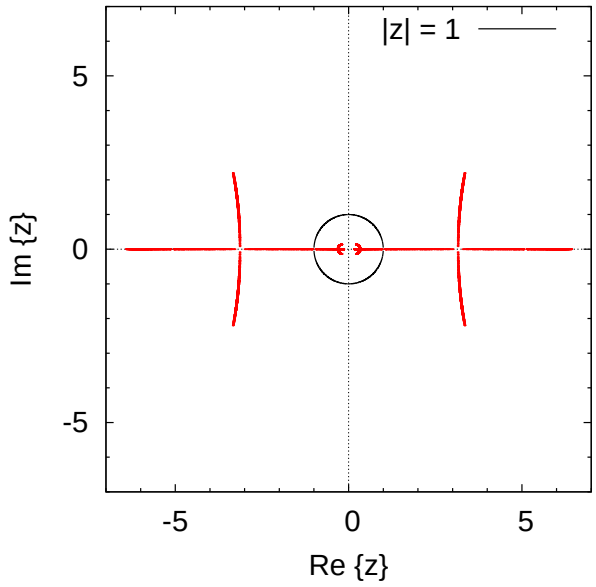

Figure C.3: Poles of the massless ASQ/HISQ fermion propagator in the complex plane

- $D > 0 \Leftrightarrow \mathring{\boldsymbol{k}}^2 > 8/9$:

$$y_1 = -2P\cosh\beta, \quad y_{2,3} = P(\cosh\beta \pm i\sqrt{3}\sinh\beta) \qquad \text{with} \quad \beta = \frac{1}{3}\operatorname{arccosh}\frac{q}{P^3}. \tag{C.7}$$

For each $\omega = y - 4$ one obtains four solutions for $z = e^{ik_0}$ as

$$z_{\pm\pm} \;=\; \pm\sqrt{1 - 2\omega \pm 2\sqrt{\omega^2 - \omega}}. \tag{C.8}$$

Fig. C.3 shows the distribution of the poles in the complex plane. The light quark mass was chosen to be zero. As above, for a given k_j the absolute value of the poles in the massless ASQ/HISQ propagator is compared to that of the poles in the naive propagator which are given as

$$z_{\pm\pm}^{(\text{naive})} \;=\; \pm\sqrt{1 + 2\mathring{\boldsymbol{k}}^2 \pm 2\sqrt{\mathring{\boldsymbol{k}}^2\,(1 + \mathring{\boldsymbol{k}}^2)}}. \tag{C.9}$$

Fig. C.4 shows the absolute values of the massless naive and ASQ/HISQ poles as a function of $\mathring{\boldsymbol{k}}^2$. For each $k_j \in [-\pi, \pi]$ the poles in the improved propagator lie outside

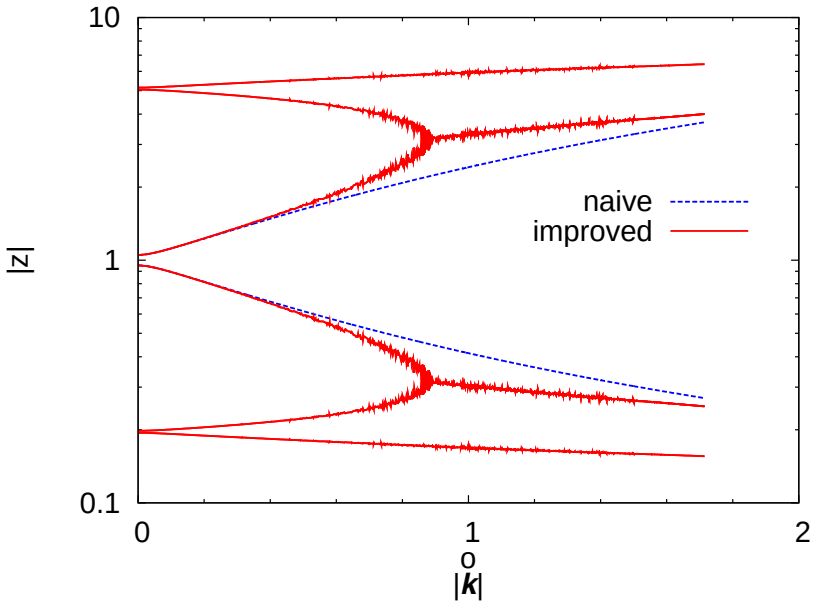

Figure C.4: Absolute value of poles in the massless naive and ASQ/HISQ fermion propagator as a function of $a|\overset{\circ}{\boldsymbol{k}}| = \sqrt{\sum_{j=1}^{3} \sin^2(k_j)}$.

the region defined by $|z_{\pm+}^{(\mathrm{naive})}| < |z| < |z_{\pm-}^{(\mathrm{naive})}|$.

I study how the poles move in the complex plane as a function of the three momentum. To take care of causality the ϵ prescription is employed by subtracting $i\epsilon$ from the denominator which becomes

$$D = \sum_{\nu} \sin^2(k_\nu) \left(1 + \frac{1}{6}\sin^2(k_\nu)\right)^2 - i\epsilon. \tag{C.10}$$

I analyse the behaviour of the poles outside the unit circle with positive real part, see Fig. C.5. All other poles can be obtained from these by replacing $z \to 1/z, -z, -1/z$. For $\overset{\circ}{\boldsymbol{k}} = 0$ the physical pole lies on the unit circle and has a small negative imaginary part. There are two additional spurious poles at larger $\mathrm{Re}\{z\}$ one with a small negative and one with a small positive part. As $|\overset{\circ}{\boldsymbol{k}}|$ increases the physical pole moves outwards whereas one of the spurious poles moves outwards just below the real axis and the other inwards just above the real axis. For $\overset{\circ}{\boldsymbol{k}}^2 = 8/9$ the physical pole touches one of the spurious poles and both, now being complex conjugates of each other, start to move away from the real axis.

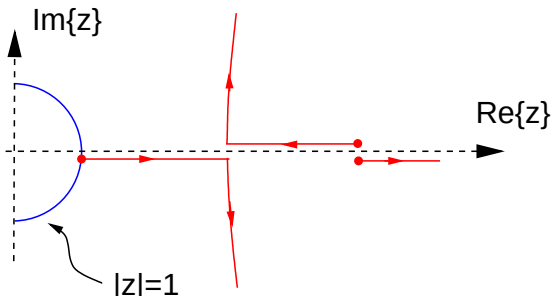

Figure C.5: Movement of three of the twelve poles in the ASQ/HISQ propagator in the complex plane. The arrows indicate increasing $|\mathring{\boldsymbol{k}}|$.

C.3 Poles of three point functions

In this section I discuss the poles of one particle irreducible three point integrals that arise in the calculation of the renormalisation of the vector- and tensor current in chapter 7.

As for the self-energy calculations in chapter 5 care has to be taken when choosing the integration contour in the k_0 plane. For certain values of the loop momentum the heavy quark pole can lie outside the unit circle and the integration contour has to be deformed to ensure that it can be Wick-rotated back to Minkowski space.

Let the position of the heavy quark pole in the z plane be denoted by z_h and the poles of the naive gluon propagator by z_- and z_+. The poles of the naive light quark action are $z_-^{(\ell)}$ and $z_+^{(\ell)}$ whereas the six poles of the improved light quark action are located at $z_{1,-}^{(\ell)}$, $z_{2,-}^{(\ell)}$, $z_{3,-}^{(\ell)}$ and $z_{1,+}^{(\ell)}$, $z_{2,+}^{(\ell)}$, $z_{3,+}^{(\ell)}$ (and the corresponding positions with opposite sign). Analytical expressions are given in section C.2. Note that only one of the poles is physical.

From the calculation of heavy quark renormalisation parameters it is known that $|z_h| < z_+$ and as the poles of the Symanzik improved gluon action lie outside the band defined by $z_- < |z| < z_+$ the same holds for improved gluons. It is thus only necessary to study the relative position of the heavy quark poles and the poles of the improved light quark propagator.

C.3.1 Simple heavy quark action.

For the unimproved heavy quark action defined in (5.26) at mass $m = 2.8$ and stability parameter $n = 2$ I generated a large number of gluon momenta k and verified that for each k one has $|z_h| < \min\{z_{1,+}^{(\ell)}, z_{2,+}^{(\ell)}, z_{3,+}^{(\ell)}\}$. I performed this check for two frame velocities, $v = 0.3$ and $v = 0.95$. In the integration code I first test whether

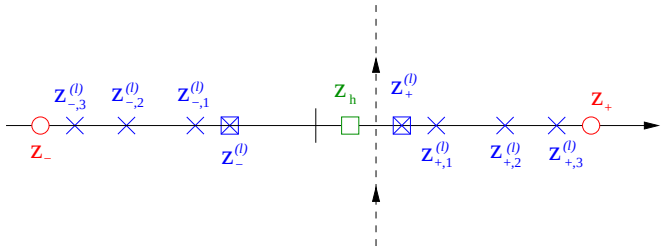

Figure C.6: Integration contour for the unimproved action. The ASQTAD light quark poles are denoted by ×, the poles in the naive light quark propagator by ⊠, the naive gluon poles by ○ and the heavy quark pole by □.

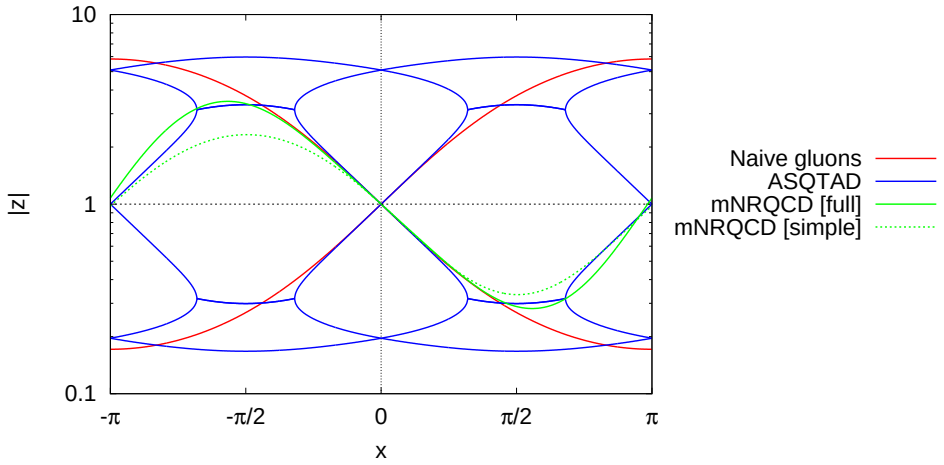

Figure C.7: Absolute values of poles as a function of x with $\boldsymbol{k} = (x, 0, 0)$. The frame velocity is $v = 0.95$, the heavy quark mass $m = 2.8$ and the stability parameter $n = 2$.

$|z_h| < \{|z_+^{(\ell)}|, |z_+|\}$ as the naive light quark positions can be calculated very easily and $|z_+^{(\ell)}| < |z_{+,j}^{(\ell)}|$. If this is the case I shift the contour halfway between $|z_h|$ and $\min\{|z_+^{(\ell)}|, |z_+|\}$, see Fig. C.6. If $|z_h| > |z_+^{(\ell)}|$ I use the smallest $|z_{+,j}^{(\ell)}|$ instead of $|z_+^{(\ell)}|$.

C.3.2 Full heavy quark action.

For the full $\mathcal{O}(1/m^2, v_{\text{rel}}^4)$ heavy quark action the situation is more complicated. It turns out that at high frame velocities and for certain configurations in momentum space the heavy quark pole can cross poles of the light propagator outside the unit circle. To illustrate this I plot the following quantities in Fig. C.7 for $\boldsymbol{k} = (x, 0, 0)$ and $-\pi < x < \pi$:

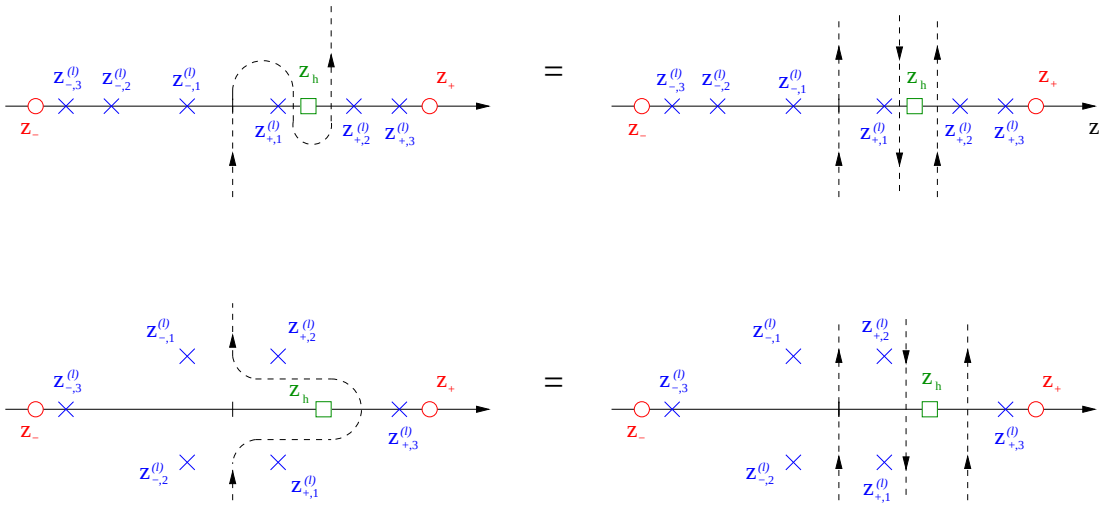

Figure C.8: Integration contour for momentum space configurations with pole crossing. The light quark poles are denoted by ×, the naive gluon poles by ○ and the heavy quark pole by □.

- $|z_h|$: Absolute value of the heavy quark poles (green) both for the full mNRQCD action and the simple action with H_0 only. The mass of the heavy quark is chosen to be $m = 2.8$ in both cases, the stability parameter is $n = 2$ and the frame velocity $v = 0.95$.

- $z_\pm$: Naive gluon poles (red)

- $|z^{(\ell)}_{\pm,j}|$: Absolute value of the light quark poles (blue), see appendix C.2.
  We have $|z^{(\ell)}_{-,3}| < |z^{(\ell)}_{-,2}| \leq |z^{(\ell)}_{-,1}| < 1 < |z^{(\ell)}_{+,1}| \leq |z^{(\ell)}_{+,2}| < |z^{(\ell)}_{+,3}|$

From the plot it can be seen that for certain negative values of x one has $|z^{(\ell)}_{+,1}| < |z_h| < |z^{(\ell)}_{+,2}|$. For the full action the dispersion relation is closer to the one in the continuum which bends $|z_h|$ up for momenta antiparallel to the frame velocity. On the other hand the dispersion relation of the light quark action has doublers at the edge of the Brillouin zone.

To be able to Wick-rotate back to Minkowski space in these cases it is necessary to deform the contour such that it encloses the heavy quark pole but not the light quark poles outside the unit circle, see Fig. C.8.

For each spatial momentum $\boldsymbol{k}$ generated by the VEGAS integration code I first check if a pole shift using the naive poles is possible. If not I compute the exact positions of the ASQ poles (see appendix C.2 and in particular Fig. C.5 which shows the movement of the light quark poles in the complex planes) and distinguish the following cases:

1. $|z_h| < |z^{(\ell)}_{-,1}|$ or $|z_h| < z_-$. Shifting the contour is not necessary.
2. $z_-, |z^{(\ell)}_{-,j}| < |z_h| < z_+, |z^{(\ell)}_{+,1}|$. I shift the contour halfway between $|z_h|$ and $\min\{z_+, z^{(\ell)}_{+,1}\}$.
3. $|z^{(\ell)}_{+,j}| < |z_h| < |z^{(\ell)}_{+,j+1}|, z_+$. It is necessary to integrate along three contours: (a) counterclockwise without shift, (b) clockwise with shifting the contour between $|z^{(\ell)}_{+,j}|$ and $|z_h|$ and (c) counterclockwise with the contour between $|z_h|$ and $\min\{|z^{(\ell)}_{+,j+1}|, z_+\}$.

Note that pole crossing only occurs for large momenta. I conclude that this is a lattice artifact which would disappear in the continuum limit.

Appendix D

Quark field renormalisation parameters in continuum QCD

In this chapter I discuss the one-loop renormalisation of the mass and wavefunction of relativistic quarks in the continuum. I work in $4-\epsilon$ dimensions to regulate UV divergences and use a gluon mass term to render the integrals IR finite. I give explicit expressions for renormalisation parameters in the on-shell- and the $\overline{MS}$-scheme.

D.1 Renormalisation of quark fields in QCD

Bare (denoted by superscript $^{(0)}$) and renormalised quantities are related via

$$\psi^{(0)} = Z_\psi \psi = (1 + \alpha_s \delta Z_\psi + \dots)\psi, \quad m^{(0)} = Z_m m = (1 + \alpha_s \delta Z_m + \dots)m. \tag{D.1}$$

The quadratic part of the QCD Lagrangian is

$$\begin{aligned} \mathscr{L} &= i Z_\psi \overline{\psi} \partial\!\!\!/ \, \psi - Z_\psi Z_m \overline{\psi} m \psi \\ &= \overline{\psi}(i\partial\!\!\!/ - m)\psi + \alpha_s \overline{\psi}(\delta Z_\psi i\partial\!\!\!/ - (\delta Z_\psi + \delta Z_m)m)\psi + \dots . \end{aligned} \tag{D.2}$$

At $\mathcal{O}(\alpha_s)$ the correction to the heavy quark self energy is given by the sum of the

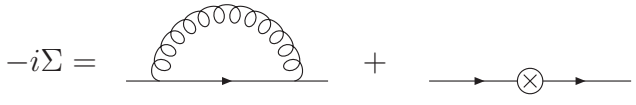

Figure D.1: $\mathcal{O}(\alpha_s)$ correction to the quark self-energy in continuum QCD

rainbow diagram and the counterterm in Fig. D.1

$$\begin{aligned} -i\Sigma(p) &= (\mu^2)^{\epsilon/2}(ig)^2 T^a T^a \int \frac{d^d k}{(2\pi)^d}\gamma_\mu \frac{i(\not{k} + \not{p} + m)}{(k+p)^2 - m^2}\gamma^\mu \frac{-i}{k^2-\lambda^2} \\ &\quad + i\alpha_s(\delta Z_\psi \not{p} - (\delta Z_\psi + \delta Z_m)m) \\ &= \frac{i\alpha_s}{3\pi}\Gamma(\epsilon/2)(4\pi)^{\epsilon/2}(\mu^2)^{\epsilon/2}\left(A(p^2)\not{p} - B(p^2)m\right) \\ &\quad + i\alpha_s(\delta Z_\psi \not{p} - (\delta Z_\psi + \delta Z_m)m) \end{aligned} \tag{D.3}$$

with

$$\begin{aligned} A(p^2) &= (2-\epsilon)\int_0^1 dx\,(1-x)\left[x(x-1)p^2 + xm^2 + (1-x)\lambda^2\right]^{-\epsilon/2} \\ B(p^2) &= (4-\epsilon)\int_0^1 dx\,\left[x(x-1)p^2 + xm^2 + (1-x)\lambda^2\right]^{-\epsilon/2}. \end{aligned} \tag{D.4}$$

D.1.1 On-shell scheme

In the on-shell scheme where the renormalised propagator is $i/(\not{p} - m)$ the counterterms are fixed by the two conditions

$$\Sigma(\not{p} = m) = 0, \qquad \frac{d\Sigma}{d\not{p}}(\not{p} = m) = 0. \tag{D.5}$$

Massless quarks. For $m = 0$ one has $A(0) = 1 - \frac{\epsilon}{4} - \frac{\epsilon}{2}\log\lambda^2$ and obtains

$$\alpha_s \delta Z_\psi^{(\mathrm{os})} = \frac{\alpha_s}{3\pi}\left(-\frac{2}{\bar{\epsilon}} + \frac{1}{2} + \log\lambda^2/\mu^2\right) \qquad \text{with} \quad \frac{2}{\bar{\epsilon}} = \frac{2}{\epsilon} - \gamma_E + \log 4\pi. \tag{D.6}$$

.

Massive quarks. The mass counterterm is IR finite and given by

$$\begin{aligned} \alpha_s \delta Z_m^{(\mathrm{os})} &= \frac{\alpha_s}{3\pi}\Gamma(\epsilon/2)(4\pi)^{\epsilon/2}(\mu^2)^{\epsilon/2}\left(A(m^2) - B(m^2)\right) \\ &= \frac{\alpha_s}{3\pi}\left(-3\frac{2}{\bar{\epsilon}} + 3\log m^2/\mu^2 - 4\right). \end{aligned} \tag{D.7}$$

The wavefunction renormalisation has IR divergent contributions, it can be written

$$\alpha_s \delta Z_\psi^{(os)} = -\frac{\alpha_s}{3\pi}\Gamma(\epsilon/2)(4\pi)^{\epsilon/2}(\mu^2)^{\epsilon/2}\left(A(m^2) + 2m^2\frac{d(A-B)}{dp^2}(m^2)\right). \tag{D.8}$$

The IR divergence is contained in the following Feynman-parameter integral

$$m^2 \frac{d(A-B)}{dp^2}(m^2) = \epsilon \int_0^1 dx \, \frac{x(x^2-1)}{x^2+(1-x)\lambda^2/m^2}. \tag{D.9}$$

Neglecting terms of $\mathcal{O}(\lambda/m)$ one can replace $x^2+(1-x)\lambda^2/m^2 \mapsto x^2+\lambda^2/m^2$ and evaluation of the remaining integral is straightforward

$$\begin{aligned} \int_0^1 dx \, \frac{x(x^2-1)}{x^2+\lambda^2/m^2} &= \frac{1}{2}\left((1+\lambda^2/m^2)\log\left[1+m^2/\lambda^2\right]-1\right) \\ &= -\frac{1}{2}(1+\log\lambda^2/m^2)+\mathcal{O}(\lambda/m). \end{aligned} \tag{D.10}$$

I find for the wavefunction counterterm

$$\alpha_s \delta Z_\psi^{(\mathrm{os})} = \frac{\alpha_s}{3\pi}\left(-\frac{2}{\bar{\epsilon}}+\log m^2/\mu^2-4-2\log\lambda^2/m^2\right). \tag{D.11}$$

D.1.2 $\overline{MS}$-scheme

In this scheme only the UV divergences are absorbed in the counterterms,

$$\alpha_s \delta Z_\psi^{(\overline{MS})} = -\frac{\alpha_s}{3\pi}\frac{2}{\bar{\epsilon}}, \qquad \alpha_s \delta Z_m^{(\overline{MS})} = -\frac{\alpha_s}{\pi}\frac{2}{\bar{\epsilon}}. \tag{D.12}$$

This implies that the mass in the $\overline{MS}$ scheme depends on the renormalisation scale μ. The relation between the masses in the two different schemes is given by

$$m^{(0)} = Z_m^{(\overline{MS})} m^{(\overline{MS})} = Z_m^{(\mathrm{os})} m^{(\mathrm{os})} \tag{D.13}$$

and at one loop one obtains

$$m^{(\overline{MS})}(\mu) = \left(1+\frac{\alpha_s}{3\pi}\left(3\log m^2/\mu^2-4\right)\right) m^{(\mathrm{os})}. \tag{D.14}$$

Appendix E

Mean field corrections

In the following I give explicit expressions for the mean field corrections to Ω_j for the simple action defined in (5.26) and the full $\mathcal{O}(1/m^2, v_{\rm rel}^4)$ mNRQCD action and "complete" cancellation of adjacent links, $U_\mu U_\mu^\dagger \mapsto 1$.

For the simple action I find for the mean field corrections with stability parameter $n = 2$

$$\hat{\Omega}_0^{(\rm tadpole)} = -\hat{\Omega}_1^{(\rm tadpole)} \;=\; u_0^{(2)}\Big(1 - \frac{v^2}{8} + \frac{3 - v^2}{\gamma m} - \frac{3 - 2v^2 + v^4}{8\gamma^2 m^2}\Big),$$

$$\hat{\Omega}_2^{(\rm tadpole)} = \hat{\Omega}_v^{(\rm tadpole)} \;=\; u_0^{(2)}\Big(-2 + \frac{v^2}{16} + \frac{-9 + 3v^2}{4\gamma m} + \frac{3 - 2v^2 + v^4}{16\gamma^2 m^2}\Big),$$

whereas for the full $\mathcal{O}(1/m^2, v_{\rm rel}^4)$ action I obtain

$$\begin{aligned}
\hat{\Omega}_0^{(\rm tadpole)} = -\hat{\Omega}_1^{(\rm tadpole)} \;=\; & u_0^{(2)}\Big(1 - \frac{v^2}{3} - \frac{19v^4}{768} - \frac{v^6}{1024} \\
& + \frac{2688 - 852v^2 + 11v^4 - 13v^6}{768\gamma m} \\
& - \frac{3456 - 4920v^2 + 2497v^4 - 264v^6 + 15v^8}{3072\gamma^2 m^2} \\
& - \frac{516 - 1264v^2 + 1058v^4 + 275v^6 - 15v^8}{768\gamma^3 m^3} \\
& - \frac{-591 + 1460v^2 - 1358v^4 + 448v^6 + 5v^8}{256\gamma^4 m^4} \\
& - \frac{81 - 216v^2 + 246v^4 - 128v^6 + 25v^8}{64\gamma^5 m^5}\Big),
\end{aligned}$$

$$
\begin{aligned}
\hat{\Omega}_2^{(\text{tadpole})} &= u_0^{(2)}\Big(-\frac{5}{3} + \frac{7v^2}{32} + \frac{13v^4}{512} + \frac{v^6}{2048} \\
&+ \frac{-10880 + 4480v^2 - 215v^4 + 35v^6}{3072\gamma m} \\
&+ \frac{-12480 + 10288v^2 + 4321v^4 - 360v^6 + 15v^8}{6144\gamma^2 m^2} \\
&+ \frac{2412 - 4864v^2 + 3974v^4 + 311v^6 - 15v^8}{1536\gamma^3 m^3} \\
&+ \frac{-879 + 2100v^2 - 1982v^4 + 640v^6 + 5v^8}{512\gamma^4 m^4} \\
&+ \frac{81 - 216v^2 + 246v^4 - 128v^6 + 25v^8}{128\gamma^5 m^5}\Big),
\end{aligned}
$$

$$
\begin{aligned}
\hat{\Omega}_v^{(\text{tadpole})} &= u_0^{(2)}\Big(-\frac{5}{3} + \frac{11v^2}{48} + \frac{29v^4}{1536} + \frac{v^6}{2048} \\
&+ \frac{-5440 + 1860v^2 - 51v^4 + 16v^6}{1536\gamma m} \\
&- \frac{12480 + 712v^2 - 3521v^4 + 320v^6 - 15v^8}{6144\gamma^2 m^2} \\
&+ \frac{2412 - 3016v^2 + 2306v^4 + 299v^6 - 15v^8}{1536\gamma^3 m^3} \\
&+ \frac{-879 + 1812v^2 - 1614v^4 + 544v^6 + 5v^8}{512\gamma^4 m^4} \\
&+ \frac{81 - 216v^2 + 246v^4 - 128v^6 + 25v^8}{128\gamma^5 m^5}\Big).
\end{aligned}
$$

Numerical values for $\hat{\Omega}_j^{(\text{tadpole})}$ and $\Omega_j^{(\text{tadpole})}$ with a heavy quark mass of $m = 2.8$ and stability parameter $n = 2$ are presented in Tabs. 5.4 and 5.5.

Appendix F

Perturbative results for a simple action

In this appendix I show results for the renormalisation parameters and matching coefficients of another simple mNRQCD action. The action has improved kinetic terms and time evolution equation. H_0 is the same as in (4.34) whereas $\delta H =$ contains the correction term $\delta H_{\rm corr.}$ and the chromomagnetic interaction term $\boldsymbol{\sigma} \cdot \boldsymbol{B}$. I use a heavy quark mass $m = 2.8$, stability parameter $n = 2$ and the Symanzik improved gluon action.

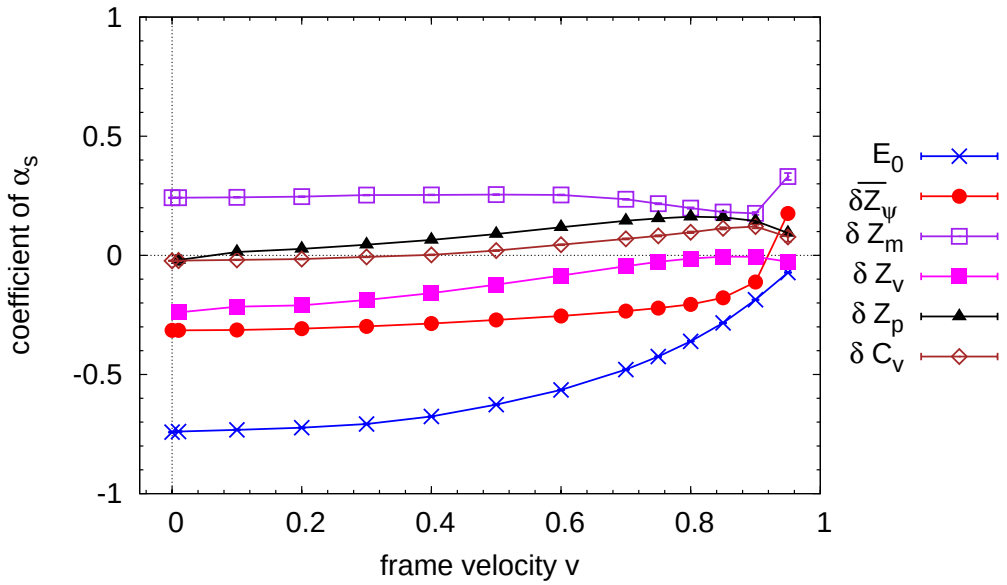

Figure F.1: Renormalisation parameters for a simple mNRQCD with improved derivatives and time evolution equation. The action is complete to $\mathcal{O}(1/m)$ and contains the chromomagnetic interaction term $\boldsymbol{\sigma}\cdot\boldsymbol{B}$ in δH. Mean field corrections for partial cancellation of $U_\mu U_\mu^\dagger$ are included in the results.

v	E_0	$\delta\overline{Z}_\psi$	δZ_M
0.00	−0.7421(19)	−0.31472(49)	0.2421(11)
0.01	−0.7394(19)	−0.31488(49)	0.2419(11)
0.10	−0.7322(19)	−0.31304(49)	0.2434(11)
0.20	−0.7235(19)	−0.30767(49)	0.2464(11)
0.30	−0.7078(19)	−0.29832(49)	0.2529(12)
0.40	−0.6763(18)	−0.28628(51)	0.2536(12)
0.50	−0.6264(17)	−0.27122(52)	0.2550(13)
0.60	−0.5648(16)	−0.25447(55)	0.2535(15)
0.70	−0.4795(14)	−0.23405(59)	0.2353(18)
0.75	−0.4247(14)	−0.22159(64)	0.2167(22)
0.80	−0.3607(13)	−0.20573(71)	0.1985(27)
0.85	−0.2834(12)	−0.17797(86)	0.1815(35)
0.90	−0.1863(11)	−0.1119(12)	0.1760(58)
0.95	−0.0721(11)	0.1757(24)	0.331(15)

v	δZ_v	δZ_p	δC_v
0.00	—	—	−0.0230(13)
0.01	−0.239(20)	−0.020(20)	−0.0222(13)
0.10	−0.2156(25)	0.0141(24)	−0.0190(13)
0.20	−0.2098(16)	0.0270(15)	−0.0155(13)
0.30	−0.1871(13)	0.0444(12)	−0.0068(13)
0.40	−0.1588(11)	0.0646(11)	0.0020(14)
0.50	−0.1231(10)	0.0896(10)	0.0203(15)
0.60	−0.0846(10)	0.1180(10)	0.0445(17)
0.70	−0.0457(10)	0.1451(11)	0.0691(21)
0.75	−0.02686(95)	0.1554(11)	0.0819(25)
0.80	−0.0138(10)	0.1622(12)	0.0967(32)
0.85	−0.0056(10)	0.1596(12)	0.1135(44)
0.90	−0.0061(11)	0.1448(14)	0.1211(75)
0.95	−0.0265(15)	0.0939(16)	0.078(20)

Table F.1: Renormalisation parameters for a simple mNRQCD with improved derivatives and time evolution equation. The action is complete to $\mathcal{O}(1/m)$ and contains the chromomagnetic interaction term $\boldsymbol{\sigma}\cdot\boldsymbol{B}$ in δH. Mean field corrections for partial cancellation of $U_\mu U_\mu^\dagger$ are included in the results.

v	$c^{(V)0}$	$c^{(V)1}$	$c^{(V)2}$
0.00	0.04393(58)	0.25368(43)	0.25304(43)

v	$c_+^{(V)0}$	$c_+^{(V)\parallel}$	$c_+^{(V)\perp}$
0.10	0.1700(25)	−0.0685(26)	0.1351(22)
0.20	0.1712(14)	−0.0639(15)	0.1340(14)
0.30	0.1778(11)	−0.0547(12)	0.1398(11)
0.40	0.18664(92)	−0.0402(11)	0.1476(10)
0.50	0.19902(84)	−0.0188(10)	0.15572(95)
0.60	0.21389(80)	0.01056(94)	0.16457(95)
0.70	0.23520(78)	0.05634(90)	0.1725(10)
0.75	0.25351(80)	0.09238(92)	0.1763(11)
0.80	0.28028(86)	0.1437(10)	0.1779(12)
0.85	0.3327(12)	0.2313(12)	0.1813(13)
0.90	0.4487(14)	0.3921(15)	0.1881(17)
0.95	0.6611(22)	0.6779(22)	0.1842(28)

v	$c_-^{(V)0}$	$c_-^{(V)\parallel}$	$c_-^{(V)\perp}$
0.10	−0.1282(25)	0.3209(25)	0.1210(20)
0.20	−0.1293(14)	0.3207(14)	0.1192(12)
0.30	−0.1404(11)	0.3128(11)	0.11005(89)
0.40	−0.15354(95)	0.30199(93)	0.09906(77)
0.50	−0.17123(88)	0.28581(87)	0.08459(71)
0.60	−0.19018(88)	0.26354(86)	0.06858(70)
0.70	−0.20794(91)	0.22948(89)	0.05292(73)
0.75	−0.2144(10)	0.20375(93)	0.04530(78)
0.80	−0.2112(10)	0.1709(10)	0.04299(88)
0.85	−0.1940(12)	0.1200(12)	0.0482(10)
0.90	−0.1419(15)	0.0340(15)	0.0674(13)
0.95	0.0496(26)	−0.1211(26)	0.1208(25)

Table F.2: Vector current matching coefficients for a simple mNRQCD with improved derivatives and time evolution equation. The action is complete to $\mathcal{O}(1/m)$ and contains the chromomagnetic interaction term $\boldsymbol{\sigma} \cdot \boldsymbol{B}$ in δH.

v	$c^{(T)0,1}$	$c^{(T)0,2}$	$c^{(T)1,2}$	$c^{(T)2,3}$
0.00	0.0712(12)	0.0713(12)	0.0713(12)	0.0713(12)

v	$c_+^{(T)0,\parallel}$	$c_+^{(T)0,\perp}$	$c_+^{(T)\parallel,\perp}$	$c_+^{(T)\perp,\perp}$
0.10	−0.0326(27)	−0.0268(24)	−0.0242(24)	−0.0327(27)
0.20	−0.0314(17)	−0.0218(16)	−0.0231(16)	−0.0283(17)
0.30	−0.0186(16)	−0.0087(15)	−0.0087(15)	−0.0161(16)
0.40	−0.0107(15)	0.0016(15)	0.0015(15)	−0.0089(15)
0.50	−0.0003(16)	0.0172(16)	0.0163(16)	−0.0006(16)
0.60	0.0048(18)	0.0324(17)	0.0329(17)	0.0047(18)
0.70	−0.0101(21)	0.0403(20)	0.0411(20)	−0.0104(21)
0.75	−0.0290(24)	0.0432(23)	0.0439(23)	−0.0286(24)
0.80	−0.0497(29)	0.0578(28)	0.0582(28)	−0.0502(29)
0.85	−0.0693(38)	0.1009(37)	0.1009(38)	−0.0698(38)
0.90	−0.0790(60)	0.2151(59)	0.2162(59)	−0.0780(60)
0.95	0.068(15)	0.591(15)	0.593(15)	0.067(15)

v	$c_-^{(T)0,\parallel}$	$c_-^{(T)0,\perp}$	$c_-^{(T)\parallel,\perp}$	$c_-^{(T)\perp,\perp}$
0.10	0.1005(25)	0.0975(21)	0.0968(21)	0.1056(24)
0.20	0.1014(12)	0.0955(11)	0.0969(11)	0.1010(12)
0.30	0.09086(87)	0.08654(87)	0.08758(88)	0.09069(87)
0.40	0.07726(75)	0.07456(76)	0.07508(77)	0.07714(75)
0.50	0.05815(76)	0.05822(76)	0.05820(77)	0.05914(76)
0.60	0.03780(74)	0.03781(76)	0.03768(76)	0.03890(74)
0.70	0.01702(76)	0.01168(78)	0.01203(78)	0.01752(76)
0.75	0.00725(80)	−0.00443(83)	−0.00404(83)	0.00753(80)
0.80	0.00272(90)	−0.01952(93)	−0.01922(93)	0.00318(90)
0.85	0.0068(11)	−0.0367(11)	−0.0371(11)	0.0068(11)
0.90	0.0273(14)	−0.0529(14)	−0.0528(14)	0.0270(14)
0.95	0.0867(25)	−0.0353(25)	−0.0357(25)	0.0863(25)

Table F.3: Tensor current matching coefficients for a simple mNRQCD with improved derivatives and time evolution equation. The action is complete to $\mathcal{O}(1/m)$ and contains the chromomagnetic interaction term $\boldsymbol{\sigma} \cdot \boldsymbol{B}$ in δH.

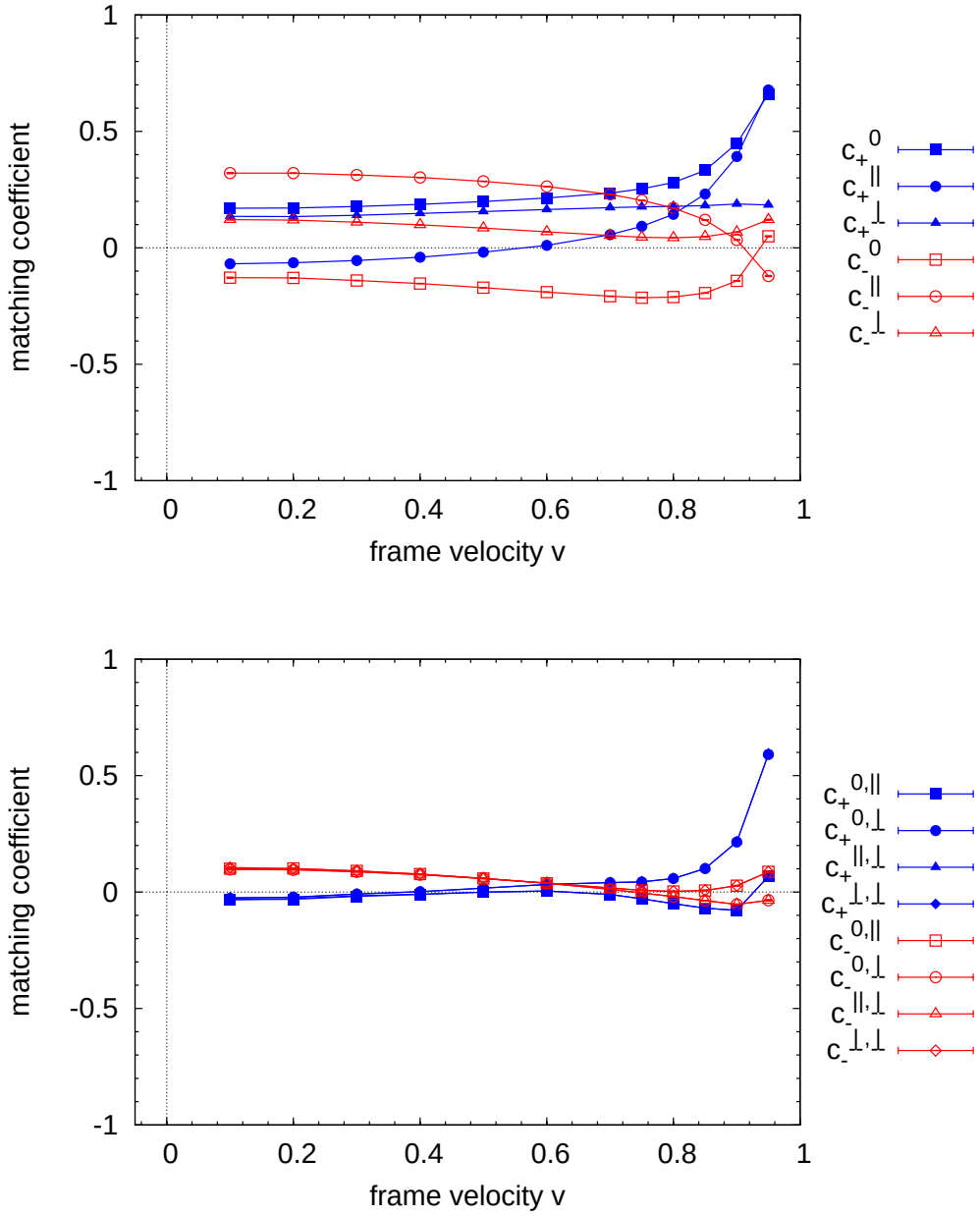

Figure F.2: Matching coefficients for a simple mNRQCD with improved derivatives and time evolution equation, vector current (top) and tensor current (bottom). The action is complete to $\mathcal{O}(1/m)$ and contains the chromomagnetic interaction term $\boldsymbol{\sigma} \cdot \boldsymbol{B}$ in δH.

Appendix G

Finite volume renormalisation parameters

In this appendix I show results for the heavy quark renormalisation parameters on a finite lattice with twisted boundary conditions.

As in the nonperturbative calculations in [108] I use two different heavy quark actions: The simple action in (5.26) with $m = 2.0$ and $n = 2$, and the full $\mathcal{O}(1/m^2, v_{\text{rel}}^4)$ action with the same stability parameter and $m = 2.8$. In both cases I use a Symanzik improved gluon action. I include mean field corrections for "partial" cancellation of $U_\mu U_\mu^\dagger$ as described in section 5.1.3. All three spatial directions are twisted.

G.1 Numerical results

I work on four different lattices of size 12×4^3, 18×6^3, 24×8^3 and 30×10^3 and for five frame velocities, $v = 0.0$, 0.2, 0.4, 0.6 and 0.8. The results for the one loop correction to the zero point energy E_0, the renormalisation of the heavy quark mass, frame velocity and the external momentum as well as the energy shift between QCD and the effective heavy quark theory are listed in Tabs. G.1 to G.5 for the simple action defined in (5.26) and for the full $\mathcal{O}(1/m^2, v_{\text{rel}}^4)$ action in Tabs. G.6 to G.10. In Figs. G.1 to G.5 I also plot the renormalisation parameters as a function of the frame velocity.

	$v = 0.0$	$v = 0.2$	$v = 0.4$	$v = 0.6$	$v = 0.8$
$4^3 \times 12$	-0.64249	-0.63066	-0.59233	-0.51905	-0.39751
$6^3 \times 18$	-0.71563	-0.70176	-0.65711	-0.57233	-0.43158
$8^3 \times 24$	-0.75045	-0.73559	-0.68786	-0.59748	-0.44736
$10^3 \times 30$	-0.77082	-0.75538	-0.70581	-0.61207	-0.45635
∞	$-0.8260(19)$	$-0.8116(19)$	$-0.7538(18)$	$-0.6507(16)$	$-0.4714(14)$

Table G.1: Zero point energy shift E_0 for the simple action defined in (5.26).

	$v = 0.0$	$v = 0.2$	$v = 0.4$	$v = 0.6$	$v = 0.8$
$4^3 \times 12$	0.35046	0.36356	0.408	0.51532	0.90748
$6^3 \times 18$	0.40063	0.417	0.47235	0.604	1.06894
$8^3 \times 24$	0.42635	0.4445	0.50585	0.65066	1.15245
$10^3 \times 30$	0.44227	0.46159	0.52682	0.68007	1.20427
∞	0.5074(12)	0.5312(12)	0.6138(13)	0.8045(17)	1.4252(33)

Table G.2: Mass renormalisation δZ_m for the simple action defined in (5.26).

	$v = 0.0$	$v = 0.2$	$v = 0.4$	$v = 0.6$	$v = 0.8$
$4^3 \times 12$	—	−0.36011	−0.34443	−0.32862	−0.33484
$6^3 \times 18$	—	−0.40693	−0.38917	−0.37146	−0.3806
$8^3 \times 24$	—	−0.43032	−0.41149	−0.39274	−0.40306
$10^3 \times 30$	—	−0.44452	−0.42503	−0.40558	−0.41639
∞	—	−0.4966(17)	−0.4748(12)	−0.4497(11)	−0.4606(12)

Table G.3: Velocity renormalisation δZ_v for the simple action defined in (5.26).

	$v = 0.0$	$v = 0.2$	$v = 0.4$	$v = 0.6$	$v = 0.8$
$4^3 \times 12$	—	−0.01155	−0.00204	0.00185	−0.02264
$6^3 \times 18$	—	−0.00689	0.00906	0.0236	0.01171
$8^3 \times 24$	—	−0.00374	0.01599	0.03701	0.03285
$10^3 \times 30$	—	−0.00146	0.02084	0.04636	0.04763
∞	—	0.0168(17)	0.0516(12)	0.1038(10)	0.14240(91)

Table G.4: Renormalisation δZ_p of the external momentum for the simple action defined in (5.26).

	$v = 0.0$	$v = 0.2$	$v = 0.4$	$v = 0.6$	$v = 0.8$
$4^3 \times 12$	0.02922	0.0396	0.07095	0.12285	0.19295
$6^3 \times 18$	0.04282	0.05625	0.0971	0.16613	0.26284
$8^3 \times 24$	0.05112	0.0662	0.11225	0.19076	0.3017
$10^3 \times 30$	0.05686	0.07301	0.12243	0.20711	0.32712
∞	0.0944(32)	0.1129(32)	0.1780(31)	0.2913(31)	0.4650(45)

Table G.5: Energy shift δC_v for the simple action defined in (5.26).

	$v = 0.0$	$v = 0.2$	$v = 0.4$	$v = 0.6$	$v = 0.8$
$4^3 \times 12$	-0.56835	-0.55623	-0.51892	-0.4481	-0.31137
$6^3 \times 18$	-0.6382	-0.6241	-0.58061	-0.49832	-0.34035
$8^3 \times 24$	-0.67193	-0.65685	-0.61026	-0.52217	-0.35341
$10^3 \times 30$	-0.6918	-0.67612	-0.62766	-0.53608	-0.3608
∞	$-0.76647(40)$	$-0.74812(39)$	$-0.69206(37)$	$-0.58682(33)$	$-0.38616(28)$

Table G.6: Zero point energy shift E_0 for the full $\mathcal{O}(1/m^2, v_{\text{rel}}^4)$ action.

	$v = 0.0$	$v = 0.2$	$v = 0.4$	$v = 0.6$	$v = 0.8$
$4^3 \times 12$	0.11692	0.10126	0.04553	-0.08422	-0.40454
$6^3 \times 18$	0.15507	0.14068	0.08988	-0.02584	-0.2959
$8^3 \times 24$	0.17505	0.1614	0.11341	0.00518	-0.23633
$10^3 \times 30$	0.18739	0.17422	0.12799	0.02426	-0.19923
∞	0.2313(12)	0.2194(12)	0.1789(13)	0.0910(15)	$-0.0901(24)$

Table G.7: Mass renormalisation δZ_m for the full $\mathcal{O}(1/m^2, v_{\text{rel}}^4)$.

	$v = 0.0$	$v = 0.2$	$v = 0.4$	$v = 0.6$	$v = 0.8$
$4^3 \times 12$	—	-0.11476	-0.0867	-0.03848	0.02601
$6^3 \times 18$	—	-0.14889	-0.11681	-0.06344	0.00187
$8^3 \times 24$	—	-0.16637	-0.1323	-0.07603	-0.01063
$10^3 \times 30$	—	-0.17698	-0.14169	-0.08355	-0.01825
∞	—	$-0.2074(15)$	$-0.1696(11)$	$-0.1037(10)$	$-0.02967(90)$

Table G.8: Velocity renormalisation δZ_v for the full $\mathcal{O}(1/m^2, v_{\text{rel}}^4)$ action.

	$v = 0.0$	$v = 0.2$	$v = 0.4$	$v = 0.6$	$v = 0.8$
$4^3 \times 12$	—	-0.01828	-0.05769	-0.14434	-0.3323
$6^3 \times 18$	—	-0.01441	-0.04918	-0.12496	-0.2907
$8^3 \times 24$	—	-0.0119	-0.04409	-0.11362	-0.26586
$10^3 \times 30$	—	-0.01014	-0.04069	-0.10628	-0.24993
∞	—	0.0025(12)	$-0.02131(89)$	$-0.06974(87)$	$-0.1746(11)$

Table G.9: Renormalisation δZ_p of the external momentum for the full $\mathcal{O}(1/m^2, v_{\text{rel}}^4)$ action.

	$v = 0.0$	$v = 0.2$	$v = 0.4$	$v = 0.6$	$v = 0.8$
$4^3 \times 12$	-0.08607	-0.09816	-0.14084	-0.2339	-0.42503
$6^3 \times 18$	-0.07286	-0.08391	-0.12242	-0.2039	-0.3655
$8^3 \times 24$	-0.06492	-0.07538	-0.11155	-0.18678	-0.33096
$10^3 \times 30$	-0.05968	-0.06975	-0.10445	-0.1759	-0.309
∞	$-0.0425(15)$	$-0.0510(15)$	$-0.0799(15)$	$-0.1350(18)$	$-0.2256(30)$

Table G.10: Energy shift δC_v for the full $\mathcal{O}(1/m^2, v_{\mathrm{rel}}^4)$ action.

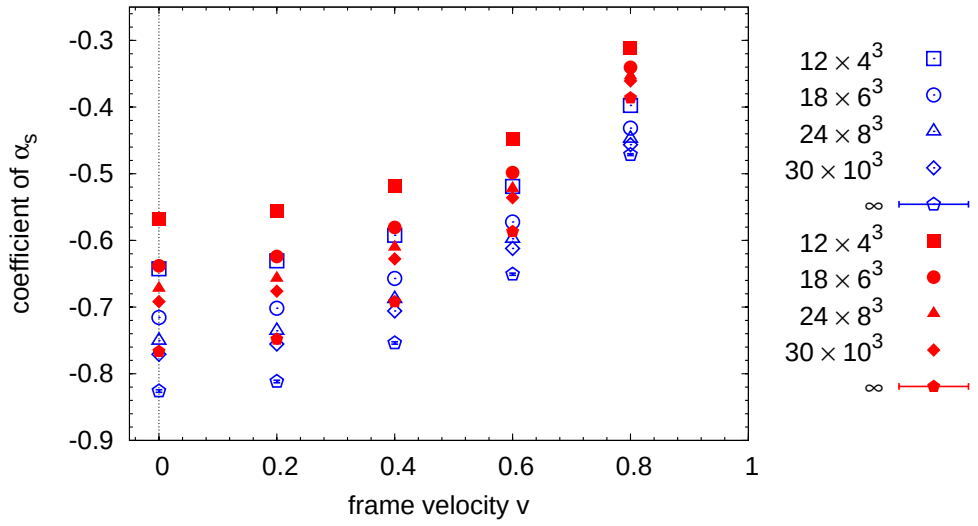

Figure G.1: Zero point energy shift E_0 for the simple action defined in (5.26) (blue, open symbols) and the full $\mathcal{O}(1/m^2, v_{\mathrm{rel}}^4)$ mNRQCD action (red, filled symbols).

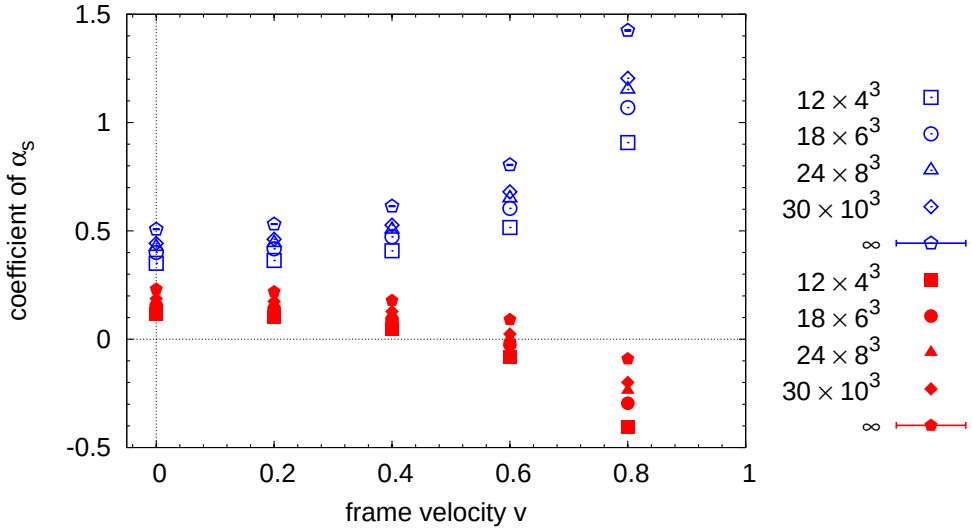

Figure G.2: Mass renormalisation for the simple action defined in (5.26) (blue, open symbols) and the full $\mathcal{O}(1/m^2, v_{\mathrm{rel}}^4)$ mNRQCD action (red, filled symbols).

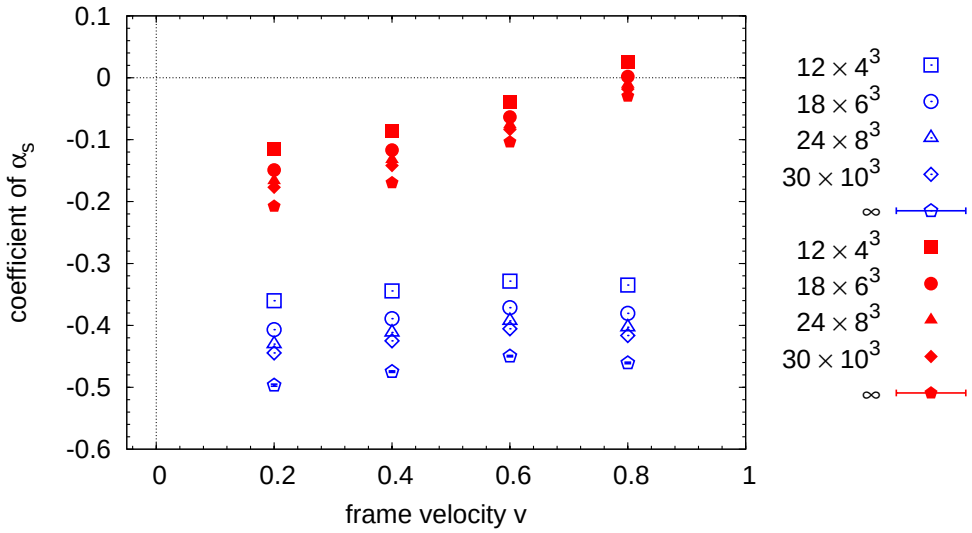

Figure G.3: Velocity renormalisation for the simple action defined in (5.26) (blue, open symbols) and the full $\mathcal{O}(1/m^2, v_{\mathrm{rel}}^4)$ mNRQCD action (red, filled symbols).

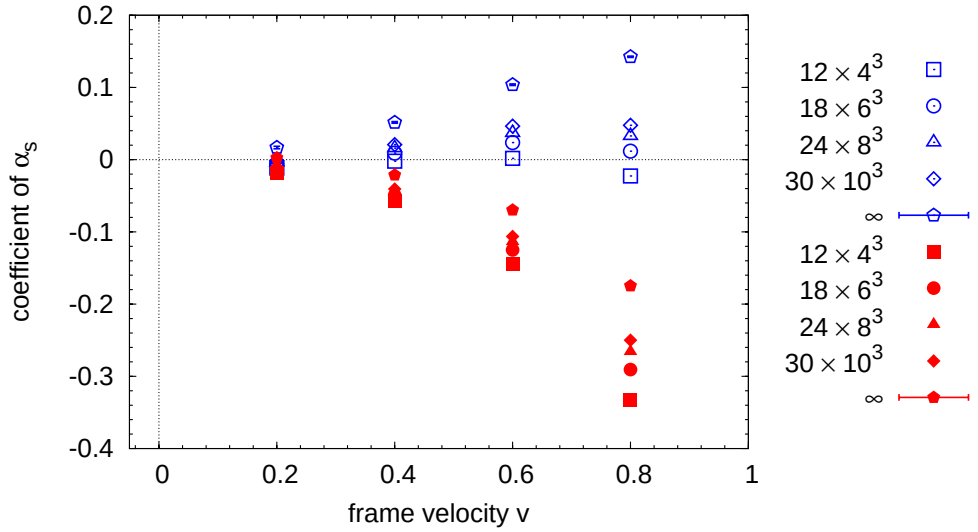

Figure G.4: External momentum renormalisation for the simple action defined in (5.26) (blue, open symbols) and the full $\mathcal{O}(1/m^2, v_{\mathrm{rel}}^4)$ mNRQCD action (red, filled symbols).

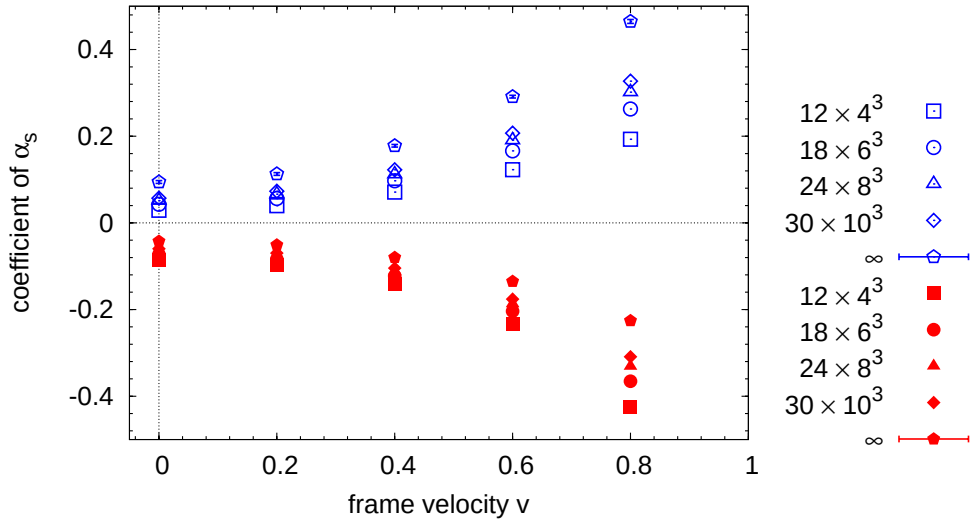

Figure G.5: Renormalisation of the energy shift C_v between QCD and mNRQCD for the simple action defined in (5.26) (blue, open symbols) and the full $\mathcal{O}(1/m^2, v_{\mathrm{rel}}^4)$ mNRQCD action (red, filled symbols).

Appendix H

Infrared stability

In this appendix I study the infrared structure of the integrals for higher order kinetic terms in the NRQCD action discussed in section 6. A thorough investigation of this region of phase space was motivated by instabilities which arose when using numerical approximations to higher order derivatives in the rainbow diagram. In the following I study the lattice integral both for numerical and analytical mixed derivatives and demonstrate that it is essential to use analytical derivatives for small gluon masses.

As the Feynman rules are very simple for the continuum NRQCD subtraction function and the instabilities arise in the infrared region of the integrand I work with the integrals $I_1^{(\mathrm{sub})}$ and $I_2^{(\mathrm{sub})}$ defined in (6.21) and (6.22). This is legitimate as the integrals have the same infrared structure as the integrals on the lattice.

H.1 Structure of the integrand

I evaluate the subtraction function for fixed spatial momentum $\boldsymbol{k}$ and a range of temporal k_0. This is done using both numerical and analytical derivatives as defined in section 6.3; in both cases the gluon mass is fixed to $\lambda^2 = 10^{-6}$.

For the spatial momentum $\boldsymbol{k} = (0, 0, 0)$ I expect both the W_1 and the W_2 subtraction functions to vanish for all k_0 (I checked this in MATHEMATICA by coding up the functions explicitly). As can be seen from Figs. H.1 and H.2 this is only true if I use analytical derivatives. Otherwise there is a narrow but sizable peak in the integrand which has large contributions to the integral.

To demonstrate that it is legitimate to use numerical derivatives for noninfrared momenta I also compare the corresponding quantities for $\boldsymbol{k} = (0.2, 0.2, 0.2)$ in Figs. H.3 and H.4. Here, even though the integrand is very large in some regions of phase space, the agreement between the two curves is very good.

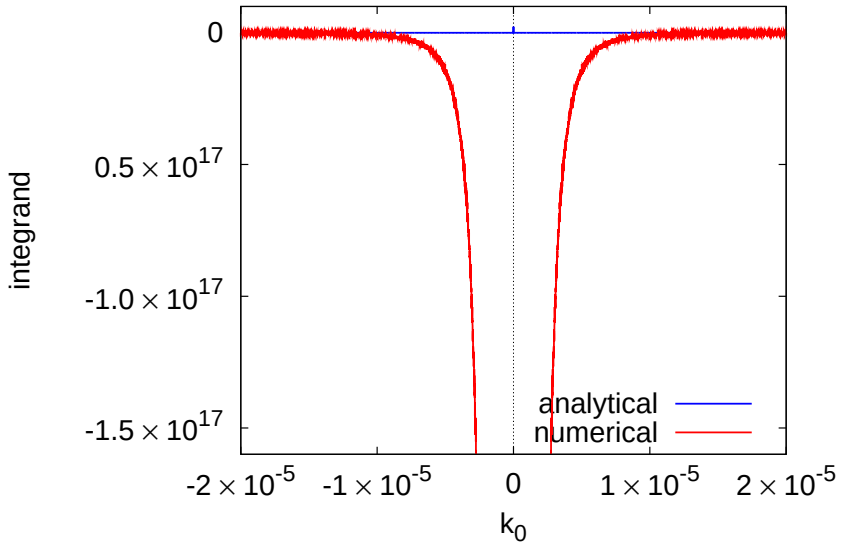

Figure H.1: W_1 subtraction function integrand $D_1 f^{(\mathrm{sub})}$ for $\boldsymbol{k} = (0, 0, 0)$.

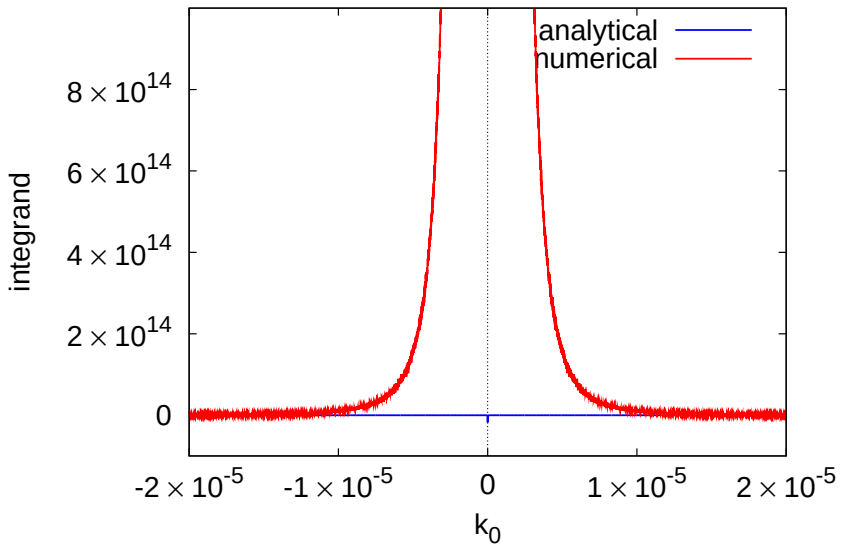

Figure H.2: W_2 subtraction function integrand $D_2 f^{(\mathrm{sub})}$ for $\boldsymbol{k} = (0, 0, 0)$.

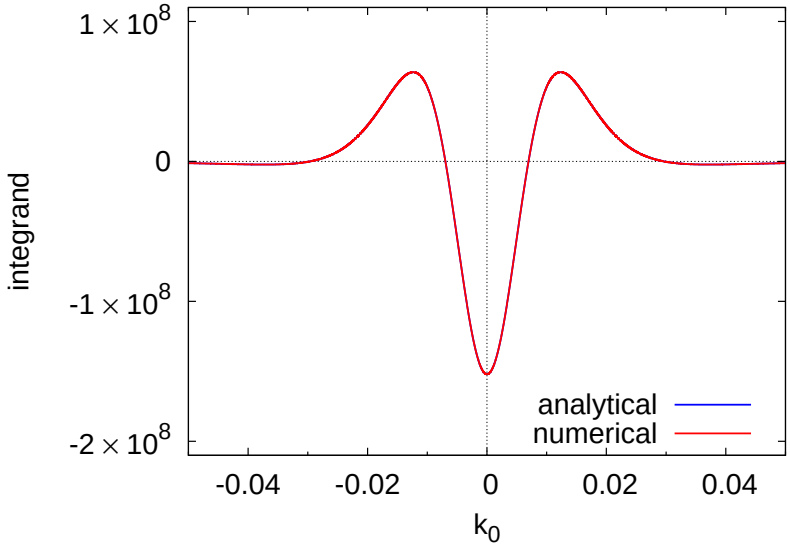

Figure H.3: W_1 subtraction function integrand $D_1 f^{(\mathrm{sub})}$ for $\boldsymbol{k} = (0.2, 0.2, 0.2)$.

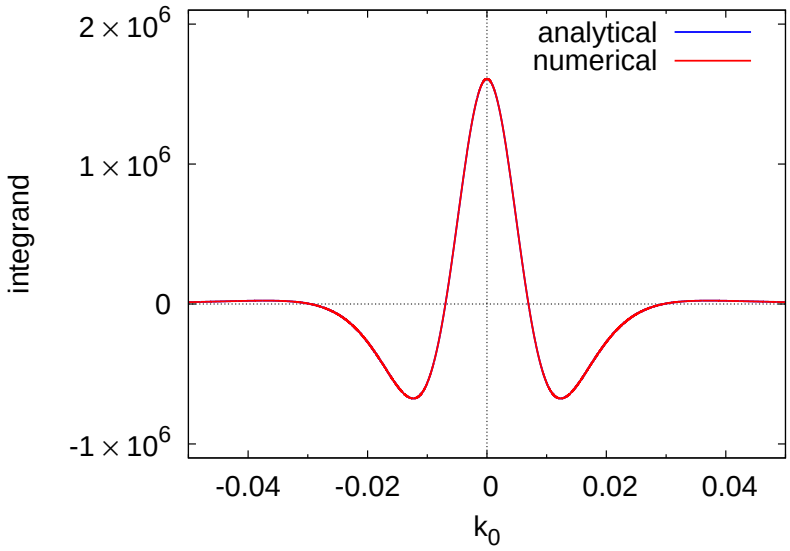

Figure H.4: W_2 subtraction function integrand $D_2 f^{(\mathrm{sub})}$ for $\boldsymbol{k} = (0.2, 0.2, 0.2)$.

λ^2	numerical	analytical
10^{-1}	$-1.556(4)$	$-1.560(5)$
10^{-2}	$-1.63(1)$	$-1.63(1)$
10^{-3}	$-1.63(3)$	$-1.63(2)$
10^{-4}	$-1.5(1)$	$-1.68(3)$
10^{-5}	$-1.2(3)$	$-1.69(3)$
10^{-6}	$-1.9(9)$	$-1.70(4)$
10^{-7}	—	$-1.65(5)$
10^{-8}	—	$-1.60(6)$
10^{-9}	$8.5(35.8)$	$-1.64(7)$
10^{-10}	—	$-1.52(9)$
10^{-11}	—	$-1.57(10)$
10^{-12}	$-9500(1300)$	$-1.54(11)$

Table H.1: Integration results for W_1 for various gluon masses λ^2 both with numerical finite differences and analytical derivatives. The results in the second column for $\lambda^2 \leq 10^{-9}$ are clearly dominated by statistical errors.

H.2 Integral for small gluon masses

Having identified a potential infrared instability I now integrate the subtraction function for W_1 for a range of gluon masses. In Tab. H.1 and Fig. H.5 I present my results (10 iterations, 20,000 function evaluations) both for numerical and analytical derivatives.

For $\lambda^2 \geq 10^{-3}$ the final value for $I_1^{(\mathrm{sub})}$ is within statistical errors independent of whether I use finite differences or analytical derivatives. For smaller gluon masses, however, the results obtained with numerical derivatives are no longer stable. The errors on the results from analytical derivatives show a slight increase as the gluon mass is reduced to below 10^{-6} but become essentially independent of λ^2. I conclude that it is legitimate to use $\lambda^2 = 10^{-6}$.

H.3 Subtracted lattice integrals

To verify that the integrals in section 6.4.1 which are constructed from lattice Feynman rules are indeed independent of the gluon mass I evaluate the different contributions to W_1 and W_2 for various values of λ. This also confirms that no instabilities are introduced by using a numerical approximation for higher order derivatives in the tadpole diagram. I carry out the calculation for the simpler action setup with a Wilson gluon action described in [122].

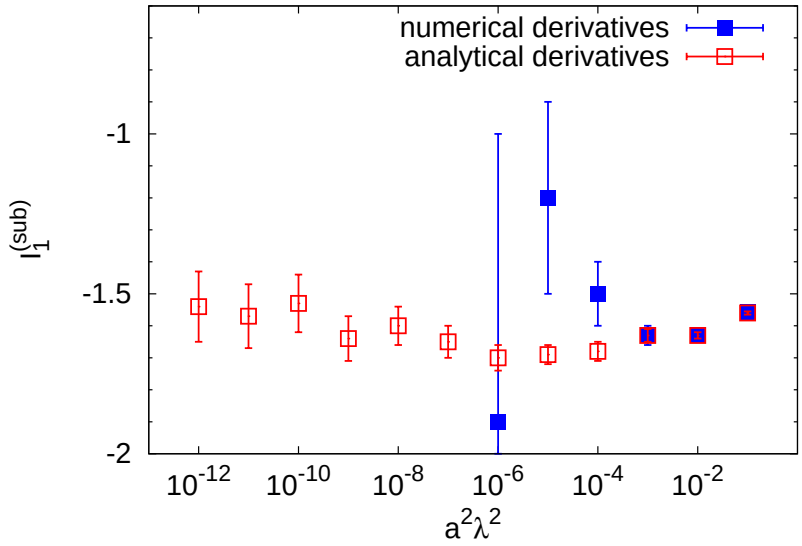

Figure H.5: W_1 for various gluon masses λ^2.

I calculate W_1 and W_2 by evaluating the integrals in (6.21) and (6.22). Due to the different action definition in [122] the derivative operators in (6.19) are modified slightly, D_1 is replaced according to

$$\begin{aligned} D_1 f \mapsto \tilde{D}_1 f \quad = \quad & \left(1+\frac{2}{m}\right)\mathrm{Re}\{f\} - 2\left(1+\frac{1}{m}\right)\frac{\partial}{\partial p_0}\mathrm{Im}\{f\} - \frac{\partial^2}{\partial p_z^2}\mathrm{Re}\{f\} \\ & + \quad (3+2m)\,\frac{\partial^2}{\partial p_z^2}\mathrm{Re}\{f\} - 2m\frac{\partial^3}{\partial p_z^2 \partial p_0}\mathrm{Im}\{f\} \\ & + \quad m^2 \frac{\partial^4}{\partial p_y^2 \partial p_z^2}\mathrm{Re}\{f\}. \end{aligned} \tag{H.1}$$

As only the derivatives generate large peaks in the integrand I use a modified version if $\tilde{D}_1$ acts on the subtraction function.

$$\tilde{D}_1^{(\mathrm{sub})} f^{(\mathrm{sub})} \quad = \quad \tilde{D}_1 f^{(\mathrm{sub})} - \left(1+\frac{2}{m}\right)\mathrm{Re}\{f^{(\mathrm{sub})}\}. \tag{H.2}$$

λ^2	$I^{(\text{lat}-\text{sub})}_{1,\text{rainbow}}$	$I^{(\text{lat})}_{1,\text{tadpole}}$	$I^{(\text{sub})}_1$	W_1
10^{-3}	5.375(4)	0.9325(9)	−5.587(4)	0.721(6)
10^{-6}	5.439(4)	0.9325(9)	−5.663(1)	0.709(4)
10^{-9}	5.442(4)	0.9326(9)	−5.665(2)	0.710(5)
10^{-12}	5.442(4)	0.9338(9)	−5.665(3)	0.711(5)

Table H.2: The integrals $I^{(\text{lat}-\text{sub})}_{1,\text{rainbow}}$, $I^{(\text{lat})}_{1,\text{tadpole}}$ and $I^{(\text{sub})}_1$ and their sum W_1 for different squared gluon masses λ^2. $I^{(\text{lat})}_{1,\text{tadpole}}$ was evaluated using numerical finite differences whereas analytical derivatives were used for the other integrals.

I finally find

$$\begin{aligned} W_1 &= I^{(\text{lat}-\text{sub})}_{1,\text{rainbow}} + I^{(\text{lat})}_{1,\text{tadpole}} + I^{(\text{sub})}_1 \qquad \text{(H.3)} \\ &= \int \frac{d^4k}{(2\pi)^4} \left[\tilde{D}_1 f^{(\text{lat})}_{\text{rainbow}} - \tilde{D}^{(\text{sub})}_1 f^{(\text{sub})}\right] + \int \frac{d^4k}{(2\pi)^4} \tilde{D}_1 f^{(\text{lat})}_{\text{tadpole}} \\ &\quad + \int \frac{d^4k}{(2\pi)^4} \tilde{D}^{(\text{sub})}_1 f^{(\text{sub})}. \end{aligned}$$

For W_2 I use the expression in (6.22).

For the action in [122] with $m = 2.0$, $n = 2$ as above I evaluate the three integrals in (6.21) for a range of gluon masses λ^2.

- Lattice rainbow. I ran 10 iterations, 200,000 function evaluations (both for thermalisation and measurement) of the integral $I^{(\text{lat}-\text{sub})}_{1,\text{rainbow}}$. On 64 cores this takes not more than two hours.
- Lattice tadpole. With the same number of iterations and function evaluations I calculate $I^{(\text{lat})}_{1,\text{tadpole}}$. As I use numerical finite differences the integration can be carried out in half an hour on 64 cores. I use $\delta p = 10^{-6}$ in the finite differences.
- Subtraction integral. Evaluation of the subtraction integral $I^{(\text{sub})}_1$ is much cheaper. On 64 cores 20,000,000 function evaluations and 10 iterations take around 30 minutes.

The results are summarised in Tab. H.2 and Fig. H.6.

As can be seen from Fig. H.6 the results are independent of the gluon mass for $\lambda^2 \leq 10^{-6}$ within statistical errors. To obtain a final result I take the weighted average of the results for $\lambda^2 \leq 10^{-6}$. This gives.

$$W_1 = 0.710(2) \qquad \text{(H.4)}$$

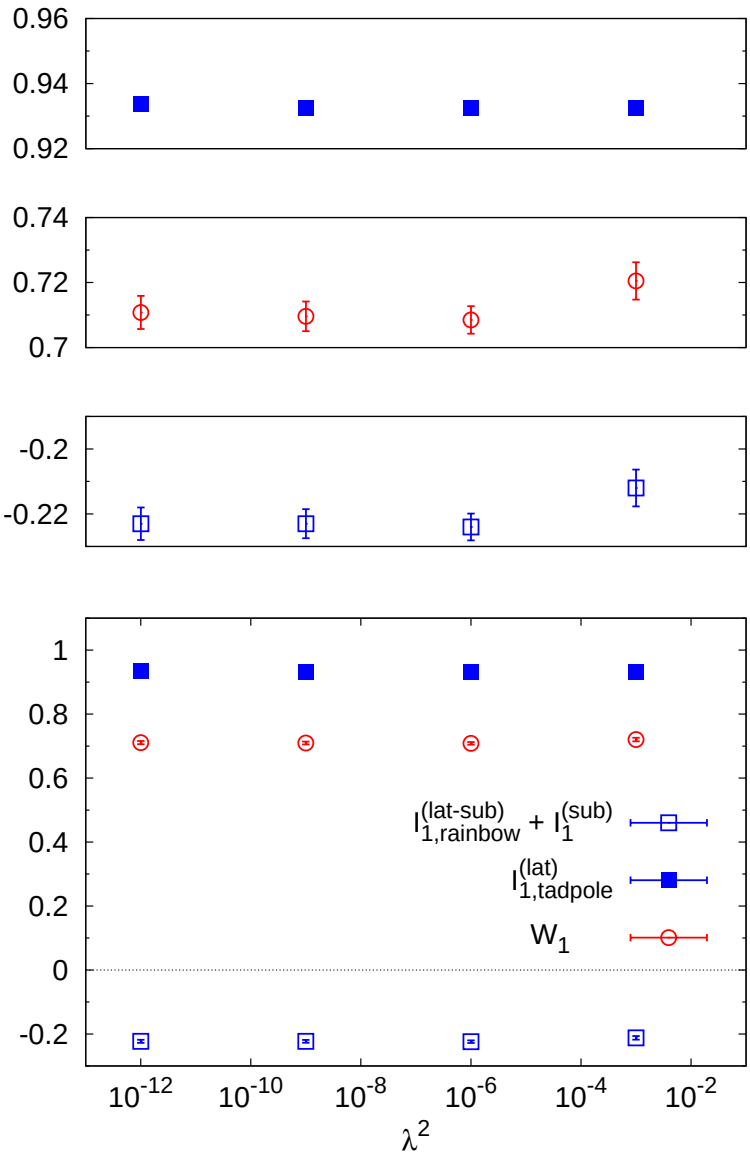

Figure H.6: The integrals $I^{(\mathrm{lat-sub})}_{1,\mathrm{rainbow}} + I^{(\mathrm{sub})}_1$, $I^{(\mathrm{lat})}_{1,\mathrm{tadpole}}$ and and their sum W_1 for different squared gluon masses λ^2. $I^{(\mathrm{lat})}_{1,\mathrm{tadpole}}$ has been evaluated using numerical finite differences whereas analytical derivatives were used for the other integrals. The top panels show the contributions from the different integrals separately.

λ^2	$I^{(\mathrm{lat-sub})}_{2,\mathrm{rainbow}}$	$I^{(\mathrm{lat})}_{2,\mathrm{tadpole}}$	W_2
10^{-3}	0.00025(7)	0.02215(2)	0.02240(7)
10^{-6}	0.00020(7)	0.02215(2)	0.02235(7)
10^{-9}	0.00026(7)	0.02214(2)	0.02240(7)
10^{-12}	0.00027(7)	0.02215(2)	0.02242(7)

Table H.3: The integrals $I^{(\mathrm{lat-sub})}_{2,\mathrm{rainbow}}$, $I^{(\mathrm{lat})}_{2,\mathrm{tadpole}}$ and their sum W_2 for different squared gluon masses λ^2. $I^{(\mathrm{lat})}_{2,\mathrm{tadpole}}$ was evaluated using numerical finite differences whereas analytical derivatives were used for the subtracted rainbow integral.

Using

$$c_1^{(2)} = -\left(\frac{1}{2n}+\frac{1}{m}\right)^{-1} W_1 \tag{H.5}$$

I finally obtain with $m = 2.0$ and $n = 2$

$$c_1^{(2)} = -0.946(3). \tag{H.6}$$

This is in perfect agreement with the value of $c_1^{(2)}$ in Fig. 2 of [122].

I repeat the same analysis for W_2. The results are listed in Tab. H.3 and plotted in Fig. H.7. Again average the results for $\lambda^2 \leq 10^{-6}$ to I find

$$W_2 = 0.02239(4). \tag{H.7}$$

Using

$$c_2^{(2)} = 24m\, W_1 \tag{H.8}$$

I finally obtain

$$c_2^{(2)} = 1.075(2). \tag{H.9}$$

This is in perfect agreement with the value of $c_2^{(2)}$ in Fig. 2 of [122].

I summarise that the dependence on the gluon mass is very weak and it is not necessary to extrapolate in λ.

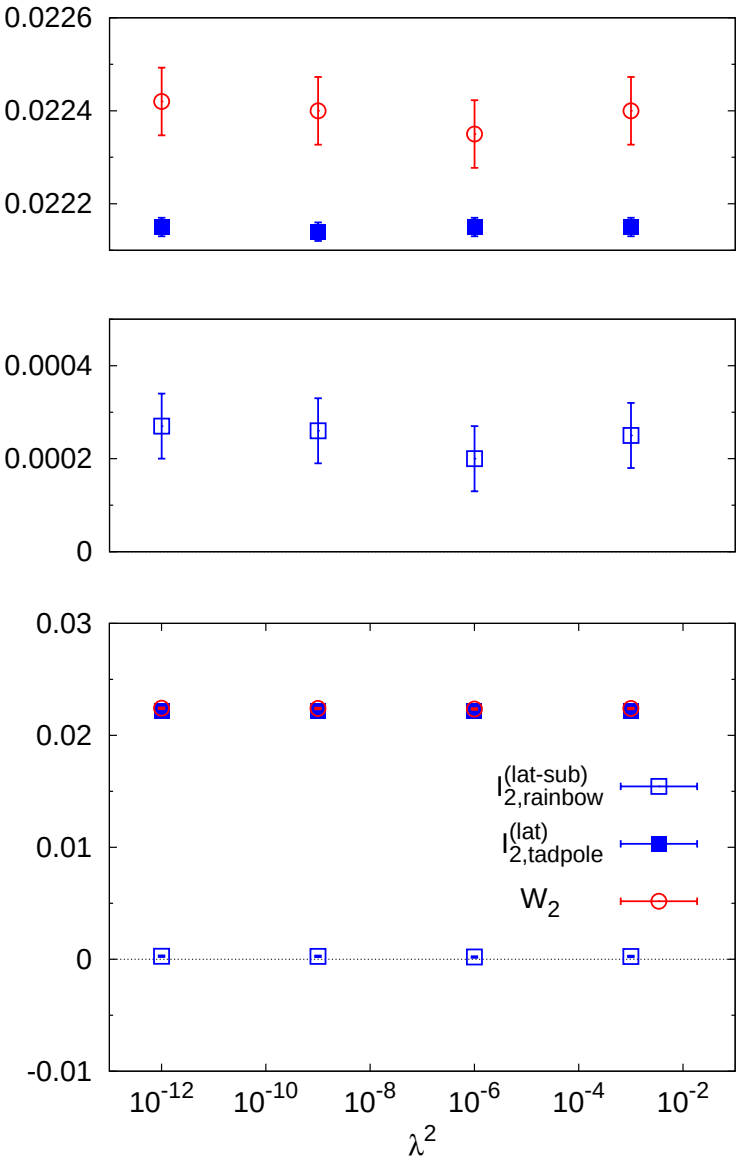

Figure H.7: The integrals $I^{(\mathrm{lat-sub})}_{2,\mathrm{rainbow}}$, $I^{(\mathrm{lat})}_{2,\mathrm{tadpole}}$ and their sum W_2 for different squared gluon masses λ^2. Numerical finite differences are used for $I^{(\mathrm{lat})}_{2,\mathrm{tadpole}}$, all other integrals are evaluated with analytical derivatives.

Appendix I

Radiative corrections to currents in the continuum

In this appendix I evaluate one-loop corrections to the vector and tensor operators with Dirac structure γ^μ and $m\sigma^{\mu\nu}$ in the continuum to $\mathcal{O}(1/m)$. In QCD they are given by

$$\begin{aligned}
\delta\mathcal{M}^{\mu}_{(V)} &= \int \frac{d^dk}{(2\pi)^d}(-igT^a\mu^{\epsilon/2})\gamma^\rho \frac{i(\not{k}+\not{p}\,')}{(k+p'^2)}\gamma^\mu \frac{i(\not{k}+\not{p}+m)}{(k+p)^2-m^2}(-igT^a\mu^{\epsilon/2})\gamma_\rho \\
&\qquad \times \frac{-i}{k^2-\lambda^2} \quad + \quad \text{(wavefunction counterterms)} \qquad \text{(I.1)} \\
&= \frac{\alpha_s}{3\pi}\int_{\perp} \gamma^\rho(\not{k}+\not{p}\,')\gamma^\mu(\not{k}+\not{p}+m)\gamma_\rho + \frac{1}{2}(\delta Z_Q+\delta Z_q)\gamma^\mu \\
\delta\mathcal{M}^{\mu\nu}_{(T)} &= \int \frac{d^dk}{(2\pi)^d}(-igT^a\mu^{\epsilon/2})\gamma^\rho \frac{i(\not{k}+\not{p}\,')}{(k+p'^2)}m\sigma^{\mu\nu} \frac{i(\not{k}+\not{p}+m)}{(k+p)^2-m^2}(-igT^a\mu^{\epsilon/2})\gamma_\rho \\
&\qquad \times \frac{-i}{k^2-\lambda^2} \quad + \quad \text{(wavefunction-, mass- and operator counterterms)} \\
&= \frac{\alpha_s}{3\pi}\int_{\perp} \gamma^\rho(\not{k}+\not{p}\,')m\sigma^{\mu\nu}(\not{k}+\not{p}+m)\gamma_\rho \qquad \text{(I.2)} \\
&\qquad + \left[\frac{1}{2}(\delta Z_Q+\delta Z_q)+\delta Z_m-\delta Z_T\right] m\sigma^{\mu\nu}
\end{aligned}$$

where I write three-point integrals as

$$\int_{\perp} f(k) = 16\pi^2(\mu^2)^{\epsilon/2}\int \frac{d^dk}{i(2\pi)^d}\frac{f(k)}{((k+p)^2-m^2)(k+p')^2(k^2-\lambda^2)}. \qquad \text{(I.3)}$$

I.1 Basis integrals

I solve integrals for up to two loop momenta in the numerator, $\int_{\perp}\{1, k^\mu, k^\mu k^\nu\}$. Introducing Feynman parameters I find

$$\int_{\perp}\{1, k^\mu, k^\mu k^\nu\} = 32\pi^2 \int_0^1 dx \int_0^1 dy\, y \int \frac{d^dk}{i(2\pi)^d} \frac{\{1, k^\mu, k^\mu k^\nu\}_{k\mapsto k-(1-y)p-y(1-x)p'}}{\left[k^2-\Delta(s)\right]^3} \tag{I.4}$$

with $\Delta(s) = (1-y)^2m^2 + y(1-y)(1-x)s + yx\lambda^2$. Expanding in $s = 2p\cdot p'$ these can be reduced to nine scalar basis integrals $a_n^{(m)}$, $\delta a_n^{(m)}$

$$\begin{aligned}
\int_{\perp} 1 &= J^{(0)}(s) = \frac{1}{m^2}a^{(0)} + \ldots, && \text{(I.5)}\\
\int_{\perp} k^\mu &= J_1^{(1)}(s)p^\mu + J_2^{(1)}(s)p'^\mu = \left(\frac{1}{m^2}a_1^{(1)} + \frac{s}{m^4}\delta a_1^{(1)}\right)p^\mu + \frac{1}{m^2}a_2^{(1)}p'^\mu + \ldots,\\
\int_{\perp} k^\mu k^\nu &= J_1^{(2)}(s)g^{\mu\nu} + J_2^{(2)}(s)p^\mu p^\nu + J_3^{(2)}(s)(p^\mu p'^\nu + p'^\mu p^\nu) + J_4^{(2)}(s)p'^\mu p'^\nu + \ldots\\
&= \left(a_1^{(2)} + \frac{s}{m^2}\delta a_1^{(2)}\right)g^{\mu\nu} + \left(\frac{1}{m^2}a_2^{(2)} + \frac{s}{m^4}\delta a_2^{(2)}\right)p^\mu p^\nu\\
&\quad + \frac{1}{m^2}a_3^{(2)}(p^\mu p'^\nu + p'^\mu p^\nu) + \ldots.
\end{aligned}$$

As an instructive example consider the evaluation of $\delta a_1^{(1)}$. In this case the numerator in (I.4) is given by $T(k-(1-y)p-y(1-x)p') = k^\mu - (1-y)p^\mu - y(1-x)p'^\mu$ and to pick up $a_1^{(1)}$ and $\delta a_1^{(1)}$ I only keep the term proportional to p^μ. I expand the denominator in s and keep the coefficient of the linear term which is

$$\frac{\partial}{\partial s}\frac{1}{\left[k^2-\Delta(s)\right]^3}\Big|_{s=0} = \frac{3y(1-y)(1-x)}{\left[k^2-\Delta(0)\right]^4}. \tag{I.6}$$

After the momentum integration I can express $\delta a_1^{(1)}$ as a Feynman parameter integral

$$\begin{aligned}
\delta a_1^{(1)} &= 32\pi^2m^4 \int_0^1 dx \int_0^1 dy\, y \int \frac{d^dk}{i(2\pi)^d} 3y(1-y)(1-x)\frac{-(1-y)}{\left[k^2-\Delta(0)\right]^4} && \text{(I.7)}\\
&= -m^4 \int_0^1 dx \int_0^1 dy \frac{(1-x)y^2(1-y)^2}{\left[(1-y)^2m^2 + xy\lambda^2\right]^2}
\end{aligned}$$

$$\begin{aligned}\delta a_1^{(1)} &= -\hat{\lambda}^{-4}\int_0^1 dy(1-y)^2\int_0^1 dx\left(\frac{1+\omega}{(x+\omega)^2}-\frac{1}{x+\omega}\right) \qquad \text{with } \omega=\frac{(1-y)^2}{y\hat{\lambda}^2}\\ &= -\hat{\lambda}^{-4}\left(\frac{1}{2}\hat{\lambda}^2-\int_0^1 dy(1-y)^2\log\left[1+\frac{y\hat{\lambda}^2}{(1-y)^2}\right]\right).\end{aligned}$$

I use the abbreviation $\hat{\lambda} = \lambda/m$. The remaining integral is evaluated using MATHEMATICA and I obtain, after expanding in $\hat{\lambda}$,

$$\delta a_1^{(1)} = -\left(\frac{2}{3}+\frac{\pi}{3\hat{\lambda}}+\frac{1}{2}\log\hat{\lambda}^2\right)+\mathcal{O}(\hat{\lambda}). \tag{I.8}$$

Ignoring terms of $\mathcal{O}(\hat{\lambda})$ and higher the remaining integrals are solved similarly, I find:

$$\begin{aligned}
a^{(0)} &= -\left(1+\frac{\pi}{\hat{\lambda}}+\frac{1}{2}\log\hat{\lambda}^2\right), && (\text{I.9})\\
a_1^{(1)} &= -\frac{1}{2}\left(1+\log\hat{\lambda}^2\right), & \delta a_1^{(1)} &= -\left(\frac{2}{3}+\frac{\pi}{3\hat{\lambda}}+\frac{1}{2}\log\hat{\lambda}^2\right),\\
a_2^{(1)} &= \frac{5}{6}+\frac{2\pi}{3\hat{\lambda}}+\frac{1}{2}\log\hat{\lambda}^2, & &\\
a_1^{(2)} &= \frac{1}{4}\left(\frac{2}{\overline{\epsilon}}-\log m^2/\mu^2+3\right), & \delta a_1^{(2)} &= \frac{1}{8}\left(\log\hat{\lambda}^2+\frac{3}{2}\right),\\
a_2^{(2)} &= -\frac{1}{2}, & \delta a_2^{(2)} &= -\frac{1}{8}\left(5+2\log\hat{\lambda}^2\right),\\
a_3^{(2)} &= \frac{1}{4}\left(\log\hat{\lambda}^2+\frac{3}{2}\right). &&
\end{aligned}$$

Note that only $a_1^{(2)}$ is ultraviolet divergent with $2/\overline{\epsilon} = 2/\epsilon - \gamma_E + \log 4\pi$.

I.2 Matrix elements

Expanding the matrix elements I find after some Dirac algebra

$$\begin{aligned}\delta\mathcal{M}^{\mu}_{(V)} &= b_1^{(V)}\gamma^\mu + b_2^{(V)}\frac{p^\mu}{m}+b_3^{(V)}s\gamma^\mu+b_4^{(V)}\frac{p'^\mu}{m}+b_5^{(V)}\frac{s}{m^2}\frac{p^\mu}{m}+\mathcal{O}(1/m^2)\\ \delta\mathcal{M}^{\mu\nu}_{(T)} &= b_1^{(T)}m\sigma^{\mu\nu}+b_2^{(T)}2i(\gamma^\mu p'^\nu-\gamma^\nu p'^\mu)+b_3^{(T)}\frac{s}{m^2}m\sigma^{\mu\nu}+\mathcal{O}(1/m^2).\end{aligned} \tag{I.10}$$

Using on-shell counterterms for the massless and heavy quark as given in (D.6), (D.7) and (D.11) and absorbing the UV divergence in the non-conserved tensor current in

the $\overline{MS}$ scheme by choosing $\delta Z_T = -4\alpha_s/(3\pi)\frac{2}{\hat{\epsilon}}$ I obtain for the vector current

$$\begin{aligned}
b_1^{(V)} &= \frac{\alpha_s}{3\pi}\left(4(1-\epsilon)a_1^{(2)} + 2a_2^{(2)} + 2a_1^{(1)}\right) + \frac{1}{2}(\delta Z_Q + \delta Z_q) \qquad \text{(I.11)}\\
&= \frac{\alpha_s}{3\pi}\left(-\frac{3}{2}\log\hat{\lambda}^2 - \frac{11}{4}\right)\\
b_2^{(V)} &= \frac{\alpha_s}{3\pi}(-4)a_2^{(2)} = \frac{\alpha_s}{3\pi}2\\
b_3^{(V)} &= 2\frac{\alpha_s}{3\pi}(2\delta a_1^{(2)} + \delta a_2^{(2)} + a_3^{(2)} + a^{(0)} + \delta a_1^{(1)} + a_2^{(1)} + a_1^{(1)})\\
&= \frac{\alpha_s}{3\pi}\left(-\frac{29}{12} - \frac{3}{2}\log\hat{\lambda}^2 - \frac{4\pi}{3\hat{\lambda}}\right)\\
b_4^{(V)} &= \frac{\alpha_s}{3\pi}(-4)(a_3^{(2)} + a_1^{(1)}) = \frac{\alpha_s}{3\pi}\left(\log\hat{\lambda}^2 + \frac{1}{2}\right)\\
b_5^{(V)} &= \frac{\alpha_s}{3\pi}(-4)\delta a_2^{(2)} = \frac{\alpha_s}{3\pi}\left(\frac{5}{2} + \log\hat{\lambda}^2\right)
\end{aligned}$$

and for the tensor current

$$\begin{aligned}
b_1^{(T)} &= \frac{\alpha_s}{3\pi}2a_1^{(1)} + \frac{1}{2}(\delta Z_Q + \delta Z_q) + \delta Z_m - \delta Z_T = \frac{\alpha_s}{3\pi}\left(-\frac{27}{4} - \frac{3}{2}\log\hat{\lambda}^2 + 4\log m^2/\mu^2\right)\\
b_2^{(T)} &= \frac{\alpha_s}{3\pi}(-2)a_1^{(1)} = \frac{\alpha_s}{3\pi}\left(1 + \log\hat{\lambda}^2\right)\\
b_3^{(T)} &= \frac{\alpha_s}{3\pi}2\left(a^{(0)} + a_1^{(1)} + \delta a_1^{(1)} + a_2^{(1)}\right) = \frac{\alpha_s}{3\pi}\left(-\frac{8}{3} - \frac{4\pi}{3\hat{\lambda}} - 2\log\hat{\lambda}^2\right) \qquad \text{(I.12)}
\end{aligned}$$

I.3 Comparison to the literature

In [140][1], eqn. (4), the expansion coefficients of the time component of the axial vector current are given as $a_1, \ldots, a_5$. Due to chiral symmetry of the light quark they can be compared to $b_1^{(V)}, \ldots, b_5^{(V)}$ in (I.11). As $s = 2p \cdot p'$ I expect $a_1 = 1 + b_1^{(V)}$, $a_2 = b_2^{(V)}$, $a_3 = 2b_3^{(V)}$, $a_4 = b_4^{(V)}$ and $a_5 = 2b_5^{(V)}$. I find perfect agreement for all IR divergent terms, there is, however, a mismatch for the IR finite term in $a_3 \leftrightarrow b_3^{(V)}$. This discrepancy is not relevant for the results presented in this thesis as I only consider radiative corrections to the leading order currents.

[1] I would like to thank Junko Shigemitsu for providing me with further details of the calculation.

Anomalous dimension of the tensor operator

The anomalous dimension of the tensor operator is given by

$$\gamma^{(T)} = \frac{1}{Z_T}\frac{dZ_T}{d\log\mu} \tag{I.13}$$

If the counterterm Z_T is expanded in inverse powers of ϵ,

$$Z_T = 1 + \sum_{k=1}^{\infty}\frac{1}{\epsilon^k}Z_T^{(k)} \tag{I.14}$$

and the μ dependence of the coupling $dg(\mu)/d\log\mu = -\epsilon g/2 + \beta(g)$ is used this implies that

$$\gamma_T^{(\mathrm{con})} = -g^2\frac{dZ_T^{(1)}}{dg^2} = \frac{8\alpha_s}{3\pi}. \tag{I.15}$$

This agrees with what is found in [45].

Appendix J

Infrared subtraction functions

In this chapter I discuss infrared subtraction functions which are added to the lattice integrand to improve the convergence of infrared divergent VEGAS integrals. I solve the subtraction integral analytically.

J.1 Wavefunction renormalisation

A subtraction function for the rainbow diagram in Fig. 5.1 needed in the calculation of the heavy quark wavefunction renormalisation can be constructed as follows:

At lowest order in the heavy quark expansion the continuum integrand (in Euclidean space) is given by

$$\alpha_s \Sigma = \int \frac{d^4k}{(2\pi)^4} (-gT^a v_\mu) D_h^{(0)}(v, k+p) (-gT^a v_\mu) \frac{1}{k^2+\lambda^2} \tag{J.1}$$

where $v_0 = i$ and the heavy quark propagator is in the static limit

$$D_h^{(0)}(v,k) = \frac{-i}{k_0 - i\boldsymbol{v}\cdot\boldsymbol{k}} \tag{J.2}$$

Furthermore the derivative with respect to p_0 at $p = 0$ is

$$\frac{\partial D_h^{(0)}(v,p+k)}{\partial p_0}\Big|_{p=0} = -i\left(\frac{-i}{k_0 - i\boldsymbol{v}\cdot\boldsymbol{k}}\right)^2. \tag{J.3}$$

Inserting this into the integral for Ω_1 one will obtain both a logarithmic infrared and a logarithmic ultraviolet divergence. To render the integral UV finite without changing the infrared behaviour I replace

$$\frac{-i}{k_0 - i\boldsymbol{v}\cdot\boldsymbol{k}} \mapsto \frac{2\gamma m}{(k+mu)^2 + m^2} \tag{J.4}$$

and find

$$\alpha_s\Omega_1^{(\mathrm{sub})} = \mathrm{Im}\{\int \frac{d^4k}{(2\pi)^4}(-gT^a v_\mu)(-i)\left(\frac{2\gamma m}{(k+mu)^2+m^2}\right)^2(-gT^a v_\mu)\frac{1}{k^2+\lambda^2}\}. \tag{J.5}$$

Evaluating integral (J.5) and neglecting all terms which vanish in the limit $\lambda/m \to 0$ I obtain the analytical expression

$$\Omega_1^{(\mathrm{sub})} = -\frac{2}{3\pi}\log\lambda^2/m^2 + \mathcal{O}(\lambda/m). \tag{J.6}$$

J.2 Higher order kinetic terms

The integrand I use as a subtraction function for the evaluation of higher order kinetic terms in the NRQCD action in section 6.4.1 is the continuum version of the rainbow diagram,

$$f^{(\mathrm{sub})} = -\frac{16\pi}{3}\,\frac{1}{\boldsymbol{k}^2+k_0^2+\lambda^2}\,\frac{1}{i(p_0+k_0)+\frac{(\boldsymbol{k}+\boldsymbol{p})^2}{2m}-\frac{((\boldsymbol{k}+\boldsymbol{p})^2)^2}{8m^3}}. \tag{J.7}$$

For $p=0$ the poles are at $i\omega_\pm \pm \epsilon$ and $i\omega_h + \epsilon$ with

$$\omega_\pm = \pm\sqrt{\boldsymbol{k}^2+\lambda^2}, \qquad \omega_h = \frac{\boldsymbol{k}^2}{2m} - \frac{(\boldsymbol{k}^2)^2}{8m^3}. \tag{J.8}$$

To be able to Wick rotate back to Minkowski space the integration contour has to separate the positive energy poles ω_+, ω_h from the negative energy gluon pole ω_-. It is easy to show that $\omega_+, \omega_h > \omega_-$ for $|\boldsymbol{k}| < 2m$ (but $\omega_h < \omega_-$ for $|\boldsymbol{k}| \to \infty$), so I impose a hard spherical cutoff $\Lambda = 2m$ on the modulus of the spatial momentum. This is legitimate as it only changes the ultraviolet behaviour. I always shift the contour midway between the two closest poles to improve convergence.

Note that the integral over $D_2 f^{(\mathrm{sub})}$ (with D_2 defined in (6.19)) vanishes due to rotational invariance, even after imposing a hard cutoff $|\boldsymbol{k}| < 2m$. The integral over $D_1 f^{(\mathrm{sub})}$ is evaluated numerically which can be done with very high statistics due to the simplicity of the integrand.

J.3 One particle irreducible corrections to heavy-light operators

I construct a subtraction function for the one particle irreducible diagrams discussed in section 7.2.1. In Euclidean space one has

$$\begin{aligned}\mathcal{M}_j &= \int \frac{d^4k}{(2\pi)^4}\Big[\overline{u}_s(p')(-igT^a\gamma_\rho)\frac{-ik\!\!\!/}{k^2}f_j\Gamma S_j U\Big]D_h^{(0)}(k)(-gT^a v_\rho)\frac{1}{k^2+\lambda^2}\\ &\equiv \alpha_s f_j\,\overline{u}_s(p')\Sigma_j^{(\mathrm{sub})}U \end{aligned}\tag{J.9}$$

where ΓS_j with $\Gamma=\{\gamma^\mu,\sigma^{\mu\nu}\}$ and $S_1=\mathrm{Id}$, $S_2=-\boldsymbol{\gamma}\cdot\hat{\boldsymbol{v}}\gamma_0$ is the Dirac structure of the operator. Again I render the integral UV finite by replacing

$$D_h^{(0)}(k)=\frac{-i}{k_0-i\boldsymbol{v}\cdot\boldsymbol{k}} \;\mapsto\; \frac{2\gamma m}{(k+mu)^2+m^2}.\tag{J.10}$$

As in (7.43) I write $\overline{u}_s(p')\Sigma_j^{(\mathrm{sub})}U$ as follows

$$\begin{aligned}f_j\overline{u}_s(p')\Sigma_j^{(\mathrm{sub})}U &= \frac{16\pi}{3}f_j\int\frac{d^4k}{(2\pi)^4}\overline{u}_s(p')(-i\gamma_\rho)\frac{-ik\!\!\!/}{k^2}\Gamma S_j U\\ &\qquad\times\;\frac{2\gamma m}{(k+p)^2+m^2}(-v_\rho)\frac{1}{k^2+\lambda^2}\\ &= \sum_{k=1,2}f_k\xi_{jk}^{(\mathrm{sub})\Gamma}\overline{u}_s(p')\Gamma S_k U.\end{aligned}\tag{J.11}$$

I evaluate the subtraction integral analytically in Minkowski space. The matrix element is given in (J.9)

$$\begin{aligned}i\mathcal{M}_j &= \int\frac{d^4k}{(2\pi)^4}\,\overline{u}_s(p')(-igT^a\gamma^\rho)\frac{i}{k\!\!\!/+i\epsilon}if_j\Gamma S_j U\\ &\qquad\times\;\frac{2m\gamma i}{(k+p)^2-m^2+i\epsilon}(-igT^a v_\rho)\frac{-i}{k^2-\lambda^2+i\epsilon}\\ &= \alpha_s\frac{16\pi}{3}f_j\int\frac{d^4k}{(2\pi)^4}\frac{2m\,\overline{u}_s(p')v\!\!\!/\,k\!\!\!/\,\Gamma S_j U}{(k^2+i\epsilon)((k+p)^2-m^2+i\epsilon)(k^2-\lambda^2+i\epsilon)}\\ &\equiv \alpha_s i f_j I_j\overline{u}_s(p')\Gamma_j^{\mu\nu}U.\end{aligned}\tag{J.12}$$

The integral which needs to be solved is

$$\int \frac{d^4k}{(2\pi)^4} \frac{k_\mu}{(k^2+i\epsilon)((k+p)^2-m^2+i\epsilon)(k^2-\lambda^2+i\epsilon)} \tag{J.13}$$
$$= -\frac{1}{2m} \frac{i}{16\pi^2}\left(1+\log\lambda^2/m^2\right)+\mathcal{O}(\lambda/m).$$

From this follows

$$I_j = -\frac{\alpha_s}{3\pi}\left(1+\log\hat{\lambda}^2\right) \qquad \text{and}$$
$$\xi_{jk}^{(sub.)} = -\frac{\delta_{jk}}{3\pi}\left(1+\log\hat{\lambda}^2\right). \tag{J.14}$$

Note that due to heavy quark symmetry this result is independent of the Dirac structure Γ of the operator.

J.4 Light quark wavefunction renormalisation

The subtraction integrand for massless light quark wavefunction renormalisation in section 7.2.1 is

$$f^{(\mathrm{sub})}(k) = -\frac{32\pi}{3}\frac{k^2-2k_0^2}{k^2(k^2+\lambda^2)}\exp\left[-k^2/\Lambda^2\right]. \tag{J.15}$$

Λ is an arbitrary UV cutoff, and the integral is readily solved to give

$$I^{(\mathrm{sub})} = \int \frac{d^4k}{(2\pi)^4} f^{(\mathrm{sub})}(k) \tag{J.16}$$
$$= \frac{1}{3\pi}\left(\gamma_E-\log a^2\Lambda^2\right)+\frac{1}{3\pi}\log a^2\lambda^2.$$

Bibliography

[1] C. Davies et al., *Moving NRQCD for High Recoil Form Factors in Heavy Quark Physics*, (2009), arXiv:0906.0945 [hep-lat].

[2] F. Halzen and A. D. Martin, *Quarks and Leptons: An Introductory Course in Modern Particle Physics* (John Wiley and Sons, 1984).

[3] M. E. Peskin and D. V. Schroeder, *An Introduction to Quantum Field Theory* (Westview Press, 1995).

[4] P. W. Higgs, *Spontaneous Symmetry Breakdown without Massless Bosons*, Phys. Rev. **145**, 1156 (1966).

[5] Particle Data Group, C. Amsler et al., *Review of Particle Physics*, Phys. Lett. **B667**, 1 (2008).

[6] D. H. Perkins, *Introduction to High Energy Physics*, 4th ed. (Cambridge University Press, 2000).

[7] S. L. Glashow, *Partial Symmetries of Weak Interactions*, Nucl. Phys. **22**, 579 (1961).

[8] A. Salam, *Elementary Particle Theory* (Almqvist and Wiksell, 1968).

[9] S. Weinberg, *A Model of Leptons*, Phys. Rev. Lett. **19**, 1264 (1967).

[10] J. Gasser and H. Leutwyler, *Chiral Perturbation Theory to One Loop*, Ann. Phys. **158**, 142 (1984).

[11] J. Gasser and H. Leutwyler, *Chiral Perturbation Theory: Expansions in the Mass of the Strange Quark*, Nucl. Phys. **B250**, 465 (1985).

[12] E. Eichten and B. R. Hill, *An Effective Field Theory for the Calculation of Matrix Elements Involving Heavy Quarks*, Phys. Lett. **B234**, 511 (1990).

[13] H. Georgi, *An Effective Field Theory for Heavy Quarks at Low Energies*, Phys. Lett. **B240**, 447 (1990).

[14] B. Grinstein, *The Static Quark Effective Theory*, Nucl. Phys. **B339**, 253 (1990).

[15] N. Cabibbo, *Unitary Symmetry and Leptonic Decays*, Phys. Rev. Lett. **10**, 531 (1963).

[16] M. Kobayashi and T. Maskawa, *CP Violation in the Renormalizable Theory of Weak Interaction*, Prog. Theor. Phys. **49**, 652 (1973).

[17] L. Wolfenstein, *Parametrization of the Kobayashi-Maskawa Matrix*, Phys. Rev. Lett. **51**, 1945 (1983).

[18] E. Dalgic et al., *B Meson Semileptonic Form Factors from Unquenched Lattice QCD*, Phys. Rev. **D73**, 074502 (2006), hep-lat/0601021.

[19] Heavy Flavor Averaging Group, E. Barberio et al., *Averages of b-Hadron and c-Hadron Properties at the End of 2007, online update:* `http://www.slac.stanford.edu/xorg/hfag`, (2008), arXiv:0808.1297 [hep-ex].

[20] J. Bailey et al., *The $B \to \pi\ell\nu$ Semileptonic Form Factor from Three- Flavor Lattice QCD: A Model-Independent Determination of $|V_{ub}|$*, (2008), arXiv:0811.3640 [hep-lat].

[21] CLEO, S. B. Athar et al., *Study of the q^2 Dependence of $B \to \pi\ell\nu$ and $B \to \rho(\omega)\ell\nu$ Decay and Extraction of $|V_{ub}|$*, Phys. Rev. **D68**, 072003 (2003), hep-ex/0304019.

[22] Belle, T. Hokuue et al., *Measurements of Branching Fractions and q^2 Distributions for $B \to \pi\ell\nu$ and $B \to \rho\ell\nu$ Decays with $B \to D^{(*)}\ell\nu$ Decay Tagging*, Phys. Lett. **B648**, 139 (2007), hep-ex/0604024.

[23] BABAR, B. Aubert et al., *Measurement of the $B^0 \to \pi^-\ell^+\nu$ Form-Factor Shape and Branching Fraction, and Determination of $|V_{ub}|$ with a Loose Neutrino Reconstruction Technique*, Phys. Rev. Lett. **98**, 091801 (2007), hep-ex/0612020.

[24] K. M. Foley and G. P. Lepage, *Moving NRQCD for B Form Factors at High Recoil*, Nucl. Phys. Proc. Suppl. **119**, 635 (2003), hep-lat/0209135.

[25] HPQCD, A. Dougall, C. T. H. Davies, K. M. Foley, and G. P. Lepage, *The Heavy Quark's Self Energy from Moving NRQCD on the Lattice*, Nucl. Phys. Proc. Suppl. **140**, 431 (2005), hep-lat/0409088.

[26] A. Dougall, K. M. Foley, C. T. H. Davies, and G. P. Lepage, *B Meson Decays at High Velocity from mNRQCD*, PoS **LAT2005**, 219 (2006), hep-lat/0509108.

[27] K. M. Foley, G. P. Lepage, C. T. H. Davies, and A. Dougall, *Moving NRQCD: B Mesons at High Velocities*, Nucl. Phys. Proc. Suppl. **140**, 470 (2005).

[28] S. Meinel, R. Horgan, L. Khomskii, L. C. Storoni, and M. Wingate, *Moving NRQCD and $B \to K^*\gamma$*, PoS **LAT2007**, 377 (2007), arXiv:0710.3101 [hep-lat].

[29] S. Meinel et al., *Rare B Decays with Moving NRQCD and Improved Staggered Quarks*, PoS **LAT2008**, 280 (2008), arXiv:0810.0921 [hep-lat].

[30] Z. Liu et al., *Form Factors for Rare B/B_s Decays with Moving NRQCD and Stochastic Sources*, PoS **LAT2009** (2009).

[31] M. Okamoto, *Full Determination of the CKM Matrix using Recent Results from Lattice QCD*, PoS **LAT2005**, 013 (2006), hep-lat/0510113.

[32] HPQCD, E. Gamiz, C. T. H. Davies, G. P. Lepage, J. Shigemitsu, and M. Wingate, *Neutral B Meson Mixing in Unquenched Lattice QCD*, (2009), arXiv:0902.1815 [hep-lat].

[33] BABAR, e. Harrison, P. F. and e. Quinn, Helen R., *The BABAR Physics Book: Physics at an Asymmetric B Factory*, (1997), Papers from Workshop on Physics at an Asymmetric B Factory (BaBar Collaboration Meeting), Rome, Italy, 11-14 Nov 1996, Princeton, NJ, 17-20 Mar 1997, Orsay, France, 16-19 Jun 1997 and Pasadena, CA, 22-24 Sep 1997.

[34] BABAR, B. Aubert et al., *Measurement of Branching Fractions and CP and Isospin Asymmetries in $B \to K^*\gamma$*, (2008), arXiv:0808.1915 [hep-ex].

[35] BABAR, B. Aubert et al., *Measurement of Branching Fractions, and CP and Isospin Asymmetries, for $B \to K^*\gamma$*, Phys. Rev. **D70**, 112006 (2004), hep-ex/0407003.

[36] BELLE, M. Nakao et al., *Measurement of the $B \to K^*\gamma$ Branching Fractions and Asymmetries*, Phys. Rev. **D69**, 112001 (2004), hep-ex/0402042.

[37] D. Atwood, M. Gronau, and A. Soni, *Mixing-induced CP Asymmetries in Radiative B Decays in and beyond the Standard Model*, Phys. Rev. Lett. **79**, 185 (1997), hep-ph/9704272.

[38] BABAR, B. Aubert et al., *Measurement of The Time-Dependent CP Asymmetry in $B^0 \to K^{*0}\gamma$ Decays*, (2007), arXiv:0708.1614 [hep-ex].

[39] Belle, Y. Ushiroda et al., *Time-dependent CP Asymmetries in $B^0 \to K^{0(S)}\pi^0\gamma$ transitions*, Phys. Rev. **D74**, 111104 (2006), hep-ex/0608017.

[40] A. J. Buras, *Weak Hamiltonian, CP Violation and Rare Decays*, (1998), hep-ph/9806471.

[41] C. Greub, T. Hurth, and D. Wyler, *Virtual $O(\alpha_s)$ Corrections to the Inclusive Decay $b \to s\gamma$*, Phys. Rev. **D54**, 3350 (1996), hep-ph/9603404.

[42] T. Inami and C. S. Lim, *Effects of Superheavy Quarks and Leptons in Low-Energy Weak Processes $K^{(L)} \to \mu\overline{\mu}$, $K^+ \to \pi^+\nu\overline{\nu}$ and $K^0 \leftrightarrow \overline{K}^0$*, Prog. Theor. Phys. **65**, 297 (1981).

[43] M. Ciuchini, E. Franco, G. Martinelli, L. Reina, and L. Silvestrini, *Scheme Independence of the Effective Hamiltonian for $b \to s\gamma$ and $b \to sg$ Decays*, Phys. Lett. **B316**, 127 (1993), hep-ph/9307364.

[44] M. Ciuchini, E. Franco, L. Reina, and L. Silvestrini, *Leading Order QCD Corrections to $b \to s\gamma$ and $b \to sg$ Decays in Three Regularization Schemes*, Nucl. Phys. **B421**, 41 (1994), hep-ph/9311357.

[45] B. Grinstein, R. P. Springer, and M. B. Wise, *Strong Interaction Effects in Weak Radiative $\overline{B}$ Meson Decay*, Nucl. Phys. **B339**, 269 (1990).

[46] A. J. Buras, A. Czarnecki, M. Misiak, and J. Urban, *Completing the NLO QCD Calculation of $\overline{B} \to X_s\gamma$*, Nucl. Phys. **B631**, 219 (2002), hep-ph/0203135.

[47] M. Misiak et al., *The First Estimate of $B(\overline{B} \to X_s\gamma)$ at $\mathcal{O}(\alpha_s^2)$*, Phys. Rev. Lett. **98**, 022002 (2007), hep-ph/0609232.

[48] A. Ferroglia, *QCD Corrections to the Radiative Decay $B \to X_s\gamma$*, (2008), arXiv:0812.0082 [hep-ph].

[49] C. Greub, H. Simma, and D. Wyler, *Branching Ratio and Direct CP violating Rate Asymmetry of the Rare Decays $B \to K^*\gamma$ and $B \to \rho\gamma$*, Nucl. Phys. **B434**, 39 (1995), hep-ph/9406421.

[50] C. E. Carlson and J. Milana, *Penguins Leaving the Pole: Bound State Effects in $B \to K^*\gamma$*, Phys. Rev. **D51**, 4950 (1995), hep-ph/9405344.

[51] H. H. Asatrian, H. M. Asatrian, and D. Wyler, *NLL Corrections for B Meson Radiative Exclusive Decays*, Phys. Lett. **B470**, 223 (1999), hep-ph/9905412.

[52] H.-Y. Cheng, *Vector Dominance Effects in Weak Radiative Decays of the B Meson*, Phys. Rev. **D51**, 6228 (1995), hep-ph/9411330.

[53] A. Khodjamirian, R. Ruckl, G. Stoll, and D. Wyler, *QCD Estimate of the Long-distance Effect in $B \to K^*\gamma$*, Phys. Lett. **B402**, 167 (1997), hep-ph/9702318.

[54] P. Ball and R. Zwicky, *New Results on $B \to \pi, K, \eta$ Decay Formfactors from Light-Cone Sum Rules*, Phys. Rev. **D71**, 014015 (2005), hep-ph/0406232.

[55] P. Ball, G. W. Jones, and R. Zwicky, *$B \to V\gamma$ Beyond QCD Factorisation*, Phys. Rev. **D75**, 054004 (2007), hep-ph/0612081.

[56] B. Grinstein and D. Pirjol, *Long-distance Effects in $B \to V\gamma$ Radiative Weak Decays*, Phys. Rev. **D62**, 093002 (2000), hep-ph/0002216.

[57] C. Greub and D. Wyler, *Decays of B Mesons into Light Hadrons*, Phys. Lett. **B295**, 293 (1992).

[58] D. Becirevic, V. Lubicz, and F. Mescia, *An Estimate of the $B \to K^*\gamma$ Form Factor*, Nucl. Phys. **B769**, 31 (2007), hep-ph/0611295.

[59] C. W. Bauer, S. Fleming, D. Pirjol, and I. W. Stewart, *An Effective Field Theory for Collinear and Soft Gluons: Heavy to Light Decays*, Phys. Rev. **D63**, 114020 (2001), hep-ph/0011336.

[60] UKQCD, L. Del Debbio, J. M. Flynn, L. Lellouch, and J. Nieves, *Lattice-constrained Parametrizations of Form Factors for Semileptonic and Rare Radiative B Decays*, Phys. Lett. **B416**, 392 (1998), hep-lat/9708008.

[61] S. Meinel, *Renormalisation of Higher Order Kinetic Terms in the NRQCD Action*, private communications (2009).

[62] D. Becirevic and A. B. Kaidalov, *Comment on the Heavy $\to$ Light Form Factors*, Phys. Lett. **B478**, 417 (2000), hep-ph/9904490.

[63] H. J. Rothe, *Lattice Gauge Theories: An Introduction*, World Sci. Lect. Notes Phys. **43**, 1 (1992).

[64] BABAR, P. Grenier, *Observation of the Bottomonium Ground State, η_b, at BaBar*, (2008), arXiv:0809.1672 [hep-ex].

[65] T. Mannel, W. Roberts, and Z. Ryzak, *A Derivation of the Heavy Quark Effective Lagrangian from QCD*, Nucl. Phys. **B368**, 204 (1992).

[66] M. E. Luke and A. V. Manohar, *Reparametrization Invariance Constraints on Heavy Particle Effective Field Theories*, Phys. Lett. **B286**, 348 (1992), hep-ph/9205228.

[67] A. V. Manohar and M. B. Wise, *Heavy Quark Physics*, Camb. Monogr. Part. Phys. Nucl. Phys. Cosmol. **10**, 1 (2000).

[68] E. Braaten, *Introduction to the NRQCD Factorization Approach to Heavy Quarkonium*, (1996), hep-ph/9702225.

[69] S. Weinberg, *Phenomenological Lagrangians*, Physica **A96**, 327 (1979).

[70] R. P. Feynman and A. R. Hibbs, *Quantum Physics and Path Integrals,* (New York, McGraw-Hill, 1965).

[71] K. G. Wilson, *Confinement of Quarks*, Phys. Rev. **D10**, 2445 (1974).

[72] HPQCD, C. T. H. Davies et al., *High-precision Lattice QCD Confronts Experiment*, Phys. Rev. Lett. **92**, 022001 (2004), hep-lat/0304004.

[73] HPQCD, E. Follana, C. T. H. Davies, G. P. Lepage, and J. Shigemitsu, *High Precision Determination of the π, K, D and D_s Decay Constants from Lattice QCD*, Phys. Rev. Lett. **100**, 062002 (2008), arXiv:0706.1726 [hep-lat].

[74] C. T. H. Davies et al., *Precision Charm Physics, m_c and α_s from Lattice QCD*, (2008), arXiv:0810.3548 [hep-lat].

[75] CLEO, J. P. Alexander, *Measurement of $B(D_s^+ \to \ell^+\nu)$ and the Decay Constant f_{D_s} from $600/pb$ of e^+e^- Annihilation Data Near $4170MeV$*, (2009), arXiv:0901.1216 [hep-ex].

[76] G. P. Lepage, *Lattice QCD for Small Computers*, (1994), hep-lat/9403018.

[77] S. Wansleben and D. P. Landau, *Monte Carlo Investigation of Critical Dynamics in the Three-dimensional Ising Model*, Phys. Rev. **B43**, 6006 (1991).

[78] M. G. Alford, W. Dimm, G. P. Lepage, G. Hockney, and P. B. Mackenzie, *Lattice QCD on Small Computers*, Phys. Lett. **B361**, 87 (1995), hep-lat/9507010.

[79] G. P. Lepage and P. B. Mackenzie, *On the Viability of Lattice Perturbation Theory*, Phys. Rev. **D48**, 2250 (1993), hep-lat/9209022.

[80] B. Sheikholeslami and R. Wohlert, *Improved Continuum Limit Lattice Action for QCD with Wilson Fermions*, Nucl. Phys. **B259**, 572 (1985).

[81] P. H. Ginsparg and K. G. Wilson, *A Remnant of Chiral Symmetry on the Lattice*, Phys. Rev. **D25**, 2649 (1982).

[82] H. Neuberger, *Exactly Massless Quarks on the Lattice*, Phys. Lett. **B417**, 141 (1998), hep-lat/9707022.

[83] D. B. Kaplan, *A Method for Simulating Chiral Fermions on the Lattice*, Phys. Lett. **B288**, 342 (1992), hep-lat/9206013.

[84] G. P. Lepage, *Flavor-symmetry Restoration and Symanzik Improvement for Staggered Quarks*, Phys. Rev. **D59**, 074502 (1999), hep-lat/9809157.

[85] HPQCD, E. Follana et al., *Highly Improved Staggered Quarks on the Lattice, with Applications to Charm Physics*, Phys. Rev. **D75**, 054502 (2007), hep-lat/0610092.

[86] G. P. Lepage and B. A. Thacker, *Effective Lagrangians for Simulating Heavy Quark Systems*, Nucl. Phys. Proc. Suppl. **4**, 199 (1988).

[87] B. A. Thacker and G. P. Lepage, *Heavy Quark Bound States in Lattice QCD*, Phys. Rev. **D43**, 196 (1991).

[88] C. T. H. Davies and B. A. Thacker, *Heavy Quark Renormalization Parameters in Nonrelativistic QCD*, Phys. Rev. **D45**, 915 (1992).

[89] G. P. Lepage, L. Magnea, C. Nakhleh, U. Magnea, and K. Hornbostel, *Improved Nonrelativistic QCD for Heavy Quark Physics*, Phys. Rev. **D46**, 4052 (1992), hep-lat/9205007.

[90] K. M. Foley, *The Quest for Flavor Physics Parameters: Highly Improved Lattice Algorithms for Heavy Quarks*, (2004), PhD thesis, UMI-31-40868.

[91] S. Meinel, *Simulation Results for Bottomonium and B Mesons with the Moving-NRQCD and AsqTad Actions [unpublished]*, 2008.

[92] E. Dalgic, J. Shigemitsu, and M. Wingate, *One-loop Matching of the Heavy-light A_0 and V_0 Currents with NRQCD Heavy and Improved Naive Light Quarks*, Phys. Rev. **D69**, 074501 (2004), hep-lat/0312017.

[93] A. Gray et al., *The Upsilon Spectrum and m_b from Full Lattice QCD*, Phys. Rev. **D72**, 094507 (2005), hep-lat/0507013.

[94] G. Martinelli, C. Pittori, C. T. Sachrajda, M. Testa, and A. Vladikas, *A General Method for Nonperturbative Renormalization of Lattice Operators*, Nucl. Phys. **B445**, 81 (1995), hep-lat/9411010.

[95] HPQCD, Q. Mason et al., *Accurate Determinations of α_s from Realistic Lattice QCD*, Phys. Rev. Lett. **95**, 052002 (2005), hep-lat/0503005.

[96] HPQCD, Q. Mason, H. D. Trottier, R. Horgan, C. T. H. Davies, and G. P. Lepage, *High-precision Determination of the Light-Quark Masses from Realistic Lattice QCD*, Phys. Rev. **D73**, 114501 (2006), hep-ph/0511160.

[97] E. Dalgic et al., *Progress on Perturbative Matching Calculations for the Charm Quark Mass Using the HISQ Action*, PoS **LAT2007**, 239 (2007).

[98] W. Dimm, G. P. Lepage, and P. B. Mackenzie, *Nonperturbative 'Lattice Perturbation Theory'*, Nucl. Phys. Proc. Suppl. **42**, 403 (1995), hep-lat/9412100.

[99] G. P. Lepage, P. B. Mackenzie, N. H. Shakespeare, and H. D. Trottier, *Perturbative Two- and Three-loop Coefficients from Large β Monte Carlo*, Nucl. Phys. Proc. Suppl. **83**, 866 (2000), hep-lat/9910018.

[100] H. D. Trottier, N. H. Shakespeare, G. P. Lepage, and P. B. Mackenzie, *Perturbative Expansions from Monte Carlo Simulations at Weak Coupling: Wilson Loops and the Static-Quark Self- Energy*, Phys. Rev. **D65**, 094502 (2002), hep-lat/0111028.

[101] K. Y. Wong, H. D. Trottier, and R. M. Woloshyn, *Perturbative Wilson Loops from Unquenched Monte Carlo Simulations at Weak Couplings*, Phys. Rev. **D73**, 094512 (2006), hep-lat/0512012.

[102] A. Hart, R. R. Horgan, and L. C. Storoni, *Perturbation Theory vs. Simulation for Tadpole Improvement Factors in Pure Gauge Theories*, Phys. Rev. **D70**, 034501 (2004), hep-lat/0402033.

[103] G. Martinelli and C. T. Sachrajda, *Computation of the b-Quark Mass with Perturbative Matching at the Next-to-Next-to-Leading Order*, Nucl. Phys. **B559**, 429 (1999), hep-lat/9812001.

[104] E. Follana and H. Panagopoulos, *The Critical Mass of Wilson Fermions: A Comparison of Perturbative and Monte Carlo Results*, Phys. Rev. **D63**, 017501 (2001), hep-lat/0006001.

[105] K. J. Juge, *Two-loop Perturbative Quark Mass Renormalization from Large β Monte Carlo*, Nucl. Phys. Proc. Suppl. **94**, 584 (2001), hep-lat/0011021.

[106] K. J. Juge, *The Charm Quark Mass to Two-loop Order*, Nucl. Phys. Proc. Suppl. **106**, 847 (2002), hep-lat/0110131.

[107] G. P. Lepage et al., *Constrained Curve Fitting*, Nucl. Phys. Proc. Suppl. **106**, 12 (2002), hep-lat/0110175.

[108] R. R. Horgan and A. Lee, *mNRQCD Renormalisation Parameters from High-β Simulations [unpublished]*, (2009).

[109] M. Luscher and P. Weisz, *Efficient Numerical Techniques for Perturbative Lattice Gauge Theory Computations*, Nucl. Phys. **B266**, 309 (1986).

[110] G. 't Hooft, *A Property of Electric and Magnetic Flux in Nonabelian Gauge Theories*, Nucl. Phys. **B153**, 141 (1979).

[111] G. P. Lepage, *VEGAS: An Adaptive Multidimensional Integration Program*, (1980), CLNS-80/447.

[112] A. Hart, G. M. von Hippel, R. R. Horgan, and L. C. Storoni, *Automatically Generating Feynman Rules for Improved Lattice Field Theories*, J. Comput. Phys. **209**, 340 (2005), hep-lat/0411026.

[113] A. Hart, G. M. von Hippel, R. R. Horgan, and E. H. Muller, *Automated Generation of Lattice QCD Feynman Rules*, (2009), arXiv:0904.0375 [hep-lat].

[114] C. J. Morningstar, *The Heavy Quark Selfenergy in Nonrelativistic Lattice QCD*, Phys. Rev. **D48**, 2265 (1993), hep-lat/9301005.

[115] A. Hart, G. M. von Hippel, and R. R. Horgan, *Perturbative Calculations for the HISQ Action: the Gluon Action at $O(N_f\alpha_s a^2)$*, PoS **LATTICE2008**, 046 (2008), arXiv:0808.1791 [hep-lat].

[116] S. Groote and J. Shigemitsu, *One-loop Self Energy and Renormalization of the Speed of Light for Some Anisotropic Improved Quark Actions*, Phys. Rev. **D62**, 014508 (2000), hep-lat/0001021.

[117] G. M. von Hippel, *TaylUR, an Arbitrary-order Automatic Differentiation Package for Fortran 95*, Comput. Phys. Commun. **174**, 569 (2006), physics/0506222.

[118] G. P. Lepage, *A New Algorithm for Adaptive Multidimensional Integration*, J. Comput. Phys. **27**, 192 (1978).

[119] ECDF, *ECDF - The Edinburgh Compute and Data Facility,* `http://www.ecdf.ed.ac.uk/`, (2008).

[120] M. Neubert, *Heavy Quark Symmetry*, Phys. Rept. **245**, 259 (1994), hep-ph/9306320.

[121] L. Khomskii, *Perturbation Theory for Quarks and Currents in Moving NRQCD on a Lattice*, PhD Thesis, (2008).

[122] C. J. Morningstar, *Radiative Corrections to the Kinetic Couplings in Nonrelativistic Lattice QCD*, Phys. Rev. **D50**, 5902 (1994), hep-lat/9406002.

[123] U. Aglietti, M. Crisafulli, and M. Masetti, *Problems with the Euclidean Formulation of Heavy Quark Effective Theories*, Phys. Lett. **B294**, 281 (1992).

[124] U. Aglietti, *Consistency and Lattice Renormalization of the Effective Theory for Heavy Quarks*, Nucl. Phys. **B421**, 191 (1994), hep-ph/9304274.

[125] M. A. Nobes, H. D. Trottier, G. P. Lepage, and Q. Mason, *Second Order Perturbation Theory for Improved Gluon and Staggered Quark Actions*, Nucl. Phys. Proc. Suppl. **106**, 838 (2002), hep-lat/0110051.

[126] J. A. M. Vermaseren, *New Features of FORM*, (2000), math-ph/0010025.

[127] S. J. Brodsky, G. P. Lepage, and P. B. Mackenzie, *On the Elimination of Scale Ambiguities in Perturbative Quantum Chromodynamics*, Phys. Rev. **D28**, 228 (1983).

[128] C. T. H. Davies, *Private Communications*, (2009).

[129] K. Hornbostel, G. P. Lepage, and C. Morningstar, *Scale Setting for α_s Beyond Leading Order*, Phys. Rev. **D67**, 034023 (2003), hep-ph/0208224.

[130] Zeuthen-Rome / ZeRo, M. Guagnelli et al., *Continuous External Momenta in Non-perturbative Lattice Simulations: a Computation of Renormalization Factors*, Nucl. Phys. **B664**, 276 (2003), hep-lat/0303012.

[131] I. N. Bronstein, K. A. Semendjajew, and E. Z. (Editor), *Teubner Taschenbuch der Mathematik* (B. G. Teubner, 1996).

[132] I. Kendall, *Renormalisation of Higher Order Kinetic Terms in the NRQCD Action*, Private Communications (2009).

[133] G. Kilcup, D. Pekurovsky, and L. Venkataraman, *On the N_f and a Dependence of B_K*, Nucl. Phys. Proc. Suppl. **53**, 345 (1997), hep-lat/9609006.

[134] C. Aubin et al., *Light Hadrons with Improved Staggered Quarks: Approaching the Continuum Limit*, Phys. Rev. **D70**, 094505 (2004), hep-lat/0402030.

[135] C. Bernard et al., *Visualization of Semileptonic Form Factors from Lattice QCD*, (2009), arXiv:0906.2498 [hep-lat].

[136] M. Okamoto et al., *Semileptonic $D \to \pi/K$ and $B \to \pi/D$ Decays in 2+1 Flavor Lattice QCD*, Nucl. Phys. Proc. Suppl. **140**, 461 (2005), hep-lat/0409116.

[137] C. Monahan, *Private Communications*, (2009).

[138] MILC Collaboration, `http://www.physics.indiana.edu/~sg/milc`, (2008).

[139] G. Parisi, *Prolegomena to any Future Computer Evaluation of the QCD Mass Spectrum*, (1983), Invited talk given at Summer Inst. Progress in Gauge Field Theory, Cargese, France, Sep 1-15, 1983.

[140] C. J. Morningstar and J. Shigemitsu, *One-loop matching of Lattice and Continuum Heavy-light Axial Vector Currents Using NRQCD*, Phys. Rev. **D57**, 6741 (1998), hep-lat/9712016.

Publications

- Stefan Meinel (speaker), Eike H. Müller, Lew Khomskii, Alistair Hart, Ronald R. Horgan and Matthew Wingate:

  Rare B decays with moving NRQCD and improved staggered quarks.

  Talk at the 26th International Symposium on Lattice Field Theory (Lattice 2008), July 2008. Published as PoS LATTICE2008:280, arXiv:0810.0921 [hep-lat]

- Ronald R. Horgan, Lew Khomskii, Stefan Meinel, Matthew Wingate, Kerryann M. Foley, G. Peter Lepage, Georg M. von Hippel, Alistair Hart, Eike H. Müller, Christine T. H. Davies, Alex Dougall and Kit Y. Wong:

  Moving NRQCD for heavy-to-light form factors on the lattice.

  Accepted for publication in Phys. Rev. D, arXiv:0906.0945 [hep-lat]

- Alistair Hart, Georg M. von Hippel, Ronald R. Horgan, Eike H. Müller:

  Automated generation of lattice QCD Feynman rules.

  Accepted for publication in Computer Physics Communications, arXiv:0904.0375 [hep-lat]

- Eike H. Müller (speaker), Christine T. H. Davies, Alistair Hart, Georg M. von Hippel, Ron R. Horgan, Iain Kendall, Andrew Lee, Stefan Meinel, Chris Monahan, Matthew Wingate:

  Radiative corrections to the m(oving)NRQCD action and heavy-light operators.

  Talk at the 27th International Symposium on Lattice Field Theory (Lattice 2009), Beijing, China, July 2009. Published as PoS (LAT2009) 241, arXiv:0909.5126 [hep-lat]

Acknowledgements

First of all and most importantly, I would like to thank Alistair Hart for supervising my thesis, our frequent discussions and his continuous help and support. I can not remember a single occasion when he was too busy to answer my questions, however trivial they might have been. I am grateful to Brian Pendleton for kindly agreeing to act as second supervisor of this thesis.
I would like to thank my collaborators and all members of the HPQCD collaboration from whom I learnt so much. In particular I want to mention Iain Kendall, Lew Khomskii, Andrew Lee, Zhaofeng Liu, Stefan Meinel, Chris Monahan and Junko Shigemitsu. I am grateful to Georg von Hippel who has provided help with the HiPPy and Fortran codes.
I would like to thank Ron Horgan and Matt Wingate for their hospitality during my visits to Cambridge and the stimulating discussions at DAMTP. Similarly I am grateful to Christine Davies for very helpful discussions in Glasgow.
Finally, I would like to express my thanks to all my colleagues in Edinburgh and the staff at the School of Physics who made me feel welcome from the very first day. During all this time Jane Patterson provided invaluable help with all administrative and practical problems.
This thesis would never have been written without the continuous support and encouragement of my friends and family. Thank you all for three unforgetable years in a wonderful country, for being great company in the hills in good and bad weather and for being there whenever I needed you.

This work has made use of the resources provided by the Edinburgh Compute and Data Facility (ECDF). (`http://www.ecdf.ed.ac.uk/`). The ECDF is partially supported by the eDIKT initiative (`http://www.edikt.org.uk`).